UC Riverside

UC Riverside Electronic Theses and Dissertations

Title

Advancement of Separation and Characterization Techniques for Ionic Analytes

Permalink

https://escholarship.org/uc/item/1z19p0hs

Author

Jones, Christopher James

Publication Date

2012

Peer reviewed|Thesis/dissertation

eScholarship.org Powered by the California Digital Library
University of California

UNIVERSITY OF CALIFORNIA
RIVERSIDE

Advancement of Separation and Characterization Techniques for Ionic Analytes

A Dissertation submitted in partial satisfaction
of the requirement for the degree of

Doctor of Philosophy

in

Chemistry

by

Christopher James Jones

June 2012

Dissertation Committee:
Dr. Cynthia K. Larive, Chairperson
Dr. Dallas Rabenstein
Dr. Ryan Julian

Copyright by
Christopher James Jones
2012

The Dissertation of Christopher James Jones is approved:

_____

_____

_____

Committee Chairperson

University of California, Riverside

Acknowledgements

Thinking back on my life up to this point it is funny to think how my goals have changed and progressed over the years to get me to this point. I clearly remember in middle school thinking about what my life would be like and thinking that I would be happy in a blue collar job like an electrician or mechanic. Now here I am some 14 or 15 years later finishing my PhD in chemistry and about to start an exciting new job at BP Biofuels. Along the way there have been many people that have guided me and encouraged me through this journey that I would like to thank. First are all of my high school sciences teachers, especially Mr. Avery who was really the first person to encourage me to pursue a life in science. I'd also like to thank the high school honors medical school program and my research advisor in the program, Dr. Robert Hickner, who introduced me to the world of research. If it hadn't been for my time in his lab I'm not sure what I would be doing today, but I doubt I'd be where I'm at today. I would also like to sincerely thank the entire chemistry faculty at ECU especially my undergraduate research advisor Dr. Yu Yang. Even from my freshman year he saw potential in me and was always there to give me advice and encouragement as I grew as chemist. Also if it hadn't been for him I would have never heard of UCR!

I want to extend sincere thanks as well to my graduate research advisor Dr. Cynthia Larive. The last five years have been a journey I will never forget! In my entire career in chemistry I don't think I've had a bigger proponent or supporter of my success than her. While we may not have agreed on all things, I can truly say that I have learned a tremendous amount of information about not only chemistry, but about myself and life

from her. I would also like to thank former lab mate Dr. John Limtiaco for all his help with NMR and his friendship. Bro, I look forward to meeting up with you again some day to share stories and maybe sing a little karaoke! To all my present and former lab mates, I'd like to thank you as well for putting up with me everyday and for making lab a fun place to be.

Of course no acknowledgements page is complete without thanking my family. Throughout my entire life they have always encouraged anything I wanted to do or be without a second thought. That even included probably the most painful thing for them in saying goodbye to me as I left NC to head out west for grad school. Even though I don't say it much thank you for everything you have done for me and I love you guys!

Finally, I would like to thank the love of my life Sara. Thank you for being my best friend and for putting up with my craziness through this whole dissertation process. I would not have gotten through this last year without you by my side and look forward to our new life together in San Diego. I Love You Sweetie!!

Acknowledgement of Copyright

Part of the text and figures in Chapter 1 and 6 are reprinted from Springer and Analytical and Bioanalytical Chemistry, Vol. 402, Christopher J. Jones and Cynthia K. Larive, Could smaller really be better? Current and future trends in high-resolution microcoil NMR spectroscopy, 61-68, 2012, with kind permission from Springer Science and Business Media.

Part of the text and figures in Chapter 1 are also reprinted from Annual Review of Analytical Chemistry, Vol. 4, Christopher J. Jones, Szabolcs Beni, John Limtiaco, Derek Langeslay, and Cynthia K. Larive, Heparin characterization: challenges and solutions, 439-465, 2011, with permission from Annual Reviews.

The text and figures in Chapter 2 are reprinted from Journal of Chromatogarphy A, Vol. 1217, Christopher J. Jones, Nellymar Membreno, and Cynthia K. Larive, Insights into the mechanism of separation of heparin and heparan sulfate disaccharides by reverse-phase ion-pair chromatography, 479-488, 2010, with permission from Elsevier.

The text and figures in Chapter 3 are reprinted from Analytical Chemistry, Vol. 83, Christopher J. Jones, Szabolcs Beni, Cynthia K. Larive, Understanding the effect of the counterion on the reverse-phase ion-pair high-performance liquid chromatography (RPIP-HPLC) resolution of heparin-related saccharide anomers, 6762-6769. Copyright (2011) American Chemical Society.

ABSTRACT OF THE DISSERTATION

Advancement of Separation and Characterization Techniques for Ionic Analytes

by

Christopher James Jones

Doctor of Philosophy, Graduate Program in Chemistry
University of California, Riverside, June 2012
Dr. Cynthia K. Larive, Chairperson

The goal of this dissertation is to develop improved analytical methods for the separation and characterization of ionic analytes while gaining insights into their underlying mechanisms. The work focuses on reversed-phase ion-pair high-performance liquid chromatography (RPIP-HPLC) and capillary isotachophoresis (cITP) separations of the highly charged molecules, heparin and heparan sulfate. Furthermore, this work explores methods to improve the sensitivity of NMR, with a focus on both microcoil and microslot NMR probes.

RPIP-HPLC is an important method for the separation of ionic solutes using lipophilic ions, referred to as ion-pairing reagents (IPR), as mobile phase modifiers to aid in their retention on a hydrophobic stationary phase. However, the fine details of the RPIP separation mechanism are still being debated. The described work investigates the role that competition between ion-pairing reagents plays in the separation of structural isomers of heparin and heparan sulfate (HS) disaccharides, and how factors such as IPR concentration and buffer pH affect the resolution of their anomeric forms.

NMR spectroscopy can yield a vast amount of structural information about a compound without destroying the sample. However, NMR is often limited by poor sensitivity and for samples containing more than one compound of interest, the spectra

obtained can quickly become convoluted, complicating interpretation. To solve these problems we use the pre-concentration/separation method cITP coupled with microcoil NMR detection. The first part of this work uses doxepin as a model compound to study both the type and strength of interactions that occur during cITP. This work focuses on the binding interactions of doxepin with the buffer modifier β-cyclodextrin and the role that the counterion acetate plays in the cITP process.

The insights gained in the doxepin cITP study were then used to develop an improved cITP-NMR method for the analysis of heparin and HS derived oligosaccharides, focusing on designing a buffer system that reduces the effects of current induced resonance broadening that occurs when cITP is coupled to microcoil NMR. Finally, this work demonstrates the coupling of cITP with a new microslot NMR probe design which eliminates the deleterious affects of the magnetic field produced by the separation.

Table of Contents

LIST OF FIGURES

LIST OF TABLES

CHAPTER ONE

Based on a papers published in Annual Reviews of Analytical Chemistry and Analytical and Bioanalytical Chemistry

Annu. Rev. Anal. Chem., 2011, 4, 439-465.

Anal. Bioanal. Chem., 2012, 402, 61-68.

Introduction

The research presented in this dissertation focuses on the development of new and more sensitive separation and characterization techniques for ionic analytes. In particular, the work will focus around heparin and heparan sulfate oligosaccharides and gaining insight into the ion-pairing interactions involved in their separations. Although heparin is an important and widely prescribed pharmaceutical anticoagulant, its high degree of sequence microheterogeneity and polydispersity make molecular-level characterization challenging. Unlike nucleic acids and proteins that are biosynthesized through template-driven assembly processes, heparin and the related glycosaminoglycan (GAG) heparan sulfate (HS) are actively remodeled during biosynthesis through a series of enzymatic reactions that lead to variable levels of *O*- and *N*-sulfonation and uronic acid epimers. As summarized in this introduction, heparin sequence information is often determined through a bottom-up approach that relies on depolymerization reactions, size- and charge-based separations, and sensitive mass spectrometric (MS) and nuclear magnetic resonance (NMR) experiments to determine the structural identity of component oligosaccharides.

This dissertation builds on the work of previous group members Valentino Almeida, Albert Korir, and Stacie Eldridge to improve and further understand the mechanisms involved in reverse-phase ion-pair (RPIP) ultra-performance liquid chromatography (UPLC) and capillary isotachophoresis (cITP) coupled to microcoil NMR which they have demonstrated to be useful techniques for the separation and characterization of heparin-derived oligosaccharides. These goals are accomplished through the following objectives:

Objective 1: Explore the mechanism of RPIP chromatography and address the interactions between the ion-pairing reagent (IPR) tributylamine (TrBA) and heparin as well as the potential role of competition between TrBA and other IPRs in the resolution of isomeric disaccharides (Chapter 2).

Objective 2: Explore the effects of counterion type and concentration, along with mobile phase pH, IPR concentration and other buffer components on the anomeric resolution of heparin disaccharides containing positively charged glucosamine (GlcN) primary amine functional groups or uncharged *N*-acetyl glucosamine (GlcNAc) residues (Chapter 3).

Objective 3: Develop a cITP separation for the isomers of doxepin and further use this separation to gain insights into the mechanism of cITP, in particular interactions of the counterion with components of both the buffer and sample. (Chapter 4).

Objective 4: Design and apply an anionic cITP buffer system for the analysis of heparin-derived oligosaccharides that minimizes current-induced broadening of NMR resonances (Chapter 5).

Objective 5: Fabricate a microslot NMR probe for coupling to cITP that allows the separation capillary to be oriented parallel to the applied magnetic field to reduce the current-induced broadening of NMR resonances (Chapter 6).

The first part of this introductory chapter presents background information about heparin's structure and function. This is followed by a discussion of the common analytical techniques used to characterize heparin. The chapter concludes with a discussion of the role of NMR in heparin characterization and strategies for improving NMR sensitivity.

1.1. Heparin Structure

Heparin, a member of the GAG family, which includes chondroitin sulfate, keratan sulfate, dermatan sulfate (DS), and HS, is a highly sulfated, linear polysaccharide. Composed of variously sulfonated hexuronic acid (1→4) D-glucosamine-repeating disaccharide building blocks, heparin is the most acidic biopolymer in nature.[1] The uronic acid residue of heparin may be either α-L-iduronic acid (IdoA) or β-D-glucuronic acid (GlcA) and can be unsubstituted or sulfonated at the 2-*O* position. The glucosamine residue may be unmodified (GlcN), *N*-sulfonated (GlcNS), or *N*-acetylated (GlcNAc), with variable patterns of *O*-sulfonation at the 3-O and 6-O positions (Figure 1.1).

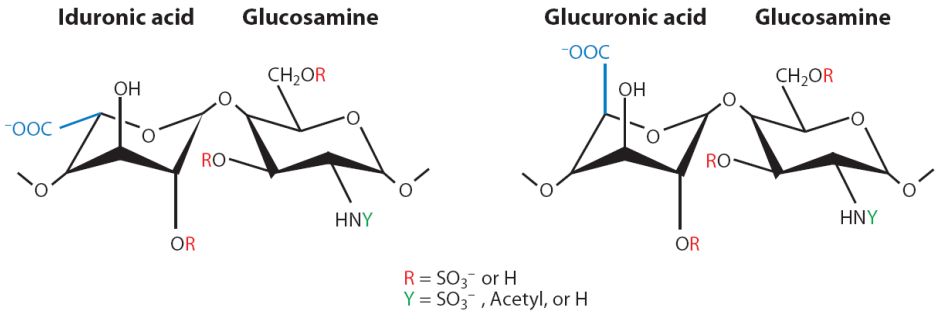

Figure 1.1. Structures of the generalized disaccharide subunits of heparin showing the substitution sites on the uronic acid and glucosamine residues and the orientation of the carboxylate moiety in the iduronic and glucuronic acid epimers.

The microheterogeneity of heparin results from variable patterns of sulfonation and the presence of hexuronic acid epimers.[1, 2] Heparin is biosynthesized in a multistep process that involves multiple enzymes in the endoplasmic reticulum and the Golgi apparatus of the mast cells of connective tissues. The specific modifications introduced by these enzymes are illustrated in Figure 1.2. Although this process appears to occur in a specific and orderly manner, its regulation is not currently well understood. The structurally related HS proteoglycans are expressed and secreted by mammalian cells and are strategically located on cell surfaces and in the extracellular matrix.[3, 4] Unlike HS, heparin lacks domain organization and possesses a higher percentage of IdoA residues and sulfonate groups (~2.5 per disaccharide). Because the biosynthesis of heparin is not template driven, it is a polydisperse mixture that contains chains of different molecular weights.

1.2 Biological Significance of Heparin

Heparin and HS influence numerous physiological[5] and pathophysiological processes,[6] including organo-,[7] morpho-,[8] angio-[9-11] and tumorigenesis;[10] growth control;[12] cell adhesion;[13] inflammation;[14] neural development and/ regeneration,[15, 16] and hemostasis[17]. Cell- surface HS proteoglycans also act as adhesion receptors for many viral and bacterial pathogens, concentrating them on cell surfaces and increasing the pathogen's ability to bind to secondary receptors responsible for internalization.[18-20]

Heparin is one of the oldest drugs in widespread clinical use. It is also one of the few currently used pharmaceutical agents derived from animal sources (namely porcine

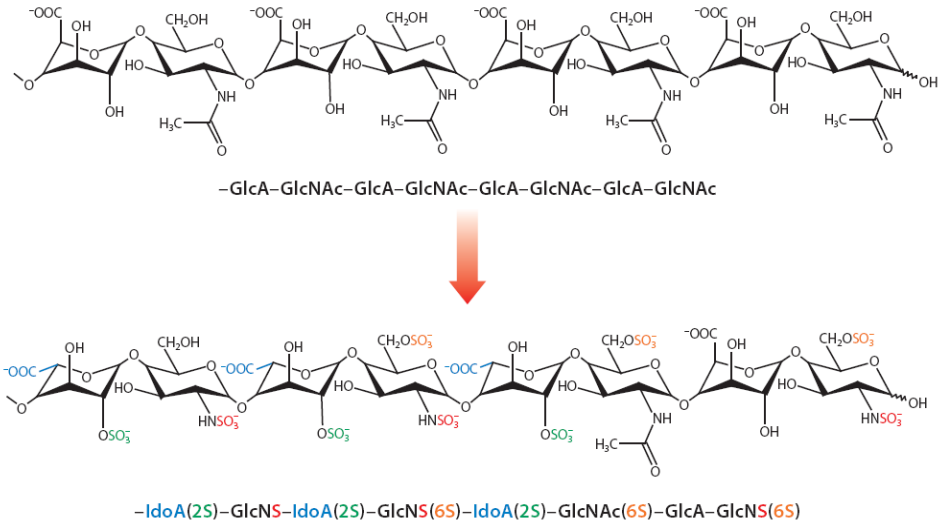

Figure 1.2. Schematic illustration of the origin of heparin's microheterogeneous structure. The final structure of heparin is the result of incomplete sequential modifications of the [GlcA-(1,4)-GlcNAc]n polymer by *N*-deacetylase/*N*-sulfotransferase-, C5 epimerase-, and 2-*O*- and 6-*O*-sulfotransferase-catalyzed reactions.

intestine). Heparin mediates its biological functions through electrostatic interactions with basic amino acid residues of target proteins.[1] The anticoagulant activity of heparin arises primarily through its interactions with the serine protease inhibitor antithrombin-III (AT-III). Binding of a specific heparin pentasaccharide sequence initiates a conformational change in AT-III that increases the flexibility of its reactive site loop and, as a result, its binding affinity for thrombin and other coagulation-cascade proteases.

Heparin is widely used in hemodialysis and in the initial treatment of venous thrombosis, pulmonary embolism, and acute coronary syndrome. A major drawback of heparin administration resides in the low predictability of coagulation parameters and the concomitant risk of potential bleeding. However, the most serious side effect is heparin-induced thrombocytopenia (low platelet count). To address these risks and limitations, low-molecular-weight heparins (LMWHs) were introduced into clinical use. [21] LMWHs are manufactured from unfractionated heparin by controlled depolymerization. The clinical success of LMWHs results largely from their enhanced subcutaneous bioavailability and improved pharmacokinetics compared to unfractionated heparin.

1.3 Challenges of Studying Heparin

A more detailed knowledge of heparin and HS structure is required to develop a better understanding of the mechanisms by which they mediate such a large number of diverse biological processes. Analytical methods that provide molecular-level structural characterization are also critical for securing the quality and safety of heparin drugs. The adulteration of pharmaceutical heparin in late 2007 and early 2008 drew attention to the

need for improvements to the analytical methods used for the rapid identification of GAGs and their potential impurities.[22] The difficulty in heparin and HS analysis resides in their high negative-charge density, polydispersity, and microheterogeneity. The molecular-level characterization of heparin and HS requires techniques that can distinguish minor differences in structure, for example, positional isomers and epimers.

1.4 Depolymerization

Due to the high degree of structural diversity of heparin and HS, most methods used to characterize them utilize a bottom-up approach, whereby the intact polysaccharide chains are chemically or enzymatically depolymerized to smaller oligosaccharides prior to analysis.[23] In an exhaustive digestion, heparin and HS are reduced to their disaccharide building blocks, permitting their compositional analysis. Studies using larger oligosaccharides, which are more biologically relevant, are conducted on samples obtained by partial depolymerization. In these studies, the digested oligosaccharides are first separated into size-uniform fractions, which are further resolved to individual oligosaccharides by subsequent charge-based separation. The purified oligosaccharides can then be characterized through the use of MS and NMR.

1.4.1. Enzymatic Digestion. Exhaustive digestions of heparin and HS are typically carried out by use of a cocktail containing the enzymes heparinase I, II, and III to selectively cleave the biopolymer at glucosamine (1→4) uronic acid glycosidic bonds. The enzymatic reaction inserts a double bond at the nonreducing end of each cleaved chain to create an ultraviolet (UV) chromophore that absorbs at a wavelength of 232 nm

(e.g., Figure 1.3), thereby facilitating detection.[24] Such heparin lyase enzymes, produced by *Flavobacterium heparinium*, are highly specific to heparin and HS and are classified according to their substrate specificity.[25] The various heparinase specificities and the structure of the resulting cleavage products are illustrated in Figure 1.4. Heparinase I cleaves the polymer chain between GlcNS and 2-*O*-sulfonated IdoA residues, the most common substitution motif in most forms of intact heparin. Heparinase II is less specific; it cleaves between glucosamine residues that can be *N*-sulfonated or *N*-acetylated and 2-*O*-sulfonated IdoA, unsubstituted IdoA, or GlcA residues.[25] Heparinase III cleaves specifically at sites between *N*-acetylated or *N*-sulfonated glucosamine and 2-*O*-unsubstituted IdoA or GlcA. Because the disaccharide GlcNAc(1→4)GlcA is commonly found in HS, heparinase III is often used for HS digestions.

1.4.2. Chemical Depolymerization. Chemical depolymerization of heparin and HS oligosaccharides can occur by several means: β-elimination, reductive deamination, and oxidation. The specificities and reaction products are shown in Figure 1.5. β-Elimination (Figure 1.5a) mimics enzymatic cleavage through a chemical reaction that introduces a double bond at the nonreducing end of each cleaved oligosaccharide. The depolymerization is carried out through a two-step reaction in which the carboxylate group on the C5 carbon of the nonreducing end hexuronic acid is first reacted with a benzyl halide to form an ester. Then, a strong base extracts the proton at the C5 position of the nonreducing end uronic acid, resulting in the formation of the double bond between C4 and C5. The benzyl ester is eliminated through hydrolysis in basic solution.[26] Reductive deamination (Figure 1.5b) is typically performed with nitrous acid; the

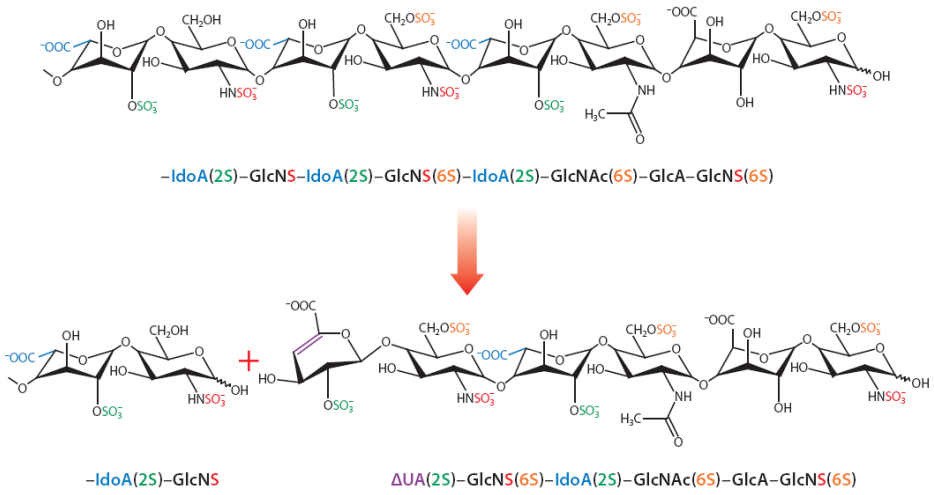

Figure 1.3. Heparinase I depolymerization of heparin results in smaller oligosaccharides that contain an unsaturated uronate residue at the nonreducing end of the cleaved chain.

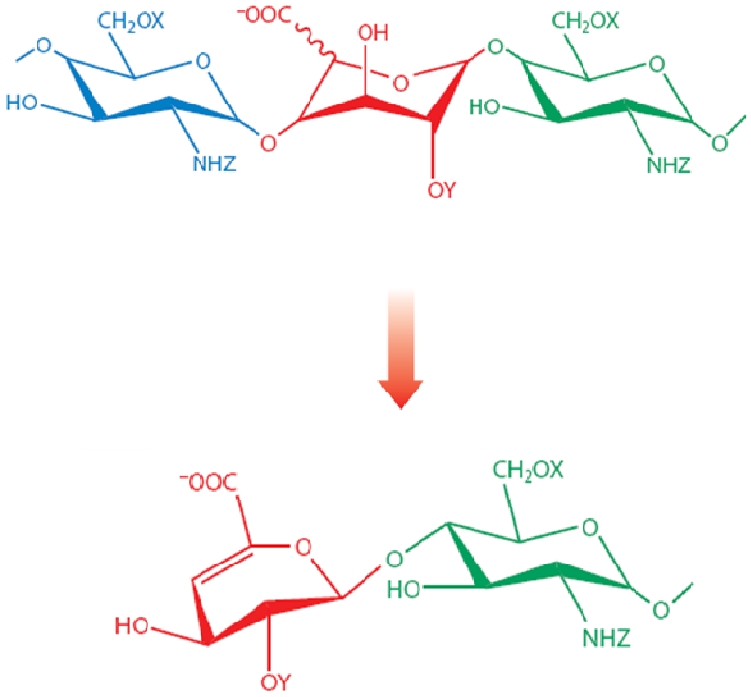

Enzymatic		
Heparinase I[a]	**Heparinase II[b]**	**Heparinase III[b]**
X = SO_3^- or H	X = SO_3^- or H	X = SO_3^- or H
Y = SO_3^-	Y = SO_3^- or H	Y = H
Z = SO_3^-	Z = SO_3^- or Ac	Z = H or Ac
[a]Hexuronic acid must be IdoA acid.		
[b]Hexuronic acid can be GlcA or IdoA.		

Figure 1.4. The depolymerization specificities and products of the enzymatic depolymerization of heparin and HS based on the substitutions at positions X, Y, and Z.

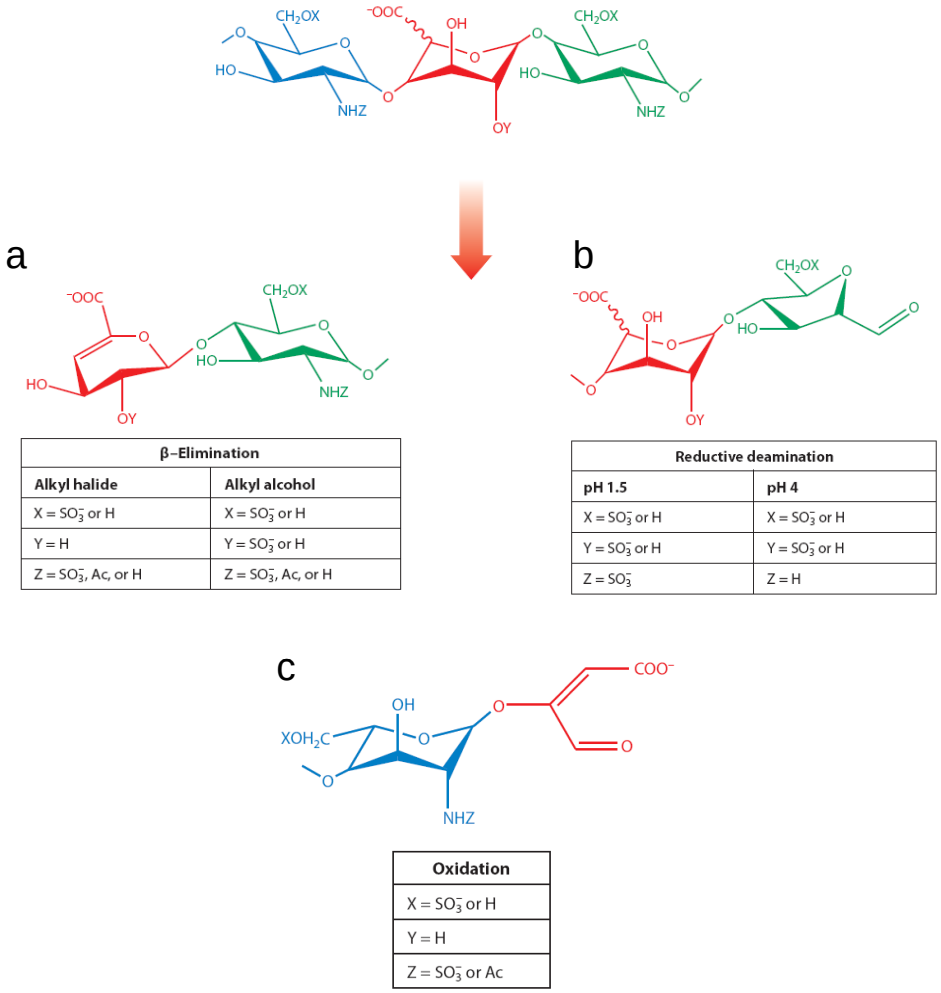

Figure 1.5. The depolymerization specificities and products of the (a) β-elimination, (b) reductive deamination, and (c) oxidation reactions of heparin and HS based on the substitutions at positions X, Y, and Z.

specificity of cleavage is determined by the solution pH. If the pH is at or below 1.5, cleavage occurs at GlcNS residues, whereas if the pH is 4.0, cleavage occurs at *N*-unsubstituted GlcN. To cleave GlcNAc glycosidic bonds via reductive deamination, samples need to be first deacetylated and then treated with nitrous acid at pH 4.0. Reductive deamination alters the structure of the glucosamine, thereby producing a 2,5-anhydro-D-mannose residue at the reducing end of the cleaved oligosaccharide (Figure 1.5b).[27] Oxidative depolymerization (Figure 1.5c) is performed with a combination of hydrogen peroxide and divalent copper or iron ions.[28] This reaction requires vicinal diols at the C2 and C3 positions of the hexuronic acid residue and results in cleavage and subsequent formation of an oxidized fragment of the hexuronic acid.[29]

1.5 Separation of Heparin-derived Oligosaccharides.

Because heparin-depolymerization reactions produce a complex mixture of variously substituted di- (or larger) oligosaccharides, it is usually necessary to incorporate one or more separation steps into the analysis. If the goal of an experiment is characterization of the disaccharide composition of a heparin sample, an exhaustive digestion must be used to reduce the biopolymer to its component disaccharides. Although the products of exhaustive digestions can be directly analyzed using MS, [30-33] most studies perform heparin compositional analysis with a separation method such as capillary electrophoresis (CE) or high-performance liquid chromatography (HPLC) to resolve the individual disaccharides. For samples that are depolymerized through

enzymatic or β-elimination reactions, compositional analysis has been simplified by the commercial availability of authentic disaccharide standards.

Frequently, the experimental goal is isolation and characterization of larger heparin oligosaccharides, often as part of a study to explore their protein-binding properties or biological activity. In such cases, the digestion is quenched before all the heparin is reduced to its component disaccharides. The analysis of the resulting mixture is complicated by the presence of variously sized oligosaccharides consisting of a diverse set of positional and configurational isomers. For such samples, a single separation cannot adequately resolve the individual components, and two or more orthogonal separation approaches may be employed.

1.5.1. Size-Exclusion Chromatography. Size-exclusion chromatography (SEC) is generally the first step in the analysis of a partially depolymerized heparin sample. This step resolves the mixture of heparin-derived oligosaccharides into size-uniform fractions.[34, 35] Figure 1.6 shows the results of the preparative-scale SEC separation of a porcine intestinal mucosa heparin sample that was partially digested with heparinase I. This SEC separation, conducted with a Bio-Gel P10 fine gel packed into a 3 cm × 200 cm column, resolved the component oligosaccharides up to the hexadecasaccharide peak. Because of the specificity of the enzymatic reaction, primarily even-numbered oligomers are produced, although small quantities of trisaccharides have also been reported. [35]

Preparative SEC can be carried out on the 100 mg to 1 g scale, which allows the resolution of size-uniform fractions for studies of heparin-protein interactions or for subsequent separation to yield purified single-component oligosaccharides. A common

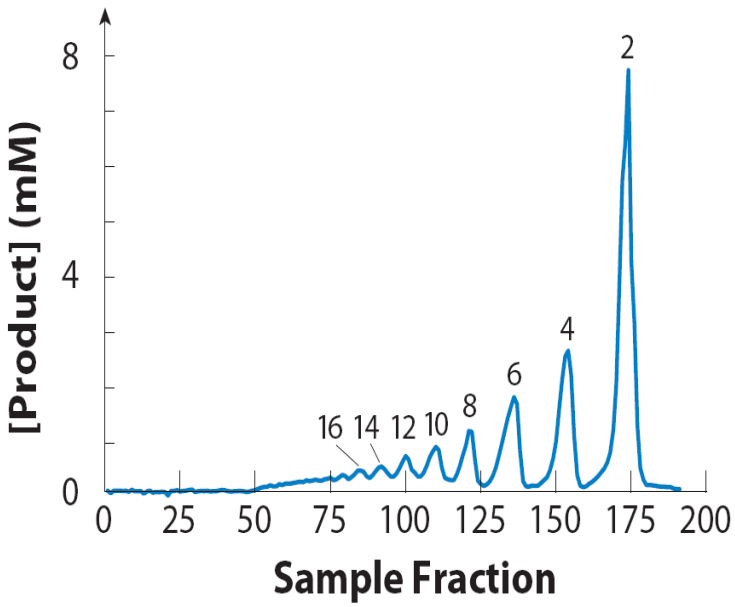

Figure 1.6. Heparin analysis normally begins with a SEC separation to fractionate digested heparin into size-uniform fractions. Shown is an example of an SEC chromatogram of the heparin oligosaccharides from a heparinase I digest of heparin with resolution up to 16-mers.

approach involves collection of the preparative SEC eluates in volumes of a few mLs to define each peak in the chromatogram. Upon completion of the separation, the collected fractions that correspond to a given oligomer size are pooled for subsequent separation according to charge. However, SEC peaks are not necessarily homogeneous, and the practice of pooling can make it more difficult to resolve trace components in the secondary separation.[35, 36] Preparative-scale SEC separations generally take on the order of days to complete and, therefore, are not useful for the rapid characterization of heparin. In contrast, analytical SEC separations require only a few hours to achieve the same size fractionation using microgram quantities of material, making this method amenable to analysis of heparin and HS samples that are available only in limited amounts. These characteristics make analytical SEC a useful tool for rapid heparin analysis, especially when coupled directly to a secondary separation or a highly selective detection method such as MS.[35, 37-39]

1.5.2. Capillary Electrophoresis and Polyacrylamide Gel Electrophoresis. CE is a useful and increasingly employed method for the separation of many types of carbohydrates.[40, 41] It is especially amenable to the separation of heparin and HS oligosaccharides due to their high negative charges. CE separations of heparin oligosaccharides are most effective in reversed-polarity mode.[36] Reversed-polarity separations use acidic buffers in the pH range of 3.5 to 4.0 to reduce electroosmotic flow. This pH range also provides the optimum resolution of heparin positional and configurational isomers, given that subtle structural variations can produce small

differences in the pK_a values of the hexuronic acid carboxylate moieties, thereby aiding in their resolution.[36]

CE has been used for disaccharide resolution and quantitation in the compositional analysis of heparin and HS;[42, 43] however, the poor reproducibility of CE can make its routine use challenging.[43] CE methods have also been extended to the analysis of larger oligosaccharides;[36] such methods include a technique developed specifically for the determination of therapeutically important LMWH samples.[44] Figure 1.7 shows an example of a CE electropherogram measured for a SEC hexasaccharide fraction. Although this electropherogram contains many peaks, some component hexasaccharides remain unresolved. CE can fairly easily resolve all of the heparin-derived disaccharide standards, including positional isomers; however, sample complexity increases rapidly with increasing chain length. For example, if all possible sulfonate positional isomers and uronic acid epimers were present, a sample composed of only hexasaccharides with eight sulfonate groups could theoretically contain 48 unique hexasaccharides having the same net charge, an analytical challenge even for a high-resolution separation method such as CE.

Polyacrylamide gel electrophoresis (PAGE), which predates CE methods, has also been used to separate heparin oligosaccharides. PAGE is a useful means of characterizing the size distribution of heparin digest samples[45-47] as well as for analysis of LMWHs.[48] Continuous elution PAGE (CE-PAGE) has been shown to be a useful technique for the preparative separation of up to milligram quantities of GAG oligosaccharides (including heparin) in under 6 hrs with higher resolution than obtained in the more commonly used

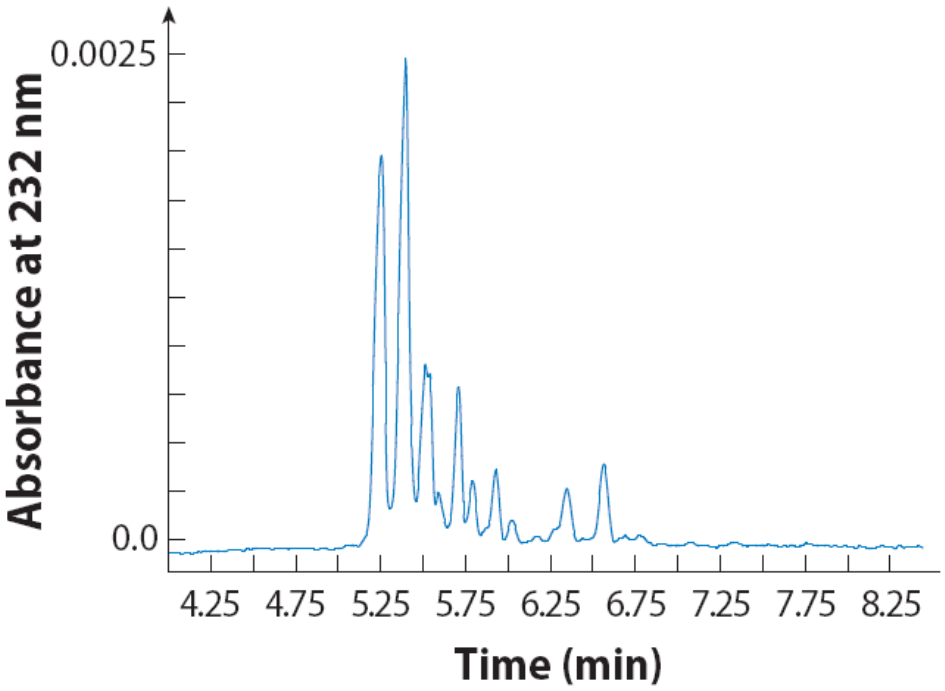

Figure 1.7. Shown is an example of a CE electropherogram for the hexasaccharide fraction of the SEC chromatogram shown in Figure 1.6.

preparative SEC separations.[45, 49, 50] However, PAGE is not used for heparin-compositional analysis because the resolution of individual disaccharides is relatively poor. In addition, this method is not easily amenable to detection by MS, which is necessary for molecular-level characterization of larger oligosaccharides.

1.5.3. Anion Exchange Chromatography. HPLC can offer a robust approach for the separation and analysis of heparin and HS oligosaccharides. Strong anion exchange (SAX)-HPLC is often used for the separation of GAG oligosaccharides, especially those derived from heparin and HS.[34, 46, 51, 52] As with other separation techniques, analytical SAX columns provide the highest resolution, whereas preparative-scale columns have greater sample capacity. Preparative or semipreparative SAX separations allow the injection of larger quantities and the isolation of purified component oligosaccharides for subsequent characterization experiments. Because of the complexity of heparin digest samples, a common protocol involves the injection of size-uniform SEC fractions onto the SAX column. The semipreparative SAX-HPLC separation of a heparin-derived SEC hexasaccharide fraction (Figure 1.8) is better able to resolve the individual hexasaccharide components than either CE or reversed-phase ion-pair (RPIP)-HPLC (discussed in Section 1.5.5). This improved resolution comes with a cost; the SAX separation requires much longer analysis times than either CE or RPIP-HPLC. Another disadvantage of SAX-HPLC is the high ionic strength mobile phase (e.g., 2 M NaCl) required for the elution of highly charged heparin oligosaccharides. As a result, SAX is not easily amenable to detection by MS, and components isolated using this approach must be desalted prior to characterization by MS or NMR.

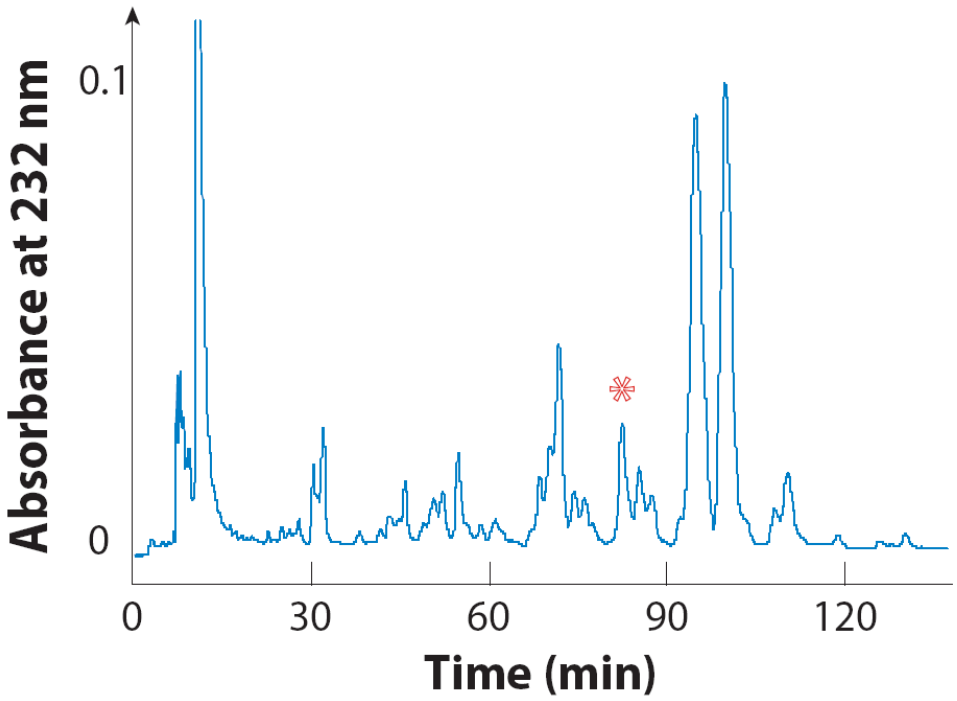

Figure 1.8. Shown is an example of SAX chromatogram for the hexasaccharide fraction of the SEC chromatogram shown in Figure 1.6. The peak marked with the asterisk represents the hexasaccharide ΔUA(2S)-GlcNS(6S)-IdoA(2S) GlcNAc(6S)-GlcA-GlcNS(6S) for which the MS and NMR spectra are shown in Figures 1.10 -1.14.

An alternative to SAX separations is weak anion exchange (WAX)-HPLC. The WAX column is packed with an amino-bonded stationary phase that interacts more weakly with anionic analytes than do the quaternary amine functionalized polymers used for SAX separations. As a result, WAX separations require less salt to elute highly charged analytes, making this method more compatible with hyphenated techniques such as HPLC-NMR. Limtiaco et al.[53] showed that WAX could be used to separate DS, heparin, and the semisynthetic oversulfated chondroitin sulfate (OSCS) through a displacement-based mechanism.

1.5.4. Hydrophilic Interaction Chromatography and Graphitized Carbon Separations. Hydrophilic interaction chromatography (HILIC) can also be used to separate heparin and HS oligosaccharides, as well as other GAGs,[54, 55] although the separations reported thus far have not been effective in resolving isomeric oligosaccharides. The inability of HILIC separations to resolve disaccharide positional isomers limits this method's utility in compositional analysis.

The use of graphitized carbon columns for the HPLC separation of heparin disaccharides has also been reported.[56] Although this method can resolve positional isomers, it offers poor resolution between the *N*-acetylated and *N*-sulfonated disaccharides. Although these disaccharides can be distinguished by MS, overlap between the chromatographic peaks containing the *N*-acetylated and *N*-sulfonated disaccharides makes it impossible to visualize the separation by UV absorbance alone.

1.5.5. Reversed-Phase Ion-Pair High-Performance Liquid Chromatography. RPIP-HPLC is an increasingly important method for the separation of heparin and HS oligosaccharides. The popularity of this approach stems from the widespread availability of reversed-phase HPLC columns and instruments as well as the ease of implementation of RPIP-HPLC with a variety of detection methods (e.g., UV, fluorescence, and MS). RPIP-HPLC is typically performed on octadecyl (C18) columns while a lipophilic alkyl ammonium salt is used as an IPR. The IPR aids in the retention and resolution of the charged analyte through electrostatic interactions. The transient analyte-IPR ion pair is relatively neutral and hydrophobic, which facilitates interactions with the hydrophobic stationary phase of the reversed-phase HPLC column.[57-59] An important application of RPIP-HPLC is the full disaccharide compositional analysis of heparin and HS.[60-62] With the incorporation of post-column fluorescent labeling,[63] RPIP-HPLC can be used for the compositional analysis of samples that are isolated from biological tissues and available only in very limited quantities.[64, 65]

Although the earliest separations used quaternary ammonium salts such as tetrabutylammonium, incorporation of more volatile reagents such as tributylamine has made RPIP-HPLC more amenable to detection by MS. Compared with UV absorbance, MS greatly improves the detection sensitivity of RPIP-HPLC separations and provides important structural information about the analytes.[62, 66-69] SAX is better able to resolve complex mixtures of larger heparin-derived oligosaccharides, but because it requires a desalting step prior to mass spectrometric analysis, RPIP-HPLC is often preferred for rapid separation and analysis.

Smaller column-packing materials (e.g., 2 μm or less) can improve the speed and sensitivity of heparin disaccharide analysis using RPIP-HPLC.[63] Ultrahigh-performance liquid chromatography (UPLC) separations allow the complete resolution of all possible heparin disaccharides, including positional isomers. Commercially available UPLC instruments utilize as small as 1.7-μm-particle columns and proprietary mobile-phase pumps that can withstand the high pressures (up to 15,000 psi) needed to push mobile phase through the column. Korir et al.[70] reported a RPIP-UPLC separation that resolves 11 commercially available heparin disaccharides in under 5 min with minimal sample preparation. Further work, discussed in detail in Chapters 2 and 3 of this dissertation, has improved upon this separation while also using the heparin disaccharides to probe the RPIP separation mechanism.[71, 72]

The speed of analysis and high resolution provided by RPIP-UPLC separations make this method an excellent choice for the full compositional analysis of heparin and HS.[70-72] The RPIP-UPLC separation of the hexasaccharide SEC fraction lacks the resolution achieved through SAX-HPLC (Figure 1.9); however, RPIP-UPLC has a distinct advantage in terms of the ease with which it can be coupled to MS detection. This advantage is especially significant given the lack of commercially available standards for heparin-derived hexasaccharides and other larger oligosaccharides.\

1.6 Mass Spectrometry

MS is a useful and sensitive technique that can provide oligosaccharide molecular weight, the degree of sulfonation and acetylation, monosaccharide composition, and

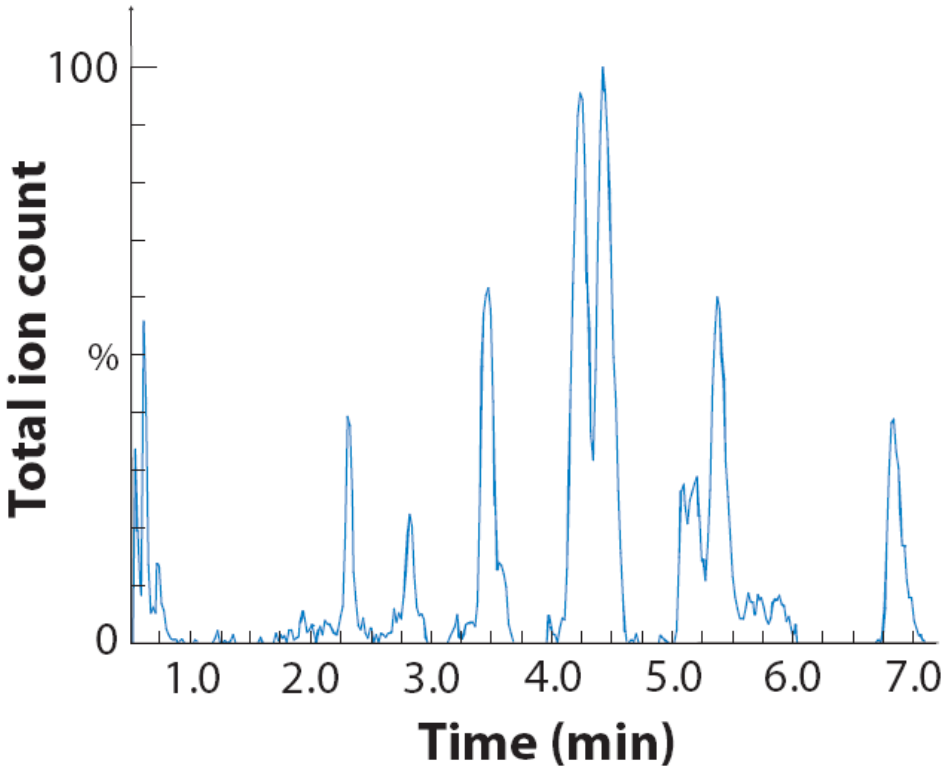

Figure 1.9. Shown is an example RPIP-UPLC chromatogram for the hexasaccharide fraction of the SEC chromatogram shown in Figure 1.6.

under controlled experimental conditions, sequence. A more detailed discussion of the use of MS for the structural and compositional analysis of GAGs can be found in Reference [73]. Most MS studies of heparin and HS utilize electrospray ionization (ESI) or matrix-assisted laser desorption/ionization (MALDI), although, as discussed in Section 1.6.2, the recently introduced method of electron detachment dissociation (EDD) shows great promise.

1.6.1. Negative-Ion Electrospray Ionization Mass Spectrometry. Because of the highly anionic nature of heparin and HS, negative-mode ESI-MS is an attractive choice for their analysis.[74] Given the complexity of depolymerized heparin samples, another benefit of ESI-MS is the ease of hyphenation with separation techniques such as CE and HPLC. Often, however, negative-ion ESI-MS spectra of heparin oligosaccharides are complicated by the presence of sodium and potassium adducts. Careful desalting, very clean sample preparation and instrumental components, and the use of ammonium buffers can reduce adduction.[33] An advantage of coupling RPIP separations with MS detection is that salt adducts can be further reduced because sodium and potassium ions are largely eluted in the void volume of the column, whereas heparin oligosaccharides are retained through their interaction with the IPR.[70]

Another challenge in the characterization of heparin and HS oligosaccharides by use of MS is the prevalence of sulfate loss during ionization. Sulfate loss from disaccharides may be catalyzed by trace amounts of acid; thus, one must be careful to remove acid from the analyte solution and source before performing MS analysis.[75] It is also important to choose ionization and ion-extraction conditions carefully, as sulfate loss

can occur within the source region of the ESI interface. Figure 1.10 shows the negative-ion ESI-time-of-flight mass spectrum acquired for a heparin-derived hexasaccharide that was isolated by SAX-HPLC and desalted prior to the RPIP-UPLC separation. As this mass spectrum shows, in addition to the doubly charged molecular ion peak, $[M-2H]^{2-}$, several related peaks including those for sulfate loss and adduction of the IPR tributylamine are also detected.

1.6.2. Matrix-Assisted Laser Desorption/Ionization Mass Spectrometry. MALDI is a soft ionization method that enables relatively high throughput MS analysis on small quantities of sample. As in ESI-MS, a common problem encountered in the use of MALDI-MS for analysis of heparin oligosaccharides is fragmentation, especially sulfate loss, during the ionization process. Early work showed that complexation of oligosaccharides by synthetic $(Arg\text{-}Gly)_n$ peptides or by the small basic protein angiogenin allowed the oligosaccharide to remain intact through the ionization process.[76] The full oligosaccharide-peptide complex was detected by positive-ion MS, and the molecular weight of the oligosaccharide was calculated by subtraction. Later studies used a similar complexation approach through the addition of quaternary ammonium or phosphonium salts as a comatrix for MALDI-MS.[77] The use of cesium salts to suppress sulfate loss when using MALDI-MS in an ionic liquid matrix has also been explored.[78] Tissot et al.[79] tested the ionic liquid 1-methylimidazolium α-cyano-4-hydroxycinnamate as a MALDI matrix and successfully ionized heparin di-, tetra-, hexa-, octa-, and decasaccharides. Dihydroxybenzoic acid and norharmane are also effective MALDI matrices for the

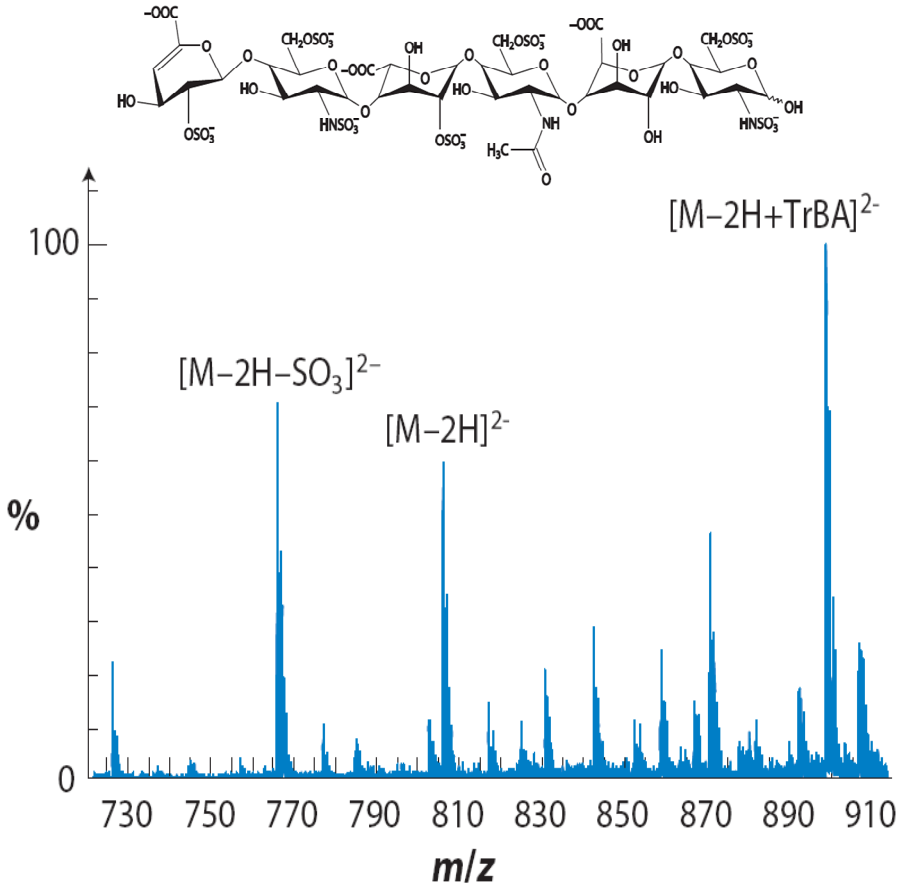

Figure 1.10. Shown is an example UPLC-MS spectrum for the hexasaccharide ΔUA(2S)-GlcNS(6S)-IdoA(2S) GlcNAc(6S)-GlcA-GlcNS(6S) isolated from the SAX-HPLC separation shown in Figure 1.8.

structural characterization of heparin and HS by MS.[80] Clearly, MALDI-MS has great potential for the characterization of heparin and HS oligosaccharides.

1.6.3. Tandem Mass Spectrometry. The use of tandem MS (MS/MS) to determine both the structure and the sequence of oligosaccharides is an ongoing area of interest in GAG research. One limitation of this approach is the propensity of heparin oligosaccharides to fragment via sulfate loss instead of through more informative ring cleavages. Zaia & Costello[74] demonstrated that the degree of fragmentation of any oligosaccharide is highly dependent upon the charge state of the ion selected for collision-induced dissociation (CID). These authors showed that through careful selection of charge states and addition of calcium ions to stabilize the sulfonate groups, the degree and abundance of ring cleavage ions can be enhanced. Meissen et al.[81] recently reported that MS/MS with CID can be used to distinguish 3-*O*-sulfonation sites from 6-*O*-sulfonation sites in heparin oligosaccharides by inducing specific cross-ring cleavages.

Ultimately, the ability to use tandem MS to sequence GAG oligosaccharides requires the generation of unique and informative fragments for each monosaccharide. In addition to cleavage of glycosidic linkages, this process also requires numerous cross-ring cleavages to distinguish variable points of sulfonation and acetylation. MALDI-LIFT-TOF/TOF and ESI-CID-MS/MS were compared for the structural analysis of oligosaccharides of *N*-acetylheparosan (a biosynthetic heparin precursor).[82] This study showed that MALDI-LIFT-TOF/TOF yielded much better cleavage specificity than did CID.

More recently, the advancement of the MS/MS technique EDD has proven useful for creating unique cross-ring cleavages in heparin and HS. By using EDD with Fourier transform ion cyclotron resonance, Wolff et al.[83] showed that diagnostic fragment ions can be created that distinguish IdoA from GlcA in heparin tetrasaccharides. In a recent report by Ly et al., MS and CID-MS/MS experiments with both FT-ICR and FTMS instruments were used to structurally characterize and sequence the simplest proteoglycan, bikunin.[49] In this work the authors showed that all of the isolated pGs studied contained a linkage region consisting of a single hexasaccharide sequence *O*-glycosidically linked to serine. Surprisingly, even beyond this linkage region the MS results revealed that the pG chains contained a predictable pattern of 4-O-sulfogalactosamine residues showing a defined sequence for bikunin. This work along with further advances in EDD, FT-ICR, and FTMS will probably lead to exciting new applications of MS/MS for the characterization of more highly complex oligosaccharides like heparin and HS.

1.7 Nuclear Magnetic Resonance Spectroscopy

NMR spectroscopy is highly sensitive to minor variations in molecular structure, making it an important technique for heparin characterization. A simple ^{1}H NMR survey spectrum can both reveal the number of monosaccharide residues present and provide a tentative compositional analysis based on comparison between ^{1}H chemical shifts and reference data.[2, 84, 85] Visual examination of the ^{1}H NMR spectrum in Figure 1.11 indicates that the hexasaccharide peak isolated by SAX-HPLC contains a single component that includes a GlcNAc residue, indicated by the singlet resonance at 2.049

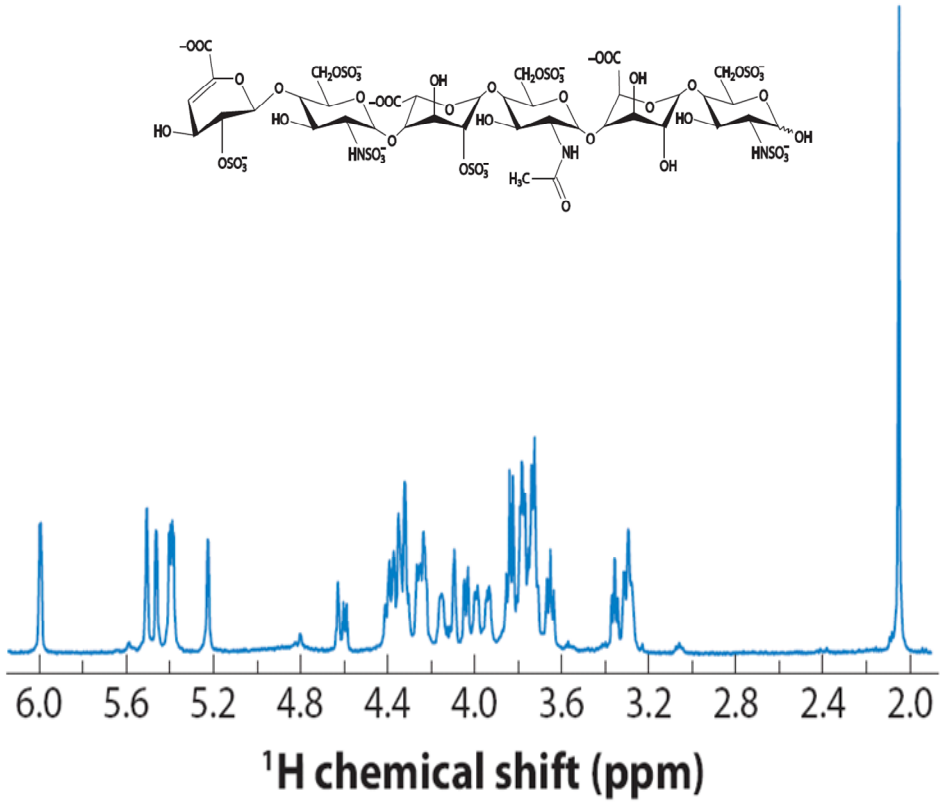

Figure 1.11. Shown is an example NMR spectrum for the hexasaccharide ΔUA(2S)-GlcNS(6S)-IdoA(2S) GlcNAc(6S)-GlcA-GlcNS(6S) isolated from the SAX-HPLC separation shown in Figure 1.8. The NMR resonance at 2.049 ppm indicates the presence of an *N*-acetyl-D-glucosamine residue.

ppm. Although this ^{1}H NMR survey spectrum provides important information about sample purity and composition, complete structural characterization of the hexasaccharide requires the use of two-dimensional NMR spectra. [46] With the powerful arsenal of two-dimensional experimental techniques available, NMR spectroscopy can be used to determine the sequence of the component monosaccharide residues and unambiguously determine sites of *N*-acetylation as well as of *N*- and *O*-sulfonation along the oligosaccharide chain. Most importantly, NMR spectroscopy can also specify the orientation of the anomeric linkage connecting the various disaccharide subunits and easily distinguishes IdoA and GlcA residues.

Because of its high level of microheterogeneity and polydisperse nature, the complete structural characterization of unfractionated heparin continues to be a major challenge. Therefore, NMR measurements are usually reserved for characterization of purified single oligosaccharides obtained by chemical or enzymatic depolymerization, followed by size- and charge-based separations. Interpretation of NMR spectral data is usually facilitated by molecular-weight and fragmentation information provided by MS. Several factors must be considered, however, to ensure that satisfactory NMR spectra are acquired for heparin structural studies. Naturally, sample purity is an important consideration. The isolated oligosaccharide components should have a purity greater than 80% to 90% to avoid complications in structural determinations. Additional NMR-silent impurities must also be minimized. Although NMR is more salt tolerant than MS, high levels of salt in oligosaccharide samples isolated from SAX separations can make it impossible to properly tune and match the NMR probe, and a desalting step is usually

required prior to analysis. As demonstrated by McIwen,[86] heparin resonance line widths are severely affected by binding of trace paramagnetic impurities. Paramagnetic transition-metal ions, which may be present as production impurities or introduced during oligosaccharide isolation, can cause line broadening through paramagnetic relaxation enhancement. The addition of a small amount of deuterated EDTA (ethylenediaminetetraacetic acid) significantly improves the spectral quality for both unfractionated heparin[86] and LMWH,[85] and it can also be helpful in the analysis of isolated oligosaccharides. Finally, if the oligosaccharide is isolated from a RPIP-HPLC separation, the sample will be contaminated by the IPR. Use of a volatile IPR such as ethylamine or removal of less volatile reagents by cation exchange can facilitate sample cleanup for NMR analysis.[87]

Another way to reduce the complexity of heparin NMR spectra without a prior separation step, especially when comparing different heparin samples, is through the use of statistical analysis methods such as principal component analysis (PCA). PCA reduces the dimensionality of the data, in this case the NMR chemical shifts and integrals of the many resonances of a heparin mixture, by simplifying the data into two principal components that represent those characteristics of the spectra that contribute most to the variance. Simplifying the data in this way allows the objective comparison of many complex spectra even when the differences between them are difficult to identify by visual inspection. The identification of contaminants in heparin samples[88-90] and the discrimination of heparin samples of different biological origins[91, 92] have been demonstrated using PCA and similar statistical analysis methods. A detailed description

of PCA and related statistical approaches is beyond the scope of this dissertation since they were not applied in this research however interested readers are referred to the book by Jolliffe for further information on this topic.[93]

1.7.1 Two-Dimensional Nuclear Magnetic Resonance Analysis of Heparin Oligosaccharides. Structural characterization of heparin-derived oligosaccharides is typically initiated by identification of the individual monosaccharide subunits in the oligosaccharide chain, using scalar couplings to provide through-bond connectivities. These connectivities can be obtained through a number of two-dimensional NMR experiments including homonuclear correlation spectroscopy (COSY) and homonuclear total correlation spectroscopy (TOCSY) experiments, as well as heteronuclear single and multiple quantum coherence spectroscopy experiments.[46, 94-96] Through the COSY spectrum (Figure 1.12), connections between coupled protons on adjacent carbon atoms within a monosaccharide ring can be identified. The well-resolved anomeric resonances and the H4 resonance of the $\Delta^{4,5}$UA residue of oligosaccharides produced by enzymatic cleavage or by β-elimination provide an entry point for analysis of the COSY spectrum. However, the limited ^{1}H NMR chemical shift dispersion of carbohydrates can make interpretation of the COSY data challenging, even for medium-sized oligosaccharides.

Because the TOCSY experiment transfers ^{1}H scalar coupling information throughout a spin system, the TOCSY spectrum allows detection of the connectivity of all the protons within each monosaccharide residue through the well-resolved anomeric resonances. The TOCSY spectrum in Figure 1.13 was used to assign resonances of the heparin-derived hexasaccharide. Through comparison of the ^{1}H chemical shift data

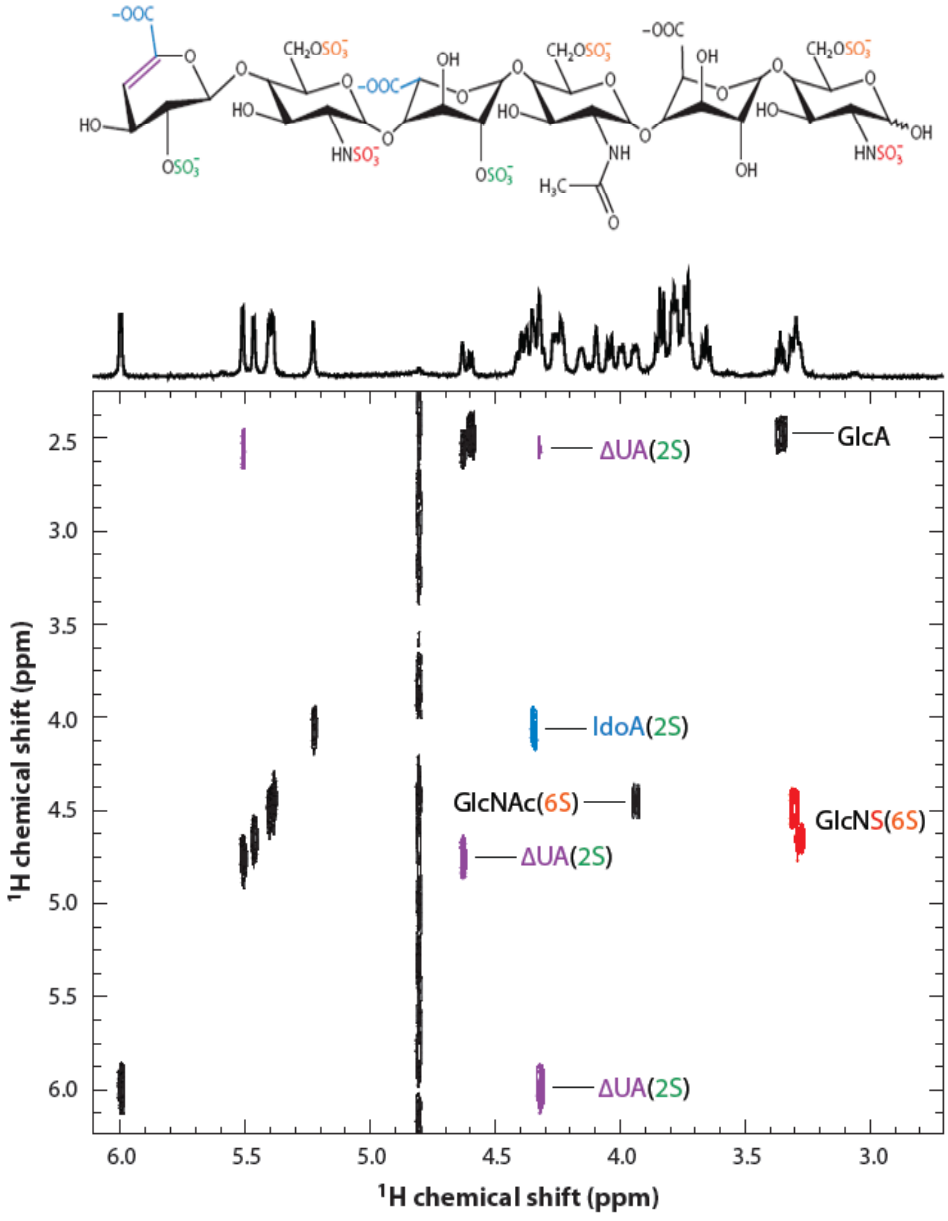

Figure 1.12. Partial correlation spectroscopy (COSY) spectrum showing cross peaks to spin-spin-coupled protons on adjacent carbons of the heparin-derived hexasaccharide ΔUA(2S)-GlcNS(6S)-IdoA(2S)-GlcNAc(6S)-GlcA-GlcNS(6S) isolated by SAX-HPLC.

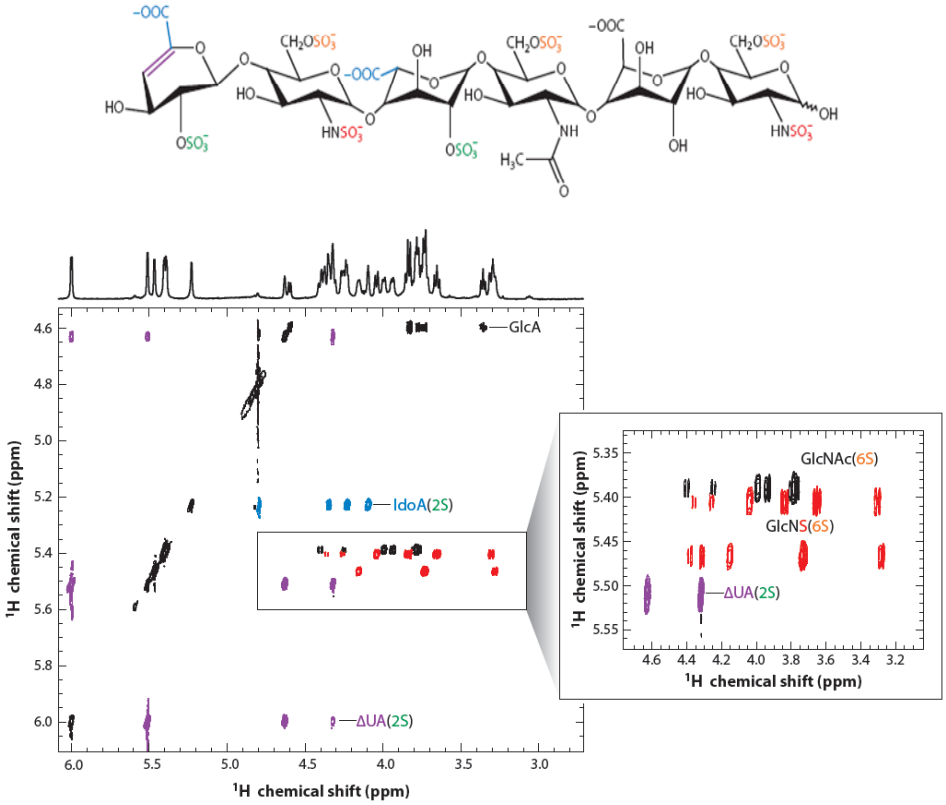

Figure 1.13. Partial total correlation spectroscopy (TOCSY) spectrum showing cross peaks of the individual monosaccharide resonances to the corresponding well-resolved anomeric resonances of the heparin-derived hexasaccharide ΔUA(2S)-GlcNS(6S)-IdoA(2S)-GlcNAc(6S)-GlcA-GlcNS(6S) isolated by SAX-HPLC. The region defined by the box is shown in the expansion.

obtained from the TOCSY spectrum with reference data, the structural identities of the monosaccharide residues can be deduced. For complicated spectra with extensive overlap in the anomeric region of the ^{1}H NMR spectrum, the band-selective homonuclear-decoupled (BASHD)-TOCSY experiment can provide improved resolution.[85]

The $^{1}H,^{13}C$ heteronuclear single quantum coherence spectroscopy (HSQC) experiment provides additional information about the type, number, and position of C-H bonds and offers improved spectral resolution by taking advantage of the greater dispersion of the ^{13}C chemical shift dimension.[97] The HEHAHA (Heteronuclear Hartmann Hahn) experiment, introduced by Bendiak et al.[98] and Jones & Bendiak,[99] is an additional tool used to characterize oligosaccharide primary structure and to identify the positions of modification, especially those introduced by *O*-acetylation.

Recent work by Langeslay et al. demonstrated experimental conditions that allowed the detection of the sulfamate ($NHSO_3^-$) ^{1}H NMR resonances of heparin and HS derived mono- and oligosaccharides in 90% H_2O.[100] These authors further showed that by using a $^{1}H,^{15}N$ HSQC experiment the sulfamate protons could be efficiently used to detect the glucosamine ^{15}N chemical shifts. Because it is only possible to have one sulfamate group per disaccharide unit of heparin and HS these spectra are much less complex than either ^{1}H and ^{13}C NMR spectra, simplifying analysis of complex mixtures. Furthermore, because of the critical role they play in heparin and HS's structure and activity, detection of the sulfamate ^{1}H and ^{15}N NMR chemical shifts should provide new insights into the inter- and intramolecular interactions in which they are involved.

Following assignment of the resonances of the individual monosaccharide residues, the oligosaccharide sequence is determined through dipolar coupling information obtained via the rotating-frame Overhauser effect spectroscopy (ROESY) experiment. The ROESY spectrum can also distinguish IdoA and GlcA through unique inter-residue cross peaks. In conjunction with the TOCSY and COSY results, the ROESY spectrum (Figure 1.14) was used to establish sequence information that conclusively determined the hexasaccharide structure. In the ROESY spectrum, cross peaks arise between resonances of the H1 and the H4 protons of adjacent residues connected via the glycosidic bond, which reveals the relative positions of the monosaccharide residues within the hexasaccharide chain. Again, in cases in which the spectrum is complicated by resonance overlap, the BASHD version of the ROESY experiment can provide enhanced resolution.[85]

1.7.2. Nuclear Magnetic Resonance Diffusion Measurements. NMR diffusion measurements are useful for the analysis of complex mixtures, such as those obtained by heparin depolymerization. Diffusion-ordered spectroscopy (DOSY) provides a noninvasive separation of the different mixture components on the basis of differences in their translational diffusion coefficients.[101-104] DOSY NMR was used for the routine screening of LMWH and unfractionated heparin by Sitkowski et al.[105] and Bednarek et al.[106] Because the ^{1}H chemical shifts of the *N*-acetyl resonances of heparin and its potential impurities DS and OSCS are well resolved spectrally, DOSY plots can resolve OSCS and DS from both unfractionated heparin and LMWH. However, care must be taken in the design of NMR diffusion experiments because viscosity effects and

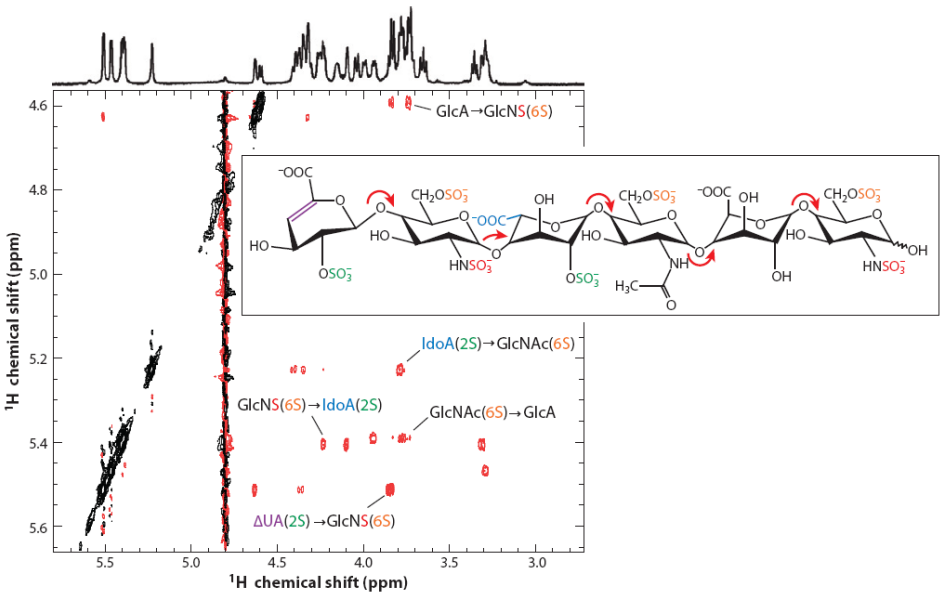

Figure 1.14. Partial ROESY spectrum showing the important peaks used to establish the sequence of the monosaccharide residues constituting the heparin-derived hexasaccharide ΔUA(2S)-GlcNS(6S)-IdoA(2S)-GlcNAc(6S)-GlcA-GlcNS(6S).

macromolecular crowding in concentrated solutions of heparin and other GAGs can dominate their translational diffusion behavior.

Limtiaco et al.[107] demonstrated the use of DOSY NMR spectra in conjunction with ^{1}H NMR and UV absorption measurements to monitor the enzymatic depolymerization of heparin with heparinase I. DOSY spectra acquired throughout the course of the enzymatic depolymerization yielded insight into the extent of the depolymerization and provided information about the size distribution of the heparin oligosaccharides produced. In addition to allowing the investigator to track and optimize the enzymatic digestion, this experiment demonstrated that DOSY NMR can be used to study mixtures of digested GAGs without employing a physical separation.

1.7.3. HPLC-NMR. As discussed in section 1.5, heparin-derived oligosaccharides resulting from enzymatic or chemical depolymerization often require an offline separation step prior to structural analysis of each isolated oligosaccharide by NMR. A potentially more efficient method would directly couple the separation and NMR analysis. However, online coupling of HPLC and NMR presents several analytical challenges. First, is the need to use deuterated mobile phases to reduce large solvent signals in the NMR spectra. This is not only expensive, but also requires adjustment of mobile phase buffer conditions to account for differences in the activity of deuterium and hydrogen (e.g. pH does not equal pD). To avoid using fully deuterated solvents, a solvent suppression technique such as WET can be used to attenuate the ^{1}H NMR resonances of mobile phase components. However, this often results in suppression of large regions of the ^{1}H NMR

spectrum, reducing the structural information available due to suppression of analyte signals that are close in chemical shift to the mobile phase resonances being suppressed.

Another consideration in HPLC-NMR experiments is that when NMR detection is used with a flowing system, the residence time, τ, of the nuclei in the coil can affect both the spin-lattice (T_1) and spin-spin (T_2) relaxation times.[108]

$$\frac{1}{T_{1\,\text{flow}}} = \frac{1}{T_{1\,\text{static}}} + \frac{1}{\tau} \qquad \text{Eq. 1.1}$$

$$\frac{1}{T_{2\,\text{flow}}} = \frac{1}{T_{2\,\text{static}}} + \frac{1}{\tau} \qquad \text{Eq. 1.2}$$

As shown in equations 1.1 and 1.2, decreasing the lifetime of the spins in the coil by increasing the flow rate ($1/\tau$) increases the rates of both T_1 and T_2 relaxation relative to their static values. Faster T_1 relaxation rates allow more rapid pulsing making it possible to acquire more transients in the short amount of time the analyte resides in the coil active volume. Shorter T_2 relaxation times, however, can lead to significant increases in line width limiting spectral resolution and reducing the degree of structural information that can be obtained.[108]

Another problem encountered in flow-based NMR experiments is that the analyte's short residence time in the coil limits the number of transients that can be acquired. As a result, it is not possible to improve the S/N of dilute peaks by extensive signal averaging or to perform 2D NMR experiments to provide additional structural information. For this reason, HPLC-NMR experiments and other flow-based

experiments are often conducted in a stop-flow mode. Typically peaks are first detected in the UV cell of the HPLC and after a calibrated amount of time the pumps are stopped, trapping the chromatographic peak in the NMR flow cell. For most HPLC separations this leads to the diffusional broadening of other analytes that elute later in the separation severely reducing chromatographic resolution. For a more in-depth review of the field of LC-NMR the reader is referred to references [108] and [109].

To date, little work has been reported on the application of LC-NMR to the characterization of heparin oligosaccharides. Most notable, is the work discussed in section 1.5.3 by Limtiaco et al.[53] The WAX column used in this study was packed with an amino-bonded stationary phase that interacted more weakly with anionic analytes than the quaternary amine functionalized polymers normally used for SAX separations. This effectively reduced the amount of salt needed to elute highly charged analytes like heparin making the separation more compatible with NMR detection which is sensitive to ionic strength. Also, because elution in this separation was driven by a displacement chromatography mechanism, analytes eluting later in the separation did not suffer from diffusional broadening, allowing both on-flow and stop-flow NMR acquisitions.

1.8 Enhancing Nuclear Magnetic Resonance Sensitivity

NMR is an invaluable technique for quantitative analysis, structure elucidation, and the study of the inter- and intramolecular interactions central to many chemical and biological processes. The main downfall of NMR is its inherent lack of sensitivity, especially compared with other popular techniques like fluorescence or mass

spectrometry. The reason for this limitation can be understood by examination of the origin of the NMR signal.[110] The signals in all spectroscopic methods arise from a transition between two or more energy states that result in the absorption or emission of electromagnetic radiation. For spin ½ nuclei in a magnetic field, B_0, the NMR signal arises from transitions between the two nuclear spin states, typically denoted as α and β. To observe an NMR signal there must be a difference in the number of spins in the two states as defined by the Boltzmann distribution (Eq. 1.3):

$$N_\alpha/N_\beta = e^{\Delta E/k_B T} \qquad \text{Eq. 1.3}$$

where N_α and N_β represent the number of nuclei in the α and β spin states, respectively, ΔE is the energy difference between the two spin states, k_B the Boltzmann constant, and T is the temperature. For most spin ½ nuclei, γ, the gyromagnetic ratio, is positive and the α spin state is lower in energy. The difference in energy between the two spin states, ΔE, is defined by Eq. 1.4:

$$\Delta E = h\gamma B_0/2\pi \qquad \text{Eq. 1.4}$$

where h is Planck's constant. Even for the highest field magnets, ΔE is generally small compared with other spectroscopic methods, limiting the sensitivity of the NMR measurement.[110]

1.8.1 Higher Magnetic Fields. Since its discovery, many technical advances have led to increases in the sensitivity of NMR measurements. The most common approach is to increase B_0, increasing the population difference between the spin states as well as the spectral dispersion. The disadvantage of this approach lies in the almost exponential increase in the price tag associated with increasing B_0. Also, investigators are generally

limited to the use of the NMR instrumentation located at their site. While use of remote instrumentation is possible, it is typically a less convenient and more expensive alternative employed as a last resort.

1.8.2 Hyperpolarization. An alternative approach to improving NMR sensitivity is hyperpolarization, of which the most common method is dynamic nuclear polarization or DNP. DNP attacks the root of the NMR sensitivity problem by selectively increasing the population of one nuclear spin state over the other. This is accomplished by first polarizing the electron spins of a radical either through microwaves or optical pumping. This polarization is then transferred from the electrons of the radical to the nuclei of the analyte followed by a fast NMR acquisition before the nuclei have time to relax. Although DNP can achieve signal enhancements up to 44,400 for ^{13}C and 23,500 for ^{15}N compared with spectra acquired at thermal equilibrium in a 9.4 T magnetic field, spectra are often limited to one dimensional experiments due to the short lifetimes of the hyperpolarized state.[111, 112] However with the advent of fast one scan NMR experiments, acquisition of 2D-NMR spectra in a few seconds when coupled with DNP is now possible.[113] Results using this technique for the characterization of heparin and HS have not yet been reported; however, future work in this area may prove useful for the characterization of mass-limited heparin oligosaccharide samples. This technique was not explored for the work described in this dissertation, as the equipment needed for DNP (e.g. a separate magnet for the polarization procedure) is still quite expensive and this instrumentation is not yet widely available.

1.8.3. Cryoprobes. To consider other approaches by which the sensitivity of NMR experiments can be improved, it is necessary to understand in greater detail the factors that contribute to the signal to noise ratio (S/N) in NMR. Equation 1.5 defines a set of constants and variables that together give rise to the S/N of an NMR experiment.[108]

$$S/N = \frac{k_0 \frac{B_1}{i} V_S N \gamma \frac{h^2}{4\pi^2} I(I+1) \frac{{\omega_0}^2}{kT3\sqrt{2}}}{V_{noise}} \qquad \text{Eq. 1.5}$$

Combining the constants in Eq. 1.5 into a single term, η, simplifies the expression (Eq.1.6) to focus only on those variables that can be manipulated to improve S/N.

$$S/N = \eta \frac{{\omega_0}^2 \frac{B_1}{i} V_s}{V_{noise}} \qquad \text{Eq. 1.6}$$

In Eq. 1.6 ω_0 is the Larmor frequency, which increases linearly with increasing B_0, B_1 is the magnitude of the oscillating magnetic field produced by the radio frequency (rf) pulse per unit of current, i, V_s is the sample volume, and V_{noise} is the root-mean-square noise in Volts of the coil and the receiver preamplifier. The term B_1/i is referred to as the quality or Q-factor of the NMR probe.

The use of high temperature (~ 20 K) superconducting alloys for coil construction in what are often termed cryoprobes has become popular as a means of achieving S/N improvements in NMR experiments. By reducing the temperature of the probe and preamplifier, cryoprobes improve S/N by decreasing the Johnson or thermal noise

contributions to V_{noise}.[114, 115] The sensitivity gains achieved by cryoprobes are relatively modest. Increases of 2-5 fold are typical, with lower gains often observed for high ionic strength aqueous solutions. While cryoprobes are more cost effective than increasing magnetic field strength, the installation (~$250,000) and ongoing maintenance costs (~$35,000 per year) are still significant. In addition, cryoprobes are typically used with a dedicated magnet to avoid frequent probe changes, making them impractical for laboratories where a wide range of NMR applications are investigated.

1.8.4. Microcoil NMR probes. Most readers are likely familiar with a process for measuring a liquid-state high-resolution NMR spectrum that involves introducing their sample into a NMR tube, placing the tube into a spinner, and dropping the tube and spinner into the probe housed inside the NMR magnet. Conventional tube-based NMR probes generally use saddle coils oriented with their long axis aligned parallel to B_0. Saddle coil probes have an air gap between the coil and the sample that allows the sample tube to be inserted and ejected pneumatically. This air gap also reduces magnetic susceptibility differences from the sample that can broaden the NMR spectrum. Magnetic susceptibility effects also require that the tube contains a sample of sufficient volume to extend above and below the coil to produce high quality spectra with narrow lines. Alternatively, special NMR tubes, such as those available from Shigemi, use glass plugs susceptibility matched to the solvent above and below the sample to restrict the volume of the sample to the coil active volume.

An alternative coil design is based on a solenoidal coil geometry oriented perpendicular to the applied magnetic field, B_0. Solenoidal coils are used in many solid-

state NMR probes,[116] and are also a popular geometry for microcoil NMR probes. Compared to other coil geometries, solenoidal coils give better sensitivity, especially for small volume samples. The B_1/i term from Eq. 1.6 can be defined for a solenoidal coil as shown in Eq. 1.7:[117]

$$\frac{B_1}{i} = \frac{\mu_0 n}{d\sqrt{1+\left[h/d\right]^2}} \qquad \text{Eq. 1.7}$$

where μ_0 is the permeability of free space, n is the number of turns of the solenoid, h is the coil length and d is the coil diameter. As shown in Eq. 1.7, for a constant length to diameter ratio (h/d), the coil sensitivity increases as the diameter is reduced. This is the fundamental premise that has driven the development of solenoidal microcoil NMR probes for improved S/N in measurements with mass-limited samples. Providing that the entire sample is soluble in the small volume interrogated by the microcoil probe, significant improvements of S/N can be achieved compared to tube-based measurements in conventional probes.[118]

Not only are solenoidal microcoils inherently more sensitive than saddle coils of the same size, they also increase sensitivity by improving the probe filling factor, defined as the ratio of V_s to the coil active volume, V_c. To increase the sample volume interrogated, a bubble cell can be etched into the capillary to more effectively fill the active volume of the coil.[119] Because solenoidal microcoils are generally wrapped directly around the capillary into which the sample is introduced, these probes have a higher filling factor than conventional probes that employ an air gap between the sample and the coil.[116] It should be noted however that the example given here is only for

conventional NMR probes, and that the saddle coils used in these probes could be fixed directly around a capillary giving them a similar filling factor as microcoils. Additionally, probe designs featuring the microcoils wound directly around the capillary can produce spectra with broad resonances due to magnetic susceptibility mismatch between the coil, capillary and sample. A major breakthrough in the development of solenoidal microcoil probes was a design that produces improved line widths by surrounding the receiver coil with a fluid susceptibility-matched to the coil material.[120] For example, immersing copper microcoils in FC-43 (a mixture of perfluoro-butylamines) approximates an infinite uniform medium surrounding the sample thereby minimizing spectral broadening due to magnetic susceptibility mismatch. Many of the other specific intricacies of solenoidal microcoil design have been reviewed in detail [108, 117, 119, 121] and some of this material will be discussed further in Chapters four, five, and six.

From a practical standpoint, sample introduction can be one of the most challenging aspects of experiments using microcoil NMR probes. Typically, the sample is introduced into the coil by injecting it into the capillary around which the coil is wound.[122] The user has the option of either filling the entire capillary with sample or limiting the sample to the active volume of the coil. To record NMR spectra with the highest possible S/N, the sample is dissolved and introduced into the probe in a volume closely matched to that of the coil. As with tube-based experiments, to obtain the uniform magnetic susceptibility necessary to produce spectra with narrow resonances, the sample must be of sufficient volume to extend beyond the edges of the solenoidal coil. This often requires a sample volume about twice that of the coil active volume.[118]

A popular way to reduce the sample volume in microcoil NMR experiments is to sandwich the sample between layers of an immiscible solvent. This creates a tight sample plug that can be positioned in the active volume of the coil for spectral acquisition, as illustrated in Fig. 1.15. This approach was first demonstrated experimentally in 1998 by Behnia and co-workers using FC-43 as the sandwiching solvent for an aqueous sample.[123] Sandwiching the sample between layers of FC-43 reduces spectral broadening due to discontinuities in the magnetic susceptibility at the ends of the sample,[120, 122] an effect similar to that obtained with susceptibility matched glass plugs in Shigemi NMR tubes. Using a 0.5 μL microcoil probe, Kautz et al. demonstrated the efficient segmented flow analysis of a diverse sample set by introducing 2 μL samples into a stream of FC-43.[124] In these segmented flow experiments, an NMR probe containing Telfon tubing was used to maximize wetting by the fluorocarbon fluid and minimize sample losses to the tubing walls. If this approach is used in probes constructed with small diameter fused silica capillaries, such as those provided in commercial CapNMR microcoil probes,[118] it can be helpful to coat the inner surface of the fused silica capillary with a fluorinated silane like perfluoro-octyl silane to prevent the FC-43 from sticking to the surface and eventually clogging the capillary. In situations where modification of the capillary is undesirable or impossible, other immiscible solvents like $CDCl_3$ can be used as the sandwiching solvent for aqueous samples.[125]

For analytes of intermediate polarity for which using an immiscible sandwiching solvent is difficult, Kc and coworkers created a probe design that uses magnetic susceptibility matched plugs to create sample cells.[126] For larger volume microcoils (15 –

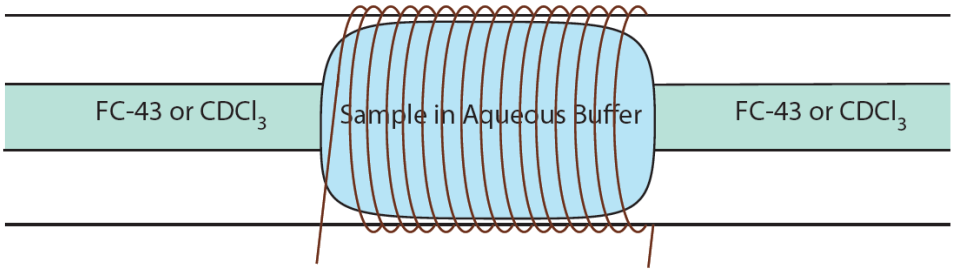

Figure 1.15. Illustration of an aqueous sample in the active volume of a microcoil sandwiched between layers of FC-43 or $CDCl_3$.

20 μL) a sample cell was constructed using Ultem plugs with small ID Teflon tubing inserted through the center. For smaller volume microcoils (0.5 – 2.0 μL) for which sufficiently small solid plugs were unavailable, a sample cell was created using Devcon two part epoxy to fill in the area between a small fused silica capillary and a larger volume thin glass capillary. In either probe design, the sample is not confined only to the active volume of the coil, but must also fill the capillary of the probe. Unlike bubble cell designs, the cell volume of these probes could be fixed to the exact volume of the microcoil decreasing the total volume needed to fill the cell and capillary.

1.8.5. Microstrip and Microslot Probes. A promising alternative to solenoidal microcoils are microstrip (or stripline) and microslot probe designs.[121, 127, 128] Both types of probes use a thin metal strip positioned parallel to B_0 to produce the perpendicular B_1 magnetic field and detect the NMR signal. Similar to a wire that produces a magnetic field that encircles it when current is applied, the B_1 magnetic field lines produced by these probes encircle the strips and run parallel to the surface. In the stripline design, B_1-field homogeneity is realized by sandwiching the metal strip between two ground planes creating a nonradiative closed system.[121] In the microslot design a small, rectangular hole is cut into a microstrip waveguide to create a pure series inductance.[127, 128] Because of their planar designs, capillaries can be oriented in any direction on-top of the microstrip or microslot allowing detection of static samples inside the capillary or those passing through the B_1 field of the probe in a flowing system. Fig. 1.16 shows a digital image taken through the lens of a microscope of a capillary fixed on-top of a microslot probe used in our lab.

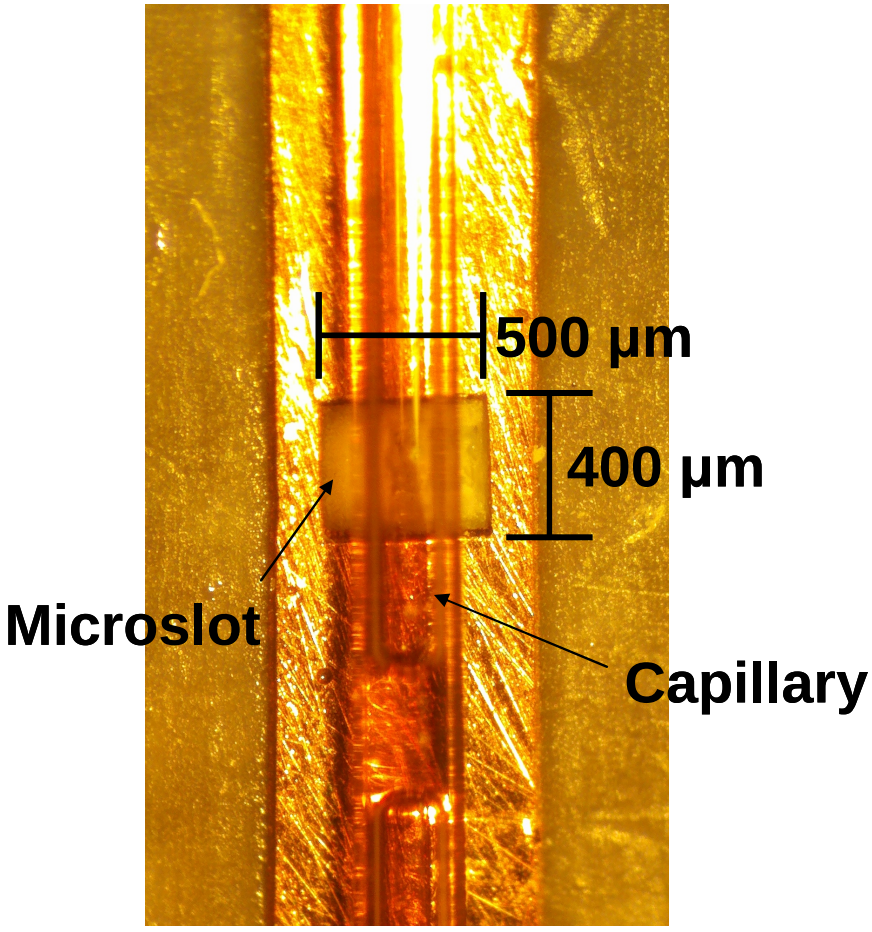

Figure 1.16. Digital image taken through the lens of a microscope of a sample capillary positioned on top of the slot in the microstrip of a microslot NMR probe.

The planar design of microstrip and microslot probes also makes their coupling to lab-on-a-chip applications relatively simple. Kentgens et al. have demonstrated that microfluidics can be easily bonded to microstrip and microslot chips without disturbing the electrical properties of the chip.[121] With the current boom in the commercial development of lab-on-a-chip devices for a wide range of chemical and biochemical applications, the added wealth of chemical and structural information that can be gained by incorporating NMR detection could be invaluable.

Another promising feature of microstrip and microslot probe designs is their ease of manufacture. Although automated fabrication techniques do exist for solenoidal microcoils, they are often hand wound by skilled probe designers. In contrast, microstrip and microslot probes are created using well established lithographic methods which could easily be translated to a commercial design process. The microstrip probe is constructed using only a single layer lithographic process and offers a full range of scalability. In the case of the microslot design, scalability is limited by the laser wavelength used to create the slot in the microstrip.

1.9. CE- and cITP-NMR

The coupling of NMR and CE was first demonstrated by Sweedler and co-workers in the mid-1990's.[129, 130] CE and capillary isotachophoresis (cITP) are both electrophoretic techniques that separate analytes based on differences in electrophoretic mobility. These separations can be carried out in fused silica capillaries with outer

diameters that allow the microcoil to be wound directly around the separation capillary, or on a polyimide sleeve through which the capillary can be inserted. This produces a probe active volume similar to the volume occupied by each separated analyte band, maximizing both the probe filling factor and sensitivity.[117]

As discussed in section 1.7.3, several problems are commonly encountered when acquiring NMR spectra on a flowing system. The first is the increase in line width due to shortened effective T_2 relaxation times which limits spectral resolution and reduces the degree of structural information that can be obtained.[108] Another problem encountered in flow-based NMR experiments is that the analyte's short residence time in the coil limits the number of transients that can be acquired. As a result, it is not possible to improve the S/N of dilute peaks by extensive signal averaging or to perform 2D NMR experiments to provide structural information. To circumvent this problem, stop-flow CE techniques have been developed that park the analyte in the active volume of the microcoil for longer NMR experiments by turning off the separation voltage when the analyte reaches the coil.[131] This halts the migration of the analyte, however, the analyte is now free to diffuse and the S/N of the detected resonances decreases over time. Turning off the separation voltage also sharpens the resonances in CE-NMR spectra by removing the B_0 inhomogeneity resulting from the secondary magnetic field, B_2, produced by the separation current.[131] The S/N of CE-NMR experiments can also be improved using a bubble cell providing that the volume detected by the microcoil is a good match for the volume of the separated bands.[132]

An alternative approach to increasing S/N is to use a preconcentration technique like cITP to focus the analytes prior to analysis.[133-135] cITP separations utilize a discontinuous buffer system to concentrate analytes by up to 2 to 3 orders of magnitude while also separating them based on their individual electrophoretic mobilities. The buffer system used for cITP separations consists of a leading electrolyte (LE) of higher mobility and a trailing electrolyte (TE) of lower mobility than the analytes being focused. Upon application of an electric potential across the separation capillary, the individual analytes stack behind the LE into separate bands the order of which is determined by their electrophorectic mobilities. To maintain a constant current the analytes will focus to a concentration proportional to the concentration of the LE. In theory, even a trace impurity can be separated from and concentrated to nearly the same concentration as a major component as long as the impurity is charged and has a different electrophoretic mobility. [136] Once the analytes are focused and stacked into concentrated bands, they migrate through the capillary to the microcoil for NMR detection. Because of the high concentration of the cITP-focused bands and the fact that they are closely stacked, turning off the voltage applied to the capillary is not an effective strategy for stopping the flow in these experiments. However, lowering the separation voltage when the analyte band reaches the microcoil can reduce the separation current improving resonance line widths and slowing the movement of the peak without significant dispersion of the focused band.[137] Using this approach, our laboratory has demonstrated the use of cITP-NMR for the measurement of ^{1}H NMR spectra for only 1-2 μg of heparin-derived di- and tetrasaccharides.[137, 138] Although the resonances in the reported spectra were broadened

by the interfering magnetic field, B_2, produced by the current in the separation capillary, the unique chemical shift fingerprints of the monosaccharide residues can be used to identify sample components and evaluate sample purity.

The movement of the focused bands in cITP-NMR experiments can also be slowed or even halted by applying a pressure to the capillary to counter the electrophoretic flow. The simplest approach is to raise the level of the leading electrolyte reservoir using a precision lab jack.[134] Figure 1.17 shows a comparison of the S/N difference between a cITP-NMR spectrum acquired on flow (Figure 1.17a) and with stop flow (Figure 1.17b) achieved by raising the leading electrolyte reservoir. Alternatively a syringe pump can be used to provide a back pressure in the closed system, although attention must be paid to the build up of gas bubbles produced at the separation electrodes.[139]

1.10 Conclusions

More efficient analytical strategies that will allow the determination of unique oligosaccharide structures are needed to improve our understanding of the role of structural elements of heparin and HS in mediating a wide range of biological processes. However, subtle variations in structure, such as sulfonation patterns, positional isomers, and hexuronic acid epimers, are almost impossible to identify in intact biopolymers. As a consequence, heparin and HS characterization proceeds through a bottom-up approach via enzymatic or chemical depolymerization, followed by size- and charge-based separations to isolate individual oligosaccharide sequences for MS and NMR

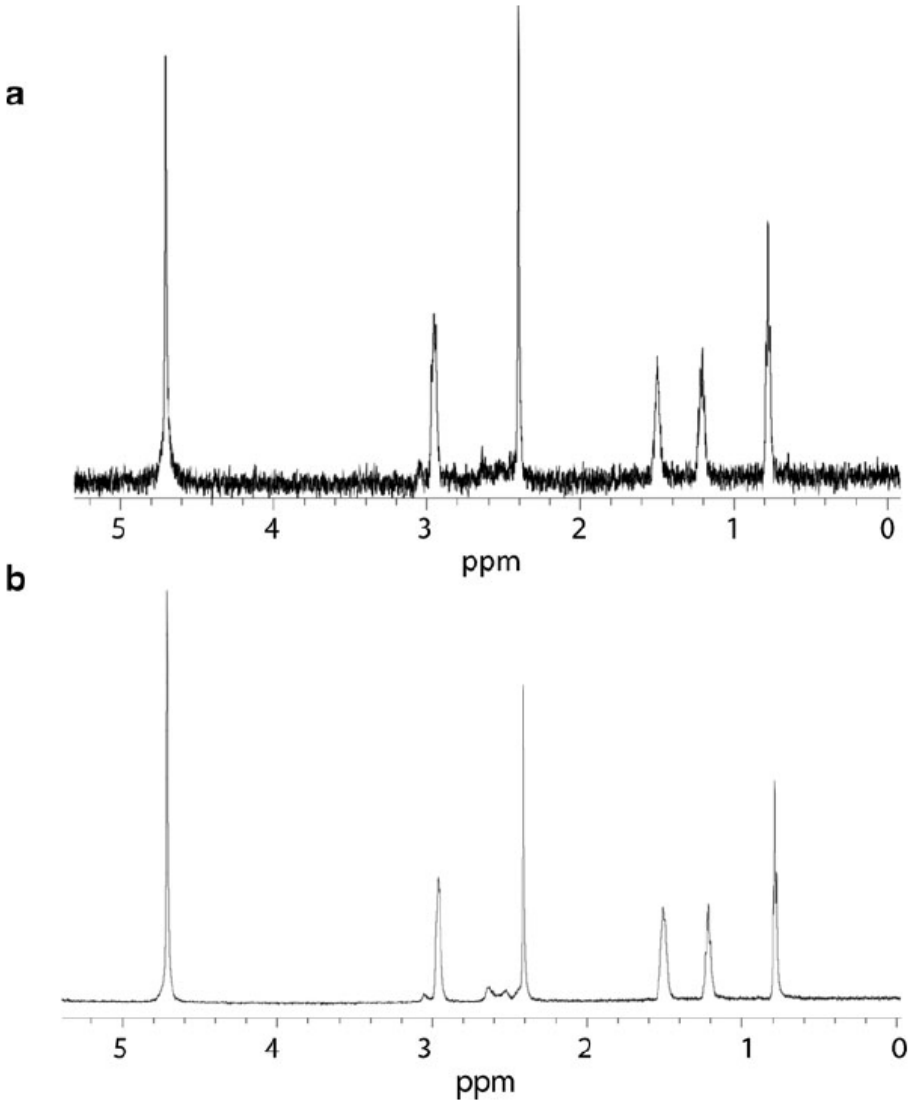

Figure 1.17. a) On-flow ^{1}H cITP-NMR spectrum acquired in 8 scans for tributylamine in a succinate buffer as the tributylamine moved through the active volume of the microcoil probe. b) Stop flow cITP-NMR spectrum for the same separation acquired by the coaddition of 50 of the 8 scan FIDs acquired in (a)

characterization. Although advances have been made, given the complexity of heparin and the difficulty in its characterization, there are still many unanswered questions regarding its molecular-level structure. Improvements to the speed and resolution of separations are increasing the throughput of the analysis, and higher information content mass spectra produced by novel methods such as EDD hold promise for the rapid sequencing of oligosaccharides. In addition, higher-field magnets, advances in cryogenically cooled and microcoil probes, and DNP experiments are increasing the sensitivity of NMR measurements, thereby removing a bottleneck in the analytical process.

The goals of this dissertation are to improve on and seek to better understand current separation methods for heparin and HS, especially RPIP-HPLC and cITP. In particular, in Chapter 2 we explore the mechanism of RPIP-HPLC with a focus on the role that competition between ion-pairing reagents play in the separation of isomeric disaccharides. This work is continued in Chapter 3 where we explore the role that mobile phase pH and counterion interactions have on resolution of the anomeric forms of the heparin derived disaccharides. In Chapter 4 we turn our attention to cITP where the cITP separation of the isomers of doxepin will be used to develop new insights into the mechanism by which all electrophoretic separations operate, in how particular buffer counterions like acetate can interact with various components of the separation system. Later in Chapter 5 we use mechanistic details of capillary isotachophoresis (cITP) gained in Chapter 4 for the cationic cITP separation of the isomers of doxepin to create a new, optimized anionic buffer system for the focusing and separation of heparin and heparan

sulfate (HS) derived oligosaccharides. Finally, in Chapter 6 we present a new microslot probe design for coupling to cITP with improved spectral resolution during the separations.

1.11 References

1. Gandhi, N. S.; Mancera, R. L., The structure of glycosaminoglycans and their interactions with proteins. *Chem. Biol. Drug Des.* **2008,** 72, 455-482.

2. Rabenstein, D. L., Heparin and heparan sulfate: structure and function. *Nat. Prod. Rep.* **2002,** 19, 312-331.

3. Linhardt, R. J., 2003 Claude S. Hudson award address in carbohydrate chemistry. Heparin: structure and activity. *J. Med. Chem.* **2003,** 46, 2551-2564.

4. Victor, X. V.; Nguyen, T. K. N.; Ethirajan, M.; Tran, V. M.; Nguyen, K. V.; Kuberan, B., Investigating the elusive mechanism of glycosaminoglycan biosynthesis *J Biol Chem* **2009,** 284, 25842-25853.

5. Mann, K. G., Biochemistry and physiology of blood coagulation. *Thromb. Haemostasis* **1999,** 82, 165-174.

6. Sasisekharan, R.; Shriver, Z.; Venkataraman, G.; Narayanasami, U., Roles of heparan-sulphate glycosaminoglycans in cancer. *Nat Rev Cancer* **2002,** 2, 521-528.

7. Mitsiadis, T. A.; Salmivirta, M.; Muramatsu, T.; Muramatsu, H.; Rauvala, H.; Lehtonen, E.; Jalkanen, M.; Thesleff, I., Expression of the heparin-binding cytokines, midkine (MK) and HB-GAM (pleiotrophin) is associated with epithelial-mesenchymal interactions during fetal development and organogenesis. **1995,** 121, 37-51.

8. Izvolsky, K. I.; Shoykhet, D.; Yang, Y.; Yu, Q.; Nugent, M. A.; Cardoso, W. V., Heparan sulfate-FGF10 interactions during lung morphogenesis. *Dev. Biol.* **2003,** 258, 185-200.

9. Crum, R.; Szabo, S.; Folkman, J., A new class of steroids inhibits angiogenesis in the presence of heparin or a heparin fragment. *Science* **1985,** 230, 1375-1378.

10. Folkman, J.; Langer, R.; Linhardt, R. J.; Haudenschild, C.; Taylor, S., Angiogenesis inhibition and tumor regression caused by heparin or a heparin fragment in the presence of cortisone. *Science* **1983,** 221, 719-725.

11. Iozzo, R. V.; San Antonio, J. D., Heparan sulfate proteoglycans: heavy hitters in the angiogenesis arena. *J. Clin. Invest.* **2001,** 108, 349-355.

12. Kresse, H.; Schönherr, E., Proteoglycans of the extracellular matrix and growth control. *J. Cell. Phys.* **2001,** 189, 266-274.

13. Lyon, M.; Gallagher, J. T., Bio-specific sequences and domains in heparan sulphate and the regulation of cell growth and adhesion. *Matrix Biol.* **1998,** 17, 485-493.

14. Li, J.-p.; Vlodavsk, I., Heparin, heparan sulfate and heparanase in inflammatory reactions. *Thromb. Haemost.* **2009,** 102, 823-828.

15. Dityatev, A.; Schachner, M., Extracellular matrix molecules and synaptic plasticity. *Nat Rev Neurosci* **2003,** 4, 456-468.

16. Holt, C. E.; Dickson, B. J., Sugar codes for axons? *Neuron* **2005,** 46, 169-172.

17. Heiden, D.; Mielke, C. H.; Rodvien, R., Impairment by heparin of primary haemostasis and platelet [^{14}C]5-hydroxytryptamine release. *Brit. J. Haematol.* **1977,** 36, 427-436.

18. Bartlett, A. H.; Park, P. W., Proteoglycans in host-pathogen interactions: molecular mechanisms and therapeutic implications. *Expert Rev. Mol. Med.* **2010,** 12, e5.

19. Rostand, K. S.; Esko, J. D., Microbial adherence to and invasion through proteoglycans. *Infect. Immun.* **1997,** 65, 1-8.

20. Van Putten, J. P. M.; Paul, S. M., Binding of syndecan-like cell surface proteoglycan receptors is required for Neisseria gonorrhoeae entry into human mucosal cells *EMBO Journal* **1995,** 14, 2144-2154.

21. Barrowcliffe, T. W., Low molecular weight heparin(s) *Brit J Haematol* **1995,** 90, 1-7.

22. Guerrini, M.; Beccati, D.; Shriver, Z.; Naggi, A.; Viswanathan, K.; Bisio, A.; Capila, I.; Lansing, J. C.; Guglieri, S.; Fraser, B.; Al-Hakim, A.; Gunay, N. S.; Zhang, Z. Q.; Robinson, L.; Buhse, L.; Nasr, M.; Woodcock, J.; Langer, R.; Venkataraman, G.; Linhardt, R. J.; Casu, B.; Torri, G.; Sasisekharan, R., Oversulfated chondroitin sulfate is a contaminant in heparin associated with adverse clinical events. *Nature Biotechnol* **2008,** 26, 669-675.

23. Langesley, D. J.; Jones, C. J.; Beni, S.; Larive, C. K., Glycoaminoglycans: Oligosaccharide analysis by liquid chromatography/specific labeling. *Methods Mol. Biol.* **2010,** In Press.

24. Jandik, K. A.; Gu, K. A.; Linhardt, R. J., Action pattern of polysaccharide lyases on glycosaminoglycans. *Glycobiology* **1994,** 4, 289-296.

25. Desai, U. R.; Wang, H. M.; Linhardt, R. J., Specificity studies on the heparin lyases from flavobacterium-heparinum. *Biochemistry* **1993,** 32, 8140-8145.

26. Mardiguian, J. Heparin esters and processes for their preparation. U.S. Patent No. 4440926, 1984.

27. Shively, J. E.; Conrad, H. E., Formation of anhydrosugars in chemical depolymerization of heparin. *Biochemistry* **1976,** 15, 3932-3942.

28. Rota, C.; Liverani, L.; Spelta, F.; Mascellani, G.; Tomasi, A.; Iannone, A.; Vismara, E., Free radical generation during chemical depolymerization of heparin. *Anal. Biochem.* **2005,** 344, 193-203.

29. Vismara, E.; Pierini, M.; Mascellani, G.; Liverani, L.; Lima, M.; Guerrini, M.; Torri, G., Low-molecular-weight heparin from Cu2+ and Fe2+ Fenton type depolymerisation processes. *Thromb. Haemost.* **2010,** 103, 613-622.

30. Behr, J. R.; Matsumoto, Y.; White, F. M.; Sasisekharan, R., Quantification of isomers from a mixture of twelve heparin and heparan sulfate disaccharides using tandem mass spectrometry. *Rapid Commun. Mass Spectrom.* **2005,** 19, 2553-2562.

31. Camara, J. E.; Satterfield, M. B.; Nelson, B. C., Quantitative determination of disaccharide content in digested unfragmented heparin and low molecular weight heparin by direct-infusion electrospray mass spectrometry. *J. Pharm. Biomed. Anal.* **2007,** 43, 1706-1714.

32. Saad, O. M.; Ebel, H.; Uchimura, K.; Rosen, S. D.; Bertozzi, C. R.; Leary, J. A., Compositional profiling of heparin/heparan sulfate using mass spectrometry: assay for specificity of a novel extracellular human endosulfatase. . *Glycobiology* **2005,** 15, 812-826.

33. Saad, O. M.; Leary, J. A., Compositional analysis and quantification of heparin and heparan sulfate by electrospray ionization ion trap mass spectrometry. . *Anal. Chem.* **2003,** 75, 2985-2995.

34. Chuang, W.-L.; McAllister, H.; Rabenstein, D. L., Chromatographic methods for product-profile analysis and isolation of oligosaccharides produced by heparinase-catalyzed depolymerization of heparin. *J. Chromatogr., A* **2001,** 932, 65-74.

35. Ziegler, A.; Zaia, J., Size-exclusion chromatography of heparin oligosaccharides at high and low pressure. *Journal of Chromatography B* **2006,** 837, 76-86.

36. Eldridge, S. L.; Korir, A. K.; Gutierrez, S. M.; Campos, F.; Limtiaco, J. F. K.; Larive, C. K., Heterogeneity of depolymerized heparin SEC fractions: to pool or not to pool? *Carbohydr. Res.* **2008,** 343, 2963-2970.

37. Henriksen, J.; Ringborg, L. H.; Roepstorrf, P., On-line size-exclusion chromatography/mass spectrometry of low molecular mass heparin. *J. Mass Spectrom.* **2004,** 39, 1305-1312.

38. Seyrek, E.; Dubin, P. L.; Henriksen, J., Nonspecific electrostatic binding characteristics of the heparin-antithrombin interaction. *Biopolymers* **2007,** 86, 249-259.

39. Zaia, J.; Costello, C. E., Compositional analysis of glycosaminoglycans by electrospray mass spectrometry. *Anal. Chem.* **2001,** 73, 233-239.

40. Campa, C.; Coslovi, A.; Flamigni, A.; Rossi, M., Overview on advances in capillary electrophoresis-mass spectrometry of carbohydrates: A tabulated review. *Electrophoresis* **2006,** 27, 2027-2050.

41. El Rassi, Z.; Mechref, Y., Recent advances in capillary electrophoresis of carbohydrates. *Electrophoresis* **1996,** 17, 275-301.

42. Gunay, N. S.; Linhardt, R. J., Capillary electrophoretic separation of heparin oligosaccharides under conditions amenable to mass spectrometric detection. *Journal of Chromatography A* **2003,** 1014, 225-233.

43. Ruiz-Calero, V.; Puignou, L.; Galceran, M. T., Use of reversed polarity and a pressure gradient in the analysis of disaccharide composition of heparin by capillary electrophoresis. *J. Chromatogr., A* **1998,** 828, 497-508.

44. Patel, R. P.; Narkowicz, C.; Hutchinson, J. P.; Hilder, E. F.; Jacobson, G. A., A simple capillary electrophoresis method for the rapid separation and determination of intact low molecular weight and unfractionated heparins. *J. Pharm. Biomed. Anal.* **2008,** 46, 30-35.

45. Laremore, T. N.; Ly, M.; Solakyildirim, K.; Zagorevski, D. V.; Linhardt, R. J., High-resolution preparative separation of glycosaminoglycan oligosaccharides by polyacrylamide gel electrophoresis. *Anal. Biochem.* **2010,** 401, 236-241.

46. Pervin, A.; Gallo, C.; Jandik, K. A.; Han, X. J.; Linhardt, R. J., Preparation and structural characterization of large heparin-derived oligosaccharides. *Glycobiology* **1995,** 5, 83-95.

47. Rice, K. G.; Rottink, M. K.; Linhardt, R. J., Fractionation of heparin-derived oligosaccharides by gradient polyacrylamide-gel electrophoresis. *Biochem. J.* **1987,** 244, 515-522.

48. Zilberstein, G.; Shlar, I.; Korol, L.; Baskin, E.; Fasoli, E.; Righetti, P. G.; Torri, G.; Bisio, A.; Bukshpan, S., Focusing of low-molecular-mass heparins in polycationic polyacrylamide matrices. *Anal. Chem.* **2009,** 81, 6966-6971.

49. Ly, M.; Leach, F. E.; Laremore, T. N.; Toida, T.; Amster, I. J.; Linhardt, R. J., The proteoglycan bikunin has a defined sequence. *Nat Chem Biol* **2011,** 7, 827-833.

50. Seelert, H.; Krause, F., Preparative isolation of protein complexes and other bioparticles by elution from polyacrylamide gels. *Electrophoresis* **2008,** 29, 2617-2636.

51. Imanari, T.; Toida, T.; Koshiishi, I.; Toyoda, H., High-performance liquid chromatographic analysis of glycosaminoglycan-derived oligosaccharides. *J. Chromatogr., A* **1996,** 720, 275-293.

52. Rice, K. G.; Kim, Y. S.; Merchant, Z. M.; Linhardt, R. J., High-performance liquid chromatographic separation of heparin-derived oligosaccharides. *Anal. Biochem.* **1985,** 150, 325-331.

53. Limtiaco, J. F. K.; Jones, C. J.; Larive, C. K., Characterization of heparin impurities with HPLC-NMR using weak anion exchange chromatography. *Anal. Chem.* **2009,** 81, 10116-10123.

54. Hitchcock, A. M.; Yates, E. A.; Costello, C. E.; Zaia, J., Comparative glycomics of connective tissue glycosaminoglycans. *Proteomics* **2008,** 8, 1384-1397.

55. Staples, G. O.; Bowman, M. J.; Costello, C. E.; Hitchcock, A. M.; Lau, J. M.; Leymarie, N.; Miller, C.; Naimy, H.; Shi, X.; Zaia, J., A chip-based amide-HILIC LC/MS platform for glycosaminoglycan glycomics profiling. *Proteomics* **2009,** 9, 686-695.

56. Karlsson, N. G.; Schulz, B. L.; Packer, N. H.; Whitelock, J. M., Use of graphitised carbon negative ion LC-MS to analyse enzymatically digested glycosaminoglycans. *J. Chromatogr., B* **2005,** 824, 139-147.

57. Cecchi, T., Ion pairing chromatography. *Crit. Rev. Anal. Chem.* **2008,** 38, 161 - 213.

58. Cecchi, T., *Ion-pair chromatography and related techniques*. Taylor & Francis Group: Boca Raton, 2009; p 215pp.

59. Cecchi, T.; Pucciarelli, F.; Passamonti, P., Extended thermodynamic approach to ion interaction chromatography. *Anal. Chem.* **2001,** 73, 2632-2639.

60. Karamanos, N. K.; Vanky, P.; Tzanakakis, G. N.; Tsegenidis, T.; Hjerpe, A., Ion-pair high-performance liquid chromatography for determining disaccharide composition in heparin and heparan sulphate. *J. Chromatogr., A* **1997,** 765, 169-179.

61. Thanawiroon, C.; Linhardt, R. J., Separation of a complex mixture of heparin-derived oligosaccharides using reversed-phase high-performance liquid chromatography. *J. Chromatogr., A* **2003,** 1014, 215-223.

62. Thanawiroon, C.; Rice, K. G.; Toida, T.; Linhardt, R. J., Liquid chromatography/mass spectrometry sequencing approach for highly sulfated heparin-derived oligosaccharides. *J. Biol. Chem.* **2004,** 279, 2608-2615.

63. Toyoda, H.; Yamamoto, H.; Ogino, N.; Toida, T.; Imanari, T., Rapid and sensitive analysis of disaccharide composition in heparin and heparan sulfate by reversed-phase ion-pair chromatography on a 2 [mu]m porous silica gel column. *J. Chromatogr., A* **1999,** 830, 197-201.

64. Sinnis, P.; Coppi, A.; Toida, T.; Toyoda, H.; Kinoshita-Toyoda, A.; Xie, J.; Kemp, M. M.; Linhardt, R. J., Mosquito heparan sulfate and its potential role in malaria infection and transmission. *J. Biol. Chem.* **2007,** 282, 25376-25384.

65. Toyoda, H.; Kinoshita-Toyoda, A.; Selleck, S. B., Structural analysis of glycosaminoglycans in Drosophila and Caenorhabditis elegans and demonstration that tout-velu, a Drosophila gene related to EXT tumor suppressors, affects heparan sulfate in vivo. *J. Biol. Chem.* **2000,** 275, 2269-2275.

66. Doneanu, C. E.; Chen, W.; Gebler, J. C., Analysis of oligosaccharides derived from heparin by ion-pair reversed-phase chromatography/mass spectrometry. *Anal. Chem.* **2009,** 81, 3485-3499.

67. Henriksen, J.; Roepstorff, P.; Ringborg, L. H., Ion-pairing reversed-phased chromatography/mass spectrometry of heparin. *Carbohydr. Res.* **2006,** 341, 382-387.

68. Kuberan, B.; Lech, M.; Zhang, L.; Wu, Z. L.; Beeler, D. L.; Rosenberg, R. D., Analysis of heparan sulfate oligosaccharides with ion pair-reverse phase capillary high performance liquid chromatography-microelectrospray ionization time-of-flight mass spectrometry. *J. Am. Chem. Soc.* **2002,** 124, 8707-8718.

69. Zhang, Z.; Xie, J.; Liu, H.; Liu, J.; Linhardt, R. J., Quantification of heparan sulfate disaccharides using ion-pairing reversed-phase microflow high-performance liquid chromatography with electrospray ionization trap mass spectrometry. *Anal. Chem.* **2009,** 81, 4349-4355.

70. Korir, A. K.; Limitiaco, J. F. K.; Gutierrez, S. M.; Larive, C. K., Ultraperformance ion-pair liquid chromatography coupled to electrospray time-of-flight mass spectrometry for compositional profiling and quantification of heparin and heparan sulfate. *Anal. Chem.* **2008,** 80, 1297-1306.

71. Jones, C. J.; Beni, S.; Larive, C. K., Understanding the effect of the counterion on the reverse-phase ion-pair high-performance liquid chromatography (RPIP-HPLC) resolution of heparin-related saccharide anomers. *Anal. Chem.* **2011,** 83, 6762-6769.

72. Jones, C. J.; Membreno, N.; Larive, C. K., Insights into the mechanism of separation of heparin and heparan sulfate disaccharides by reverse-phase ion-pair chromatography. *J. Chromatogr., A* **2010,** 1217, 479-488.

73. Chi, L. L.; Amster, J.; Linhardt, R. J., Mass spectrometry for the analysis of highly charged sulfated carbohydrates. *Curr. Anal. Chem.* **2005,** 1, 223-240.

74. Zaia, J.; Costello, C. E., Tandem mass Spectrometry of sulfated heparin-like glycosaminoglycan oligosaccharides. *Anal. Chem.* **2003,** 75, 2445-2455.

75. Zaia, J.; Miller, M. J. C.; Seymour, J. L.; Costello, C. E., The role of mobile protons in negative ion CID of oligosaccharides. *J. Am. Soc. Mass Spectrom.* **2007,** 18, 952-960.

76. Juhasz, P.; Biemann, K., Utility of noncovalent complexes in the matrix-assisted laser-desorption ionization mass-spectrometry of heparin-derived oligosaccharides. *Carbohydr. Res.* **1995,** 270, 131-147.

77. Ueki, M.; Yamaguchi, M., Analysis of acidic carbohydrates as their quaternary ammonium or phosphonium salts by matrix-assisted laser des orption/ionization mass spectrometry. *Carbohydr. Res.* **2005,** 340, 1722-1731.

78. Laremore, T. N.; Linhardt, R. J., Improved matrix-assisted laser desorption/ionization mass spectrometric detection of glycosaminoglycan

disaccharides as cesium salts. *Rapid Commun. Mass Spectrom.* **2007,** 21, 1315-1320.

79. Tissot, B.; Gasiunas, N.; Powell, A. K.; Ahmed, Y.; Zhi, Z. L.; Haslam, S. M.; Morris, H. R.; Turnbull, J. E.; Gallagher, J. T.; Dell, A., Towards GAG glycomics: Analysis of highly sulfated heparins by MALDI-TOF mass spectrometry. *Glycobiology* **2007,** 17, 972-982.

80. Bultel, L.; Landoni, M.; Grand, E.; Couto, A. S.; Kovensky, J., UV-MALDI-TOF mass spectrometry analysis of heparin oligosaccharides obtained by nitrous acid controlled degradation and high performance anion exchange chromatography. *J. Am. Soc. Mass Spectrom.* **2010,** 21, 178-190.

81. Meissen, J. K.; Sweeney, M. D.; Girardi, M.; Lawrence, R.; Esko, J. D.; Leary, J. A., Differentiation of 3-O-sulfated heparin disaccharide isomers: Identification of structural aspects of the heparin CCL2 binding motif. *J. Am. Soc. Mass Spectrom.* **2009,** 20, 652-657.

82. Minamisawa, T.; Suzuki, K.; Hirabayashi, J., Systematic identification of N-acetylheparosan oligosaccharides by tandem mass spectrometric fragmentation. *Rapid Commun. Mass Spectrom.* **2006,** 20, 267-274.

83. Wolff, J. J.; Chi, L. L.; Linhardt, R. J.; Amster, I. J., Distinguishing glucuronic from iduronic acid in glycosaminoglycan tetrasaccharides by using electron detachment dissociation. *Anal. Chem.* **2007,** 79, 2015-2022.

84. Chuang, W. L.; Christ, M. D.; Peng, J.; Rabenstein, D. L., An NMR and molecular modeling study of the site-specific binding of histamine by heparin, chemically modified heparin, and heparin-derived oligosaccharides. *Biochemistry* **2000,** 39, 3542-3555.

85. Chuang, W. L.; Christ, M. D.; Rabenstein, D. L., Determination of the primary structures of heparin- and heparan sulfate-derived oligosaccharides using band-selective homonuclear-decoupled two dimensional H-1 NMR experiments. *Anal. Chem.* **2001,** 73, 2310-2316.

86. McEwen, I., Broadening of H-1 NMR signals in the spectra of heparin and OSCS by paramagnetic transition metal ions. The use of EDTA to sharpen the signals. *J. Pharm. Biomed. Anal.* **2010,** 51, 733-735.

87. Mourier, P. A. J.; Viskov, C., Chromatographic analysis and sequencing approach of heparin oligosaccharides using cetyltrimethylammonium dynamically coated stationary phases. *Anal. Biochem.* **2004,** 332, 299-313.

88. Ruiz-Calero, V.; Saurina, J.; Galceran, M. T.; Hernandez-Cassou, S.; Puignou, L., Potentiality of proton nuclear magnetic resonance and multivariate calibration methods for the determination of dermatan sulfate contamination in heparin samples. *Analyst* **2000,** 125, 933-938.

89. Ruiz-Calero, V.; Saurina, J.; Hernandez-Cassou, S.; Galceran, M. T.; Puignou, L., Proton nuclear magnetic resonance characterisation of glycosaminoglycans using chemometric techniques. *Analyst* **2002,** 127, 407-415.

90. Zang, Q.; Keire, D. A.; Wood, R. D.; Buhse, L. F.; Moore, C. M. V.; Nasr, M.; Al-Hakim, A.; Trehy, M. L.; Welsh, W. J., Combining 1H NMR spectroscopy and chemometrics to identify heparin samples that may possess dermatan sulfate (DS) impurities or oversulfated chondroitin sulfate (OSCS) contaminants. *J. Pharm. Biomed. Anal.* **2011,** 54, 1020-1029.

91. Rudd, T. R.; Skidmore, M. A.; Guimond, S. E.; Cosentino, C.; Torri, G.; Fernig, D. G.; Lauder, R. M.; Guerrini, M.; Yates, E. A., Glycosaminoglycan origin and structure revealed by multivariate analysis of NMR and CD spectra. *Glycobiology* **2009,** 19, 52-67.

92. Ruiz-Calero, V.; Saurina, J.; Galceran, T.; Hernández-Cassou, S.; Puignou, L., Estimation of the composition of heparin mixtures from various origins using proton nuclear magnetic resonance and multivariate calibration methods. *Anal. Bioanal. Chem.* **2002,** 373, 259-265.

93. Jolliffe, I., *Principal Component Analysis*. Springer: New York, 2002.

94. Mascellani, G.; Guerrini, M.; Torri, G.; Liverani, L.; Spelta, F.; Bianchini, P., Characterization of di- and monosulfated, unsaturated heparin disaccharides with terminal N-sulfated 1,6-anhydro-beta-D-glucosamine or N-sulfated 1,6-anhydro-beta-D-mannosamine residues. *Carbohydr. Res.* **2007,** 342, 835-842.

95. Yamada, S.; Yoshida, K.; Sugiura, M.; Sugahara, K., One-fimensional and 2-fimensional H-1-NMR characterization of 2 series of sulfated disaccharides prepared from chondroitin sulfate and heparan-sulfate heparin by bacterial eliminase digestion. *J. Biochem.* **1992,** 112, 440-447.

96. Yates, E. A.; Santini, F.; Guerrini, M.; Naggi, A.; Torri, G.; Casu, B., H-1 and C-13 NMR spectral assignments of the major sequences of twelve systematically modified heparin derivatives. *Carbohydr. Res.* **1996,** 294, 15-27.

97. Guerrini, M.; Naggi, A.; Guglieri, S.; Santarsiero, R.; Torri, G., Complex glycosaminoglycans: profiling substitution patterns by two-dimensional nuclear magnetic resonance spectroscopy. *Anal. Biochem.* **2005,** 337, 35-47.

98. Bendiak, B.; Fang, T. T.; Jones, D. N. M., An effective strategy for structural elucidation of oligosaccharides through NMR spectroscopy combined with peracetylation using doubly C-13-labeled acetyl groups. *Can. J. Chem. -Revue Canadienne De Chimie* **2002,** 80, 1032-1050.

99. Jones, D. N. M.; Bendiak, B., Novel multi-dimensional heteronuclear NMR techniques for the study of 13C-O-acetylated oligosaccharides: Expanding the dimensions for carbohydrate structures. *J. Biomol. NMR* **1999,** 15, 157-168.

100. Langeslay, D. J.; Beni, S.; Larive, C. K., Detection of the ^{1}H and ^{15}N NMR resonances of sulfamate groups in aqueous solution: A new tool for heparin and heparan sulfate characterization. *Anal. Chem.* **2011,** 83, 8006-8010.

101. Jayawickrama, D. A.; Larive, C. K.; McCord, E. F.; Roe, D. C., Polymer additives mixture analysis using pulsed-field gradient NMR spectroscopy. *Magn. Reson. Chem.* **1998,** 36, 755-760.

102. Johnson Jr, C. S., Diffusion ordered nuclear magnetic resonance spectroscopy: principles and applications. *Prog. Nucl. Magn. Reson. Spectrosc.* **1999,** 34, 203-256.

103. Morris, K. F.; Johnson, C. S., Diffusion-ordered two-dimensional nuclear magnetic resonance spectroscopy. *J. Am. Chem. Soc.* **1992,** 114, 3139-3141.

104. Morris, K. F.; Stilbs, P.; Johnson, C. S., Analysis of mixtures based on molecular size and hydrophobicity by means of diffusion-ordered 2D NMR. *Anal. Chem.* **1994,** 66, 211-215.

105. Sitkowski, J.; Bednarek, E.; Bocian, W.; Kozerski, L., Assessment of oversulfated chondroitin sulfate in low molecular weight and unfractioned heparins diffusion ordered nuclear magnetic resonance spectroscopy method. *J. Med. Chem.* **2008,** 51, 7663-7665.

106. Bednarek, E.; Sitkowski, J.; Bocian, W.; Mulloy, B.; Kozerski, L., An assessment of polydispersed species in unfractionated and low molecular weight heparins by diffusion ordered nuclear magnetic resonance spectroscopy method. *J. Pharm. Biomed. Anal.* **2010,** 53, 302-308.

107. Limtiaco, J. F. K.; Beni, S.; Jones, C. J.; Langesley, D.; Larive, C. K., NMR methods to monitor the enzymatic depolymerization of heparin. *Anal. Bioanal. Chem.*
2011, 399, 593-603.

108. Webb, A., Radiofrequency microcoils in magnetic resonance. *Prog. Nucl. Magn. Reson. Spectrosc.* **1997,** 31, 1-42.

109. Exarchou, V.; Krucker, M.; van Beek, T. A.; Vervoort, J.; Gerothanassis, I. P.; Albert, K., LC–NMR coupling technology: recent advancements and applications in natural products analysis. *Magn. Reson. Chem.* **2005,** 43, 681-687.

110. Claridge, T. D. W., *High-Resolution NMR techniques in organic chemistry*. Elsevier: Oxford, 2008; Vol. 19, p 372.

111. Ardenkjaer-Larsen, J. H.; Fridlund, B.; Gram, A.; Hansson, G.; Hansson, L.; Lerche, M. H.; Servin, R.; Thaning, M.; Golman, K., Increase in signal-to-noise ratio of > 10,000 times in liquid-state NMR. *Proc. Natl. Acad. Sci. U.S.A.* **2003,** 100, 10158-10163.

112. Bowen, S.; Hilty, C., Time-resolved dynamic nuclear polarization enhanced NMR spectroscopy. *Angew. Chem. Int. Ed.* **2008,** 47, 5235-5237.

113. Zeng, H.; Bowen, S.; Hilty, C., Sequentially acquired two-dimensional NMR spectra from hyperpolarized sample. *J. Magn. Reson.* **2009,** 199, 159-165.

114. Serber, Z.; Richter, C.; Moskau, D.; Bohlen, J.-M.; Gerfin, T.; Marek, D.; Haberli, M.; Baselgia, L.; Laukien, F.; Stern, A. S.; Hoch, J. C.; Dotsch, V., New carbon-detected protein NMR experiments using cryoProbes. *J. Am. Chem. Soc.* **2000,** 122, 3554-3555.

115. Spraul, M.; Freund, A. S.; Nast, R. E.; Withers, R. S.; Maas, W. E.; Corcoran, O., Advancing NMR Sensitivity for LC-NMR-MS Using a Cryoflow Probe: Application to the Analysis of Acetaminophen Metabolites in Urine. *Anal. Chem.* **2003,** 75, 1536-1541.

116. Doty, F. D., Probe design and construction. In *Enc Mag Res*, Wiley: New York, 1996; pp 3753-3763.

117. Lacey, M. E.; Subramanian, R.; Olson, D. L.; Webb, A. G.; Sweedler, J. V., High-resolution NMR spectroscopy of sample volumes from 1 nL to 10 μL. *Chem. Rev.* **1999,** 99, 3133-3152.

118. Schroeder, F. C.; Gronquist, M., Extending the scope of NMR spectroscopy with microcoil probes. *Angew. Chem., Int. Ed. Engl.* **2006,** 45, 7122-7131.

119. Jones, C. J.; Beni, S.; Limtiaco, J. F. K.; Langeslay, D. J.; Larive, C. K., Heparin characterization: challenges and solutions. *Annu. Rev. Anal. Chem.* **2011,** 4, 439-465.

120. Olson, D. L.; Peck, T. L.; Webb, A. G.; Magin, R. L.; Sweedler, J. V., High-resolution microcoil ^{1}H-NMR for mass-limited, nanoliter-volume samples. *Science* **1995,** 270, 1967-1970.

121. Kentgens, A. P. M.; Bart, J.; van Bentum, P. J. M.; Brinkmann, A.; van Eck, E. R. H.; Gardeniers, J. G. E.; Janssen, J. W. G.; Knijn, P.; Vasa, S.; Verkuijlen, M. H. W., High-resolution liquid- and solid-state nuclear magnetic resonance of nanoliter sample volumes using microcoil detectors. *J. Chem. Phys.* **2008,** 128.

122. Lacey, M. E.; Sweedler, J. V.; Larive, C. K.; Pipe, A. J.; Farrant, R. D., ^{1}H NMR characterization of the product from single solid-phase resin beads using capillary NMR flow probes. *J. Magn. Reson.* **2001,** 153, 215-222.

123. Behnia, B.; Webb, A. G., Limited-Sample NMR Using Solenoidal Microcoils, Perfluorocarbon Plugs, and Capillary Spinning. *Anal. Chem.* **1998,** 70, 5326-5331.

124. Kautz, R. A.; Goetzinger, W. K.; Karger, B. L., High-throughput microcoil NMR of compound libraries using zero-dispersion segmented flow analysis. *J. Comb. Chem.* **2004,** 7, 14-20.

125. Limtiaco, J. F. K.; Beni, S.; Jones, C. J.; Langeslay, D. J.; Larive, C. K., The efficient structure elucidation of minor components in heparin digests using microcoil NMR. *Carbohydr. Res.* **2011,** 346, 2244-2254.

126. Kc, R.; Gowda, Y. N.; Djukovic, D.; Henry, I. D.; Park, G. H. J.; Raftery, D., Susceptibility-matched plugs for microcoil NMR probes. *J. Magn. Reson.* **2010,** 205, 63-68.

127. Krojanski, H. G.; Lambert, J.; Gerikalan, Y.; Suter, D.; Hergenröder, R., Microslot NMR probe for metabolomics studies. *Anal. Chem.* **2008,** 80, 8668-8672.

128. Maguire, Y.; Chuang, I. L.; Zhang, S.; Gershenfeld, N., Ultra-small-sample molecular structure detection using microslot waveguide nuclear spin resonance. *Proc. Natl. Acad. Sci.* **2007,** 104, 9198-9203.

129. Wu, N.; Peck, T. L.; Webb, A. G.; Magin, R. L.; Sweedler, J. V., Nanoliter volume sample cells for ^{1}H NMR: Application to online detection in capillary electrophoresis. *J. Am. Chem. Soc.* **1994,** 116, 7929-7930.

130. Wu, N.; Peck, T. L.; Webb, A. G.; Magin, R. L.; Sweedler, J. V., ^{1}H-NMR spectroscopy on the nanoliter scale for static and online measurements. *Anal. Chem.* **1994,** 66, 3849-3857.

131. Olson, D.; Lacey, M.; Webb, A.; Sweedler, J., Nanoliter-volume ^{1}H NMR detection using periodic stopped-flow capillary electrophoresis. *Anal. Chem.* **1999,** 71, 3070-3076.

132. Rodat, A.; Gavard, P.; Couderc, F., Improving detection in capillary electrophoresis with laser induced fluorescence via a bubble cell capillary and laser power adjustment. *Biomed. Chromatogr.* **2009,** 23, 42-47.

133. Eldridge, S. L.; Almeida, V. K.; Korir, A. K.; Larive, C. K., Separation and analysis of trace degradants in a pharmaceutical formulation using on-line capillary isotachophoresis-NMR. *Anal. Chem.* **2007,** 79, 8446-8453.

134. Kautz, R. A.; Lacey, M. E.; Wolters, A. M.; Foret, F.; Webb, A. G.; Karger, B. L.; Sweedler, J. V., Sample concentration and separation for nanoliter-volume NMR spectroscopy using capillary isotachophoresis. *J. Am. Chem. Soc.* **2001,** 123, 3159-3160.

135. Korir, A.; Larive, C., On-line NMR detection of microgram quantities of heparin-derived oligosaccharides and their structure elucidation by microcoil NMR. *Anal. Bioanal. Chem.* **2007,** 388, 1707-1716.

136. Bocek, P.; M. Demi; Gebauer, P.; Dolnik, V., *Analytical isotachophoresis*. VCH Publishers: New York, 1988; p 237.

137. Korir, A. K.; Larive, C. K., On-line NMR detection of microgram quantities of heparin-derived oligosaccharides and their structure eluctdation by microcoil NMR. *Anal. Bioanal. Chem.* **2007,** 388, 1707-1716.

138. Korir, A. K.; Almeida, V. K.; Malkin, D. S.; Larive, C. K., Separation and analysis of nanomole quantities of heparin oligosaccharides using on-line capillary isotachophoresis coupled with NMR detection. *Anal. Chem.* **2005,** 77, 5998-6003.

139. Wolters, A. M.; Jayawickrama, D. A.; Larive, C. K.; Sweedler, J. V., Capillary Isotachophoresis/NMR extension to trace impurity analysis and improved instrumental coupling. *Anal. Chem.* **2002,** 74, 2306-2313.

CHAPTER TWO

Insights into the Reverse-Phase Ion-pair Separation of Heparin Derived Oligosaccharides

Based on a paper published in Journal of Chromatography, A

J. Chromatogr., A, 2010, 1217, 479-488.

This chapter uses the diverse family of commercially available heparin-derived disaccharides as a probe to explore the mechanism of reverse-phase ion-pair high-performance liquid chromatography (RPIP-HPLC). More specifically the study investigates the role that competition between ion-pairing reagents with different steric bulk and hydrophobicity plays in the separation of structural isomers of heparin and heparan sulfate (HS) disaccharides. Additionally, high-resolution magic angle spinning saturation transfer difference (HR-MAS STD) NMR experiments were used in an attempt to ascertain the degree to which ion-pair formation takes place in the mobile phase and at the stationary phase surface.

2.1 Introduction

Reverse-phase ion-pair high pressure liquid chromatography (RPIP-HPLC) and ultraperformance liquid chromatography (RPIP-UPLC) are promising and increasingly popular methods for the separation of organic and inorganic ionic solutes using lipophilic ions, referred to as ion-pairing reagents (IPR), as mobile phase modifiers to aid in the

retention and resolution of these species on a hydrophobic stationary phase.[1-3] The mechanism of retention in RPIP-HPLC is however, a matter of some debate. In the classical model of retention in RPIP-HPLC (Figure 2.1A), the hydrophobic IPR and the analyte ion of opposite charge combine in the mobile phase to form a neutral species which then partitions into the hydrophobic stationary phase.[4-6] The dynamic ion-exchange model (Figure 2.1B), however, suggests that the IPR is first adsorbed onto the surface of the stationary phase creating charge sites which then act as ion exchange sites for the oppositely charged analyte.[7-9] The presence of evidence for both theories suggest that RPIP separations occur through a combination of both mechanisms and that the extent to which each contributes to analyte retention may be controlled by experimental conditions.[1, 10]

To provide further insights into the separation mechanism of RPIP-HPLC, a set of test compounds is needed that provides a diversity of charges as well as subtle structural variations relative to the position of these charges, for example through positional isomers. Such a class of compounds would allow the evaluation of subtle changes in resolution and retention times as a result of varying experimental conditions, e.g., the type and concentration of IPR, mobile phase composition and pH. Through careful observations of the effect of separation conditions on the chromatographic resolution of a class of compounds having regular differences in charge and structure, the mechanistic details of RPIP-HPLC can be better inferred. The heparin and heparan sulfate disaccharides presented in Table 2.1 are an ideal set of test compounds for this purpose. As a group, they are a family of congeners with a range of molecular charge states as well

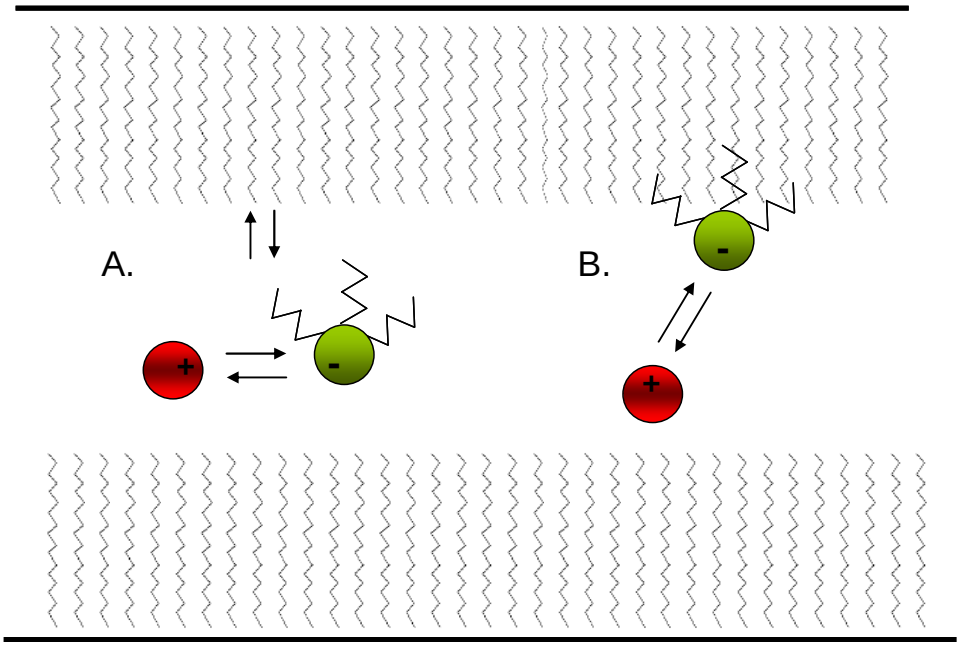

Figure 2.1. Ilustration depicting the dynamic equilibria involved between charged analytes and ion-pairing reagent in both the A) classic model and B)dynamic ion-exchange model of ion-pairing

Table 2.1. Designation, structures, and net charge states at pH 7.0 of the family of heparin disaccharides studied.

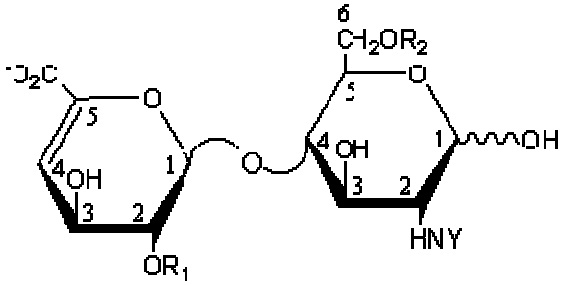

Disaccharide	R_1	R_2	Y	Charge
IS	SO_3^-	SO_3^-	SO_3^-	-4
IIS	H	SO_3^-	SO_3^-	-3
IIIS	SO_3^-	H	SO_3^-	-3
IVS	H	H	SO_3^-	-2
IA	SO_3^-	SO_3^-	Ac	-3
IIA	H	$SO3^-$	Ac	-2
IIIA	SO_3^-	H	Ac	-2
IVA	H	H	Ac	-1
IH	SO_3^-	SO_3^-	H	-2
IIH	H	SO_3^-	H	-1
IIIH	SO_3^-	H	H	-1
IVH	H	H	H	0

as several isomeric (as well as anomeric) species that have previously been demonstrated to be resolvable through RPIP-HPLC and UPLC methods.[11, 12]

High resolution magic angle spinning (HR-MAS) saturation transfer difference (STD) NMR experiments can also be used to provide spectroscopic evidence about the relative strength of interactions between IPR's, analyte, stationary phase, and mobile phase.[13-15] HR-MAS is ideal for these types of experiments because spinning the sample, which will include the stationary phase in the suspended state, at the magic angle (θ_m) of 54.7° (the angle where the equation for dipolar coupling (Eq. 2.1) equals zero) will

$$0 = 3\cos^2\theta_m \qquad \text{Eq 2.1}$$

reduce spectral broadening due to dipolar coupling between nuclei. More importantly, differences in magnetic susceptibility between the suspended stationary phase and the mobile phase will be averaged out by the spinning of the samples.

This chapter explores the mechanism of RPIP chromatography through the use of the RPIP-UPLC and HR-MAS STD NMR experiments. The ability of RPIP-UPLC to resolve heparin disaccharides based on differences in charge and subtle variations in compound structure makes it a useful probe of the mechanism of RPIP separations. This investigation also specifically addresses the interactions between the IPR tributylamine (TrBA) and heparin derived disaccharides as well as the potential role that competition between TrBA and other IPRs plays in the resolution of isomeric disaccharides. In the HR-MAS STD NMR experiments, saturation of the methyl resonances of the C18

stationary phase can be transfered to the IPR. These experiments have the potential to reveal which parts of each molecule are involved in RPIP interactions. Additionally, by monitoring the magnitude of saturation transfer under different mobile phase conditions we can potentially evaluate the extent to which IPR-analyte interactions occur in the mobile phase and at the stationary phase surface.

2.2 Experimental

2.2.1. Materials and reagents. All heparin disaccharide standards were purchased from the Sigma Chemical Company (St. Louis, MO). Table 2.1 shows the structures, designations, and net charge states at pH 7 of the commercially available disaccharides studied. The ion paring reagent TrBA (purity ≥99.5%) and benzene sulfonic acid were also purchased from Sigma. Butylamine (MBA) (99.5%), trimethylamine, and ammonium acetate were purchased from Fisher Scientific (Pittsburgh, PA). Acetonitrile (optima grade) and water (HPLC grade) were purchased from Sigma and Honeywell Burdick & Jackson, respectively. Deuterium oxide (D_2O, 99% D), sodium deuteroxide, deuterated acetonitrile and deuterated acetic acid were purchased from Cambridge Isotope Laboratories, Inc. (Andover, MA).

2.2.2. UPLC Separation. All chromatographic separations were performed on a 2.1 x 100 mm Acquity^{TM} UPLC BEH C18 column with 1.7 μm particles (Waters Corporation, Milford, MA). A guard column packed with the same 1.7 μm C18 particles was utilized prior to the analytical column. The column temperature was maintained at 40°C throughout the separation, and a flow rate of 0.5 mL/min was used. A sample

volume of 10 μL of a 0.2 mM disaccharide mixture prepared in water was injected for each separation. A binary solvent system was used for gradient elution. Solvent A consisted of 5% acetonitrile in water while solvent B consisted of 80% acetonitrile in water. Both solvents contained the same IPR concentrations and were adjusted using pH meter readings to an apparent pH between pH 6.9 and 7.0 using acetic acid. This yielded an acetate concentration for the 20, 10, 5.0, and 2.5 mM TrBA solutions of 20.0, 9.4, 4.7, and 2.4 mM, respectively. Chromatographic separations using 20 mM TrBA and 2.5 mM ammonium acetate contained an acetate concentration of 22.2 mM.

The pH meter was calibrated using a three point calibration with pH 4.00 (0.05 M potassium biphthalate buffer), pH 7.00 (0.05 M potassium phosphate monobasic-sodium hydroxide buffer), and pH 12.00 (NaOH, KCl buffer) buffers. The pH 4.00 and pH 7.00 buffers were purchased from Fisher Scientific (Pittsburgh, PA) while the pH 12.00 buffer was purchased from Ricca Chemical Company (Arlington, TX). For separations studying the effects of varying TrBA concentration, the ion-pair composition of both solvents consisted of 2.5-20 mM TrBA with no other IPR. For the separations studying the effects of varying MBA concentration both solvents contained 10, 15, and 20 mM MBA while the TrBA concentration was maintained at 2.5 mM. The buffers for the MBA experiments contained acetate concentrations of 11.1, 16.7 and 22.2 mM, respectively. Retention factors were calculated for Tables 2.1-2.5 by subtracting the retention time of the void from the retention time of the analyte peak and then dividing this value by the retention time of the void.

The gradient profile consisted of a 1 min isocratic step of 100% solvent A after which the fraction of solvent B was increased to 3% over the next 1.5 min. The fraction of solvent B was then increased to 25% over the next 2.5 min and maintained at 25% for 1 min before it was increased to 35% over a 1 min period. The fraction of solvent B was then increased over the next 4 min to 100%. A 5 min equilibration was utilized prior to the next injection. Isocratic experiments to probe the effect of varying TrBA and acetate concentrations were performed with a fixed mobile phase composition of 30% solvent B.

2.2.3. Mass Spectrometry. Total ion chromatograms were obtained using a Waters ESI quadrupole time-of-flight mass spectrometer (Waters Corporation, Millford, MA). Data acquisition was performed using Masslynx 4.1 software. All spectra were obtained in negative mode using the following instrument parameters: capillary voltage, 3 kV; cone voltage, 12 V; source temperature, 120 °C; desolvation temperature, 200 °C; extractor voltage, 1 V; radio frequency lens, 0.5 V; interscan delay, 0.1 sec; m/z range, 215-1000.

2.2.4. HR-MAS STD-NMR. HR-MAS samples were prepared by packing a 4 mm rotor insert with 145 mg of Waters BEH-C18 1.7 μm particles that were removed from a Waters 2.1 x 100 mm Acquity^{TM} UPLC BEH C18 column. To simulate the chromatographic mobile phase the following three IPR buffers were prepared in deuterated solvents: (1) 30 mM trimethylamine (TMA) titrated to pD 7.0 with acetic acid in 85% D_2O and 15% deuterated-ACN (containing 100 mM protonated ACN), (2) 30 mM TMA and 30 mM benzenesulfonic acid titrated to pD 7.0 with NaOD in 85% D_2O and 15% deuterated-ACN (100 mM protonated ACN), and (3) 30 mM TMA and 30 mM

benzenesulfonic acid titrated to pD 7.0 with NaOD in 70% D_2O and 30% deuterated-ACN (100mM protonated ACN). Thirty microliters of each buffer was added to the appropriate rotor insert by injecting the buffers in 10μL aliquots on top the packed C18 and then centrifuging the inserts at 9,000 rpms for 1min to force the buffers to wet the C18. The inserts were then closed and inserted into a 4mm zirconium rotor for analysis by NMR.

All ^{1}H NMR spectra were measured using a Bruker Avance NMR spectrometer operating at a frequency of 600.10 MHz equipped with a 4 mm dual resonance (^{1}H and ^{13}C) HR-MAS probe. All samples were spun at the magic angle at a frequency of 5,000 Hz. The probe and samples were kept at a constant temperature of 25°C by routing the bearing gas used to spin the rotor through a variable temperature unit prior to running it to the probe. STD-NMR experiments were performed using the standard Bruker defined stddiff.2 pulse sequence which features a 3 ms homospoil gradient pulse applied at the beginning of the pulse sequence to eliminate unwanted transverse magnetization. A 50 ms saturation pulse at 40.0 dB was applied to the larger of the two C18 resonances ~1.10 ppm for the on-resonance spectrum and at 18,000 Hz for the off-resonance spectrum. Both the on- and off-resonance STD spectra were measured for 128 scans with 8 dummy scans. Line broadening of 1 Hz was applied to each spectrum to improve the signal-to-noise ratio of the subtracted spectra.

2.3. Results

The complete resolution of a mixture of eleven heparin disaccharides was previously demonstrated by Korir et al. by RPIP-UPLC utilizing 50 mM ammonium

acetate as a pH buffer and 5mM TrBA as an IPR.[12] Although this method allowed for the rapid and efficient separation of the mixture components, presumably due to differential ion-pairing interactions of the disaccharides with TrBA, the presence of ammonium ions was also required for complete resolution of isomeric disaccharide pairs IIH/IIIH, IIA/IIIA and IIS/IIIS at the TrBA concentration used. A disadvantage of the use of ammonium as a mobile phase buffer is that it reduces the ESI-MS ionization efficiency, thereby limiting the sensitivity of the analysis. As shown in Figure 2.2, the ionization efficiency of heparin disaccharide IS is dramatically reduced by increasing ammonium ion concentration. Motivated by our desire to reduce MS ion suppression while maintaining good chromatographic resolution, experiments were designed to explore the effects of IPR structure and buffer composition on the chromatographic retention time and resolution of a heparin disaccharide mixture. This study also addresses the possibility that competition between TrBA and other positive IPRs such as ammonium and MBA for ion-pair formation may contribute to the chromatographic resolution of isomeric heparin disaccharides.

The heparin disaccharides shown in Table 2.1 comprise an interesting class of analytes for exploring the nature of ion-pairing interactions in RPIP chromatography. The disaccharides are all very hydrophilic and are poorly retained on the reverse phase column unless an ion-pairing reagent is employed. This family is comprised of species with similar structures and charge states, ranging from zero net charge at neutral pH

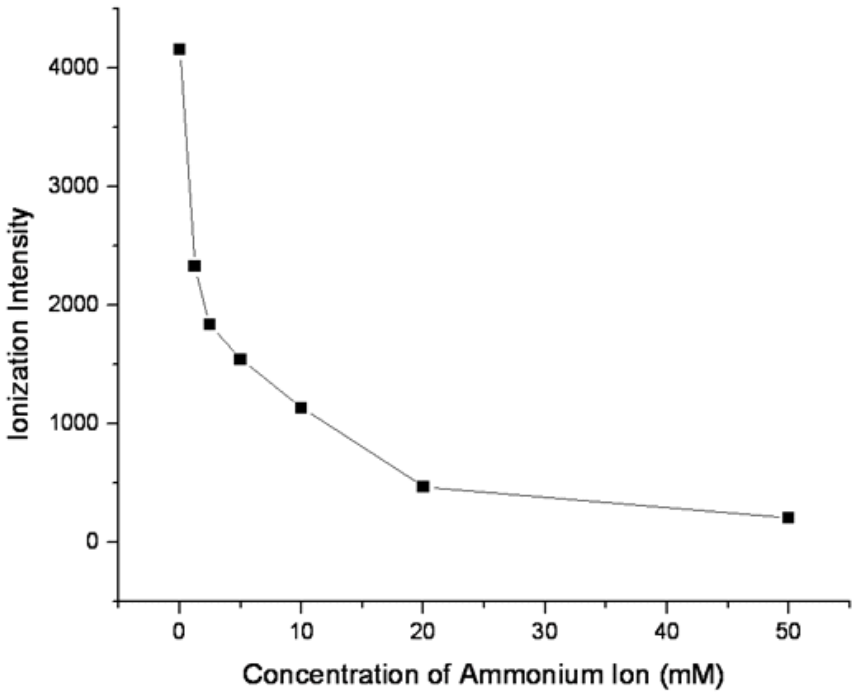

Figure 2.2. Graph of ionization intensity of the IS disaccharide as a function of increasing ammonium concentration while maintaining a constant TrBA concentration of 5 mM. Experiment was performed by direct infusion into the MS.

(IVH) to a charge of -4 (IS). In this family, negative charges result from the carboxylate group and from 2-*O* sulfonation of the iduronic acid, and from 6-*O* and *N*-sulfonation of the glucosamine residue. Disaccharides containing an unmodified glucosamine (IH, IIH, IIIH, and IVH) will have a positively charged amino group at the mobile phase pH employed in these experiments. Additionally, the disaccharides comprising charge states -1 (IVA, IIH, and IIIH), -2 (IIA, IIIA, and IH) and -3 (IA, IIS and IIIS) offer structural motifs that differ only in the nature and position of charged functional groups. Although one might expect to be able to resolve components with very different structures but similar charges, for example IIH and IVA, through different ion-pairing interactions, the ion-pairing interactions leading to separation of the isomeric pairs IIH/IIIH, IIA/IIIA and IIS/IIIS are likely to be more complex. Therefore, examining the effects of varying IPR structure and concentration on the resolution of this disaccharide family should yield insights into the finer details of the RPIP separation mechanism.

2.3.1. Effect of TrBA Concentration. Figure 2.3A shows the effect of varying mobile phase TrBA concentration on the separation of the heparin disaccharide mixture. The mobile phase used to measure these chromatograms contained no ammonium acetate, so TrBA acetate also served as the pH buffer in these experiments. In cases of peak overlap, compound identity was verified using the mass spectra, and for isomeric species which give rise to identical molecular ions, through injection of spiked samples. Tables 2.2-2.5 show calculated retention factors, widths at half height and peak areas for all 11 commercial disaccharides studied at the varying mobile phase TrBA

A.

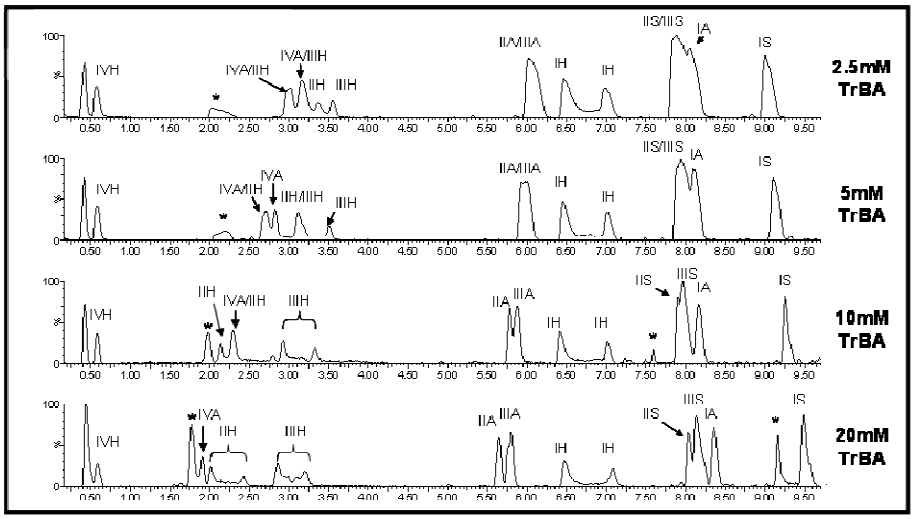

B.

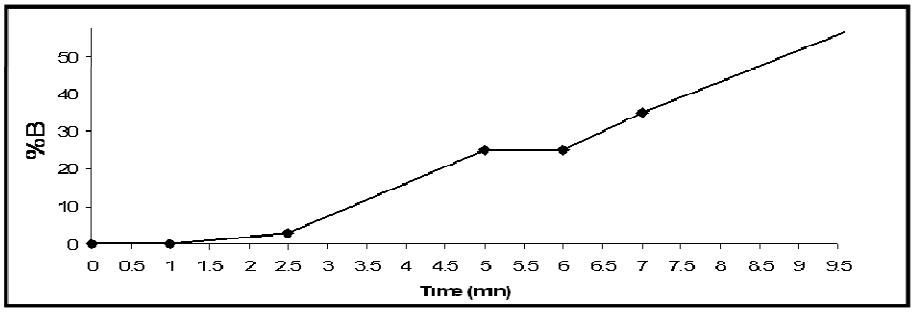

Figure 2.3. (A) The effect of increasing TrBA concentration on chromatographic resolution and retention of the commercially available heparin-derived disaccharides. (B) Illustration of the gradient profile showing the change in percentage of mobile phase buffer solution B as a function of time.

Table 2.2. Retention factors, widths at half height and peak areas for the RPIP-UPLC separation of the 11 commercially available disaccharides with 2.5 mM TrBA.

Disaccharide	[TrBA]	Retention Factor	$W_{1/2}$ (min)	Peak Area
IVH	2.5 mM	0.36 ± 0.02	0.076 ± 0.001	1932± 33
IVA	2.5 mM	5.85 ± 0.01	0.068 ± 0.002	594± 11
IVA anomer	2.5 mM	6.13 ± 0.03	0.078± 0.002	N/A
IIH	2.5 mM	5.74 ± 0.03	0.085 ± 0.001	2028± 16
IIH anomer	2.5 mM	6.67 ± 0.00	0.091 ± 0.004	988± 46
IIIH	2.5 mM	6.66 ± 0.00	0.071 ± 0.002	1407± 70
IIIH anomer	2.5 mM	7.52 ± 0.01	0.068 ± 0.001	784± 17
IIA	2.5 mM	13.18 ± 0.00	0.120 ± 0.001	4164± 20
IIIA	2.5 mM	14.00 ± 0.02	0.117 ± 0.006	3459± 14
IH	2.5 mM	14.93 ± 0.00	0.109 ± 0.003	2949± 54
IH anomer	2.5 mM	16.08 ± 0.03	0.093 ± 0.002	1764± 26
IIS	2.5 mM	17.67 ± 0.00	0.137 ± 0.001	4371± 43
IIIS	2.5 mM	18.70 ± 0.02	0.160 ± 0.011	5428± 36
IA	2.5 mM	17.98 ± 0.00	0.143 ± 0.001	6071 ± 54
IS	2.5 mM	19.93 ± 0.00	0.253 ± 0.003	10374± 36

Table 2.3. Retention factors, widths at half height and peak areas for the RPIP-UPLC separation of the 11 commercially available disaccharides using 5.0 mM TrBA.

Disaccharide	[TrBA]	Retention Factor	$W_{1/2}$ (min)	Peak Area
IVH	5 mM	0.37 ± 0.00	0.072± 0.002	1666± 37
IVA	5 mM	5.05 ± 0.00	0.075± 0.003	420± 20
IVA anomer	5 mM	5.40 ± 0.03	0.085± 0.001	N/A
IIH	5 mM	5.16 ± 0.00	0.088± 0.001	1498± 24
IIH anomer	5 mM	6.24 ± 0.03	0.093± 0.002	669± 37
IIIH	5 mM	6.53 ± 0.01	0.080± 0.002	999 ± 3
IIIH anomer	5 mM	7.45 ± 0.01	0.075± 0.003	624 ± 11
IIA	5 mM	13.00 ± 0.02	0.101± 0.001	3066± 38
IIIA	5 mM	13.90 ± 0.02	0.102± 0.001	2536± 19
IH	5 mM	15.06 ± 0.03	0.091± 0.001	1921± 22
IH anomer	5 mM	16.29 ± 0.02	0.079± 0.002	1147± 2
IIS	5 mM	17.91 ± 0.01	0.133± 0.003	3267± 42
IIIS	5 mM	18.94 ± 0.03	0.128± 0.001	3783± 20
IA	5 mM	18.28 ± 0.00	0.119± 0.006	4253± 38
IS	5 mM	20.38 ± 0.01	0.201± 0.008	7265± 143

Table 2.4. Retention factors, widths at half height and peak areas for the RPIP-UPLC separation of the 11 commercially available disaccharides with 10 mM TrBA.

Disaccharide	[TrBA]	Retention Factor	$W_{1/2}$ (min)	Peak Area
IVH	10 mM	0.37 ± 0.00	0.069 ± 0.002	532 ± 7
IVA	10 mM	3.88 ± 0.01	0.077 ± 0.004	216 ± 3
IVA anomer	10 mM	4.20 ± 0.01	0.081 ± 0.004	N/A
IIH	10 mM	4.20 ± 0.01	0.074± 0.002	444 ± 17
IIH anomer	10 mM	5.26 ± 0.00	0.063 ± 0.005	227 ± 3
IIIH	10 mM	5.77 ± 0.00	0.085 ± 0.004	538 ± 40
IIIH anomer	10 mM	6.61 ± 0.03	0.082 ± 0.004	290 ± 28
IIA	10 mM	12.49 ± 0.02	0.081 ± 0.001	1166 ± 22
IIIA	10 mM	12.78 ± 0.01	0.097 ± 0.002	1203 ± 57
IH	10 mM	13.95 ± 0.01	0.071 ± 0.001	666 ± 8
IH anomer	10 mM	15.13 ± 0.03	0.083 ± 0.002	491 ± 4
IIS	10 mM	17.74 ± 0.00	0.095 ± 0.001	1211 ± 5
IIIS	10 mM	17.87 ± 0.01	0.109 ± 0.004	1298 ± 29
IA	10 mM	18.23 ± 0.00	0.094 ± 0.002	1425 ± 6
IS	10 mM	20.40 ± 0.00	0.123 ± 0.004	1760 ± 25

Table 2.5. Retention factors, widths at half height and peak areas for the RPIP-UPLC separation of the 11 commercially available disaccharides with 20 mM TrBA.

Disaccharide	[TrBA]	Retention Factor	$W_{1/2}$ (min)	Peak Area
IVH	20 mM	0.44 ± 0.04	0.069± 0.002	861 ± 77
IVA	20 mM	3.07 ± 0.00	0.066± 0.002	272 ± 14
IVA anomer	20 mM	N/A	N/A	N/A
IIH	20 mM	3.33 ± 0.00	0.068± 0.002	945 ± 17
IIH anomer	20 mM	4.15 ± 0.01	0.088± 0.003	450 ± 24
IIIH	20 mM	5.20 ± 0.01	0.103± 0.007	534 ± 11
IIIH anomer	20 mM	5.96± 0.01	0.099± 0.005	520 ± 17
IIA	20 mM	11.95 ± 0.01	0.082± 0.001	1319 ± 64
IIIA	20 mM	12.40 ± 0.02	0.100± 0.008	1436 ± 43
IH	20 mM	13.71 ± 0.01	0.071± 0.002	601 ± 22
IH anomer	20 mM	14.75 ± 0.01	0.071± 0.002	622 ± 9
IIS	20 mM	17.73 ± 0.01	0.094± 0.002	2321 ± 18
IIIS	20 mM	18.00 ± 0.02	0.113± 0.004	2665 ± 52
IA	20 mM	18.47 ± 0.02	0.089± 0.003	1914 ± 40
IS	20 mM	20.95 ± 0.00	0.117± 0.005	3353 ± 42

concentrations. At a TrBA concentration of 2.5 mM, peaks are broad and are poorly resolved. As the TrBA concentration is increased to 20 mM, the peaks sharpen and resolution of all of the disaccharides in this sample is achieved. As expected, ion-pairing with TrBA resolves the disaccharides primarily based on charge. Disaccharide IVH, with a net charge of zero, is barely retained and elutes shortly after the column void while the most highly charged disaccharide, IS, with a net charge of -4 is the most highly retained. Within these extremes, groups of disaccharides having similar charges, elute in the expected order: disaccharides with a -1 net charge (IVA, IIH and IIIH) before those with a -2 net charge (IIA, IIIA, and IH) followed by the disaccharides having a net charge of -3 (IIS, IIIS and IA). For the compounds containing a free glucosamine residue, two peaks are detected for each compound due to resolution of the α and β anomers formed by mutarotation of the reducing-end glucosamine residue.[16] This phenomenon is explored in greater depth in Chapter 3. It is interesting that increasing the TrBA concentration does not produce large changes in the retention time for most species, and that the improved resolution achieved at higher concentrations can be attributed at least in part to sharpening of the peaks. It is also important to note that increasing the TrBA concentration of the mobile phase also increases ion suppression during MS detection similar to the behavior observed in Figure 2.2 with increasing ammonium concentration. For this reason when using MS detection the IPR mobile phase concentration should be optimized to maintain adequate analyte resolution and retention while minimizing ion suppression. Additionally this change in ion intensity with changing TrBA concentration

makes it difficult to extract useful information from the peak areas derived from the total ion chromatograms, for example in Tables 2.2-2.5.

2.3.2. Competition between TrBA and Ammonium Ion. Except for the incomplete resolution of the isomeric disaccharides IIS and IIIS, the quality of the separation in Figure 2.3A obtained with 20 mM TrBA is nearly as good as that reported by Korir et al. using 5 mM TrBA and 50 mM ammonium acetate.[12] Figure 2.4 shows the effect of adding 2.5 mM ammonium acetate to the mobile phase buffer containing 20 mM TrBA. As can be seen from the chromatogram in Figure 2.4, addition of a small amount of ammonium ion results in complete resolution of the disaccharide isomers IIS and IIIS, as well as partial resolution of the α and β anomers of disaccharides IVA and IS. The results achieved in Figure 2.4 suggest that competition between TrBA and ammonium for ion-pairing interactions with these disaccharides is at least partially responsible for their separation. Additionally, the overall decrease in retention of all disaccharides observed in Figure 2.4 is most likely a result of the lower hydrophobicity of the ammonium ion. Thus, any analyte interactions with ammonium take place in the mobile phase only, causing a decrease in retention time. Figure 2.5 also shows the application of the full isomer separation method used for Figure 2.4 to a heparin sample that had been exhaustively digested with heparinase I, II and III. The results in Figure 2.5 demonstrate the applicability of this separation to a real sample, and confirm the ability of the method to resolve disaccharide IVS, which was not included in Figure 2.4 because it was not commercially available at the time.

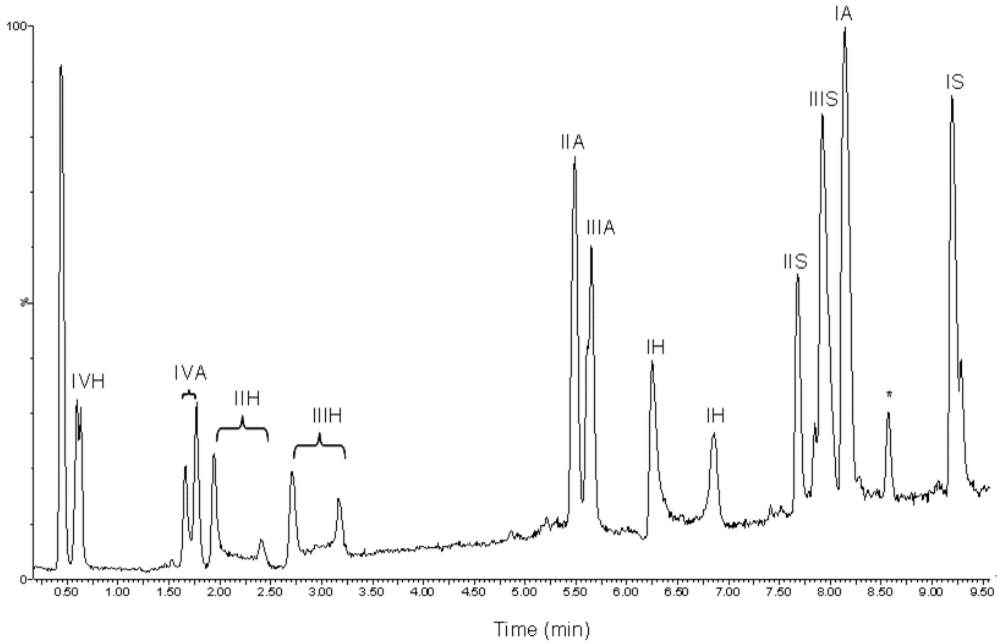

Figure 2.4. Optimized ion-pair separation of commercially available heparin-derived disaccharides. Mobile phase IPR concentration: 20mM TrBA, 2.5 mM ammonium acetate. The peak marked with an asterisk is an impurity.

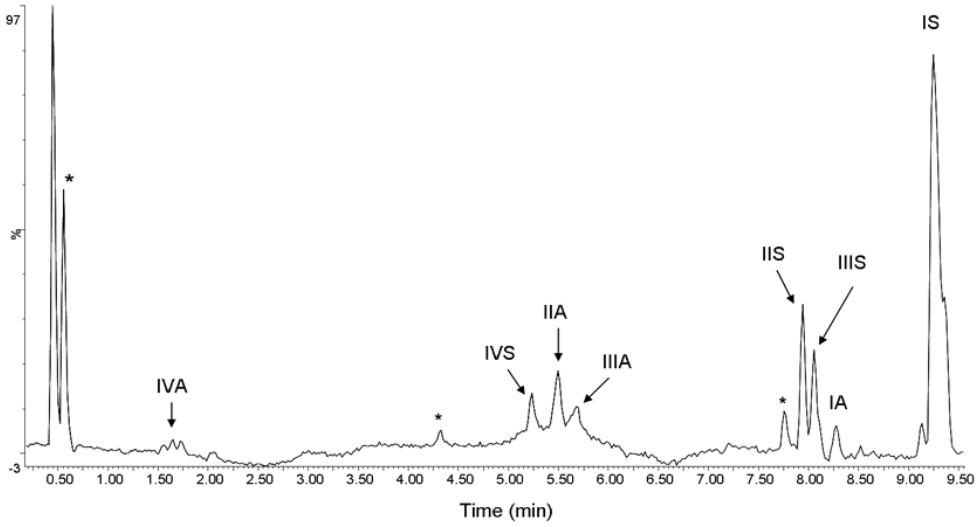

Figure 2.5. Separation of a heparin sample exhaustively digested with a cocktail of heparinase enzymes I, II and III. Mobile phase IPR concentration: 20 mM TrBA, 2.5 mM ammonium acetate. The peaks marked with an asterisk are impurities.

2.3.3. Competition between TrBA and MBA. To further investigate the possibility that competition between IPRs occurs and is an important component of the separation mechanism, the effects of varying the MBA concentration while maintaining a constant TrBA concentration of 2.5 mM was studied. MBA was chosen because its single butyl side chain should allow some retention of the MBA-disaccharide ion-pair on the reverse phase column. However, because MBA is less hydrophobic than TrBA, competition between these ions should be visible through changes in retention time. The results presented in Figure 2.6 show the effect of increasing MBA concentration on the separation of the isomeric disaccharides IIA and IIIA, selected because the glucosamine nitrogen of these compounds is *N*-acetylated simplifying the nature of the interactions with the IPR.

As can be seen in Figure 2.4, disaccharide IIIA, which elutes after disaccharide IIA, has a greater ion-pairing affinity for TrBA under the separation conditions employed, 20 mM TrBA and 2.5 mM ammonium. In Figure 2.6A, when only 20 mM MBA is used as an IPR (no TrBA is present), sharp peaks are obtained for both disaccharides at 0.78 min. With a mobile phase containing 20 mM MBA and 2.5 mM TrBA, shown in Figure 2.6B, each disaccharide produces several relatively sharp chromatographic peaks between 1.00 and 2.00 min. Close examination reveals that IIIA has greater peak dispersion and retention of the later eluting components. We attribute these peaks to the partial chromatographic resolution of species in which the disaccharides are bound to MBA and TrBA over the course of the separation, and are in slow exchange on the time scale of the chromatographic separation. Even though TrBA

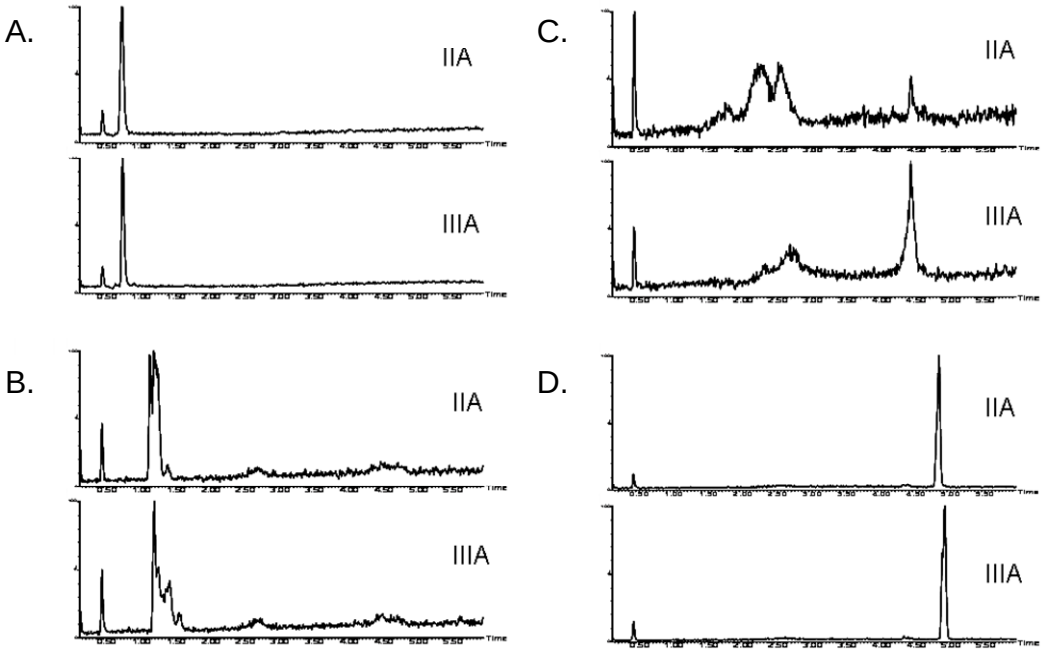

Figure 2.6. The effect of competition between the IPRs MBA and TrBA on the *N*-acetylated disaccharides IIA and IIIA. Mobile phase IPR concentration: (A) 20 mM MBA (B) 20 mM MBA, 2.5 mM TrBA (C) 15 mM MBA, 2.5 mM TrBA (D) 10 mM MBA, 2.5 mM TrBA.

is more hydrophobic and should have a greater effect on retention, MBA is present at a much higher concentration and the poor retention suggests that MBA interactions dominate. At an intermediate concentration of 15 mM MBA, shown in Figure 2.6C, a transition point is reached in the retention of both the IIA and the IIIA isomers at which two types of ion-pair species are both present and resolved in the chromatogram. As expected from the separation in Figure 2.4, disaccharide IIIA appears to have a greater ion-pairing interaction with TrBA than disaccharide IIA in Figure 2.6C. The broad peaks detected in this separation further suggest that exchange between MBA and TrBA ion-pairs is occurring on the chromatographic time scale. It is also interesting that there appears to be two different types of ion-pair species formed, and with different populations for disaccharides IIA and IIIA. The broad peaks observed between 2 and 3 min suggest involvement of both MBA and TrBA in ion-pairing. The sharper and more highly retained peaks at around 4.5 min likely results from stable TrBA ion-pairs. Figure 2.6D, shows that when the MBA concentration is decreased to 10 mM, a single chromatographic peak is now detected for each disaccharide. The longer retention time observed in Figure 2.6D likely reflects the larger relative population of TrBA–disaccharide ion-pairs. The sharpness of these peaks suggests either that competition between the TrBA and MBA is fast on the time scale of the separation, or more likely that TrBA dominates the ion-pairing interactions. MS analysis of the mass spectra for the chromatographic peaks did not yield further insights into this matter as no MBA or TrBA adducts to the heparin disaccharides could be detected in either negative or positive mode ESI. In fact, no disaccharide ions were detected positive mode. It is also important to

note that the overall lower retention of the disaccharides in Figure 2.6B-D as compared to Figure 2.2A where only 2.5 mM TrBA is present is most likely due to the presence of the less hydrophobic MBA thus reducing the surface potential of the stationary phase.

2.3.4. Competition between TrBA and DBA. Experiments exploring the competition between TrBA and dibutylamine (DBA) were also conducted. As a result of the similarity in the hydrophobicities of TrBA and DBA, competition between the two could not be easily visualized through changes in retention of any of the disaccharides as was observed for the competition of TrBA and MBA. Interestingly, the extracted MS spectrum for the IS disaccharide peak shown in Figure 2.7 reveals that unlike TrBA and MBA, DBA efficiently adducts to IS. However, this is only observed for the IS disaccharide. It is also important to note that little to no sulfate loss is observed in MS spectrum in Figure 2.7 suggesting that the formation of adduct ions may increase the stability of the sulfate group which could be important for structurally characterizing larger heparin derived oligosaccharides by MS/MS.

2.3.5. HR-MAS STD NMR. To explore whether the ion-pair interactions discussed thus far occur primarily in solution or at the stationary phase surface, HR-MAS STD NMR experiments were performed. In these experiments resonances on the C18 stationary phase were saturated and the transfer of this saturation to the IPR, TMA, and its ion-pairing partner BSFA were monitored. TMA was chosen as the IPR instead of TrBA in this experiment because its only NMR resonance is a singlet that is well resolved from the resonances of the C18. BSFA was chosen because its only NMR

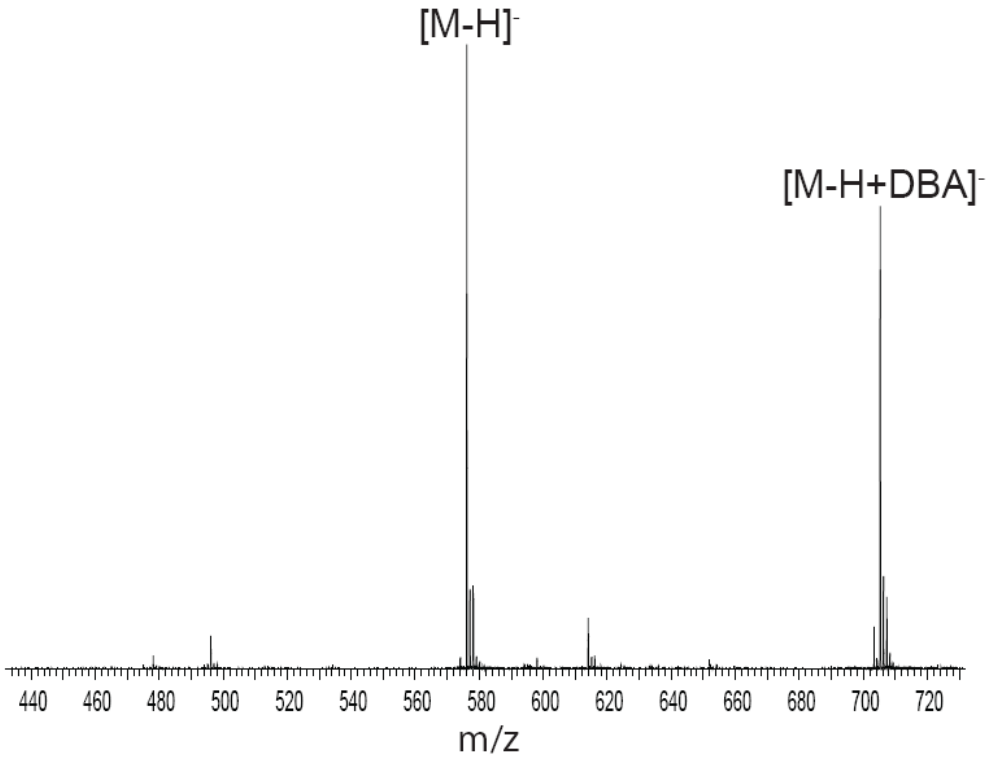

Figure 2.7. Extracted MS spectrum of the IS disaccharide from the separation of the commercially available heparin derived disaccharides with mobile phase buffers consisting of 20 mM TrBA and 2.5 mM DBA at pH 6.5.

resonances are in the aromatic region of the ^{1}H spectrum which are also well resolved from both those of C18 and TMA.

As a control experiment, Figure 2.8A, shows the HR-MAS STD NMR spectrum of buffer containing only 30 mM TMA at pD 7.0 and a solvent composition of 85% D_2O/15% deuterated-ACN (containing 100 mM protonated ACN to allow monitoring of the ACN resonance) in a rotor insert packed with C18 stationary phase. This spectrum clearly shows transfer of saturation from the C18 stationary phase to the methyl groups of TMA and to the ACN resonance. This result suggests that under these conditions the hydrophobic methyl groups of TMA interact with the C18 stationary phase creating an ion-exchange like stationary phase.

In Figure 2.8B 30 mM BSFA was added to the buffer solution used in Figure 2.8A to see if the formation of an ion-pair between BSFA and TMA would change the degree of interaction between TMA and the stationary phase surface. In Figure 2.8B we see a slight increase in the intensity of TMA compared to Figure 2.8A. This suggests that by ion-pairing with BSFA, TMA's interaction with the stationary phase is strengthened. Furthermore, comparing Figure 2.8B to Figure 2.8C where the percentage of ACN in the buffer was increased to 30% there is almost no visible intensity difference between the TMA resonances. This suggests that addition of ACN to the buffer had very little effect on the interaction between TMA and the stationary phase. In Figures 2.9B and C we further see that saturation is also being transferred to the BSFA molecules either through transfer of saturation from the TMA molecules it ion-pairs or by interaction of the benzene group of BSFA directly with the stationary phase.

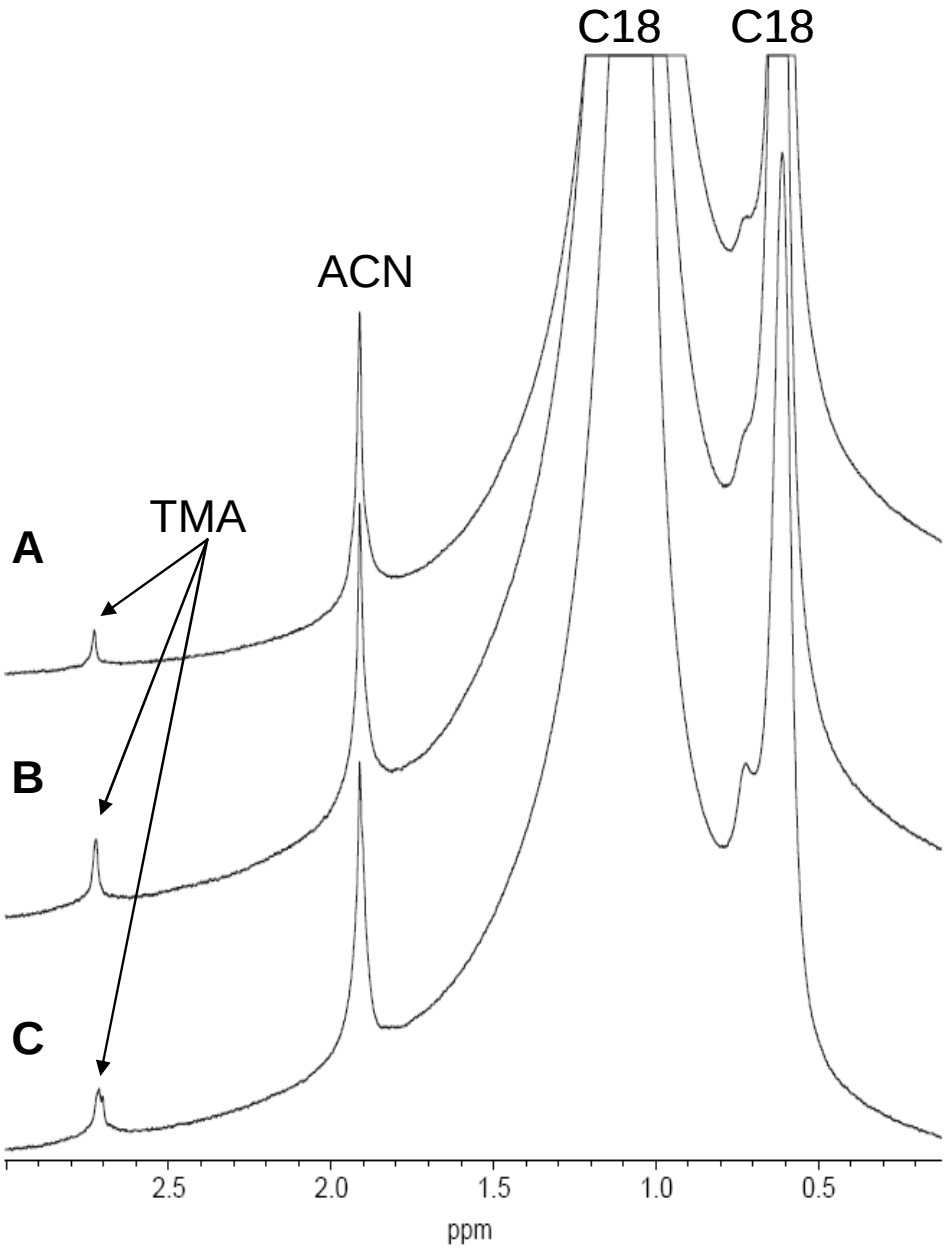

Figure 2.8. HR-MAS STD NMR spectra measured for rotor inserts packed with C18 stationary phase and 30 μL of A) 30 mM TMA pD 7.0 in 85:15 D_2O:deuterated ACN (100 mM protonated), B) 30 mM TMA and 30 mM BSFA pD 7.0 in 85:15 D_2O:deuterated ACN (100 mM protonated) and C) 30 mM TMA and 30 mM BSFA pD 7.0 in 70:30 D_2O:deuterated ACN (100 mM protonated).

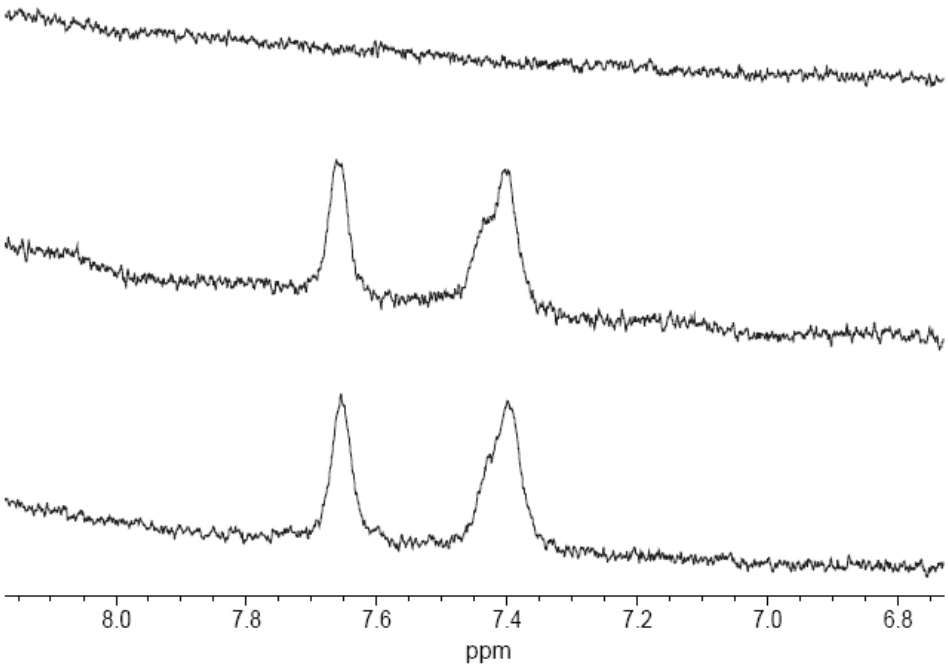

Figure 2.9. Expansion of the aromatic region of the HR-MAS STD NMR spectra of rotor inserts packed with C18 stationary phase and 30 μL of A) 30 mM TMA pD 7.0 in 85:15 D_2O:deuterated ACN (100 mM protonated), B) 30 mM TMA and 30 mM BSFA pD 7.0 in 85:15 D_2O:deuterated ACN (100 mM protonated) and C) 30 mM TMA and 30 mM BSFA pD 7.0 in 70:30 D_2O:deuterated ACN (100 mM protonated).

2.4. Discussion

In RPIP separations, the retention of analytes is determined by several factors. These include the hydrophobicity of the stationary phase, organic concentration of the mobile phase, charge of analytes at the experimental pH, as well as charge, concentration and hydrophobicity of the IPR.[1, 10] In the electrostatic model of retention through ion-paring, the hydrophobic IPRs are first adsorbed onto the surface of the hydrophobic stationary phase where, in the case of this study, the disaccharides interact electrostatically with the positive charge of the alkyl ammonium IPR through the negative surface potential that is generated by their carboxylate and sulfonate groups. Electrostatic ion-pair formation can also occur in the mobile phase prior to interaction with the stationary phase with retention of the ion-pair occurring at the stationary phase surface.

From these models, certain retention trends for this series of disaccharides can be hypothesized. First, as discussed previously, as the concentration of the IPR is increased the retention of the disaccharides should also increase.[17] However, as seen in Figure 2.3A, this is only the case for the later eluting disaccharides IIS, IIIS, IA, and IS. The retention times of disaccharides IH and IVH are unaffected by the increase in TrBA concentration, while disaccharides IIA, IIIA, IVA, IIH, and IIIH show a decrease in retention time as the concentration of TrBA is increased. This phenomenon could be explained in part by the mechanism of stationary phase volume exclusion resulting from coating of the stationary phase with TrBA, similar to the “cation exclusion” mechanism

described by Loeser et al.[18] In this mechanism, instead of the surface charge of the stationary phase causing volume exclusion, it is the size of the TrBA molecules coating the surface of the stationary phase that blocks the disaccharides from accessing the stationary phase pore volume. Thus as the TrBA concentration is increased, more of the pore volume will be blocked resulting in less retention of the disaccharides by the stationary phase. However, at higher organic mobile phase concentrations, a portion of the TrBA coating is washed away and normal retention trends are expected, as observed in Figure 2.3A for disaccharides IIS, IIIS, IA, and IS which elute at higher organic concentrations produced by the gradient profile shown in Figure 2.3B.

An alternative explanation for these results is that as the TrBA concentration is increased the concentration of the counterion, in this experiment acetate, is also increased relative to the constant concentration of heparin disaccharides. Because acetate is negatively charged it can compete with heparin for interaction with TrBA and thus lower the overall surface potential of the stationary phase causing a decrease in retention of the disaccharides. Additionally, it is possible that the disaccharides with a -1 and -2 net charge have a higher propensity to ion-pair in the mobile phase which would remove these analyte ions from interacting with the stationary phase decreasing their retention factor.[3] With increasing TrBA concentration there would be an increased percentage of TrBA in the mobile phase making this effect more pronounced and reducing the retention of these disaccharides.

To test which theory best explains the observed retention behavior, a series of isocratic separations were performed with 30% buffer B (the approximate percentage at

which disaccharide IS elutes) while increasing the TrBA concentration. Table 2.6 summarizes the changes in retention factor for each disaccharide as a function of TrBA concentration. As can be seen from this table, the poorly retained disaccharides IVH, IVA, IIH, and IIIH show an initial small increase in retention factor when the TrBA concentration is increased from 2.5 to 5.0 mM followed by a small decrease in retention factor when the concentration of TrBA is increased further to 10 and 20 mM. A similar but more pronounced trend is observed for disaccharides IIA and IIIA. The retention factor for disaccharide IH decreases with increasing TrBA concentration while disaccharides IIS, IIIS, IA and IS show an increase in retention factor with increasing TrBA concentration. It is interesting that while disaccharide IIIS has a higher retention factor for 20 mM TrBA than for 2.5 mM there is an initial spike in its retention factor at 5.0 mM TrBA similar to that observed for the -1 and -2 charge state disaccharides. This is in contrast to the trend seen for IIS, for which the retention factor increases with increasing TrBA concentration. The results summarized in Table 2.6 show similar retention trends to those seen in Figure 2.3 but with a higher organic concentration. This suggests that the reason the -1 and -2 charge state disaccharides show a decrease in retention with increasing TrBA concentration may be due to the increasing concentration of acetate, which can also ion pair with TrBA. However, because the -1 and -2 charge state disaccharides are so poorly retained in this isocratic experiment it is hard to judge whether the observed trends are sufficiently significant to completely eliminate a role of pore exclusion effects on the disaccharide retention factors. The results of the HR-MAS STD experiments in Figures 2.8 and 2.9 suggest that at least for the IPR TMA that the

Table 2.6. Retention factors for the 11 commercially available disaccharides using 30% mobile phase buffer B at 2.5, 5, 10 and 20 mM TrBA concentration.

Disaccharide	[TrBA]	Retention Factor	[TrBA]	Retention Factor	[TrBA]	Retention Factor	[TrBA]	Retention Factor
IVH	2.5 mM	0.11 ± 0.00	5 mM	0.13± 0.00	10 m M	0.12 ± 0.01	20 mM	0.11± 0.00
IVA	2.5	0.34 ± 0.00	5	0.37± 0.00	10	0.35 ± 0.02	20	0.34± 0.00
IIH	2.5	0.30 ± 0.00	5	0.33± 0.00	10	0.30 ± 0.02	20	0.27± 0.01
IIIH	2.5	0.30 ± 0.00	5	0.33± 0.00	10	0.33 ± 0.00	20	0.27± 0.00
IIA	2.5	0.62 ± 0.00	5	0.65± 0.00	10	0.64 ± 0.02	20	0.59± 0.01
IIIA	2.5	0.65 ± 0.02	5	0.70± 0.00	10	0.67 ± 0.03	20	0.58± 0.01
IH	2.5	0.69 ± 0.00	5	0.65± 0.00	10	0.66 ± 0.02	20	0.61± 0.00
IIS	2.5	0.89 ± 0.00	5	1.07± 0.00	10	1.08± 0.05	20	1.09± 0.02
IIIS	2.5	0.99 ± 0.02	5	1.17± 0.00	10	1.14 ± 0.03	20	1.08± 0.02
IA	2.5	0.96 ± 0.02	5	1.17± 0.00	10	1.16 ± 0.03	20	1.21± 0.00
IS	2.5	1.30 ± 0.00	5	1.83± 0.00	10	1.89 ± 0.04	20	2.21± 0.00

interaction between the IPR and the stationary phase doesn't change much with increasing organic concentration further shedding doubt on the role of pore exclusion effect.

The separation of groups of disaccharides according to their net negative charge, as is observed in Figures 2.3 and 2.4, can be explained simply by an increase in the average number of ion-pair interactions with increasing disaccharide charge. However, this simple mechanism fails to fully explain the chromatographic resolution of the structurally similar isomeric pairs IIH/IIIH, IIA/IIIA, and IIS/IIIS, for which the only difference is sulfonation at either the C6 position of the glucosamine residue or the C2 position of the uronic acid residue. To understand how these compounds might be resolved in RPIP separations, the sites of electrostatic interaction with the IPR must be considered as well as the role that competition between different IPRs may play in the resolution of the individual isomers.

As shown in Figure 2.3A, all of the disaccharide isomers except IIS and IIIS can be resolved simply by using 20 mM TrBA as the IPR. Further examination of the structures of the IIH/IIIH and IIA/IIIA isomers suggests that a mechanism based on the sterics of the ion-pairing interaction may be involved in this separation. In disaccharides IIH and IIA, the sulfonate at the glucosamine C6 is in close proximity to the negatively charged carboxylate moiety of the uronic acid residue in comparison to length of the TrBA butyl arms. Interaction of a TrBA cation with either the glucosamine C6 sulfonate or the carboxylate group would sterically hinder ion-pairing with a second TrBA ion at the other site. However, in the case of disaccharides IIIH and IIIA, which are more

highly retained than their isomeric analogs, the uronic acid C2 sulfonate and the carboxylate moiety are oriented away from each other in space allowing ion-paring with TrBA at both sites simultaneously, leading to greater interactions with the stationary phase. For disaccharides IIS and IIIS, N-sulfonation of the glucosamine adds another point of interaction with the IPR, increasing their retention relative to IIH/IIIH or IIA/IIIA. The glucosamine *N*-sulfonate and uronic acid C2 sulfonate are sufficiently close in disaccharide IIIS that ion-pairing with one TrBA sterically hinders interaction of second TrBA ion with the other site. Therefore, the net ion-pairing interactions of IIS and IIIS are similar, and they have similar retention times as shown in Figure 2.3A.

Addition of 2.5 mM ammonium ion improves the resolution of disaccharides IIS and IIIS, as shown in Figure 2.4, suggesting that competition between the TrBA and ammonium ions is responsible for the separation of these isomers. A separation mechanism involving competition of the smaller ammonium ion with the much larger TrBA should be reflected in changes in the retention time of the isomer with the greatest degree of steric crowding at TrBA interaction sites. Comparison of Figures 2.3A and 2.4 indicate that the retention time of IIIS is essentially unchanged in the presence of 2.5 mM ammonium ion, while the retention time of IIS decreases from 7.93 min in Figure 2.3a to 7.67 min in Figure 2.4. As was observed for disaccharides IIH and IIA, this result suggests that steric effects have a more significant impact on ion-pairing interactions with TrBA and disaccharide IIS.

The results shown in Figure 2.6 further probe the nature of competition between IPRs in this separation. Figure 2.6C shows that at an intermediate concentration of 15

mM MBA a transition point is reached in the retention of the isomeric pair IIA/IIIA where two ion-pair species are resolved in the chromatogram shown in Figure 2.6C. In addition to the sharper peak at 4.48 min that we attribute to the TrBA ion-pair, two broad peaks are also detected between 2 and 3 min for each disaccharide. Because these peaks have a retention time that is intermediate between that of MBA and TrBA alone, they might be attributed to ion-pairs with both MBA and TrBA. Even at concentrations of 20 mM MBA and 2.5 mM TrBA (Figure 2.6B), slow exchange between multiple ion-pair species leads to partial resolution and broadening compared to the peak widths obtained when only 20 mM MBA is present. Overall lower retention of the disaccharides is observed in Figures 2.6B-D compared with Figure 2.3A where only 2.5 mM TrBA is present. As mentioned previously, this is most likely due to a reduction in the surface potential of the stationary phase induced by MBA, a less hydrophobic IPR. Although this study examined only the mass spectrometry-compatible IPRs: TrBA, MBA, and ammonium, other IPRs used for ion-pairing with heparin such as tetrabutylammonium (TBA), should have similar separation mechanisms as previous heparin disaccharide separations using these alternate IPRs show identical elution orders as those presented in this work.[11, 19] One would expect similar separation mechanisms to apply to other classes of closely related hydrophilic anions, but the extent of competition effects should be highly dependent on the strength of the ion-pairing interactions themselves. If the IPR interacts tightly with the analyte it would be more difficult for another IPR to compete for that interaction. In this regime steric interactions would be expected to dominate the separation mechanism.

Beyond the factors already discussed, peak width also affects the chromatographic resolution of the heparin disaccharide family. As observed in Figure 2.3A, increasing the TrBA concentration decreases the peak width. It is this decrease in peak broadening at high TrBA concentrations, more so than changes in relative retention times, that is responsible for the partial resolution of the IIS and IIIS isomers. With such a complex system, peak broadening effects must be interpreted with some caution, considering that multiple equilibria are involved. However, the results in Figure 2.3A suggest that when TrBA is at high concentration, stable ion-pairs are formed, decreasing the peak broadening that would result from partial resolution of ion-pairs with different configurations (e.g. those having either one or two associated TrBA ions). This hypothesis is reinforced by the results presented in Figure 2.6 showing clear chromatographic resolution of different types of disaccharide ion-pairs.

While the previous mechanisms serve well to explain isomer separation, the phenomena of anomeric resolution requires an alternative explanation. As seen in Figures 2.3 and 2.4, chromatographic resolution of the α and β anomers is most significant for disaccharides with an unsubstituted glucosamine residue, suggesting that the partial positive charge state of this amine plays a role in the chromatographic resolution of these anomers. This phenomenon has also been observed in CE separations of heparin disaccharides and glucosamine.[16, 20] Our initial hypothesis was that the resolution of the α and β anomers of the disaccharides IH, IIH and IIIH in these separations could be attributed to differences in the pKa values of the glucosamine primary amine group. For example, Blaskó et al. report that the β-anomer ammonium

group of glucosamine is more acidic (pKa = 7.87) compared to the α anomer (pKa = 8.12).[21] This suggests that under our separation conditions, the α-anomers of disaccharides IH, IIH and IIIH have a higher average population of species with a positively charged primary amine, and thus an overall lower net negative charge. This lower negative electrostatic charge would reduce the overall interaction of the α anomers with the IPRs causing them to elute prior to the corresponding β anomers. However, unless the specific goal of the experiment required resolution of the α and β anomers, better chromatographic resolution and quantitation of heparin disaccharides could be achieved by adjusting the mobile phase pH away from the glucosamine pKas, providing that effective resolution of the entire disaccharide family could still be achieved. This phenomenon is explored in detail in the next chapter in which the effects of the mobile phase pH, IPR counterion, and buffer components on the anomeric resolution of heparin-derived disaccharides containing positively charged GlcN primary amine functional groups or uncharged *N*-acetyl glucosamine (GlcNAc) residues is studied.

2.5. Conclusions

Because of the potential versatility and effectiveness of RPIP-HPLC and UPLC in the separation and study of a wide range of charged hydrophilic analytes, including heparin and HS disaccharides, it is important to improve our mechanistic understanding of separations based on ion-pairing interactions. An improved understanding of the separation mechanism assists in the development and refinement of new separation

methods for complex mixtures of structurally similar analytes. This study focused on the effects of competition between TrBA and two other positive but less hydrophobic IPRs, MBA and ammonium, on the UPLC resolution of structural isomers of heparin disaccharides having subtle differences in charge and structure. Although the results of this work focused primarily on the mechanism of heparin disaccharide separation using TrBA as an IPR, it should be noted that we expect other bulky cationic IPRs such as TBA to operate by a similar separation mechanism. The knowledge gained from this study could provide significant insights leading to the development of RPIP-UPLC methods for the separation of larger heparin oligosaccharides, as well as other complex mixtures of structurally-similar ionic compounds.

In chapter 3 the effects of the mobile phase pH, IPR counterion, and buffer components on the anomeric resolution of heparin-derived disaccharides containing positively charged GlcN primary amine functional groups or uncharged *N*-acetyl glucosamine (GlcNAc) residues is further explored. Also an optimized separation of the 11 commercially available heparin disaccharides with minimal resolution of the anomeric species is presented.

2.6. References

1. Cecchi, T., Ion pairing chromatography. *Crit. Rev. Anal. Chem.* **2008,** 38, 161 - 213.

2. Cecchi, T., *Ion-pair chromatography and related techniques*. Taylor & Francis Group: 2009.

3. Cecchi, T.; Pucciarelli, F.; Passamonti, P., Extended thermodynamic approach to ion interaction chromatography. *Anal. Chem.* **2001,** 73, 2632-2639.

4. Horvath, C.; Melander, W.; Molnar, I.; Molnar, P., Enhancement of retention by ion-pair formation in liquid chromatography with nonpolar stationary phases. *Anal. Chem.* **1977,** 49, 2295-2305.

5. Knox, J. H.; Laird, G. R., Soap chromatography--a new high-performance liquid chromatographic technique for separation of ionizable materials : Dyestuff intermediates. *J. Chromatogr.* **1976,** 122, 17-34.

6. Wittmer, D. P.; Nuessle, N. O.; Haney, W. G., Simultaneous analysis of tartrazine and its intermediates by reversed phase liquid chromatography. *Anal. Chem.* **1975,** 47, 1422-1423.

7. Hoffman, N. E.; Liao, J. C., Reversed phase high performance liquid chromatographic separations of nucleotides in the presence of solvophobic ions. *Anal. Chem.* **1977,** 49, 2231-2234.

8. Kissinger, P. T., Reverse-phase ion-pair partition chromatography. Comments. *Anal. Chem.* **1977,** 49, 883-883.

9. Kraak, J. C.; Jonker, K. M.; Huber, J. F. K., Solvent-generated ion-exchange systems with anionic surfactants for rapid separations of amino acids. *J. Chromatogr.* **1977,** 142, 671-688.

10. El Rassi, Z., Recent progress in reversed-phase and hydrophobic interaction chromatography of carbohydrate species. *J. Chromatogr., A* **1996,** 720, 93-118.

11. Karamanos, N. K.; Vanky, P.; Tzanakakis, G. N.; Tsegenidis, T.; Hjerpe, A., Ion-pair high-performance liquid chromatography for determining disaccharide composition in heparin and heparan sulphate. *J. Chromatogr., A* **1997,** 765, 169-179.

12. Korir, A. K.; Limitiaco, J. F. K.; Gutierrez, S. M.; Larive, C. K., Ultraperformance ion-pair liquid chromatography coupled to electrospray time-of-flight mass spectrometry for compositional profiling and quantification of heparin and heparan sulfate. *Anal. Chem.* **2008,** 80, 1297-1306.

13. Albert, K., NMR investigations of stationary phases. *J. Sep. Sci.* **2003,** 26, 215-224.

14. Friebolin, V.; Bayer, M. P.; Matyska, M. T.; Pesek, J. J.; Albert, K., ^{1}H HR/MAS NMR in the suspended state: Molecular recognition processes in liquid chromatography between steroids and a silica hydride-based cholesterol phase. *J. Sep. Sci.* **2009,** 32, 1722-1728.

15. Hellriegel, C.; Skogsberg, U.; Albert, K.; LÃ¤mmerhofer, M.; Maier, N. M.; Lindner, W., Characterization of a chiral stationary phase by HR/MAS NMR spectroscopy and investigation of enantioselective interaction with chiral ligates by transferred NOE. *J. Am. Chem. Soc.* **2004,** 126, 3809-3816.

16. Skelley, A. M.; Mathies, R. A., Rapid on-column analysis of glucosamine and its mutarotation by microchip capillary electrophoresis. *J. Chromatogr., A* **2006,** 1132, 304-309.

17. Kuberan, B.; Lech, M.; Zhang, L.; Wu, Z. L.; Beeler, D. L.; Rosenberg, R. D., Analysis of heparan sulfate oligosaccharides with ion pair-reverse phase capillary high performance liquid chromatography-microelectrospray ionization time-of-flight mass spectrometry. *J. Am. Chem. Soc.* **2002,** 124, 8707-8718.

18. Loeser, E.; Drumm, P., Investigation of anion retention and cation exclusion effects for several C18 stationary phases. *Anal. Chem.* **2007,** 79, 5382-5391.

19. Toyoda, H.; Yamamoto, H.; Ogino, N.; Toida, T.; Imanari, T., Rapid and sensitive analysis of disaccharide composition in heparin and heparan sulfate by reversed-phase ion-pair chromatography on a 2 [mu]m porous silica gel column. *J. Chromatogr., A* **1999,** 830, 197-201.

20. Eldridge, S. L.; Korir, A. K.; Gutierrez, S. M.; Campos, F.; Limtiaco, J. F. K.; Larive, C. K., Heterogeneity of depolymerized heparin SEC fractions: to pool or not to pool? *Carbohydr. Res.* **2008,** 343, 2963-2970.

21. Blaskó, A.; Bunton, C. A.; Bunel, S.; Ibarra, C.; Moraga, E., Determination of acid dissociation constants of anomers of amino sugars by 1H NMR spectroscopy. *Carbohydr. Res.* **1997,** 298, 163-172.

CHAPTER THREE

Understanding the Role that Counterions play in the Anomeric Resolution of Heparin Related Oligosaccharides by Reverse-Phase Ion-Pair High-Performance Liquid Chromatography

Based on a paper published in Analytical Chemistry

Anal. Chem., 2011, 83, 6762-6769.

In this chapter, the effects of ion-pairing reagent (IPR) concentration, counterion and mobile phase pH on the quality of the RPIP-UPLC separation were examined with particular emphasis on how these factors impact the separation of heparin-derived disaccharide anomers. This work builds on the separation presented in chapter 2 and explores mobile phase conditions that minimize anomeric resolution. These results highlight the role of the IPR counterion and demonstrate that the resolution of disaccharide anomers can be minimized by conducting the separation at low pH, simplifying chromatographic analysis and improving resolution. I performed the experiments, processed the data and interpreted the results with helpful contributions from Dr. Szabolcs Beni.

3.1 Introduction

In chapter two efforts were made to probe the mechanism of the RPIP-UPLC separation of the 11 commercially available heparin derived disaccharides focusing on the nature of specific interactions between the analytes and the IPR tributylamine (TrBA)

as well as the role that competition between different IPR's plays in the resolution of sulfonation isomers. That work also demonstrated the unintentional resolution of the anomeric forms of several of the disaccharide standards, particularly those containing an unsubstituted amino moiety. Although it is interesting that the different anomeric forms of the same disaccharide can be resolved through RPIP-UPLC, this is usually not desirable and better chromatographic resolution and sensitivity could be achieved by minimizing the separation of the disaccharide anomers. The work in this chapter explores the effects of the mobile phase pH, IPR counterion, and buffer components on the anomeric resolution of heparin-derived disaccharides containing positively charged GlcN primary amine functional groups or uncharged N-acetyl glucosamine (GlcNAc) residues. Finally, in this chapter the optimized separation of 11 commercially available heparin disaccharides with minimal resolution of the anomeric species is presented.

3.2 Experimental

3.2.1 Materials and Reagents. All *N*-sulfonated and *N*-amino heparin disaccharide standards were purchased from the Sigma Chemical Company (St. Louis, MO). All *N*-acetylated heparin disaccharide standards were purchased from V-labs (Covington, LA). Table 3.1 lists the names and structures of the disaccharides studied. Glucosamine derivatives and the internal standard, ΔUA2S-GlcNCOEt6S (IP) were also purchased from V-Labs (Covington, LA). The IPR TrBA (purity ≥ 99.5%) and acetonitrile (optima grade) were also purchased from Sigma. HPLC grade water was

Table 3.1. Names and structures of the family of heparin disaccharides studied.

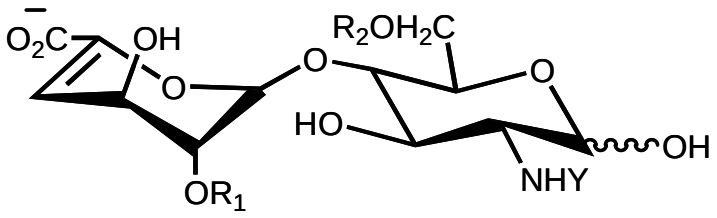

Disaccharide	R_1	R_2	Y
IS	SO_3^-	SO_3^-	SO_3^-
IIS	H	SO_3^-	SO_3^-
IIIS	SO_3^-	H	SO_3^-
IA	SO_3^-	SO_3^-	Ac
IIA	H	SO_3^-	Ac
IIIA	SO_3^-	H	Ac
IVA	H	H	Ac
IH	SO_3^-	SO_3^-	H
IIH	H	SO_3^-	H
IIIH	SO_3^-	H	H
IVH	H	H	H

purchased from Honeywell Burdick & Jackson. Ammonium acetate, ammonium formate, formic acid, and acetic acid were purchased from Fisher Scientific (Pittsburgh, PA).

3.2.2 UPLC Separation. All chromatographic separations were performed on a 2.1 x 100 mm AcquityTM UPLC BEH C18 column with 1.7 μm particles (Waters Corporation, Milford, MA). A guard column packed with the same 1.7 μm C18 particles was utilized prior to the analytical column. A sample volume of 10 μL of a 0.2 mM solution of either a disaccharide or monosaccharide mixture prepared in water was injected for each separation. A binary solvent system was used for gradient elution. Solvents A and B consisted of 5% and 50 % acetonitrile in aqueous buffer, respectively.

3.2.2.1 Study of the Effect of Mobile Phase pH and Counterion Makeup on Mono- and Disaccharide Anomer Resolution and Retention. Initial separations using the chromatographic method from chapter 2 for resolving heparin-derived disaccharides used a buffer containing 20 mM TrBA and 2.5 mM ammonium acetate at pH 6.5. To study the effect that buffer pH has on the resolution and retention of the anomers of N-unsubstituted disaccharides as well as the monosaccharides GlcN(6S), GlcNS, and GlcNS(6S), buffers were prepared containing 20 mM TrBA and either 2.5 mM ammonium acetate or 2.5 mM ammonium formate at the studied pH. In both cases the buffers were initially prepared by making an aqueous solution of 40 mM TrBA and either 5.0 mM ammonium acetate or ammonium formate and were titrated to the desired pH with either acetic acid or formic acid. The buffers were then diluted to their final concentration with the appropriate volumes of water and acetonitrile to give buffers containing 5% (A) or 50% (B) acetonitrile.

The gradient profile for the experiments studying the effect of pH on anomer resolution consisted of a 1 min isocratic step of 100% solvent A after which the fraction of solvent B was increased to 4.8% over the next 1.5 min. The fraction of solvent B was increased to 40% over the next 2.5 min and maintained at 40% for 1 min before it was increased to 56% over a 1 min period. The fraction of solvent B was then increased over the next 3 min to 96%. Finally, the fraction of solvent B was increased to 100% over the next two minutes. A 5 min equilibration period was utilized prior to the next injection. This gradient program was selected because in chapter 2 we found it to provide the best separation of the 11 commercially available disaccharide standards. For these experiments the column temperature was maintained at 40°C and the flow rate was kept at a constant 0.5 mL/min. All the chromatograms were measured in triplicate and representative chromatograms are shown.

3.2.2.2 Mobile Phase pH and Gradient Parameters for Separation Conditions that Minimize Anomer Resolution. As will be discussed in the results section, a buffer system was identified that minimized resolution of the anomers of the 11 disaccharides studied while still achieving full separation of the isomeric components. This buffer contained 30 mM TrBA at pH 3.5 and was prepared from an aqueous solution of 60 mM TrBA titrated to pH 3.5 with formic acid. This solution was diluted with water and acetoniltrile to make mobile phase buffers containing 30 mM TrBA and either 5% (A) or 50% (B) acetonitrile. Subsequent experiments designed to observe the effect of column temperature on the resolution of *N*-acetylated di- and monosaccharides also used this buffer system. However, separations to evaluate the effects of TrBA concentration on the

retention of *N*-acetylated disaccharides used a series of buffers titrated to pH 3.5 with formic acid and diluted as described above to give final TrBA concentrations ranging from 2.5 to 20 mM.

The gradient profile used for these experiments consisted of a 1 min isocratic step of 100% solvent A after which the fraction of solvent B was increased to 4.8% over the next 1.5 min. The fraction of solvent B was then increased to 40% over the next 2.5 min and maintained at 40% for 2 min while the flow rate was increased from 0.5 mL/min to 0.6 mL/min. Over the next 5 min period the fraction of solvent B was increased to 100% while the flow rate was further increased to 0.65 mL/min. The fraction of solvent B was then maintained at 100% for 2 min. Finally, the system was returned to its initial conditions over the next 2 min and allowed to equilibrate for 5 min. The column temperature was varied between 25 and 50 °C for the temperature studies, but was maintained at 25°C in the final optimized separation.

3.2.3 Mass Spectrometry. Total ion chromatograms were measured using a Waters ESI quadrupole time-of-flight mass spectrometer (Waters Corporation, Millford, MA). Data acquisition was performed using Masslynx 4.1 software. All spectra were acquired in negative mode using the following instrument parameters: capillary voltage, 3 kV; cone voltage, 12 V; source temperature, 120 °C; desolvation temperature, 200 °C; extractor voltage, 1 V; radio frequency lens, 0.5 V; interscan delay, 0.1 sec; m/z range, 215-1500.

For determination of the MS response factors presented in Table 3.2, average peak area was measured for each disaccharide in a series of four replicate experiments for

analyte concentrations ranging from 0.025 mM to 2.0 mM for the separations represented in Figure 3.1B and C. For each solution, the average analyte peak area was plotted versus analyte concentration and a linear regression performed. For the normalized response factors presented in supplemental Table 3.3, the average peak area for each analyte was divided by the average peak area of the internal standard, which was held at constant concentration. This ratio was then plotted versus the analyte concentration, and linear regression performed.

3.2.4 NMR Spectroscopy. All ^{1}H NMR spectra were measured using a Bruker Avance NMR spectrometer operating at a frequency of 599.84 MHz equipped with a 5-mm broadband inverse probe. Samples were prepared in 90% H_2O/10% D_2O at a disaccharide concentration of 0.4 mM with 30 mM TrBA to mimic the mobile phase IPR concentration. Samples were titrated to pH 3.5 with deuterated formic acid. WATERGATE was used to suppress the water resonance in all spectra. ^{1}H survey spectra were acquired by averaging 512 transients with 8 dummy scans. A relaxation delay of 3 s was used, and FIDs were acquired into 26,452 data points following the application of the 90° pulse. FIDs were apodized by multiplication by an exponential function equivalent to 1.0 Hz line broadening prior to Fourier transform and zero-filled to 131072 points.

TOCSY spectra were acquired using the standard mlevgpph19 Bruker pulse sequence with WATERGATE solvent suppression during the 1.5 s relaxation delay. A total of 208 transients were acquired in F2 with 8 dummy scans for each of the 128 increments measured in the F1 dimension. A 120 ms mixing time was used. The spectra

were zero-filled to 4096 points in the F2 dimension and 512 points in the F1 dimension. All processing was performed using Bruker Topspin software (version 1.3).

3.3 Results

Chapter 2 demonstrated that the 11 heparin-derived disaccharides shown in Table 3.1 can serve as a unique probe to explore the mechanism of RPIP chromatography. The optimized separation (Figure 3.1A) resolved all of the components including the isomeric compounds. This family of disaccharides comprises an interesting set of hydrophilic molecules with similar structures spanning a range of charge states from neutral to -4. For most of the disaccharides, the net charge is derived from the combination of the carboxylate group and the 2-*O*, 6-*O* or *N*-sulfo substituents. However, the disaccharides designated as IH, IIH, IIIH, and IVH also have a contribution to their net charge from the unmodified glucosamine (GlcN) amino group which is positively charged under conditions commonly employed in RPIP separations. In chapter 2, we suggested that the resolution of isomeric disaccharides was enhanced through competition of TrBA with ammonium, and that chromatographic resolution of the α and β anomers of several disaccharides including IH, IIH, IIIH, and to a lesser extent IVH, (Figure 3.1A) could result from differences in the pK_a values of the GlcN amino groups. As reported for amino sugars by Blaskó et al.[1] and for heparin disaccharides by Eldridge et al.,[2] the pK_a of the α anomer ammonium group is on average ~0.4 pH units lower than in the β form.

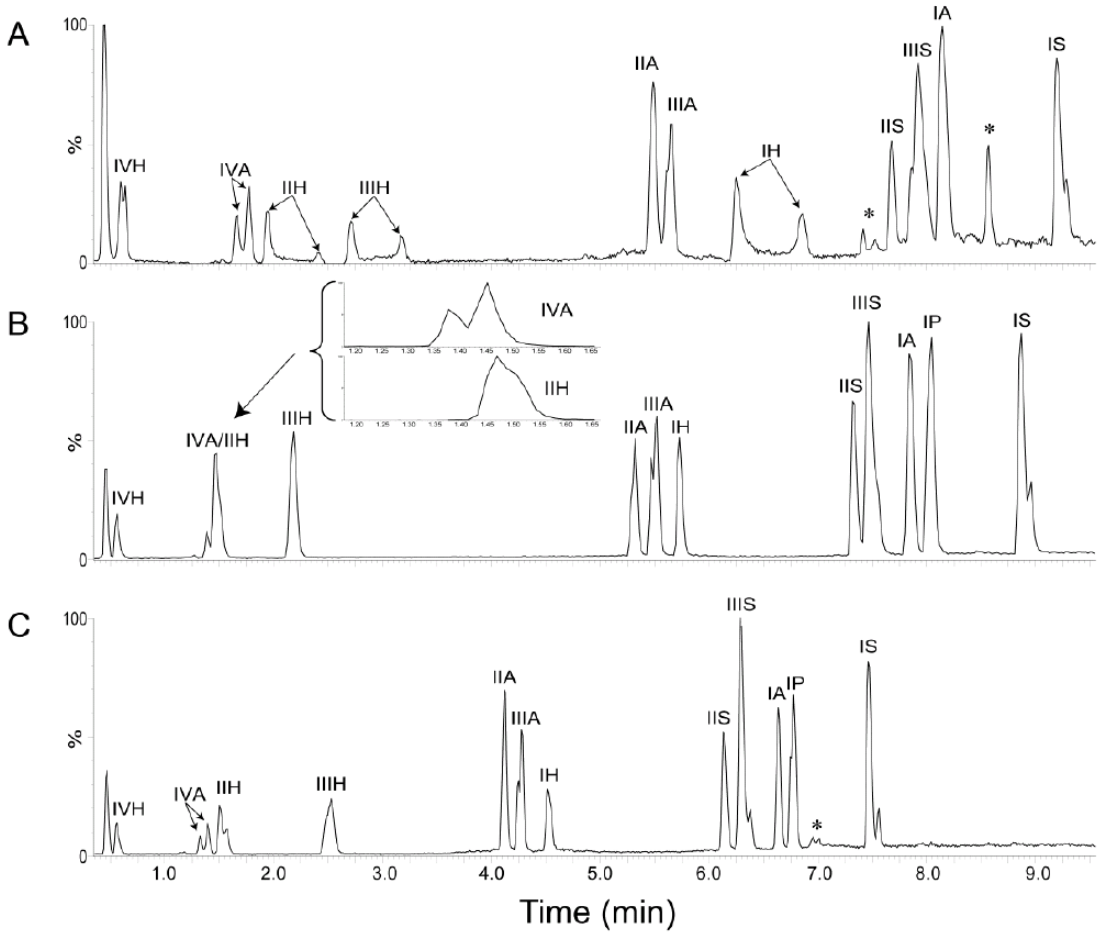

Figure 3.1. TICs for the 11 heparin disaccharides studied and the internal standard ΔUA2S-GlcNCOEt6S (IP) using (A) disaccharide separation method from chapter 2 with 20 mM TrBA, 2.5 mM NH_4COOH buffers at pH 6.5 and column temperature of 40°C, (B) the same separation conditions at pH 3.5 and (C) 30 mM TrBA and column temperature of 25°C at pH 3.5 with a new gradient profile optimized for the higher IPR concentration. The peaks marked with an asterisk are impurities.

This observation led us to hypothesize that for the α anomer the greater population of positively charged GlcN ammonium groups reduces its electrostatic interactions with the IPR causing it to elute prior to the β anomer under the neutral pH conditions used in the chromatographic method developed in chapter 2. If this hypothesis is correct, choosing mobile phase pH values significantly lower than the ammonium pK_a should reduce or eliminate the chromatographic resolution of the GlcN-containing disaccharide anomers, as the amino groups of the α and β forms would both be fully protonated. Collapse of the anomers into a single chromatographic peak would improve the sensitivity of the method for those disaccharides and could increase the resolution of the separation providing that the remaining members of the disaccharide family remain resolved at the lower mobile phase pH.

Figure 3.2A shows a series of chromatograms measured for the disaccharides IVH, IIH, IIIH, and IH (listed in order of elution) as a function of mobile phase pH, which was adjusted with acetic acid. The mobile phase buffer consisted of 20 mM TrBA and 2.5 mM ammonium acetate. Assignment of the anomer peaks of the disaccharides containing an unmodified GlcN amino group was performed by comparison of the intensities of the chromatographic peaks with those reported by ^{1}H NMR.[2] In each case, the less intense β anomer peak is most affected by the change in mobile phase pH. Rather than coalescence of the α and β anomer peaks at an average retention time, a greater decrease in the retention time of the β anomer is observed with decreasing pH.

For the earliest eluting disaccharide, IVH, a slight decrease in retention time can be seen as the mobile phase pH is lowered with little change in peak shape. At the pH

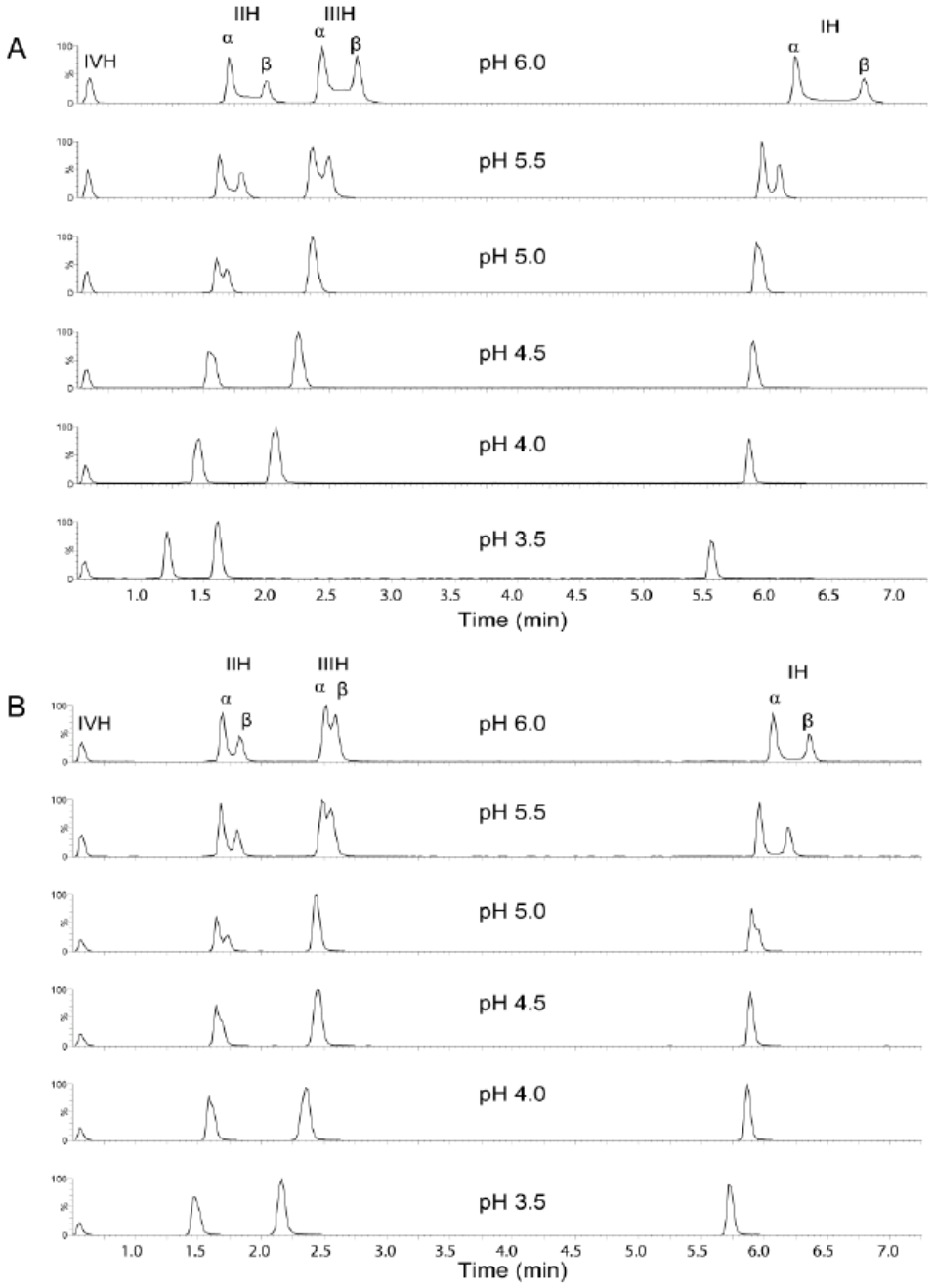

Figure 3.2. TICs showing changes in retention time and anomeric resolution as a function of pH for IVH, IIH, IIIH, and IH. Gradient elution used mobile phase buffers containing 20 mM TrBA and either (a) 2.5 mM NH_4OAc, or (b) 2.5 mM NH_4COOH.

values examined, the net charge of disaccharide IVH ranges from neutral to partially positive. Therefore it elutes just after the column void and is unlikely to be retained through an ion-pairing mechanism. The pronounced effect of mobile phase pH on the retention of the other disaccharides can be more clearly seen in Figure 3.2A. Compared with the chromatogram measured at pH 6.0, reducing the pH to 5.5 produces a significant decrease in the resolution of the anomers. Complete collapse of the anomer peaks of disaccharides IIIH and IH occurs at pH 5.0, while collapse of the earlier eluting IIH anomers does not occur until pH 4.5. Moving from pH 4.0 to 3.5, the peaks for disaccharides IIH, IIIH and IH shift dramatically to shorter retention times.

Two types of ion-pair interactions, illustrated in Figure. 3.3, are possible in the chromatograms shown in Fig. 3.2. First is the most obvious heparin disaccharide-TrBA interaction that drives the RPIP separation. A second possible interaction is ion-pairing between TrBA and its buffer counterion, acetate. Because ion-pairs of this type compete with the desired disaccharide-TrBA interactions, the effects of the counterion were addressed by performing an analogous series of experiments with a mobile phase containing 20 mM TrBA and 2.5 mM ammonium formate, and using formic acid to adjust the solution pH. Only acetate and formate were studied as counterions because other commonly used mobile phase counterions such as phosphate are not amenable to MS detection. Fig. 3.2B shows a series of chromatograms for IVH, IIH, IIIH, and IH measured as a function of pH with formate replacing acetate as the TrBA counterion. Compared with the chromatograms in Figure 3.2A, a similar trend is observed as the pH

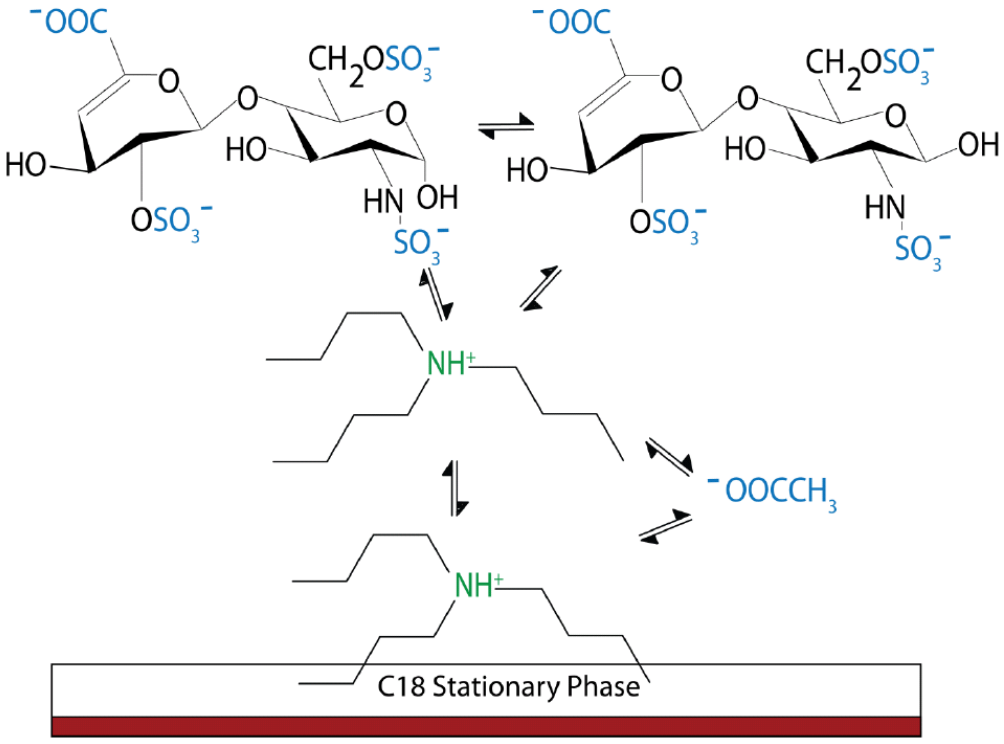

Figure 3.3. Illustration of the possible dynamic equilibria involved in RPIP-HPLC separations.

is lowered by addition of formic acid with some subtle but important differences. In Figure 3.2B at pH 6.0, the anomeric peaks of each disaccharide are less well resolved than in the corresponding separation in Figure 3.2A. At pH 5.5 the retention times of the IIH and IIIH anomers are fairly similar to their values in acetate buffer and as the mobile phase is lowered, the same gradual decrease in the retention times of the disaccharides is observed in Figure 3.2B with full collapse of the anomeric peaks for all the disaccharides at pH 4.5. At pH 3.5, again a larger decrease in the retention times of disaccharides IIH, IIIH, and IH is seen in Figure 3.2B, however the shift is not as dramatic as that observed in Fig. 3.2A.

Because the lower values of pH examined in Figure 3.2 begin to approach the pKa values of the disaccharide carboxylate moieties,[2] experiments were designed using a series of sulfonated glucosamine monosaccharides, structures shown in Figure 3.4, which should have a constant net charge over the pH range examined. These monosaccharides represent the possible glucosamine residues of the "H" and "S" disaccharides listed in Table 3.1. Figure 3.4 shows the changes in retention time measured as a function of mobile phase pH for glucosamine-6-sulfate, GlcN(6S), glucosamine-*N*-sulfate, GlcNS, and glucosamine-*N*,6-disulfate, GlcNS(6S) with acetate or formate as counterions. The chromatograms used to create Figure 3.4 are presented as Fig. 3.5. The small β anomer peaks of GlcNS and GlcNS(6S) are neglected in Fig. 3.4. At pH 6.0 GlcN(6S), like the IVH disaccharide, is zwitterionic and has no formal net charge at the pH values examined; even so it does show a slight decrease in retention time with decreasing pH.

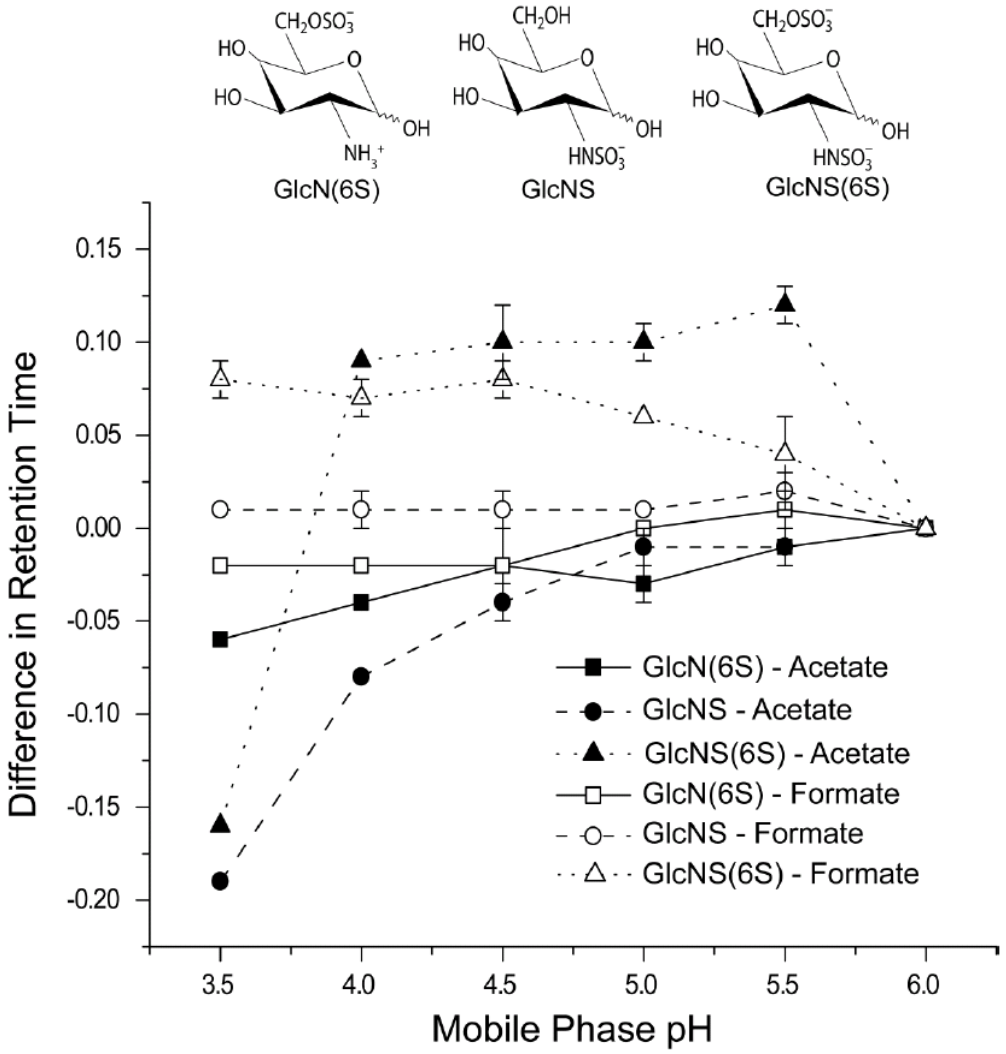

Figure 3.4. The change in retention time plotted as a function of pH for the monosaccharides GlcNS, GlcN(6S), and GlcNS(6S).

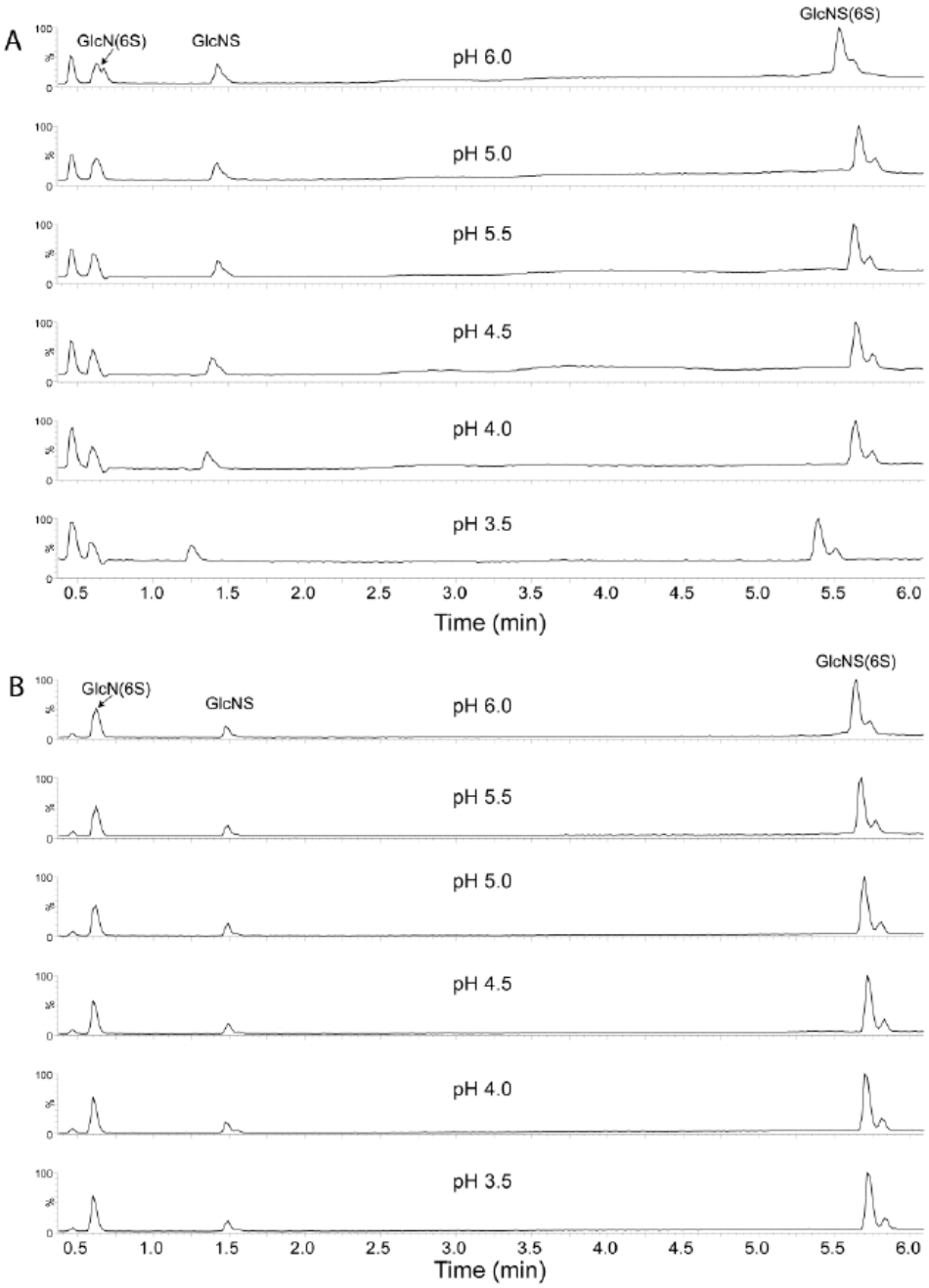

Figure 3.5. A series of total ion chromatograms showing the change in retention times and the resolution of the anomers as a function of pH for the monosaccharides GlcNS, GlcN(6S), and GlcNS(6S). The monosaccharides were eluted using the gradient program provided in the experimental section with mobile phase buffers containing 20 mM TrBA and either (A) 2.5 mM NH_4OAc or (B) 2.5 mM NH_4COOH.

In the presence of acetate, GlcNS and GlcNS(6S) show a remarkable change in their retention behavior as the pH is lowered with acetic acid. At first, lowering the mobile phase pH causes the monosaccharides to be slightly more retained reaching a retention time maximum around pH 5.0. As the pH is lowered further, the retention times begin to shift again to lower values with a pronounced drop from pH 4.0 to pH 3.5. In contrast, when formate is the counterion only small changes in the retention times of GlcN(6S) and GlcNS are observed as the pH is lowered by addition of formic acid. For GlcNS(6S) the retention time gradually increases as the pH is lowered. Overall, formate produces sharper peaks than acetate.

An important goal of this research was to design a chromatographic separation that resolves all 11 disaccharides with sharp peaks and minimal resolution of the anomeric forms. The results presented in Figures 3.2 and 3.4 suggest that the chromatogram shown in Figure 3.1A might be improved by using formate-based buffer system. Figure 3.1B shows the separation obtained for the 11 disaccharides and the internal standard ΔUA2S-GlcNCOEt6S (IP) measured using a 2.5 mM ammonium formate buffer containing 20 mM TrBA at pH 3.5 (reduced by addition of formic acid). The gradient program and mobile phase compositions were the same as that used to measure the chromatograms in Figure 3.2 and Figure 3.4. Table 3.2 shows response factors measured for each of the heparin disaccharides. Table 3.3 also lists the response factors relative to the internal standard, IP. With the exception of a small β-anomer shoulder for IS, resolution of the α and β anomers is almost completely eliminated in

Table 3.2. Response factors for disaccharides determined from TICs in Figures 3.1B and 3.1C. In the separation using 20 mM TrBA, the response factor for IVA can be calculated using the well resolved peak for the β anomer, however, the response for IIH cannot be determined due to overlap with the IVA α anomer peak. NC = not reported

	20 mM TrBA and 2.5 mM NH_4COOH, pH 3.5		**30 mM TrBA pH 3.5**	
Disaccharide	**Response Factor**	**r^2**	**Response Factor**	**r^2**
IVH	y = 1680.1x + 30.245	0.9918	y = 272.43x + 0.0873	0.9905
IVA	y = 601.43x + 0.5676	0.9992	y = 385.13x - 4.3999	0.9935
IIH	NR	NR	y = 669.23x - 3.0421	0.9983
IIIH	y = 3997.2x + 84.206	0.9908	y = 940.3x - 4.4463	0.999
IIA	y = 5160.6x + 139.7	0.9883	y = 1408.3x - 5.3248	0.999
IIIA	y = 5784.9x + 143.5	0.9886	y = 1295.8x - 12.024	0.996
IH	y = 3760.5x + 78.451	0.9927	y = 721.4x - 4.5774	0.9975
IIS	y = 5644.4x + 110.54	0.9942	y = 1256.7x - 8.9529	0.9992
IIIS	y = 4328.8x + 58.178	0.9997	y = 2865.4x - 41.154	0.9964
IA	y = 6263.8x + 135.98	0.9928	y = 1255.1x + 1.3083	0.9995
IS	y = 11766x + 355.37	0.9904	y = 2275.6x - 11.775	0.9990

Table 3.3. Response factors calculated relative to the internal standard IP for the chromatograms shown in Figures 3.1B and 3.1C. In the separation using 20 mM TrBA, the response factor for IVA can be calculated using the well resolved peak for the β anomer, however, the response for IIH cannot be determined due to overlap with the IVA α anomer peak.

	20 mM TrBA and 2.5 mM NH_4COOH, pH 3.5		**30mM TrBA, pH 3.5**	
Disaccharide	**Response Factor**	**r^2**	**Response Factor**	**r^2**
IVH	y = 0.9587x + 0.013	0.9924	y = 0.858x + 0.0021	0.9945
IVA	y = 0.3533x – 6E-06	0.9993	y = 1.2169x – 0.012	0.9966
IIH	NR	NR	y = 2.1114x – 0.0056	0.9998
IIIH	y = 2.2978x + 0.0352	0.9905	y = 2.9677x – 0.0083	1
IIA	y = 2.9414x + 0.0724	0.9903	y = 4.4444x – 0.0081	1
IIIA	y = 3.2353x + 0.0751	0.9901	y = 4.0928x – 0.031	0.9981
IH	y = 2.1572x + 0.0333	0.9921	y = 2.2767x – 0.0102	0.9993
IIS	y = 3.2271x + 0.0476	0.9937	y = 3.9686x – 0.0212	1
IIIS	y = 2.4374x + 0.0274	0.9993	y = 9.055x – 0.1166	0.9982
IA	y = 3.6042x + 0.0569	0.9916	y = 3.9593x + 0.0125	0.9999
IS	y = 6.8752x + 0.1835	0.9905	y = 7.1813x – 0.0237	1
NR: Not reported				

Figure 3.1B. Unfortunately these conditions compromise the overall resolution of this disaccharide family. The IVA and IIH disaccharides now coelute and the peaks for the IIS and IIIS disaccharides are no longer baseline resolved as demonstrated in Figure 3.1A and in other RPIP separations.[3-5]

The peaks for IVA and IIH elute at such a low acetonitrile percentage (between 5 and 7%) in the chromatogram shown in Figure 3.1B that it proved difficult to resolve them based on changes to the mobile phase gradient. Temperature can be a useful parameter to fine tune HPLC separations through subtle changes to capacity factors.[6] To better resolve these disaccharides, the column temperature was lowered to room temperature and the concentration of TrBA was increased to enhance the interaction of disaccharides IVA and IIH with TrBA. Optimization of the method showed that the presence of ammonium in the mobile phase had no effect on disaccharide retention under these new conditions and it was eliminated from the buffer system. Figure 3.1C shows the optimized separation of the 11 disaccharides and IP. Disaccharides IVA and IIH are now baseline resolved, and compared with Figure 3.1B, the resolution of IIS and IIIS has been improved. Compared with Figure 3.1A, there is less problem from resolution of the α and β anomeric forms, although some splitting of the IVA, IIH, IIIA, IIIS, and IS peaks is observed with the most significant anomeric resolution for disaccharide IVA. The reproducibility of the method was tested by performing 10 consecutive separations. The maximum standard deviation in retention time for any disaccharide was found to be 0.01 min for disaccharide IIIS. Table 3.2 lists response factors for each of the 11 heparin

disaccharides for this separation compared to those for the separation shown in Figure 3.1B. The response factors calculated relative to IP are given in Table 3.3.

The chromatograms in Figure 3.2 and Figures 3.1B and C demonstrate that the anomeric resolution of disaccharides containing an unsubstituted GlcN residue can be significantly reduced by lowering the mobile phase pH. However these results do not provide mechanistic insights into the resolution of the anomeric forms of disaccharides containing an *N*-acetyl substituted glucosamine residue for which the only charges are those that arise from the negatively charged carboxylate and sulfonate groups. Therefore, experiments were performed to test the effects of column temperature and IPR concentration on the anomeric resolution of the *N*-acetylated heparin disaccharides.

Figure 3.6 shows the chromatograms measured over the temperature range 25-50 °C. Disaccharides IA and IIA, which were present as single peaks in Figures 3.1B and C, show little change in retention time or peak width with changing temperature. As the temperature is increased, the resolution of the anomers of disaccharide IVA decreases slightly, but even at 50 °C two peaks are still observed. Similar behavior is observed in Figure 3.6 for disaccharide IIIA; at 50 °C the anomeric peak appears as a shoulder on the right side of the main peak, and with decreasing temperature these two peaks become better resolved.

In Figure 3.6 we observe that for disaccharides IIIA and IVA the less abundant anomer elutes first, which is opposite of the trend in the chromatograms of GlcN disaccharides (Figure 3.2). For the GlcN disaccharides, assignments of the α and β anomers were made by comparing the intensity of the chromatographic peaks to the

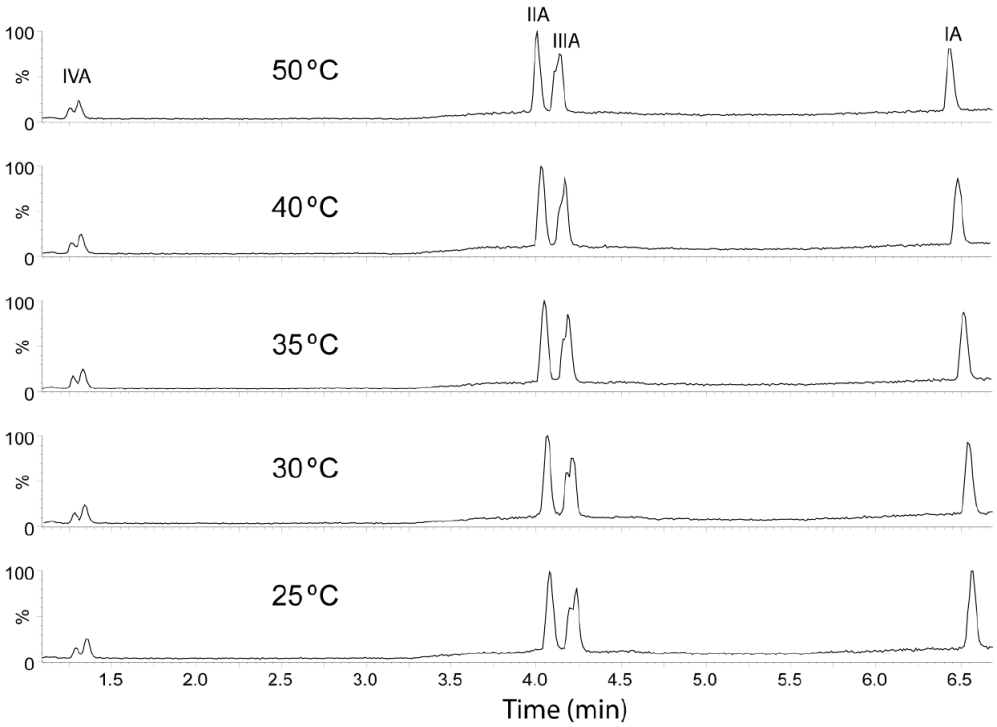

Figure 3.6. Series of total ion chromatograms for the disaccharides IVA, IIA, IIIA, and IA to examine possible changes in anomer peak resolution and retention time as a function of column temperature.

relative integrals of the ^{1}H NMR resonances of the anomeric forms.[2] The results presented in Figure 3.6 could be explained by a change in the order of elution, with the less abundant β anomer eluting first, or by a shift in the equilibrium between the two forms to favor a later-eluting β anomer. To distinguish these possibilities we turned to ^{1}H NMR spectroscopy. Although poor resolution of the carbon-bound ^{1}H resonances of the anomeric forms of disaccharides IIIA and IVA prevented their quantitation in D_2O solution, spectra measured in 90% H_2O/10% D_2O allowed detection of the amide proton resonances of each anomeric form (Figure 3.7). A TOCSY spectrum measured for IIIA (Figure 3.8) allowed the unambiguous assignment of the amide resonances through cross peaks to the H-1 protons of the α and β anomers of the disaccharides. The relative intensity of the anomer ^{1}H NMR resonances was used to assign the chromatographic peaks confirming that for the GlcNAc-containing disaccharides IIIA and IVA, the less abundant β anomer elutes prior to the α form.

To probe further the ion-pairing interactions of disaccharides IIIA and IVA, chromatograms were measured as a function of TrBA concentration. Figure 3.9A shows the effect of increasing TrBA concentration on the retention time and anomer resolution of IIIA. Although the IIIA anomers are not resolved at the lower TrBA concentrations, at 20 mM TrBA where the disaccharide is most highly retained, the β anomer is partially resolved as a shoulder on the main peak. Interestingly, the effect of TrBA concentration on the retention time and degree of anomer resolution of disaccharide IVA (Figure 3.9B) is opposite that observed for IIIA, but is consistent with trends reported in our previous

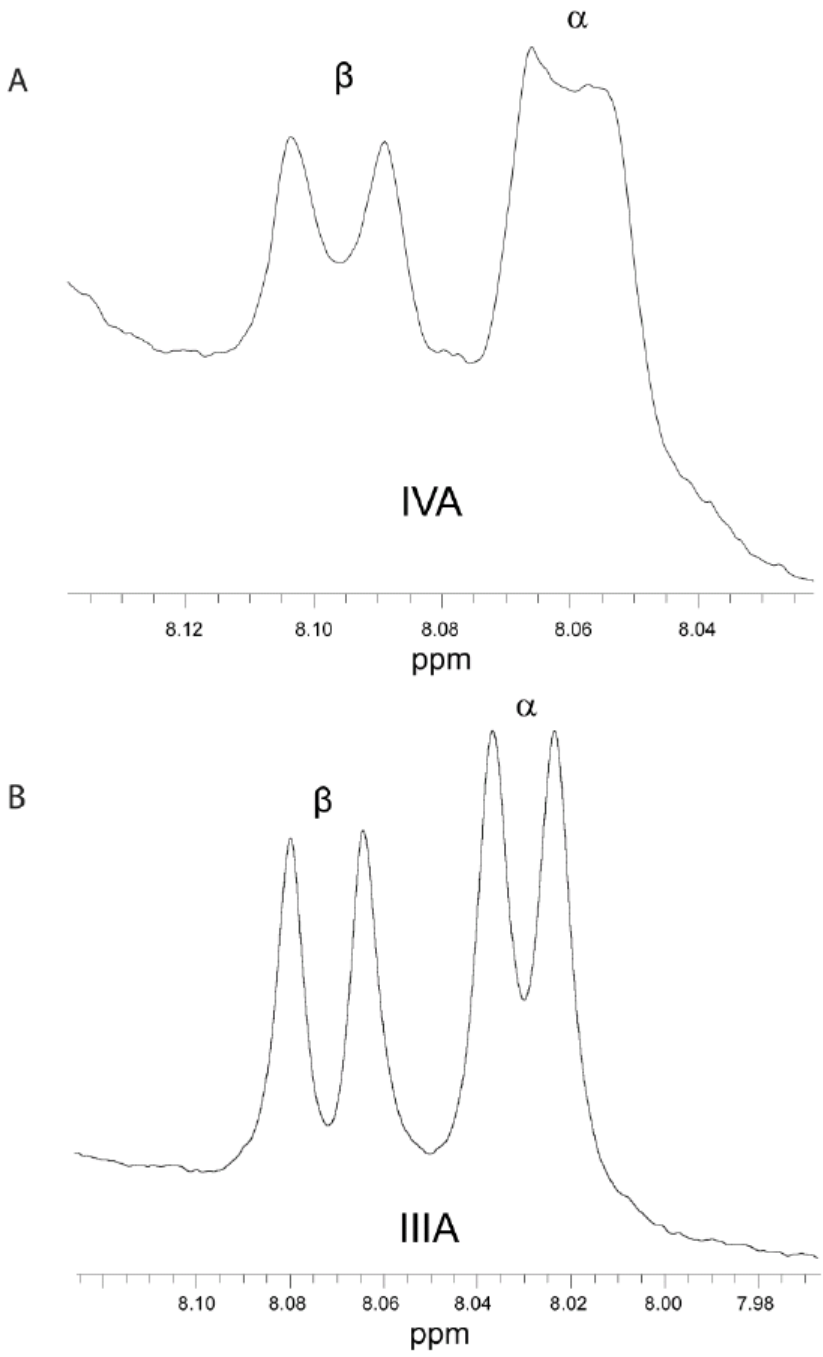

Figure 3.7. An expansion of the ^{1}H NMR spectra showing the amide resonances of the α and β anomers of the disaccharides IIIA and IVA.

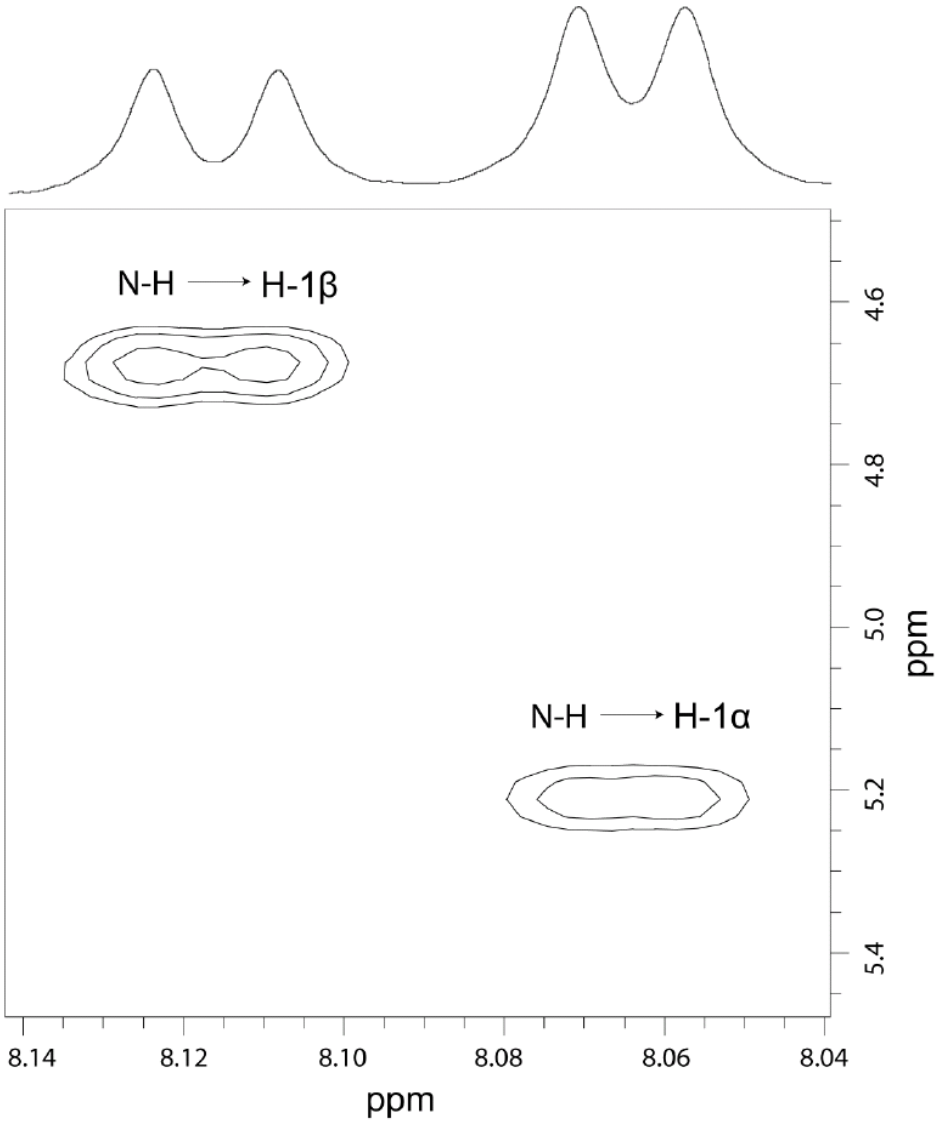

Figure 3.8. The TOCSY spectrum measured for disaccharide IIIA to determine the assignment of the amide resonances through cross peaks to the H-1 protons of the α and β anomers.

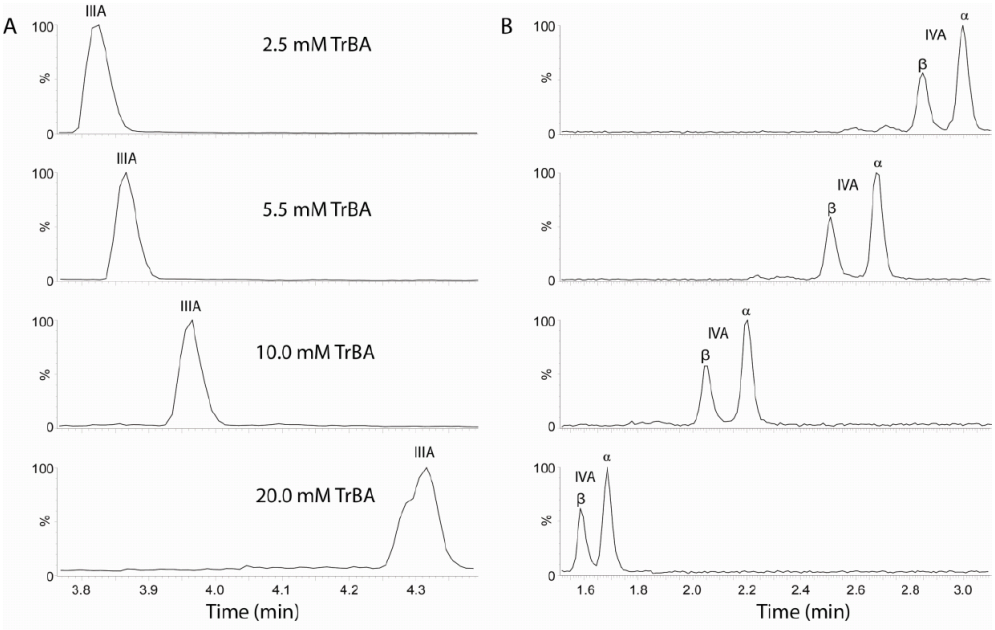

Figure 3.9. Series of total ion chromatograms showing changes in retention as a function of TrBA concentration for the disaccharides (A) IIIA and (B) IVA.

study in chapter 2 evaluating the retention patterns of heparin-derived disaccharides as a function of TrBA concentration.[3]

To further explore the contribution of the *N*-acetyl group on the retention of *N*-acetylated compounds, the isocratic separation of GlcNAc, IVA and GlcNAc(6S) was measured (Figure 3.10). GlcNAc, which contains no charged groups and therefore should not engage in ion-pairing interactions, was slightly retained, eluting shortly after the column void. This suggests that the *N*-acetyl group is involved in hydrophobic interactions with the C18 stationary phase, contributing to the retention of GlcNAc containing mono- and disaccharides. Of the three compounds, GlcNAc(6S) with one sulfonate group is the most highly retained, eluting at 2.2 min with a similar degree of anomer resolution as observed for IVA which elutes earlier in the separation around 1.4 min.

3.4 Discussion

In RPIP separations, the retention behavior of analytes is determined by a complex balance of factors that include the strength of the ion-pair interaction, IPR hydrophobicity and concentration, pH, counterion concentration, analyte charge, column temperature, and as discussed in chapter 2, competition between IPR's.[3] While our previous report explained the separation order of the 11 heparin disaccharides studied herein, including the resolution of isomeric compounds, it is more difficult to understand the mechanism of separation of disaccharide anomers differing only in the orientation of

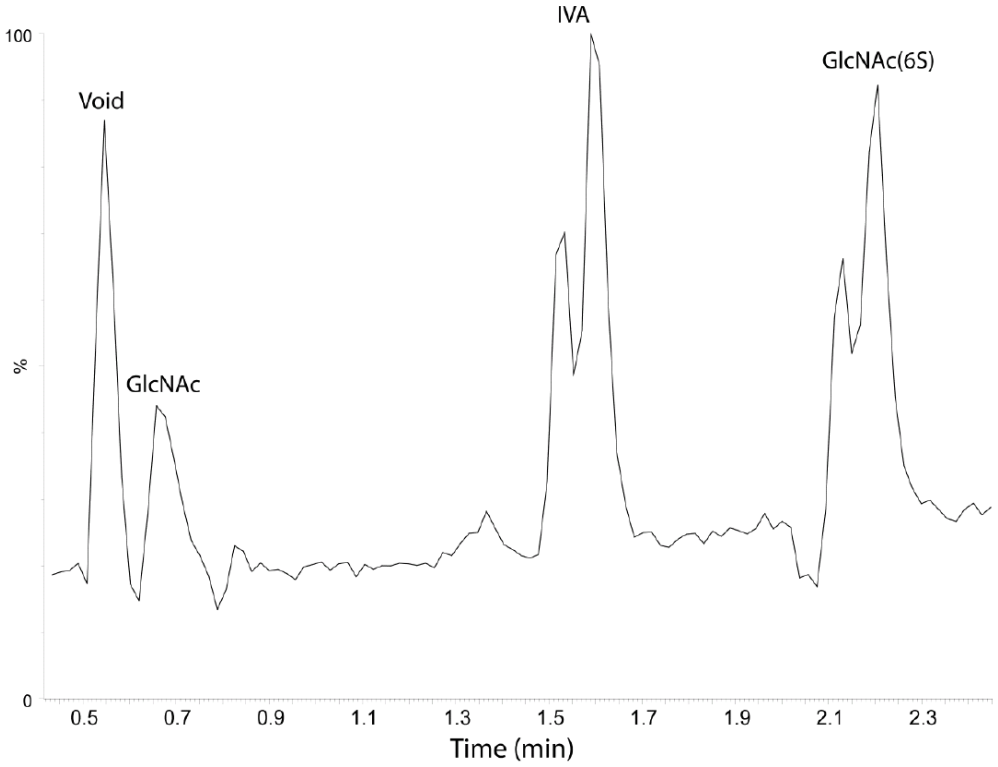

Figure 3.10. Total ion chromatogram for the isocratic separation of GlcNAc, IVA, and GlcNAc(6S). Mobile phase consisted of 30 mM TrBA at pH 3.5 and 95% H_2O, 5% ACN at a flow rate of 0.5 mL/min.

a single hydroxyl group in either the axial or equatorial position of the reducing end sugar residue. Given that the basic mechanism of RPIP involves electrostatic interaction of a charged analyte with an oppositely charged IPR, resolution of the anomeric forms of heparin disaccharides could be caused by either a difference in the anomer net charge, for example due to differences in pK_a values, or due to differences in the steric hindrance of charged sites as a result of structural differences between the anomers.

3.4.1 Separation of Glucosamine-Containing Saccharides. For the disaccharides IH, IIH, IIIH, and IVH, which contain a positively charged primary amine, the data presented in Figure 3.2 counters our initial hypothesis that the difference in the fractional protonation of the amino group is responsible for the resolution of the anomeric forms. With a net charge that ranges from neutral to partially positive, disaccharide IVH is poorly retained by either reverse-phase or ion-pairing interactions and elutes near the void. For IH, the most-highly retained disaccharide in this group, the pK_a(D) values of the α and β anomers have been reported as 8.78 and 8.31, respectively.[2] As shown in Figure 3.2A the IH anomers can be resolved chromatographically even at a nominal pH of 5.5, where the calculated fractions of the protonated amino forms are 0.9994 (α) and 0.9984 (β). Even taking into account the different solution conditions for the measured pK_a values in Reference 2 (D_2O solution, 0.1 M $NaNO_3$) and this separation (77% H_2O/23% ACN, 20 mM TrBA, 2.5 mM ammonium acetate), it is difficult to attribute the resolution of the IH anomers to differences in the fractional protonation of the GlcN amine. Although ACN can cause shifts in the pK_a values, the low percentage used in this separation is not likely responsible,[7] and the similar degree of chromatographic resolution

of the anomers of IIH (6.1% ACN), IIIH (7.2% ACN), and IH (23% ACN) at pH 5.5 supports this assertion. It may be instructive to consider the source of the amino group pK_a differences for these disaccharides. As illustrated in Figure 3.3, in the β anomer the equatorial position of the anomeric OH group orients itself away from the molecule and out into solution while in the α anomer, the C1 OH group is in the axial position where it can hydrogen bond with the amino group, stabilizing the positive charge and shifting its pK_a by around +0.4 pH units. Charge repulsions between the positively charged GlcN amino group and the IPR should reduce interactions of TrBA with neighboring negatively charged groups, although it is difficult to envision why this effect should be less significant for the α anomer. The unusual chromatographic peak shape for the disaccharides IH, IIH, and IIIH, especially in Figure 3.2A, reflects the dynamic equilibrium between the α and β anomers on the time scale of the separation.[8]

Comparison of Figures 3.2A and B reveals that the choice of IPR counterion affects the degree of anomeric resolution of disaccharides IH, IIH, and IIIH. Ion-pairing of the disaccharide amino moiety with acetate or formate could reduce the effective positive charge of the glucosamine moiety and enhance interactions with TrBA. As the mobile phase pH is lowered the resolution of the anomers decreases, primarily due to decreases in the retention of the β anomer. Decreasing the mobile phase pH by addition of either acetic or formic acid causes the acetate and formate concentrations in the mobile phase to stay relatively constant at approximately 22.5 mM (the sum of the buffer counterion concentrations: 20 mM TrBA + 2.5 mM NH_4^+). In the α anomer, the anomeric hydroxyl group is in an axial orientation with respect to the glucosamine ring,

as illustrated in Figure 3.3, and may partially block ion-pair formation by the amino group with acetate or formate. As the pH is lowered excess acetic or formic acid is added to the mobile phase which could cause a change in the mobile phase dielectric constant, altering the extent of interactions between the buffer counterion and the GlcN amino group. An interaction mechanism that incorporates differences in steric effects for the anomers is also consistent with the observation of greater resolution of the anomers in the presence of acetate (Figure 3.2A) than with formate (Figure 3.2B).

More difficult to explain in Figure 3.2 is the greater degree of resolution of the anomers of IIH relative to IIIH. As shown in Table 3.1, the difference between IIH and IIIH is only in the position of sulfonation, with 6-*O*-sulfo substitution of the glucosamine ring in IIH and 2-*O*-sulfo substitution of the ΔUA ring of IIIH. Hinterwirth et al. reported similar resolution of the anomers of glucose-6-phosphate, and glucosamine-6-phosphate by reversed-phase weak anion exchange chromatography (WAX), while the anomers of glucose-1-phosphate and glucosamine-1-phosphate eluted as a single peak.[8] Adsorption of TrBA onto the surface of the stationary phase in our separations could result in a separation based on a pseudo-WAX mechanism.[3, 9, 10] The separations of the monosaccharides GlcN(6S), GlcNS, and GlcNS(6S) in Figure 3.5 confirm the importance of 6-*O*-sulfo substitution on retention of the β anomer suggesting a possible role of for the equatorial orientation of the anomeric OH group in stabilizing the 6-*O*-sulfonate – TrBA interaction.

Figure 3.4 compares the changes in retention time for the glucosamine analogs as the pH is lowered with either acetic or formic acid. In the solutions containing formic

acid, pH-dependent shifts in retention times are smaller, but the trends are similar to those observed with acetic acid. In both buffers, the retention time of GlcNS(6S) increases as the pH is lowered, with the effect more pronounced in the presence of acetate. Acetate and formate can also ion pair with TrBA and therefore compete with GlcNS(6S) for ion-pairing interactions as illustrated in Figure 3.3. Therefore, as the pH is lowered, interactions between TrBA and acetate or formate may change making TrBA more available to ion pair with GlcNS(6S) leading to an increase in its retention time. When the pH is lowered from 4.0 to 3.5 using acetic acid, a pronounced drop in the retention time of GlcNS(6S) and, to a less extent, GlcNS occurs that is not observed with formic acid. A similar decrease in retention time of IH, IIH and IIIH is observed between pH 4 and 3.5 in acetate buffer (Figure 3.2A) that is not observed in Figure 3.2B in the presence of formate.

Because the glucosamine monosaccharides examined in Figure 3.4 do not contain a carboxylate group, as the pH is lowered from 4.0 to 3.5 a change in the net charge cannot be a factor in the decrease in retention of GlcNS and GlcNS(6S). It is also interesting that in the formate buffer system the retention trends for the glucosamine monosaccharides are essentially constant and a sharp decrease in retention time is not observed at pH 3.5. The mobile phase pH was lowered in these experiments by addition of either acetic or formic acid. Because of the differences in their pK_a values, a much larger amount of acetic acid (pK_a 4.75) is required than formic acid (pK_a 3.85) to reach the lower pH values examined. Therefore, we attribute the decrease in retention times observed at pH 3.5 in Figures 3.2A and 3.4 to the large excess of acetic acid, ~0.9 M,

which increases the effective organic composition of the mobile phase decreasing analyte retention times by desorbing TrBA from the surface of the stationary phase and by increasing TrBA/saccharide interactions in the mobile phase. Not only is a greater amount of acetic acid used to lower the mobile phase pH from 4.0 to 3.5, acetic acid is more hydrophobic than formic acid. For example, in the separation of a series of carboxylic acids using a mixed-mode 1:1 C18:dialkylamine stationary phase, Saari-Nordhaus and Anderson noted that at low pH, carboxylic acids including acetic, propionic, isobutyric and butyric acid are retained by reverse-phase interactions, whereas formic acid behaves more like an inorganic anion.[11] The results of our experiments support this interpretation and further highlights the role that TrBA absorbed on the surface of the stationary phase may play in the separations of the saccharides examined, as surface-sorbed TrBA may mimic the mixed-mode stationary phase described in reference 11.

3.4.2 Optimization of the Heparin Disaccharide Separation. The results discussed above suggest that performing the separation at low pH in a formic acid buffer system could collapse the anomeric peaks of IH, IIH and IIIH and produce a chromatogram with improved resolution compared with Figure 3.1A. The chromatogram obtained for the 11 disaccharide mixture using 20 mM TrBA, and 2.5 mM ammonium formate at pH 3.5 and 40 °C is shown in Figure 3.1B. Except for IVA and IIH, which coelute, the other disaccharides are well-resolved. Although they overlap in the TIC, using selected ion monitoring IVA and IIH can be resolved because of their different molecular masses (Figure 3.1B inset).

To achieve our goal of resolving chromatographically all of the disaccharides including IVA and IIH while minimizing the resolution of the α and β anomers, the TrBA concentration was increased to 30 mM and the column temperature reduced to 25 °C producing the chromatogram shown in Figure 3.1C. Although the chromatograms in Figures 3.1B and C were measured for samples prepared from the same stock solution, Figure 1C has a noticeably poorer signal-to-noise ratio due to increased ionization suppression. Even with the poorer chromatographic resolution of IVA and IIH in Figure 3.1B, these separation conditions will generally be preferable for negative ESI mass spectrometry detection due to the greater sensitivity, indicated by the much larger response factors obtained with lower TrBA concentrations (Table 3.2). If further improvements in sensitivity are needed, recent work by Yang and co-workers suggest that using hexylamine as the IPR can provide better ionization efficiency than TrBA.[12] A standard practice in LC-MS measurements is to report normalized response factors (Table 3.3) calculated relative to the intensity of the internal standard,[13, 14] however this approach is not useful for comparing the sensitivity of different separation conditions, as in Figures 3.1B and C, because the ionization of the internal standard IP also changes with TrBA concentration.

The retention times of IVA and IIH both decrease in Figure 3.1C, but the resolution of the peaks is increased because the change in retention time is greater for IVA. Under these conditions, split peaks are observed for the anomeric forms of several disaccharides: IIIA, IVA, IIH, IIIS and IS, although the splitting is less severe than observed in Figure 3.1A. Although not completely resolved, the peak for disaccharide

IIIH is clearly broadened by the lower temperatures used in Figure 3.1C. The less abundant β anomers of IIIA and IVA appear to elute first, a trend counter to that observed for the disaccharides containing amino or *N*-sulfonated glucosamine residues. The elution order of the IIIA and IVA anomers was determined from the ratio of the intensities of the α and β amide resonances in the ^{1}H NMR spectra of IIIA and IVA (Figure 3.7) and is also consistent with observations of Blumberg et al. for reverse-phase separations of GlcNAc saccharides.[15]

In Figure 3.1, the anomers of IVA are better resolved than for the later eluting IIIA suggesting that hydrophobic interactions, likely between the *N*-acetyl methyl group and the hydrophobic stationary phase, play an important role in the retention and resolution of the anomers of the weakly retained IIIA and IVA disaccharides. This is further supported by the data shown in Figure 3.10 in which the GlcNAc monosaccharide elutes after the column void even though it has no functional groups that can participate in ion-pairing interactions.

3.4.3 Separation of *N*-Acetyl Glucosamine-Containing Saccharides. Figure 3.9 shows the effect of the TrBA concentration on the extent of anomeric resolution and the retention times of IIIA and IVA. Retention of IIIA is likely through a combination of hydrophobic interactions of the *N*-acetyl group with the stationary phase and ion-pairing interactions with TrBA. For IVA, as the TrBA concentration increases the retention time decreases due to pore exclusion effects.[16] The greater retention of the α anomers of IIIA and IVA may be attributed to hydrogen bonding between the axial anomeric OH group with the glucosamine nitrogen, stabilizing a conformation in which the *N*-acetyl moiety is

more available for hydrophobic interactions with the column. This hypothesis is supported by the smaller $^{3}J_{NH\text{-}C2H}$ of the β anomer NMR resonances (Figure 3.7), reflecting a greater dihedral angle positioning the *N*-acetyl group further from the glucosamine ring and making it more available to interact with the column.[17] This is again supported by the chromatogram in Figure 3.10 in which the uncharged GlcNAc monosaccharide is retained past the column void through hydrophobic interactions with the C-18 stationary phase. Disaccharides IA and IIA, which have 6-*O*-sulfo substituted glucosamine residues, appear in Figure 3.1 as single chromatographic peaks with no resolution of the α and β anomers. This suggests that sulfonation at the 2-*O* position of the uronic acid residue may help to exaggerate the availability of the acetyl group for interaction with the column through steric effects.

3.5 Conclusions

This chapter focused on the effects of mobile phase pH, IPR concentration, IPR counterion, and column temperature on the chromatographic resolution of heparin disaccharide and monosaccharide anomers. For the disaccharides containing a free GlcN amino group, ion-pairing interactions of the buffer counterions acetate and formate could explain the collapse of the anomer peaks as the pH was reduced. For the variously substituted di- and monosaccharides, the retention differences for the α and β anomers reflected differences in the position of *O*-sulfonation and the orientation of the anomeric OH group relative to the *N*-acetyl group. The conclusions drawn from this study are likely generalizable to other sugars, particularly those with charged substituents such as

phosphate. Although our motivation to understand the separation mechanisms was to develop separation conditions that minimize anomer resolution, the insights gained could also be used to maximize the separation of the anomers, for example to measure interconversion rates. In chapter 4, the study of buffer counterions is continued with the exploration of their effects on the capillary isotachophoresis separation of the isomers of the tricyclic antidepressant doxepin.

3.6 References

1. Blaskó, A.; Bunton, C. A.; Bunel, S.; Ibarra, C.; Moraga, E., Determination of acid dissociation constants of anomers of amino sugars by 1H NMR spectroscopy. *Carbohydr. Res.* **1997,** 298, 163-172.

2. Eldridge, S. L.; Higgins, L. A.; Dickey, B. J.; Larive, C. K., Insights into the capillary electrophoresis separation of heparin disaccharides from nuclear magnetic resonance, pKa, and electrophoretic mobility measurements. *Anal. Chem.* **2009,** 81, 7406-7415.

3. Jones, C. J.; Membreno, N.; Larive, C. K., Insights into the mechanism of separation of heparin and heparan sulfate disaccharides by reverse-phase ion-pair chromatography. *J. Chromatogr., A* **2010,** 1217, 479-488.

4. Karamanos, N. K.; Vanky, P.; Tzanakakis, G. N.; Tsegenidis, T.; Hjerpe, A., Ion-pair high-performance liquid chromatography for determining disaccharide composition in heparin and heparan sulphate. *J. Chromatogr., A* **1997,** 765, 169-179.

5. Zhang, Z.; Xie, J.; Liu, H.; Liu, J.; Linhardt, R. J., Quantification of heparan sulfate disaccharides using ion-pairing reversed-phase microflow high-performance liquid chromatography with electrospray ionization trap mass spectrometry. *Anal. Chem.* **2009,** 81, 4349-4355.

6. Dolan, J. W., Temperature selectivity in reversed-phase high performance liquid chromatography. *J. Chromatogr., A* **2002,** 965, 195-205.

7. Subirats, X.; Martí, R.; Bosch, E., On the effect of organic solvent composition on the pH of buffered HPLC mobile phases and the pK a of analytes-A review. *Sep. Purif. Rev.* **2007,** 36, 231 - 255.
8. Hinterwirth, H.; Lämmerhofer, M.; Preinerstorfer, B.; Gargano, A.; Reischl, R.; Bicker, W.; Trapp, O.; Brecker, L.; Lindner, W., Selectivity issues in targeted metabolomics: Separation of phosphorylated carbohydrate isomers by mixed-mode hydrophilic interaction/weak anion exchange chromatography. *J. Sep. Sci.* **2010,** 33, 3273-3282.

9. Cecchi, T., *Ion-pair chromatography and related techniques*. Taylor & Francis Group: 2009.

10. El Rassi, Z., Recent progress in reversed-phase and hydrophobic interaction chromatography of carbohydrate species. *J. Chromatogr., A* **1996,** 720, 93-118.

11. Saari-Nordhaus, R.; Anderson, J., Ion chromatographic separation of inorganic anions and carboxylic acids on a mixed-mode stationary phase. *Anal. Chem.* **1992,** 64, 2283-2287.

12. Yang, B.; Weyers, A.; Baik, J. Y.; Sterner, E.; Sharfstein, S.; Mousa, S. A.; Zhang, F.; Dordick, J. S.; Linhardt, R. J., Ultra-performance ion-pairing liquid chromatography with on-line electrospray ion trap mass spectrometry for heparin disaccharide analysis. *Anal. Biochem.* **2011,** 415, 59-66.

13. Brustkern, A. M.; Buhse, L. F.; Nasr, M.; Al-Hakim, A.; Keire, D. A., Characterization of currently marketed heparin products: reversed-phase ion-pairing liquid chromatography mass spectrometry of heparin digests. *Anal. Chem.* **2010,** 82, 9865-9870.

14. Korir, A. K.; Limitiaco, J. F. K.; Gutierrez, S. M.; Larive, C. K., Ultraperformance ion-pair liquid chromatography coupled to electrospray time-of-flight mass spectrometry for compositional profiling and quantification of heparin and heparan sulfate. *Anal. Chem.* **2008,** 80, 1297-1306.

15. Blumberg, K.; Liniere, F.; Pustilnik, L.; Bush, C. A., Fractionation of oligosaccharides containing N-acetyl amino sugars by reverse-phase high-pressure liquid chromatography. *Anal. Biochem.* **1982,** 119, 407-412.

16. Loeser, E.; Drumm, P., Investigation of anion retention and cation exclusion effects for several C18 stationary phases. *Anal. Chem.* **2007,** 79, 5382-5391.

17. Karplus, M., Contact electron-spin coupling of nuclear magnetic moments. *J. Chem. Phys.* **1959,** 30, 11-15.

CHAPTER FOUR

Microcoil-NMR Study of the Interactions Between Doxepin, β-Cyclodextrin, and Buffer Components During Capillary Isotachophoresis.

The work in this chapter studies the capillary isotachophoresis (cITP) separation of the isomers of the tricyclic antidepressant doxepin by online microcoil NMR. Also, because the isomers have identical electrophoretic mobilities under normal cITP conditions this work explores the use of β-CD as a buffer additive to resolve the isomers. The work also uses CE to determine the binding constant of the Z isomer and β-CD which to date has not been reported in the literature. Finally, the doxepin cITP separation will be used to develop new insights into the mechanism by which all electrophoretic separations operate, in how particular buffer counterions like acetate can interact with various components of the separation system. The insights learned from this chapter will be valuable for the development and optimization of future cITP separations of other analytes.

4.1 Introduction

As discussed in Section 1.8.4, the coupling of capillary separations with microcoil NMR detection can enhance the structural and chemical analysis of mass limited samples.[1] Although capillary separations are more commonly coupled to detection methods such as fluorescence and mass spectrometry that provide greater sensitivity,

NMR offers the ability to unambiguously differentiate structural and positional isomers of molecules and is by nature non-destructive to the sample. Additionally, the sensitivity of NMR to experimental conditions such as buffer pH and temperature as well as intermolecular interactions makes NMR a useful tool for studying the mechanism of separations.[2-5]

In previous studies, capillary isotachophoresis (cITP) has been successfully coupled to microcoil NMR allowing the analysis of as little as a few nanograms of sample.[2, 3, 6-13] cITP separations utilize a discontinuous buffer system to concentrate analytes by up to 2 to 3 orders of magnitude while also separating components based on their individual electrophoretic mobilities.[14] The buffer system used for cITP separations consists of a leading electrolyte (LE) of higher mobility and a trailing electrolyte (TE) of lower mobility than the analytes being focused. Upon application of an electric potential across the separation capillary, the individual analytes stack into separate bands behind the LE, the order of which is determined by their electrophorectic mobilities. To maintain a constant current, the analytes will focus to a concentration proportional to the LE concentration. In theory, this means that even trace compounds can be separated from and concentrated to nearly the same concentration as a major component of a sample as long as the trace compound is charged and has a different electrophoretic mobility.[4, 6] Once the analytes are focused and stacked into concentrated bands, they migrate through the capillary at a constant velocity to the detector (in this case the NMR microcoil).

The coupling of cITP to microcoil NMR can provide unique insights into the separation mechanism of cITP by allowing changes in NMR line width, resonance integrals, and chemical shifts to be followed with changing experimental conditions. Previous work by Wolters et al. used these techniques to track changes in pD, temperature, and concentrations of the leading ion, sample, and trailing ion throughout the course of the cITP experiment.[5] This work was followed up by Korir et al. who studied the movement of buffer ions in both cationic and anionic cITP and also showed the spectral effects of magnetic susceptibility differences within the analyte band.[3] Almeida et al. used microcoil NMR experiments to probe the molecular level interactions of several beta-blockers with β-cyclodextrin (β-CD) during cITP concentration.[2] This work demonstrated a direct relationship between the complexation equilibrium constant and the maximum concentration of neutral β-CD molecules that focused along with the beta-blocker, demonstrating that binding information can be inferred from cITP experiments.

The work detailed in this chapter builds on these three sets of experiments by studying the cITP focusing and separation of the isomers of the tricyclic antidepressant doxepin using microcoil NMR. Doxepin is found in two isomeric forms in commercial preparations with the E isomer being ~ 85% abundant and the Z isomer ~15% abundant (structures shown in Figure 4.1). As one would expect, under normal experimental conditions it is impossible to electrophoretically separate the two isomers. However, cyclodextrins are widely used as buffer additives for the capillary electrophoresis (CE) separation of compounds with similar or even identical electrophoretic mobilities, for

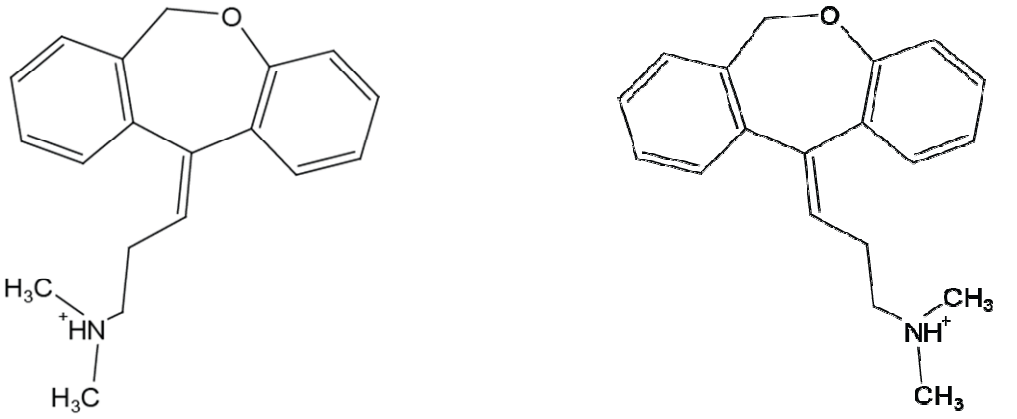

Figure 4.1. The structures of A) the more abundant E isomer of the tricyclic antidepressant doxepin and B) the less abundant Z isomer.

example enantiomers,[15-18] and previous work[19] showed that the doxepin isomers can be separated by CE with the addition of β-CD to the run buffers. To date however, studies have only reported the β-CD/doxepin binding constant for the more abundant E isomer, but not the Z form of this compound.[20] This chapter describes the design of a cITP separation for the doxepin E and Z isomers through which relative binding affinities of the two isomers with β-CD can be inferred. These cITP-NMR results are compared to the results of binding constant measurements using CE and ^{1}H NMR. Through these experiments, online microcoil NMR also provided unique insights into the cITP separation mechanism, in particular interactions of the buffer counterion acetate with various components of the separation system.

4.2 Methods and Materials

4.2.1. Material and Reagents. Fused silica capillaries were purchased from Polymicro (Phoenix, AZ) and surface-modified to produce zero electroosmotic flow (EOF) by MicroSolv Technology Corporation (Eatontown, NJ). Polyurethane-coated copper wire (99.99% Cu) was purchased from California Fine Wire Company (Grover Beach, CA). Non-magnetic trimmer capacitors were purchased from Voltronics. Doxepin hydrochloride, β-CD, optima grade acetonitrile and sodium acetate were purchased from Sigma-Aldrich, Inc. (St. Louis, MO). HPLC grade water was purchased from Honeywell Burdick & Jackson. Triethylamine was purchased from Alfa Aesar (Ward Hill, MA). Chloroform was purchased from Thermo Fisher Scientific (Waltham, MA). Deuterium oxide (D_2O, 99.9% D low paramagnetic) and deuterated acetic acid

were purchased from Cambridge Isotope Laboratories, Inc. (Andover, MA). The 0.2 μm nylon syringe filters used in this work were purchased from MicroSolv (Eatontown, NJ).

4.2.2. Solenoidal Microcoil Probe Construction. The design of the solenoidal microcoil probe used in this work has been described previously.[21] In short, a 50 μm thin copper wire (California Fine Wire Co., Grove Beach, CA) was wrapped around and glued with devcon 5-minute (Riviera Beach, FL) to a polyimide sleeve (MicroLumen, Tampa, FL) to obtain a 16-turn solenoidal coil with a diameter of 430 μm and an observe volume of ~25 nL. The coil and sleeve were fixed to a circuit board with epoxy and enclosed in a plastic bottle containing fluorinert, FC-43 (3M, St. Paul, MN), which has a magnetic susceptibility that closely matches that of copper. The coil leads were soldered to the tuning and matching capacitors of the probe and tuned to 600 MHz.

4.2.3. On-line cITP-Microcoil-NMR Experiments. The cITP buffers were prepared in low paramagnetic D_2O. The leading electrolyte (LE) consisted of 160 mM sodium acetate (NaAcetate) titrated to pD 5.0 with deuterated acetic acid. The trailing electrolyte solution (TE) consisted of 160 mM deuterated acetic acid. For experiments using β-CD as a buffer modifier, the appropriate amount of β-CD was added to the buffers prior to adjusting the pD with deuterated acetic acid. For the cITP experiment, the capillary was filled with LE using a disposable syringe and a 1 mM doxepin sample, prepared in 50/50 H_2O/TE, introduced by hydrodynamic injection at a height differential of 18 cm for 7 min. Next the TE was injected for a total of 7 min at the same height differential. After completion of the injection protocol, the voltage across the capillary was raised to -15 kV for the duration of the cITP experiment. ^{1}H NMR spectra were

acquired using a Bruker Avance spectrometer operating at 599.84 MHz. After the start of the cITP experiment, NMR acquisition was initiated to acquire an array of ^{1}H NMR spectra using 90° pulses with an acquisition time of 1.99 s and a spectral width of 11.03 ppm using the Bruker defined zg_8pulse pulse sequence which uses a composite 90° pulse to suppress background signals from the probe by only detecting resonances in the most homogeneous part of the B_1 field.[22] Each spectrum was acquired by coaddition of eight transients with no dummy scans. Line broadening equivalent to 1.0 Hz and zero-filling to 65,536 points were applied prior to Fourier transformation. Except for experiments studying the migration of β-CD, once doxepin reached the microcoil a hydrodynamic back pressure was applied to the LE buffer reservoir to slow its movement through the active volume of the probe. Data displayed as an array of spectra was produced by the coaddition of 20 free induction decays (FIDs) of 8 scans each to produce each spectrum shown in the array after first manually aligning the spectra to account for spectral drift during data acquisition due to the lack of a lock channel. Data displayed as a pseudo two-dimensional plot was produced by processing only the F2 dimension of the pseudo-2D data dataset obtained using the Bruker experiment lc2originally designed for HPLC-NMR and modified to incorporate the zg_8pulse sequence.

4.2.4. Capillary Electrophoresis Separation of Doxepin Isomers. CE separations were carried out using a Beckman Coulter PA800 CE (Brea, CA). For CE separations without β-CD, a 50 mM NaAcetate buffer at pH 4.6 was prepared as the run buffer. For all other experiments containing β-CD as a buffer modifier the appropriate concentration of β-CD was added to a 50 mM NaAcetate buffer prior to titrating to pH 4.6 with glacial

acetic acid. For the binding study by CE, solutions of 0.0, 0.5, 1.0, 2.0, 4.0, 6.0, 8.0, and 10 mM β-CD with 50 mM NaAcetate at pH 4.6 were used. Samples containing 0.15 mM doxepin and 0.1% methanol were prepared in each of the run buffers just prior to analysis. Between experiments, the capillary was rinsed with 0.1 M NaOH, followed by HPLC grade water (Honeywell Burdick & Jackson) for 2 min and phosphate buffer for 5 min, all at high pressure (50 psi). Samples were pressure injected at 0.5 psi for 7 s. The separation voltage was 22.0 kV, and total run time was 20 min. No pressure was applied during the separations.

4.2.5. Normal Phase HPLC Separation of Doxepin Isomers. All chromatographic separations were performed on a 4.6 x 150 mm Kromasil silica column (Sigma-Aldrich, Inc., St. Louis, MO) using an Agilent 1100 series HPLC. An isocratic solvent system of 25% chloroform and 75% acetonitrile containing 0.1% triethylamine was used for elution. The separation was run at a constant flow rate of 1.0 mL/min and was monitored using UV detection at 254 nm.

4.2.6. Structure Elucidation of the Doxepin Z Isomer by NMR. All ^{1}H NMR spectra were measured using a Bruker Avance NMR spectrometer operating at a frequency of 599.84 MHz equipped with a Protasis/MRM TXI microcoil probe. The lyophilized sample isolated by HPLC was reconstituted in 4 μL of D_2O. The sample was sandwiched between layers of chloroform and injected into capillary of the probe until the sample was positioned completely in the active volume of the microcoil, as monitored by the spectrometer lock level. ^{1}H NMR survey spectra were acquired by averaging 1024 transients with 16 dummy scans. A relaxation delay of 3 s was used, and FIDs were

acquired into 26,452 data points following the application of the 90° pulse. FIDs were apodized by multiplication by an exponential function equivalent to 1.0 Hz line broadening prior to Fourier transform and zero-filled to 131072 points.

The COSY spectrum was acquired using the standard cosyphpr Bruker pulse sequence with presaturation during the 1.5 s relaxation delay. A total of 32 transients were acquired in F2 with 64 dummy scans for each of the 256 increments measured in the F1 dimension. The spectra were zero-filled to 4096 points in the F2 dimension and 2048 points in the F1 dimension. All processing was performed using Bruker Topspin software (version 1.3).

The TOCSY spectrum was acquired using the standard mlevphpr Bruker pulse sequence with presaturation during the 1.5 s relaxation delay. A total of 32 transients were acquired in F2 with 64 dummy scans for each of the 512 increments measured in the F1 dimension. A 200 ms mixing time was used. The spectra were zero-filled to 4096 points in the F2 dimension and 1024 points in the F1 dimension. All processing was performed using Bruker Topspin software (version 1.3).

The NOESY spectrum was acquired using the standard noesyphpr Bruker pulse sequence with presaturation during the 1.5 s relaxation delay and during the NOESY mixing time. A total of 40 transients were acquired in F2 with 64 dummy scans and 448 increments measured in the F1 dimension. A 400 ms mixing time was used. The spectra were zero-filled to 4096 points in the F2 dimension and 2048 points in the F1 dimension. All processing was performed using Bruker Topspin software (version 1.3).

4.2.7 NMR Titration to Determine the Binding Constant of β-CD and doxepin.

To determine the binding constant between β-CD and doxepin by NMR solutions of doxepin at concentrations of 0.0, 0.1, 0.2, 0.4, 0.6, 0.8, 1.0, 2.0, 4.0, 6.0, 8.0 and 10.0 mM were prepared in a 50mM NaAcetate buffer at pD 5.0 and 1.0mM β-CD. For analysis each sample was added to a 1.7 mm capillary (New Era, Vineland, NJ) and inserted into a micro NMR tube fitted for a 5 mm Bruker probe (New Era, Vineland, NJ). The volume outside the capillary was filled with a 2 mM solution of deuterated DSS in D_2O as an external reference (note: deuterated DSS was not used as an internal reference to prevent binding of DSS and β-CD).

^1H NMR spectra were measured by averaging 128 transients with 8 dummy scans using a Bruker Avance NMR spectrometer operating at a frequency of 599.84 MHz equipped with a BBI probe. A relaxation delay of 1.5 s was used, and FIDs were acquired into 32,768 data points following the application of the 90° pulse. The FIDs were apodized by multiplication by an exponential function equivalent to 1.0 Hz line broadening prior to Fourier transform and zero-filled to 131072 points. To construct a binding plot the chemical shift of the anomeric proton of β-CD was plotted vs. the concentration of doxepin and the data was fitted to a quadratic function in Scientist (St. Louis, MO).

4.2.8 NMR Measurements to Examine Binding between Acetate and β-CD. To determine if binding occurs between acetate and β-CD two samples were prepared. The first contained only 1 mM NaAcetate at pD 5.0 in D_2O and the second contained 10 mM β-CD with 1 mM NaAcetate at pD 5.0 in D_2O. ^1H NMR spectra were measured for both

samples by averaging 1024 transients with 16 dummy scans using a Bruker Avance NMR spectrometer operating at a frequency of 599.84 MHz equipped with a BBI probe. A relaxation delay of 3 s was used, and FIDs were acquired into 26,452 data points following the application of the 90° pulse. The FIDs were apodized by multiplication by an exponential function equivalent to 1.0 Hz line broadening prior to Fourier transform and zero-filled to 131072 points.

4.3. Results and Discussion

4.3.1 Online cITP Microcoil NMR of Doxepin. The electrophoretic separation of the isomers of doxepin presents an interesting analytical challenge. From the theory of CE, we know that electrophorectic separations are driven by differences in the electrophoretic mobility of the analytes which is dependent on both the size (more specifically the hydrodynamic radius) and charge of the molecules. Because both doxepin isomers have identical pKa's and nearly identical hydrodynamic radii they also have essentially the same electrophoretic mobility. For this reason it is unlikely that the isomers will be resolved under normal electrophoretic conditions. To separate the isomers of doxepin electrophoretically the migration rate of one or both of the isomers must be modified so that they have different effective mobilities. Similar to techniques for the electrophoretic resolution of enantiomers, one approach for modifying the mobilities of the two isomers is by introducing into the buffer system a counter ion or neutral molecule (such as a cyclodextrin) with which the two isomers interact with different affinities.[23] In most separations, these interactions are relatively weak and

therefore the free analyte and complex are in dynamic equilibrium on timescale that is fast compared to that of the separation. The isomer that interacts with the buffer additive most strongly will have an effective mobility closer to that of the complex and thus will migrate more slowly than the weaker interacting isomer which will have an effective mobility that is more similar to the free form. Lin et al. reported that the isomers of doxepin could be resolved by adding β-CD to the CE running buffer.[19] To demonstrate the resolution of the isomers for a CE buffer system (50mM NaAcetate pD 5.0) that is more analogous to the LE used in cationic cITP experiments in our lab, Figure 4.2 shows a comparison of the CE electropherograms acquired both with (Figure 4.2B) and without (Figure 4.2A) β-CD present in the run buffers. Comparison of the electropherograms in Figure 4.2 shows that addition of 0.8 mM β-CD to the run buffer produces baseline resolution of the Z and E isomers. Also from their migration times in Figure 4.2B (effective mobilities for Z: 6.15×10^{-5} cm^2/sV and E: 5.80×10^{-5} cm^2/sV) it is clear that the Z isomer forms a lower affinity complex with β-CD. To determine each isomer's binding affinity to β-CD in this buffer system, a series of CE buffers were prepared with 0.0, 0.5, 1.0, 2.0, 4.0, 6.0, 8.0, and 10 mM β-CD and 50 mM NaAcetate at pH 4.6. A sample of 0.15 mM doxepin with 0.1% methanol (as a neutral marker) was prepared and separated in each buffer to determine the effect of the βCD on the migration times of the doxepin isomers. From the migration times of each isomer and the neutral marker in their respective buffers, double reciprocal plots (Figure 4.3) were prepared as detailed by Al Azzam et al. with linear fits of $y = -0.1982x - 4490$ $R^2 = 0.9906$ for the Z isomer and $y = -0.1253x – 4503.7$ $R^2 = 0.9969$ for the E isomer.[24] From these plots the binding

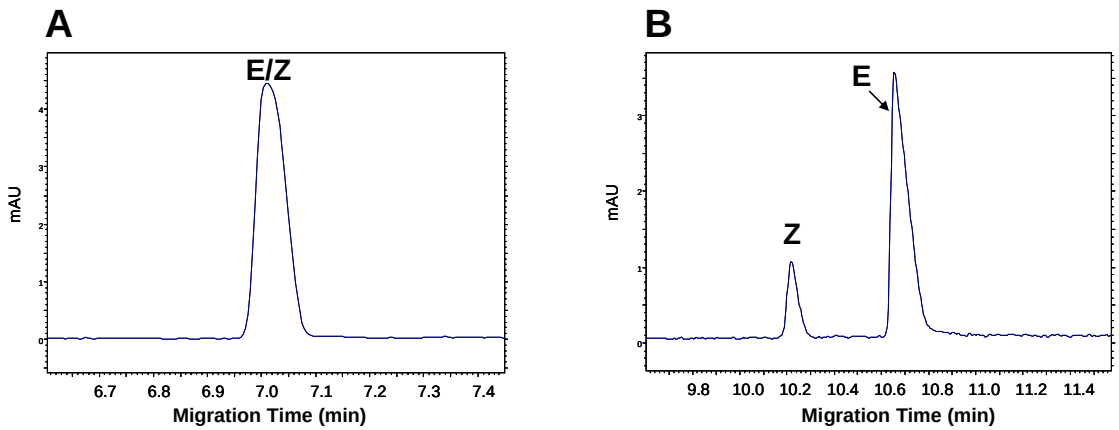

Figure 4.2. Electropherograms showing CE electropherograms of the isomers of doxepin using A) a 50 mM NaAcetate buffer at pH 4.6 and B) a 50 mM NaAcetate buffer at pH 4.6 and 0.8 mM β-CD.

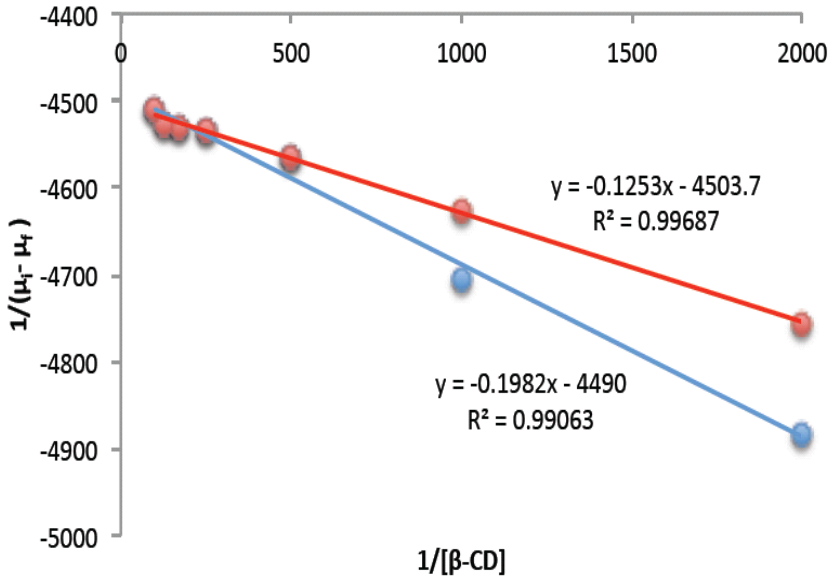

Figure 4.3. Double reciprocal plots for both the Z (blue) and E (red) isomers showing their respective linear fits.

constants for the Z and E isomers were found to be 2.27 x 10^4 $M^{-1}$and 3.60 x 10^4 M^{-1}, respectively. Important to note is that to the best of our knowledge this is the first report of the β-CD binding constant for the doxepin Z isomer.

We also attempted to calculate the binding constant for doxepin and β-CD by NMR. In these experiments the concentration of β-CD was kept constant at 1 mM and the concentration of doxepin was varied. The chemical shift of the anomeric resonance of β-CD was then plotted vs. the concentration of doxepin. This data was fit in Scientist using a non-linear least squares fit (Figure 4.4) to a 1:1 binding model (full model is shown in Appendix 1) with a reported binding constant of 3.77 x 10^4 M^{-1}. Although the binding constant calculated from the NMR data is in good agreement with the value determined for the E isomer by CE, the poor fit of the 1:1 binding model to the NMR data at the highest doxepin concentrations suggests that the actual binding equilibrium is more complex. While this type of NMR analysis is effective for single components, the situation for doxepin is more complicated since the two isomers are both present in solution and simultaneously compete for β-CD with different affinities.

Closer examination of the CE electropherograms in Figure 4.2 reveals that the peaks are broad, and in Figure 4.2B there is significant tailing for both the Z and E isomer peaks. Lin et al. attributed these problems to interactions of the positively charged doxepin molecule with the negatively charged capillary wall and used a PDMA coated capillary to prevent these interactions.[19] However, there are many interactions that occur during the electrophoretic process that do not necessarily manifest themselves in the form of changes in peak shape or in phenomena that can be easily observed by UV

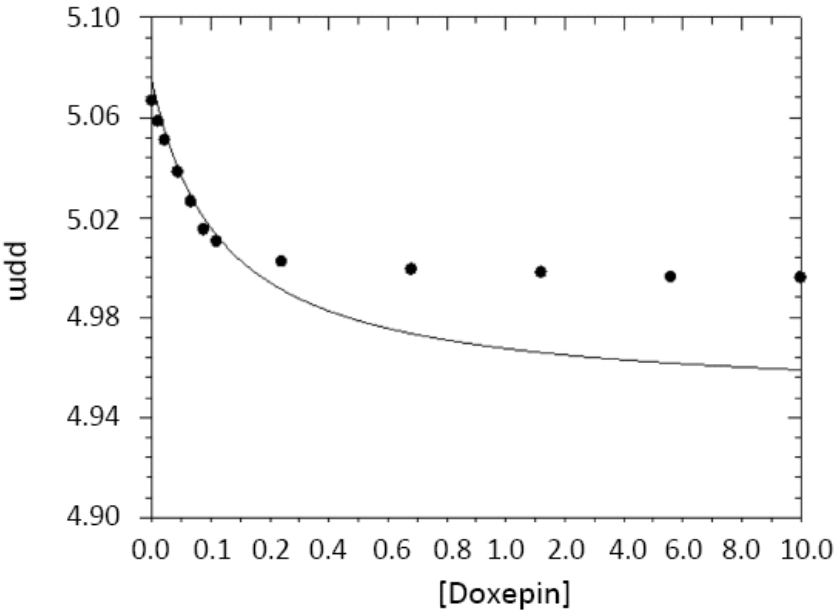

Figure 4.4. The results of the non-linear least squares fit of the 1:1 binding model in Appendix 1 to the NMR chemical shift of the anomeric resonance of β-CD measured as a function of the doxepin concentration.

detection. These include changes in pH, counterion interactions with various components of the buffer, intracapillary movement of ions that do not possess a UV chromophore, and conformational flexibility/changes in the analytes that do not lead to direct changes in mobility. The latter is especially important in the analysis of doxepin where its conformational flexibility often complicates its analysis.[25-28]

Figure 4.5 shows a ^{1}H NMR survey spectrum of a mixture of doxepin isomers in its commercial preparation. From quick examination of the survey spectrum several things are immediately noticeable. First is the presence of two broad resonances for the H-6 proton of doxepin. These result from inequivalent H-6 protons that exchange by ring inversion that occurs on the millisecond time scale which is intermediate on the NMR chemical shift time scale.[25] Second, is the presence of two methyl resonances for the dimethylamine group of the E isomer. This is thought to be the result of electrostatic interactions with negatively charged molecules in solution which slow down the rotation of the dimethyl amine group. This in turn creates a condition where the methyl resonances are in slow exchange between two different chemical environments.[26] Upon binding to β-CD, as in the CE separation shown in Figure 4.2B, the rates at which ring inversions and rotation of the dimethylamine group occur slow significantly.[29] In fact, it has been shown that the rotation of the entire doxepin side chain slows down causing the H-β and H-γ proton resonances to split into two resonances as well.[29] To better understand the extent to which these phenomena and other interactions occur during electrophoretic separations of doxepin, online cationic cITP-NMR analysis was performed.

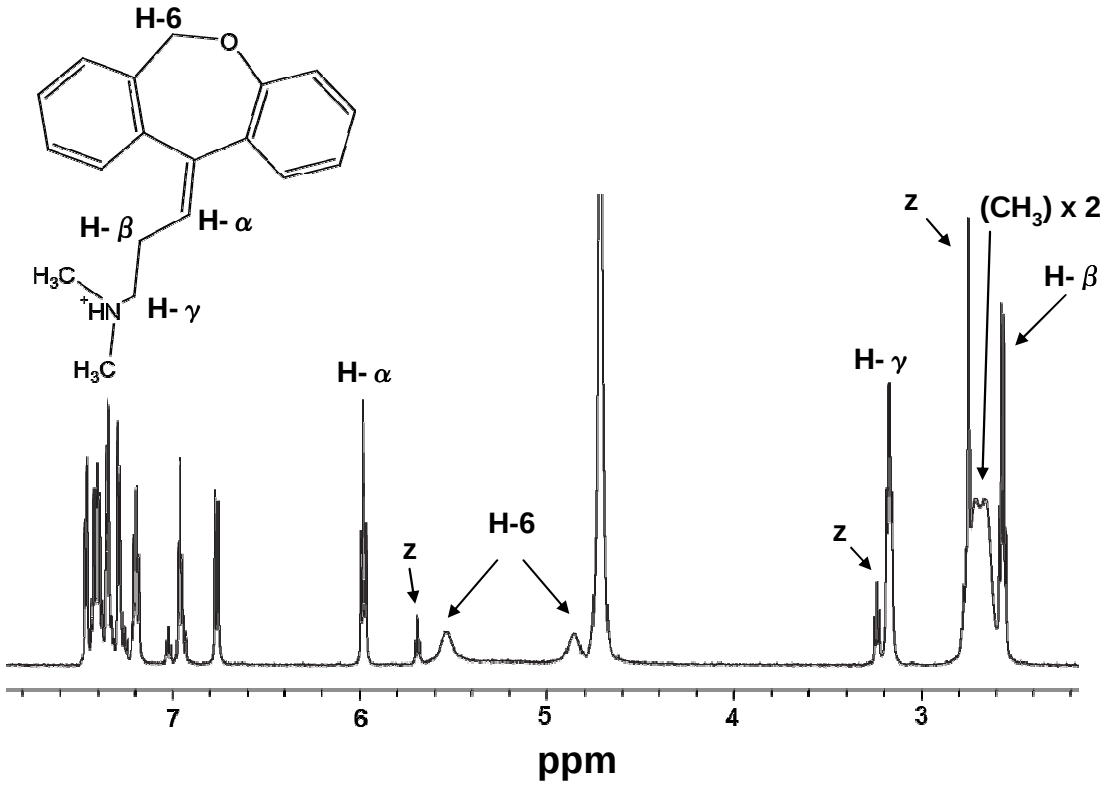

Figure 4.5. ^{1}H NMR survey spectrum of a commercial preparation of doxepin. The structure of the E isomer is shown to indicate the resonance assignments.

Figure 4.6 shows the results of the online cationic cITP-NMR analysis of 9 nanomoles of doxepin with an LE of 160 mM NaAcetate at pD 5.0 and a TE of 160 mM deuterated acetic acid. In Figure 4.6 we see that both doxepin isomers focus well using this cationic cITP buffer system, but there is no visible resolution between the isomers similar to the CE result shown in Figure 4.2A. In fact, after coaddition of the spectra in Figure 4.6 that contain resonances of the focused doxepin band, we are left with a spectrum (Figure 4.7) that looks very similar to the survey spectrum shown in Figure 4.5. Further inspection of H-6 resonances in Figure 4.7 shows that same ring inversion process detected in Figure 4.5 occurs during the cITP separation as well. Interestingly, the methyl resonances of the dimethylamine group of the E isomer are no longer split into two resonances, but instead appear as a single one broad resonance. The broadness of this resonance is likely due to the fact that at higher concentrations (like those in cITP) the dimethylamine groups at the end of the side chain of two different doxepin molecules are thought to interact to form a dimer, again slowing the rotation of the dimethylamine group.[26, 28] The primary differences between the spectra in Figures 4.5 and 4.7 are the poorer spectral resolution observed in Figure 4.7, produced in part by current-induced broadening from the separation capillary (discussed in greater detail in Chapters 5 and 6) and by changes in chemical shift of some resonances that result from pH differences between the two experiments.

Additional experiments were performed to investigate the intermolecular interactions and changes in conformational dynamics that occur during cITP upon the addition of β-CD. Figure 4.8 shows the results of the online cITP-NMR analysis of

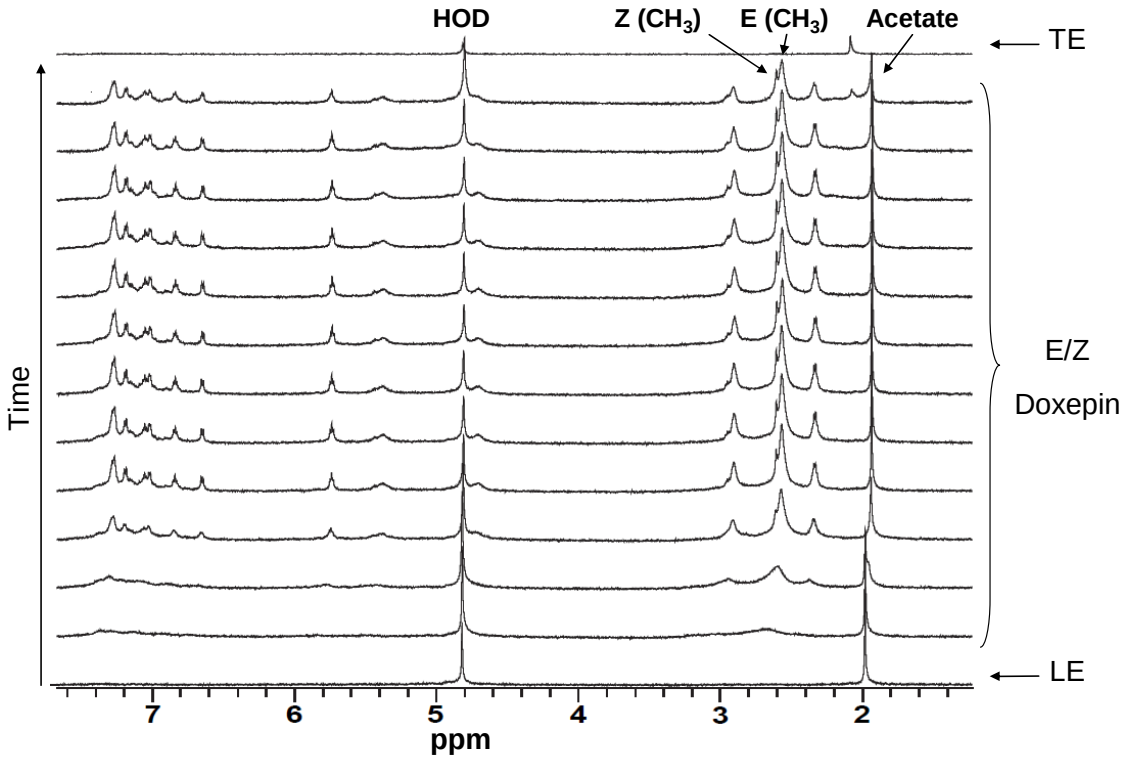

Figure 4.6. Results of the online cationic cITP- NMR analysis of 9 nanomoles of doxepin with a LE of 160 mM NaAcetate at pD 5.0 and a TE of 160 mM deuterated acetic acid.

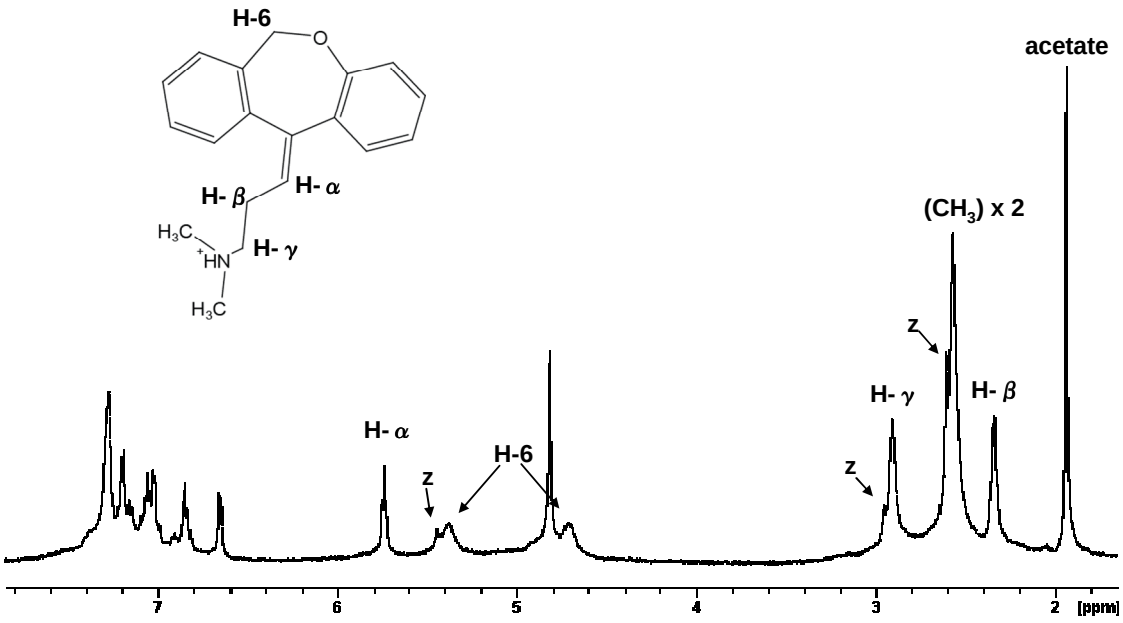

Figure 4.7. Spectrum resulting from coaddition of all of the cITP-NMR spectra in Figure 4.6 containing resonances of doxepin. The structure of the E isomer is shown to indicate the resonance assignments.

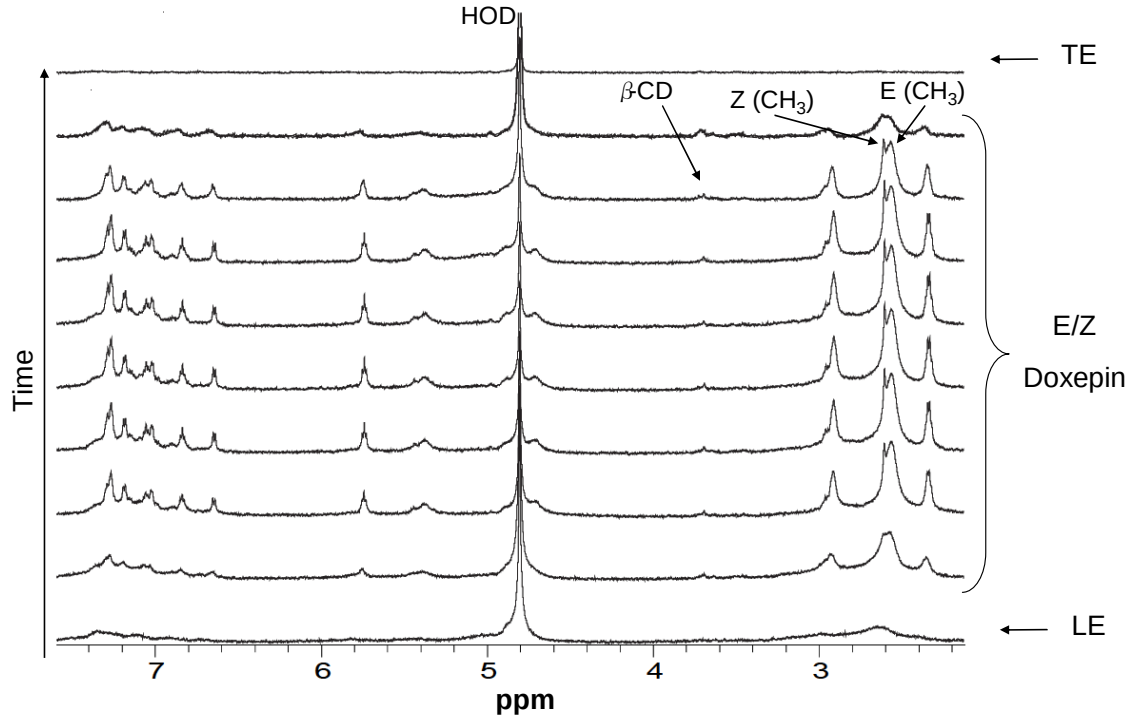

Figure 4.8. Results of the online cationic cITP- NMR analysis of 9 nanomoles of doxepin with a LE of 160 mM NaAcetate at pD 5.0 and a TE of 160 mM deuterated acetic acid. The LE and TE both contain 0.8 mM β-CD.

doxepin with 0.8 mM β-CD added to both the LE and TE buffers. The spectra of the focused doxepin resonances are nearly identical to those presented in Figures 4.6 and 4.7, with no visible separation of the isomers. Additionally, the lack of change in chemical shift of the doxepin isomers in Figure 4.8, which would be expected if doxepin was complexed to β-CD,[29] suggests that the concentration of β-CD was too low compared to the final concentration of the cITP-focused doxepin isomers to induce significant binding. Interestingly, looking at the spectra that correspond to the interfaces between the LE/sample and sample/TE in Figure 4.8 and at the LE/sample interface in Figure 4.6 we see a significant degree of broadening of the resonances in these spectra. This most likely a result of changes in the local magnetic susceptibility changes at the analyte boundaries and from the focusing of trace amounts of paramagnetic ions at the boundaries.[3, 9, 30, 31]

This cITP-NMR experiment was repeated using 10.0 mM β-CD (the aqueous solubility limit) in both the LE and TE, with the results presented in Figure 4.9. The changes in the doxepin spectra in Figure 4.9 compared to those shown in Figures 4.8 and 4.6 reflect the binding between doxepin and β-CD. Furthermore, compared to their positions in the spectra of the LE and TE, pronounced ring-current induced shifts are observed for the β-CD resonances resulting from the inclusion of the doxepin aromatic rings in the β-CD cavity.[29] Furthermore, a splitting of the H-γ resonance into two resonances is also observed indicating a decrease in the rate of rotation of the doxepin side chain creating a condition where the H-γ protons are in two different chemical enviroments.[29] A significant increase in the intensity of the β-CD resonances is also

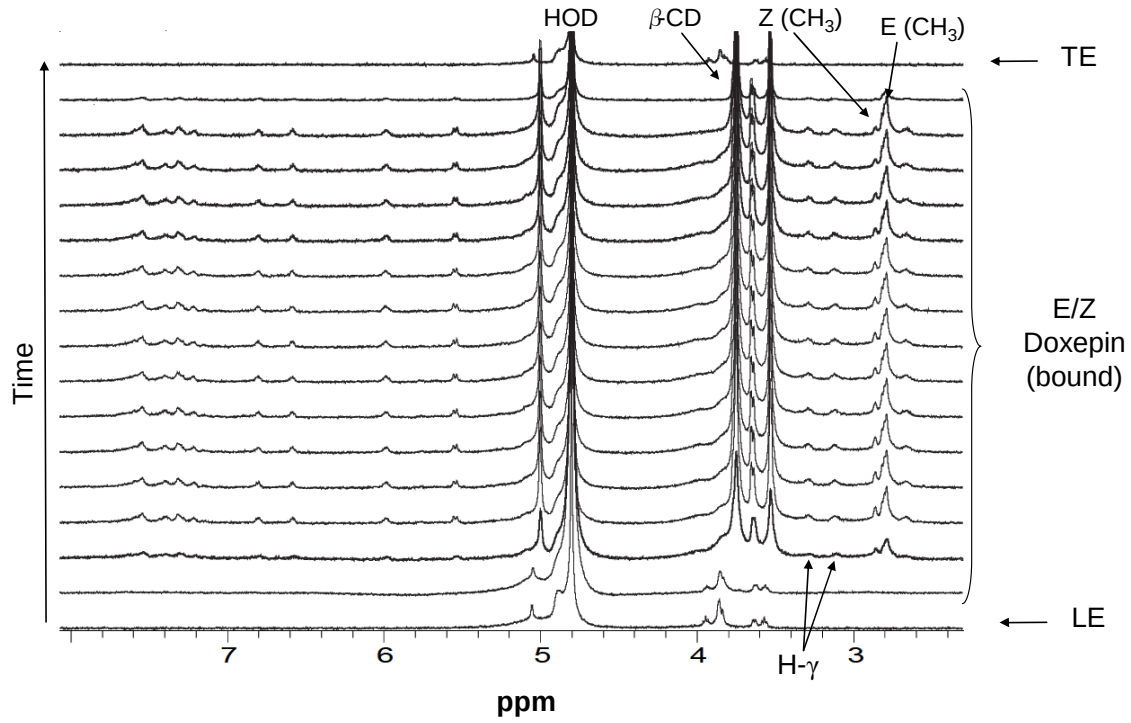

Figure 4.9. Results of the online cationic cITP- NMR analysis of 9 nanomoles of doxepin using a LE of 160 mM NaAcetate at pD 5.0 and a TE of 160 mM deuterated acetic acid. The LE and TE both contained 10.0 mM β-CD.

detected in the spectra of the cITP-focused doxepin indicating that β-CD co-concentrated along with doxepin during cITP stacking as a result of their host–guest interactions. This phenomenon was previously reported in the focusing and separation of several commercial β-blockers by cITP using various cyclodextrins as buffer additives.[2, 7] However, as in the previous cITP separations reported herein, no visible separation of the doxepin isomers was achieved in Figure 4.9. This is likely a result of saturating the buffer system with an excess of β-CD compared to doxepin. In this situation both isomers will be fully complexed with β-CD and have the same mobilites and thus can not be resolved. To achieve a separation using this approach one isomer needs to have a greater fraction present as the complex creating a difference in their respective electrophoretic mobilities. We hypothesized that by reducing the concentration of β-CD to an intermediate value between the 10 mM and 0.8 mM concentrations already tested that the stronger binding E isomer will be fully complexed with the available β-CD leaving the Z isomer in its free or partially complexed form.

Figure 4.10 shows the results of the online cITP microcoil NMR analysis of doxepin using a buffer system containing 4.5 mM β-CD in the LE and TE. Immediately noticeable is a distinct change in chemical shift of the doxepin resonances visible at the very front of the analyte band compared to those found in the rest of the band. This change in chemical shift also seems to correspond with a co-concentration of β-CD within the band suggesting that the change in chemical shift is a result of a differential degree of binding between doxepin and β-CD in different parts of the band. The expansion of the region of the spectra between 1.5 and 4.5 ppm (Figure 4.11) shows that

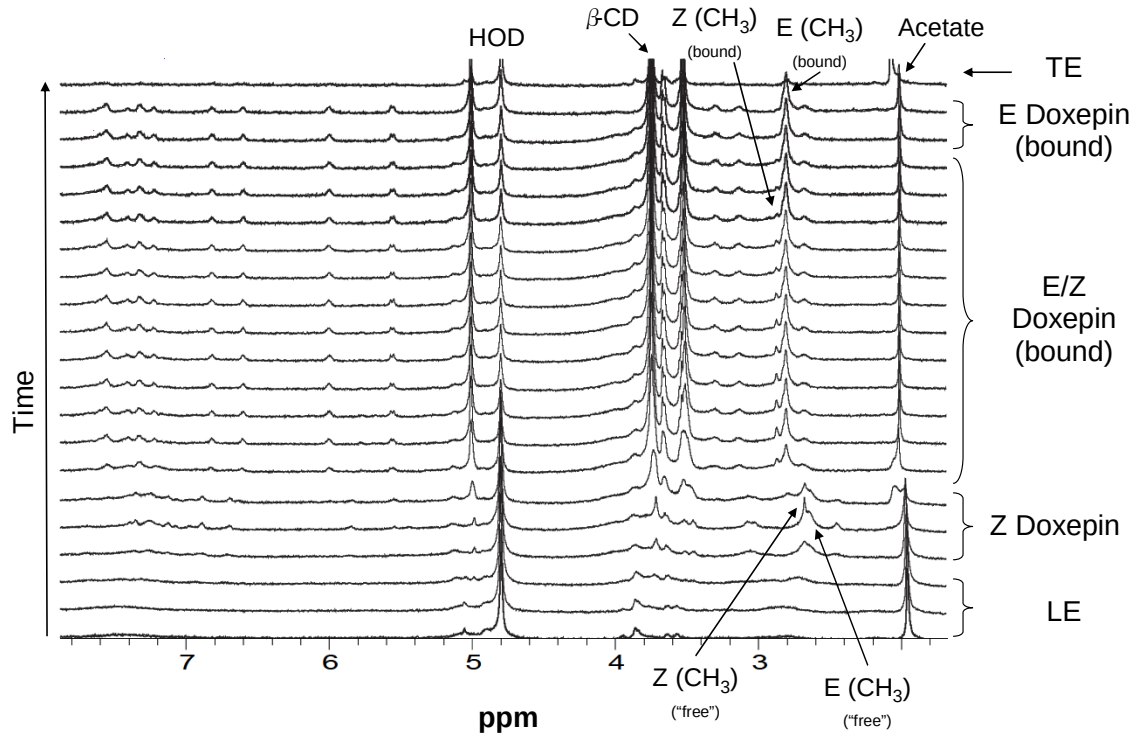

Figure 4.10. Results of the online cationic cITP- NMR analysis of 9 nanomoles of doxepin with a LE of 160 mM NaAcetate at pD 5.0 and a TE of 160 mM deuterated acetic acid. The LE and TE both contain 4.5 mM β-CD. Following the methyl resonances, a noticeable change in the chemical shift of the doxepin resonances is visible at the very front of the analyte band compared to those found in the rest of the band indicating differential degree of binding between doxepin and β-CD in different regions of the band.

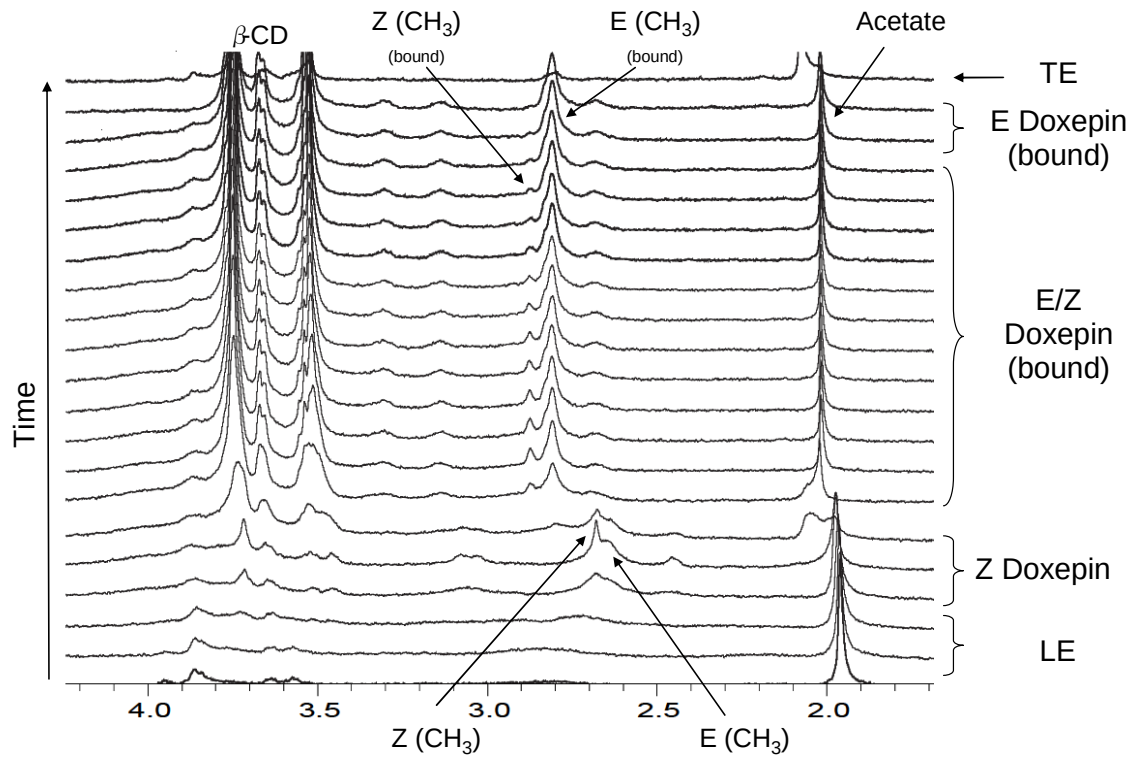

Figure 4.11. Spectral expansion of Figure 4.10 showing that the spectra containing resonances of doxepin near the beginning of the analyte band have chemical shifts that are more like the fully free form of doxepin and that the Z isomer is the dominant species in this region. Resonances in the latter portion of the band seem to indicate that doxepin is in a mostly bound form with the E isomer being the more dominant isomer.

the spectra containing resonances of doxepin near the beginning of the analyte band have chemical shifts that are more like the fully free form of doxepin although the chemical shifts of the β-CD resonances in these spectra suggest an intermediate degree of binding between the fully free and fully bound form. Additionally, the broadened resonances in beginning of the band imply that either the magnetic susceptibility is changing throughout this portion of the band or that in this portion of the band there is an intermediate degree of exchange between the bound and free forms of doxepin. This suggests that this part of the analyte band is a diffuse transition zone between the LE and the more focused latter portion of the band. Furthermore, looking at the methyl resonances, it seems that the dominant isomer in the front of the band is the Z isomer suggesting at least a partial separation of the two species. This fits well with the CE binding results that showed that the Z isomer has a smaller binding affinity towards β-CD than does the E isomer, and therefore a higher electrophoretic mobility.

Moving farther along the band a distinct shift in the pD of the buffer is detected by the sharp change in chemical shift of the acetate resonance. This shift in pD is accompanied by a change in the chemical shifts of the doxepin resonances reflecting the bound form and a co-concentration of β-CD. Following the methyl resonance of the Z isomer in Figure 4.11 through the band towards the TE, a gradual decrease in the intensity is observed until only the resonances of the E isomer are detected just prior to the sample/TE interface. Additional cITP experiments were also performed with buffer concentrations of β-CD at 3.0 and 5.0 mM (data not shown) but these experiments did not provide better resolution of the two isomers. The results in Figures 4.10 and 4.11 show

that a separation of the isomers was achieved with mostly the free form of the Z isomer focusing at the beginning of the band, followed by a transition to a mixture of the two isomers in a bound form with β-CD. Finally, resolution of only the E-isomer in the bound form was achieved just prior to the TE. It is interesting to note the significant increase in the concentration of β-CD needed to exact this separation using cITP compared to that used in Figure 4.2B using CE (4.5 mM vs. 0.8 mM). This is likely a function of the higher concentration of doxepin in the focused analyte band compared to that in the analyte peaks of the CE separation. It stands to reason that the high concentration of the focused doxepin would require a higher concentration of β-CD to reach a similar β-CD to doxepin ratio during the cITP separation as is effective in the CE separation.

Finally, to confirm the identity of the Z isomer resonances near the beginning of the analyte band we isolated ~0.5 mg of the Z isomer through a normal phase HPLC separation of the isomers as described in Section 4.2.5. To confirm the identity of the Z isomer, the isolated material was subjected to one- and two-dimensional ^{1}H-NMR experiments using a commercial TXI-microcoil probe from Protasis. Figure 4.12 shows the ^{1}H-NMR survey spectrum of the isolated material. Assignments of the doxepin proton resonances as well as those of the triethylamine (TEA) impurity were made using the COSY and TOCSY spectra shown in Figures 4.13 and 4.14 and by comparison to reference chemical shift data for the E isomer.[29] To confirm the stereochemistry of the isolated doxepin molecule Figure 4.15 shows an enlargement of the aromatic region of the NOESY spectrum. The NOE cross-peaks between the α proton near the double bond

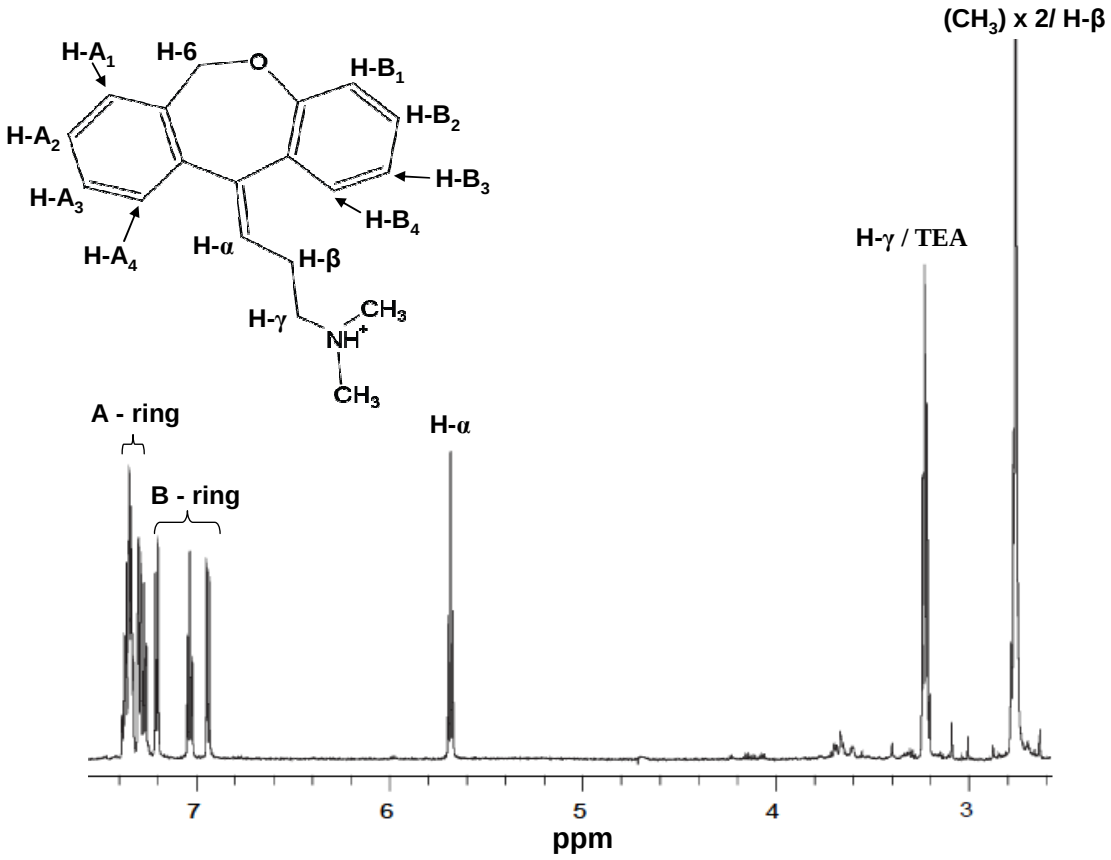

Figure 4.12. ^{1}H NMR survey spectrum for ~0.5 mg of the doxepin Z isomer isolated by normal phase HPLC and reconstituted in 4 μL of D_2O. The spectrum was acquired in a commercial Protasis TXI microcoil probe.

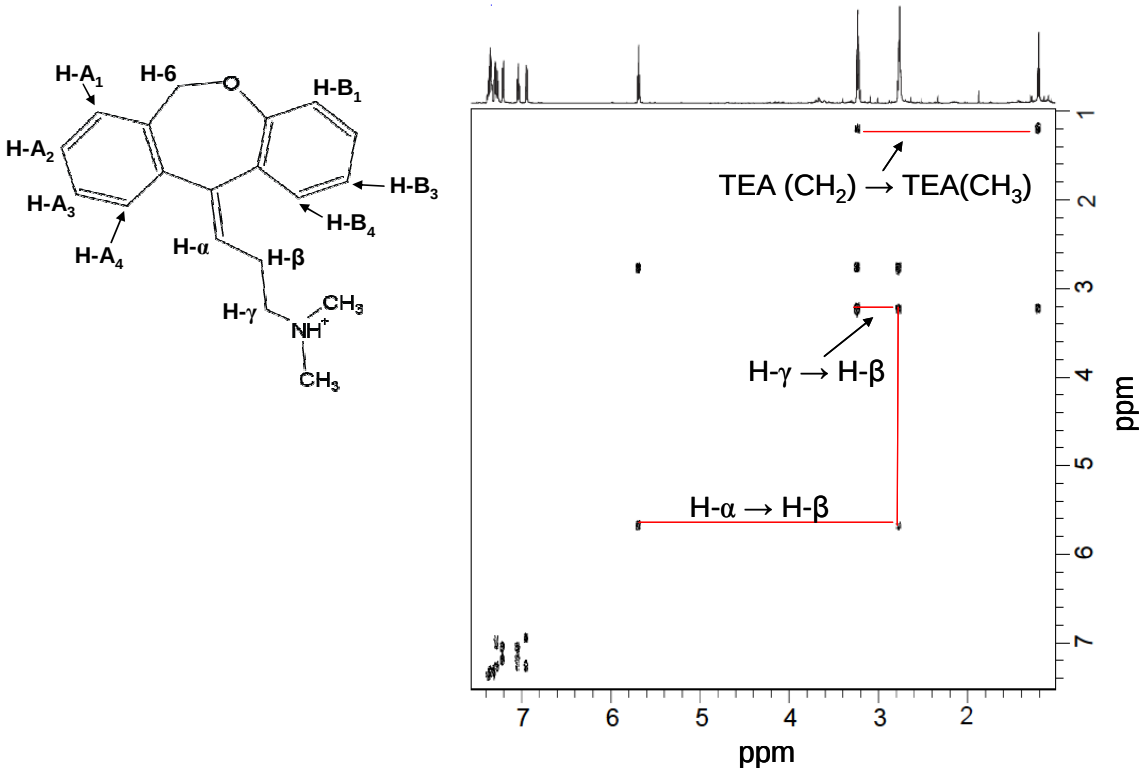

Figure 4.13. COSY NMR spectrum for ~0.5 mg of the doxepin Z isomer isolated by normal phase HPLC and reconstituted in 4 µL of D_2O. The spectrum was acquired in a commercial Protasis TXI microcoil probe. The red lines indicate cross peaks that correspond to the through bond coupling of the H-β proton to both the H-α and H-γ protons of doxepin. The cross peaks near 1 ppm represent through bond coupling of the methyl and methylene protons of TEA, an impurity introduced in the HPLC separation.

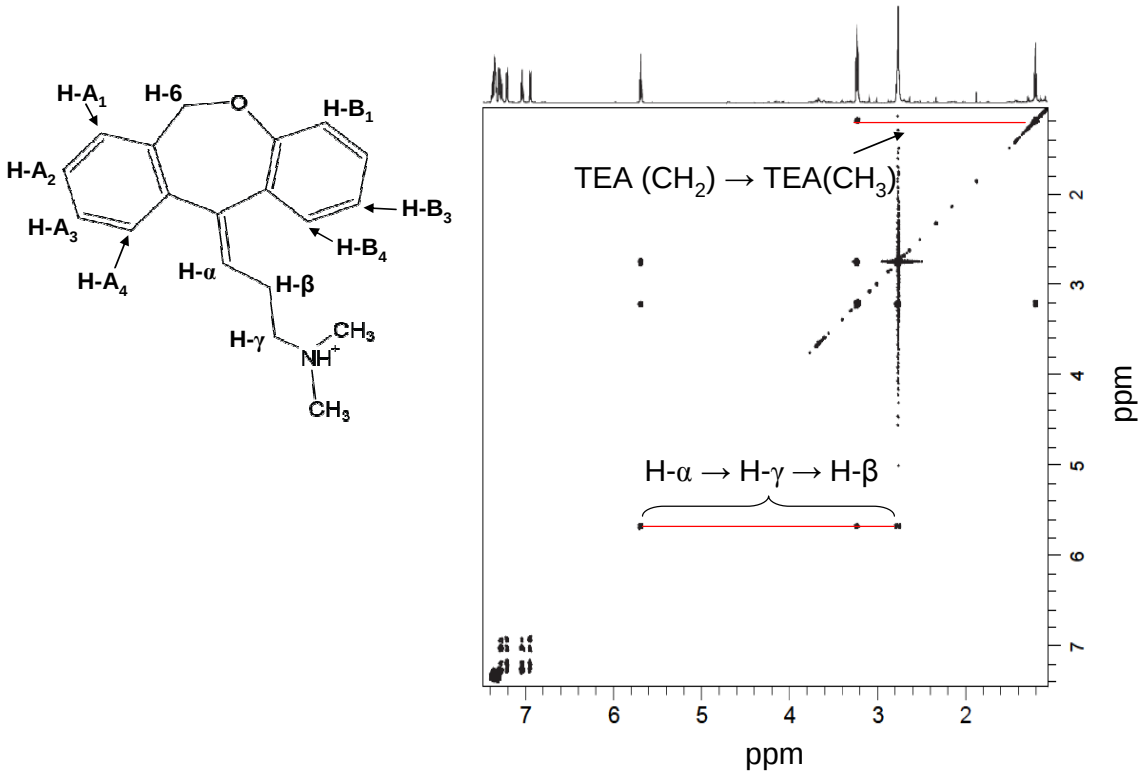

Figure 4.14. TOCSY NMR spectrum for ~0.5mg of the doxepin Z isomer isolated by normal phase HPLC and reconstituted in 4 μL of D_2O. The spectrum was acquired in a commercial Protasis TXI microcoil probe. The red lines indicate cross peaks that correspond to the coupling through multiple bonds in the same spin system. The cross peaks around 5.7 ppm in the F1 dimension indicate that the H-α, H-β, and H-γ protons are all in the same spin system (as expected). The cross peaks near 1 ppm in the F1 dimension again represent through bond coupling of the methyl and methylene protons of TEA, an impurity introduced in the HPLC separation.

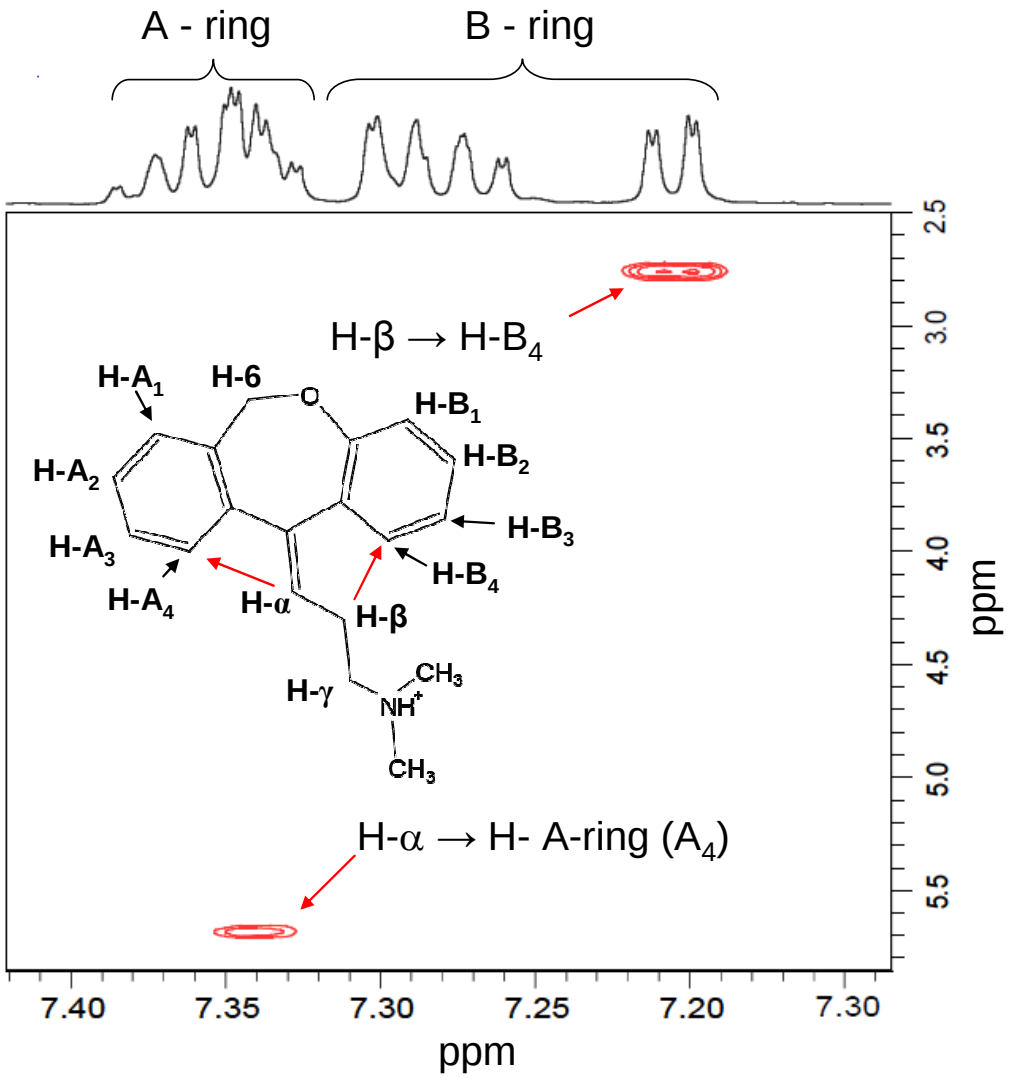

Figure 4.15. NOESY NMR spectrum for ~0.5 mg of the Z isomer of doxepin isolated by normal phase HPLC and reconstituted in 4 μL of D_2O. The spectrum was acquired in a commercial Protasis TXI microcoil probe. The NOE cross-peaks (shown in red) between the α proton near the double bond to a proton on the "A" ring (most likely the A_4 proton), and between the β proton to "B" ring (most likely the B_4 proton) confirms that the isolated compound is the doxepin Z isomer.

to a proton on the "A" ring (most likely the A_4 proton), and between the β proton to "B" ring (most likely the B_4 proton) confirm that the isolated compound was the doxepin Z isomer.

After confirming its identity, the isolated Z isomer was subjected to analysis by cationic cITP-NMR. The experiment was performed with no β-CD in the buffer system because in Figure 4.10 the resolved Z isomer appeared to be in a mostly unbound state. Figure 4.16 shows a comparison of the spectrum from the cITP separation in Figure 4.10 that we suspected might contain only the resolved Z isomer (Figure 4.16A) with the coadded spectrum from the online cITP-NMR analysis of the isolated Z isomer (Figure 4.16B). Although the Z isomer was concentrated to a concentration similar to that of the E isomer in Figure 4.16A, there are a number of E isomer resonances (indicated by blue asterisks) that indicate that complete resolution of the two isomers did not occur. Even so, the increased concentration of the Z isomer in Figure 4.16A compared to Figure 4.6 makes visualization of the Z isomer resonances much easier, although full structural characterization would still be very difficult using the current cITP-NMR platform.

4.3.2. Intracapillary pD and Magnetic Susceptibility Effects. While the cITP separation in Figure 4.10 was not successful in completely resolving the lower abundance Z isomer, the results are still useful for further probing the mechanism of cITP. In previous work the chemical shift of the LE counterion, acetate, was used to monitor online the pD of the solution in the LE, analyte band, and TE during cationic cITP.[3, 5, 32] In addition to using NMR to monitor the intracapillary pD, Korir et al. also compared the unreferenced chemical shifts of acetate and *tert*-butanol to address the spectral effects of

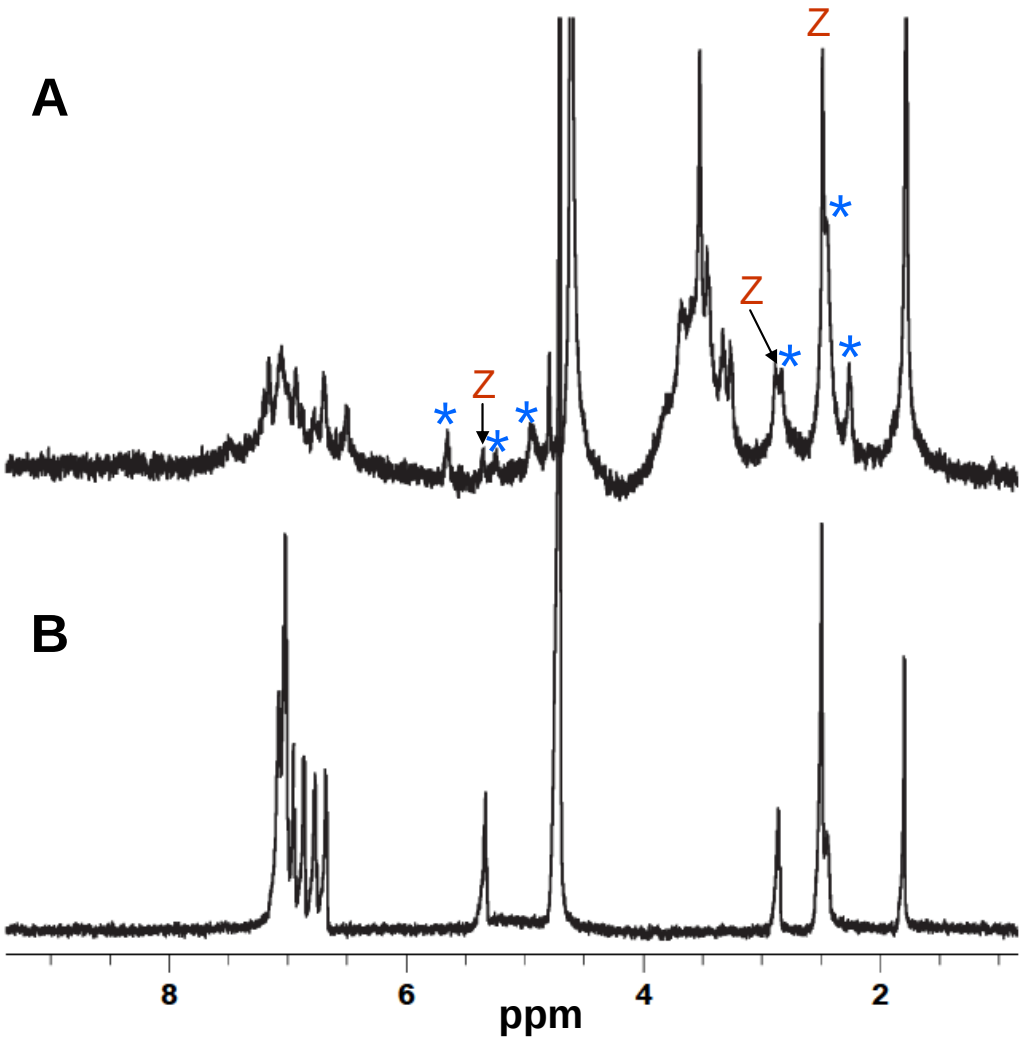

Figure 4.16. Comparison of the cITP-NMR spectra of A) the separation of doxepin shown in Figure 4.10 and B) the coadded spectrum of the isolated Z isomer analyzed by using a buffer system consisting of LE: 160 mM NaAcetate pD 5.0 and TE: 160 mM deuterated acetic acid. Resolved resonances of the E isomer are indicated with blue asterisks and resonances of the Z isomer are indicated by a red "Z".

differences in magnetic susceptibility of the sample band, TE and LE buffers.[3] Korir et al. concluded that for a cationic buffer system similar to the one used in Figure 4.5 with no β-CD, in both the LE and TE the acetate chemical shift directly related to real pD changes in the buffer. However, in the analyte band the chemical shift of acetate was dominated by the difference in magnetic susceptibility in the band compared to that of the LE or TE.[3] Figure 4.17 shows a similar trend in the acetate chemical shift for the cITP-NMR experiment shown in Figure 4.5. In Figure 4.17 the constant acetate chemical shift suggests that the pD of LE region of the capillary is uniform until the transition between the LE and analyte band is reached where a sharp upfield transition is observed in the chemical shift of the acetate resonance. From NMR titration curves for acetate, we know that if this change in chemical shift were due solely to pH effects, it would correspond to an increase in pD to a value higher than that of both the LE and the TE, which is highly unlikely in cationic cITP buffer systems.[3, 5, 32] However, this transition to a lower chemical shift is consistent with the report by Korir et al. in which the unreferenced chemical shift of acetate was measured and compared to that of the chemical shift reference *tert*-butanol. In this work the unusual change in the chemical shift of the acetate resonance was attributed to a difference in the magnetic susceptibility of the analyte band and was thought to not be reflective of the pD.[3] While the spectra shown in Figure 4.17 were referenced to the chemical shift of the HOD resonance and not *tert*-butanol, we still suspect that the odd change in the acetate chemical shift is a result of a change in magnetic susceptibility. Especially, since in Figure 4.17 we see that once the

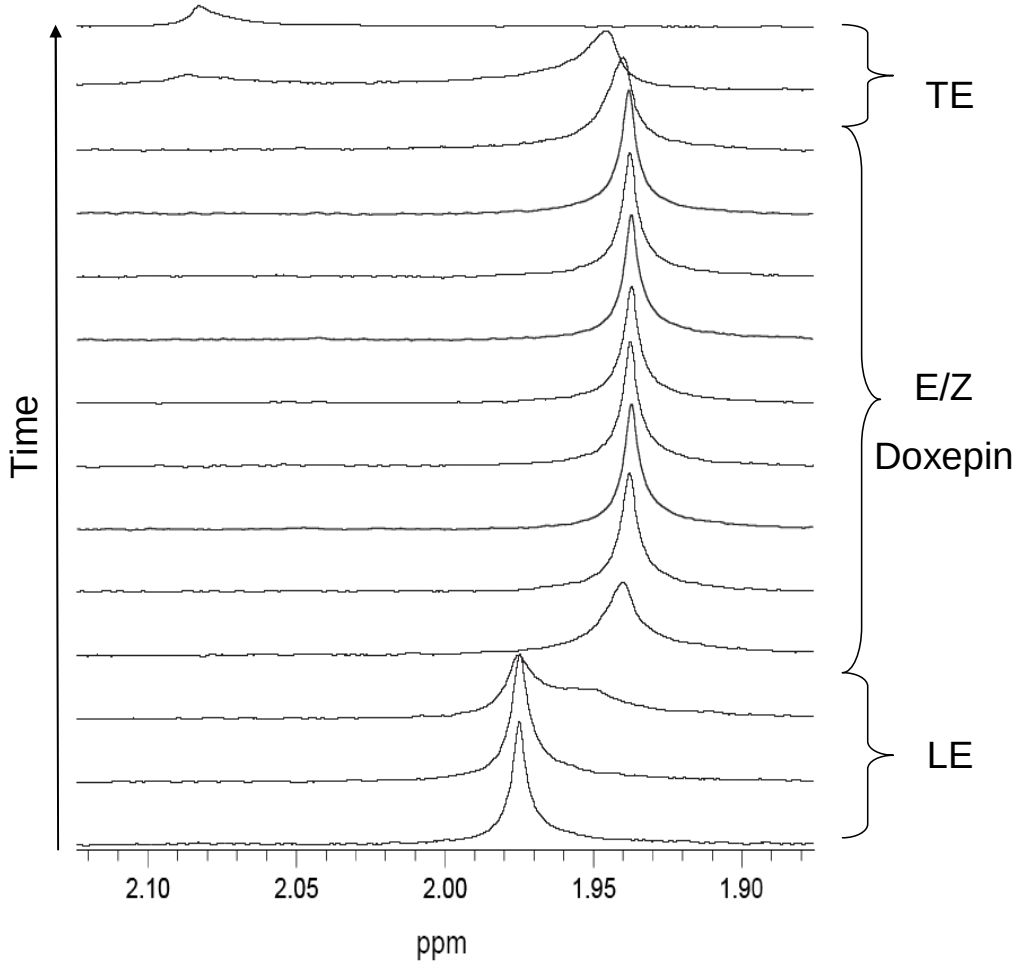

Figure 4.17. Expansion of the cITP-NMR spectra from Figure 4.3 showing the changes of the acetate resonance chemical shift over the course of the separation.

transition to the TE is reached that the chemical shift of acetate increases to a value we would expect given the pD of the TE (2.55).

Figure 4.18 shows the changes in acetate chemical shift for the cationic cITP separation of doxepin in Figure 4.10 in which 4.5 mM β-CD was used as a buffer modifier. A very different chemical shift profile is observed in Figure 4.18 from that observed in Figure 4.17. In the LE we see that the chemical shift of acetate starts at a chemical shift similar to its initial position in Figure 4.17, but as the transition zone between the LE and the analyte is approached, the acetate chemical shift drifts downfield. Even once doxepin appears in the active volume of the coil, the acetate resonance chemical shift continues a gradual downfield drift. Finally at the transition point between the free doxepin isomers and the β-CD complexed isomers there is a distinct change in the chemical shift of doxepin. This seems to confirm that the region at the beginning of the analyte band that contained what seemed to be the isomers in their free form was a poorly focused, diffuse transition zone between the LE and the more focused portion of the band where the bound doxepin isomers are observed. Additionally, in the transition zone between the diffuse portion of the band and the better focused portion of the sample band an extreme downfield transition in the acetate chemical shift suggests a local pD at that point similar to the TE (although it is difficult to put an exact value on the shift because of the broadness of the resonance). Spectrally, this is observed as two broad resonances likely indicating that the spectrum at the transition point shows acetate moving between the two very distinct pD zones (one at a low pD and one near the pD of the LE). This presence of the low pD zone suggests a buildup of D^+ at this transition

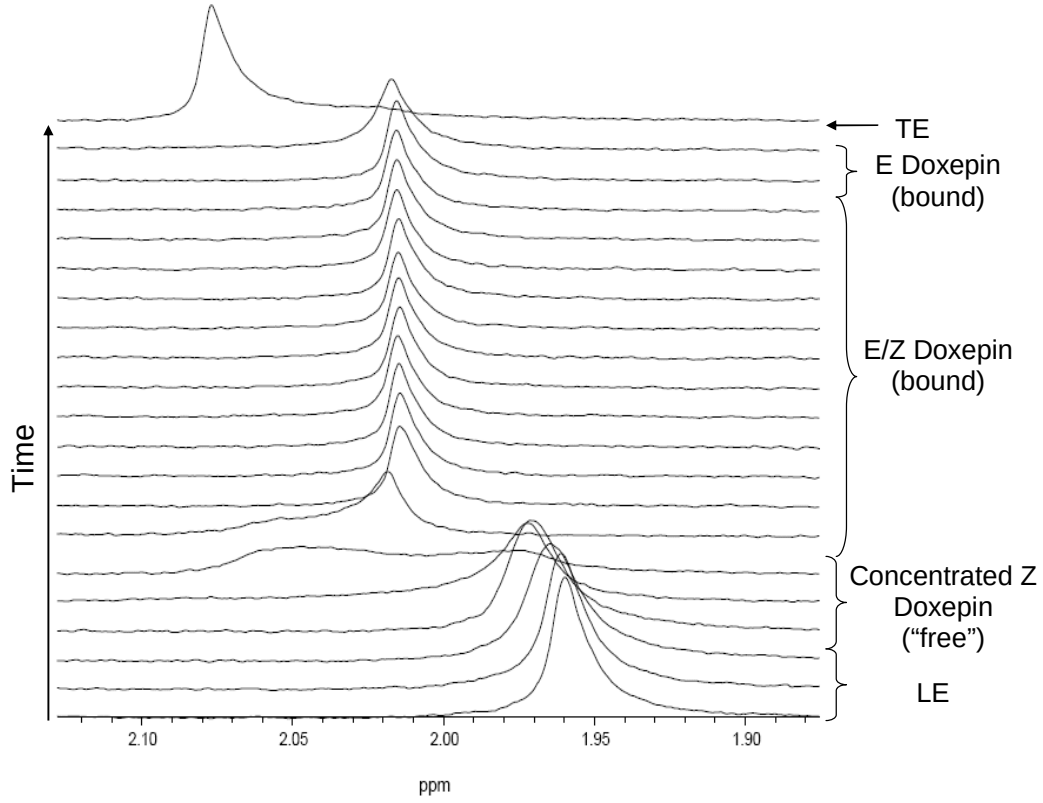

Figure 4.18. The expansion of the cITP-NMR spectra from Figure 4.8 showing the changes of the acetate resonance chemical shift over the course of the separation.

zone similar to that seen by Korir et al.[3] However, after this quick transition the chemical shift of acetate quickly shifts back upfield where it remains constant throughout the rest of the analyte band. In contrast to Figure 4.17 the shift in this region does not seem to be influenced by a change in magnetic susceptibility although this is difficult to say for sure without comparing the unreferenced chemical shifts to a pD independent internal reference like *tert*-butanol. In the cITP-NMR experiments performed in this chapter, an internal reference was not used to avoid complications from binding to β-CD. Finally, once the transition between the sample and TE is reached another sharp chemical shift transition is seen indicating the transition to the lower pD TE.

4.3.3. Evaluation of Differential Binding of Doxepin Isomers with β-CD by cITP.

In Section 4.3.1. we showed that the binding constants for the both the E and Z isomers of doxepin to β-CD could be determined by measuring the change in mobility of each isomer as a function of β-CD concentration of the running buffer. However, determining binding information in such a way is a very time consuming and work intensive process. In previous work our group has shown that the concentration of β-CD that co-concentrates with a given analyte during cationic cITP is correlated with the binding constant.[2] Furthermore, from experiments conducted in a 5 mm probe we have shown that the chemical shift of the β-CD resonances are dependent on the ratio of the concentrations of β-CD:doxepin.[29] To test if our cationic cITP method could yield similar information about the binding constants of the E and Z isomers of doxepin, the Z isomer isolated by HPLC was subjected to analysis by cITP NMR using a buffer containing 10 mM β-CD in both the LE and the TE. Figure 4.19 shows the comparison

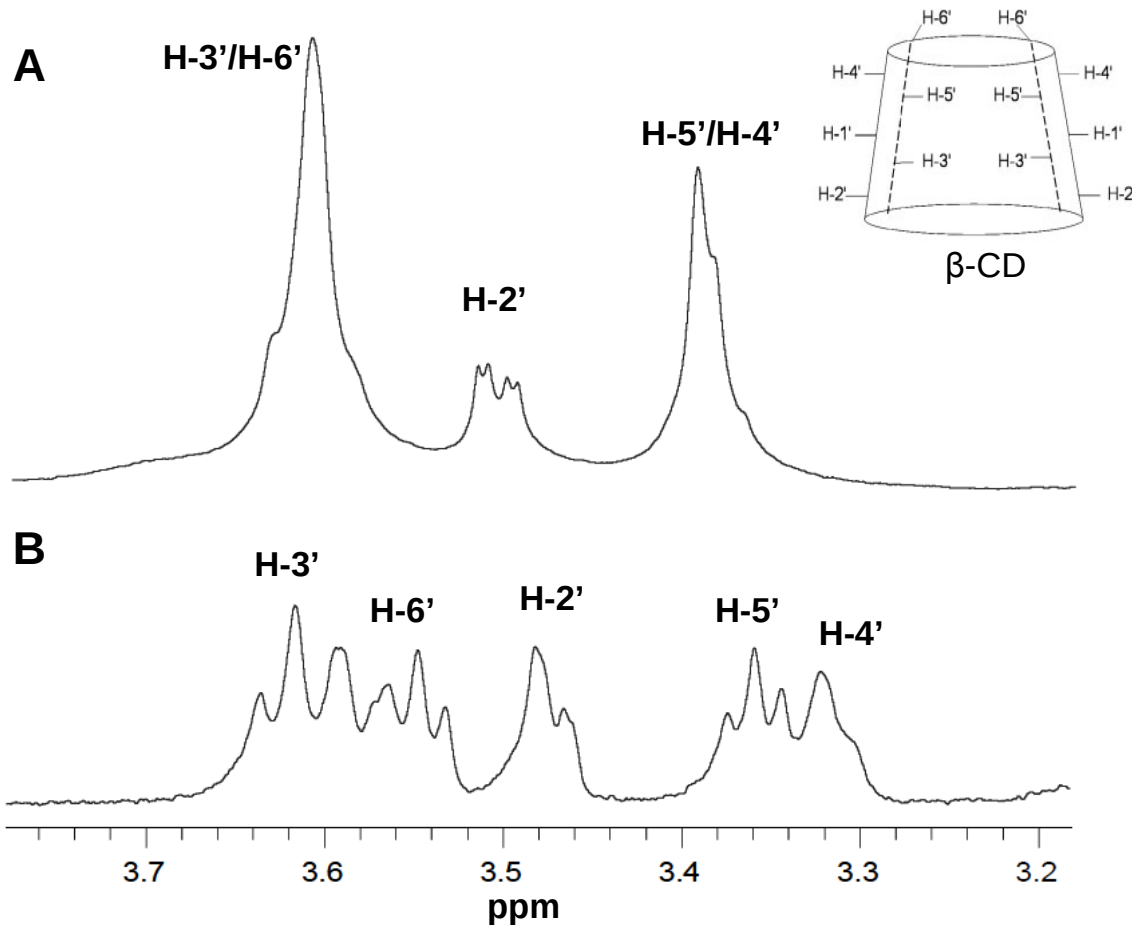

Figure 4.19. Results comparing the β-CD resonances for A) the online cITP-NMR analysis of a mixture of E and Z isomers of doxepin using a cITP buffer system of LE: 160 mM NaAcetate, 10 mM β-CD (pD 5.0); TE: 160 mM deuterated acetic acid, 10 mM β-CD to B) the online cITP NMR analysis of only the Z isomer of doxepin using the same buffer system.

the of the β-CD resonances for the coadded spectrum from this experiment and the β-CD resonances of the coadded spectrum of the experiment in Figure 4.9 where the mixture of E and Z isomers were focused with the same amount of β-CD in the LE and TE (the assignments of the β-CD resonances are based off on those of Cruz et al.[29]). Comparing the spectra in Figure 4.19A and B, a clear difference in the chemical shifts of the β-CD resonances is observed indicating differential degrees of binding. Using the results reported by Cruz et al., the β-CD chemical shifts in Figure 4.19A indicate a 1:1 β-CD:doxepin ratio in the focused analyte band.[29] However, the chemical shifts of β-CD in Figure 4.19B where only the Z isomer was focused indicates a β-CD:doxepin ratio closer to 1:5. While binding constants can not be derived from this data, relative binding strengths can easily be inferred for the two isomers from these experiments which only took a total of about 4 hrs to run compared to a day or more for the CE experiments described earlier. Additionally, because these separations only need ~9 nanomoles of material the time needed for offline HPLC enrichment prior to analysis is greatly reduced.

4.3.4. Visualizing Intracapillary Movement of β-CD. As discussed in the previous section work from our group, as well as others, has shown that during cITP β-CD in the buffer system co-concentrates with charged analytes with which it forms complexes.[2, 7] However, none of the previous work has addressed the question of where the β-CD that co-concentrates in the analyte band comes from. Because β-CD is an uncharged molecule, its mobility within the capillary should be limited to diffusional movement (with a diffusion coefficient around 3×10^{-6} cm^2s^{-1})[33] and from interactions with charged analytes in the buffer. In the work by Jayawickrama et al. movement of β-

CD into the analyte band was accomplished by adding a small concentration of sulfated β-CD to the LE in addition to 150 mM α-CD, which carries no charge. Because the β-CD was sulfated it migrated through the capillary in the opposite direction as the analyte band where it interacted with the sample.[7] To try to elucidate where in our separation the uncharged β-CD that co-concentrated in the analyte band during cITP NMR analysis came from, a series of doxepin cITP-NMR experiments were designed to investigate the degree of co-concentration and intracapillary movement of β-CD. Figure 4.20 shows a pseudo two-dimensional plot of the results of the online cITP analysis of doxepin using an LE buffer of 160 mM NaAcetate and 10 mM β-CD at pD 5.0 and a TE buffer of 160 mM deuterated acetic acid, no β-CD. Similar to Figure 4.9 where 10 mM β-CD was present in both the LE and TE, in Figure 4.20 we see the co-concentration of β-CD within the doxepin analyte band. From the chemical shifts of the doxepin resonances, it is clear that doxepin is in the bound form. Additionally, a diffuse trail of β-CD from the back of the analyte band is observed extending into the TE. Because there is no β-CD in the TE buffer, the β-CD in this trail must have come from the LE. Because of the high concentration of β-CD that co-concentrated in the analyte band we initially postulated that this trail is likely from neutral β-CD that diffused out of the analyte band and into the TE.

To test this hypothesis we performed the experiment again but this time with no sample so that the β-CD could not concentrate inside the capillary. Figure 4.21 shows the results of this experiment. Following the acetate resonance a sharp transition zone is observed between the LE and the TE where the analyte band would have been. As

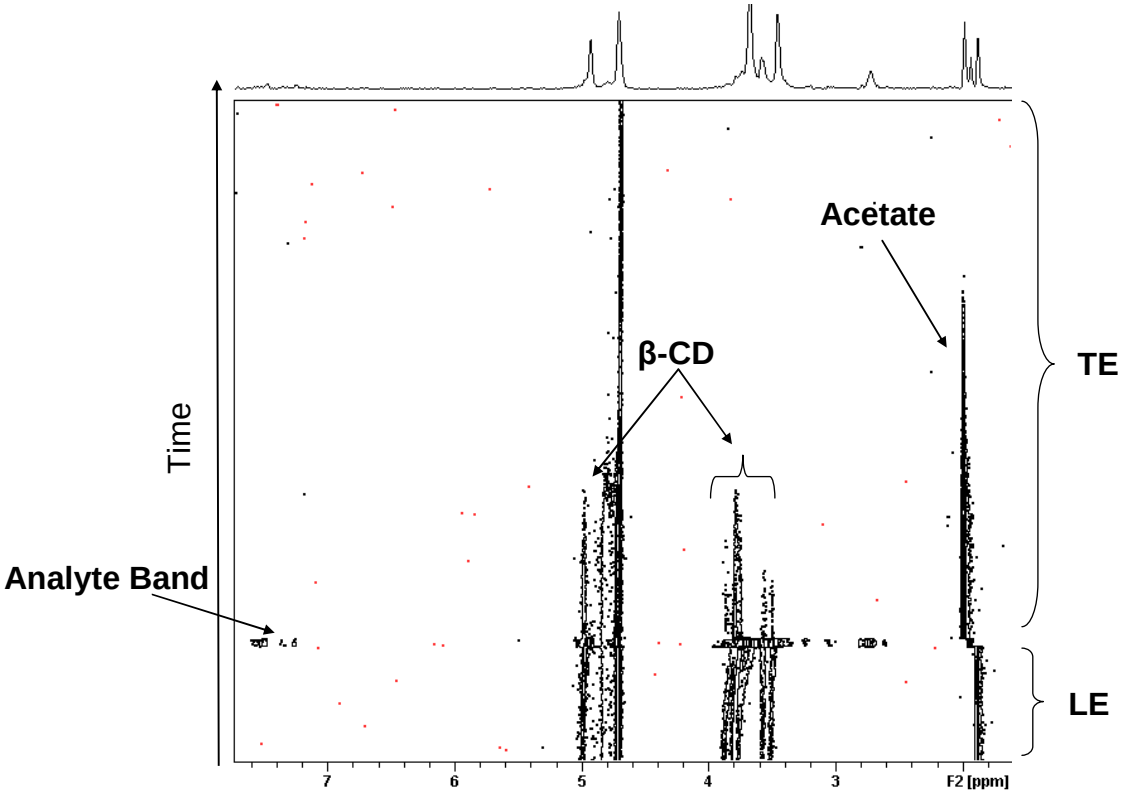

Figure 4.20. Pseudo two-dimensional plot of the online cITP NMR analysis of a mixture of E and Z isomers of doxepin using a cITP buffer system of LE: 160 mM NaAcetate, 10 mM β-CD (pD 5.0); TE: 160 mM deuterated acetic acid and no β-CD.

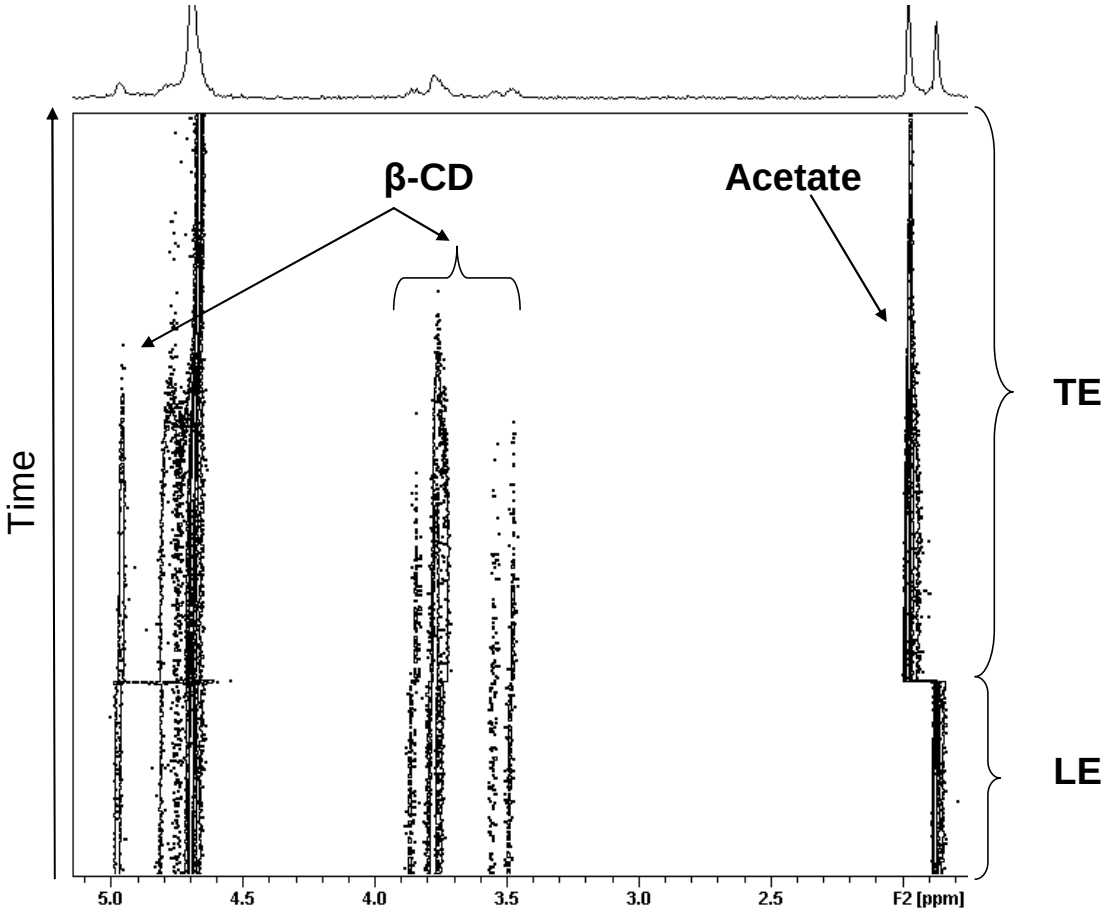

Figure 4.21. Pseudo two-dimensional plot of the online cITP NMR experiment with no sample using a cITP buffer system of LE: 160 mM NaAcetate, 10 mM β-CD (pD 5.0); TE: 160 mM deuterated acetic acid no β-CD.

expected, β-CD does not concentrate at the LE/TE interface in the spectra shown in Figure 4.21, but a diffuse trail of β-CD into the TE is still observed similar to that in Figure 4.20. It seemed unlikely the movement of β-CD into the TE in Figure 4.21 was the result of simple diffusion because β-CD was not concentrated between the LE and TE, and yet the β-CD trail extends as far into the TE as it did in Figure 4.20 where β-CD was concentrated in the analyte band exaggerating the concentration gradient of β-CD between the LE and TE.

To explain these results, we postulated that the trail resulted from β-CD being pulled into the TE by interactions with a negatively charged ion like acetate that can migrate from the LE through the analyte band and into the TE. To test this hypothesis a cITP-NMR experiment (Figure 4.22) was performed for doxepin using a buffer system consisting of an LE of 160 mM NaAcetate (pD 5.0) and a TE of 160 mM deuterated acetic acid with 10 mM β-CD. No β-CD was added to the sample or to the LE, and the use of protonated acetate in the LE and deuterated acetic acid in the TE allows the transport of acetate from the LE into the TE to be monitored by NMR. Although doxepin is focused in Figure 4.22A, β-CD does not co-concentrate in the analyte band. Interestingly, in Figure 4.22A, the resonances of β-CD also do not appear anywhere in the beginning of the TE. In fact, in Figure 4.22B we see that the resonances of β-CD do not appear until after the acetate resonance disappears. At this point, the acetate from the LE has been fully converted to acetic acid and can no longer migrate towards the anode.

The results in Figure 4.22 suggest that when acetate and β-CD are both present in the LE, a binding interaction between them allows the β-CD to migrate with the acetate

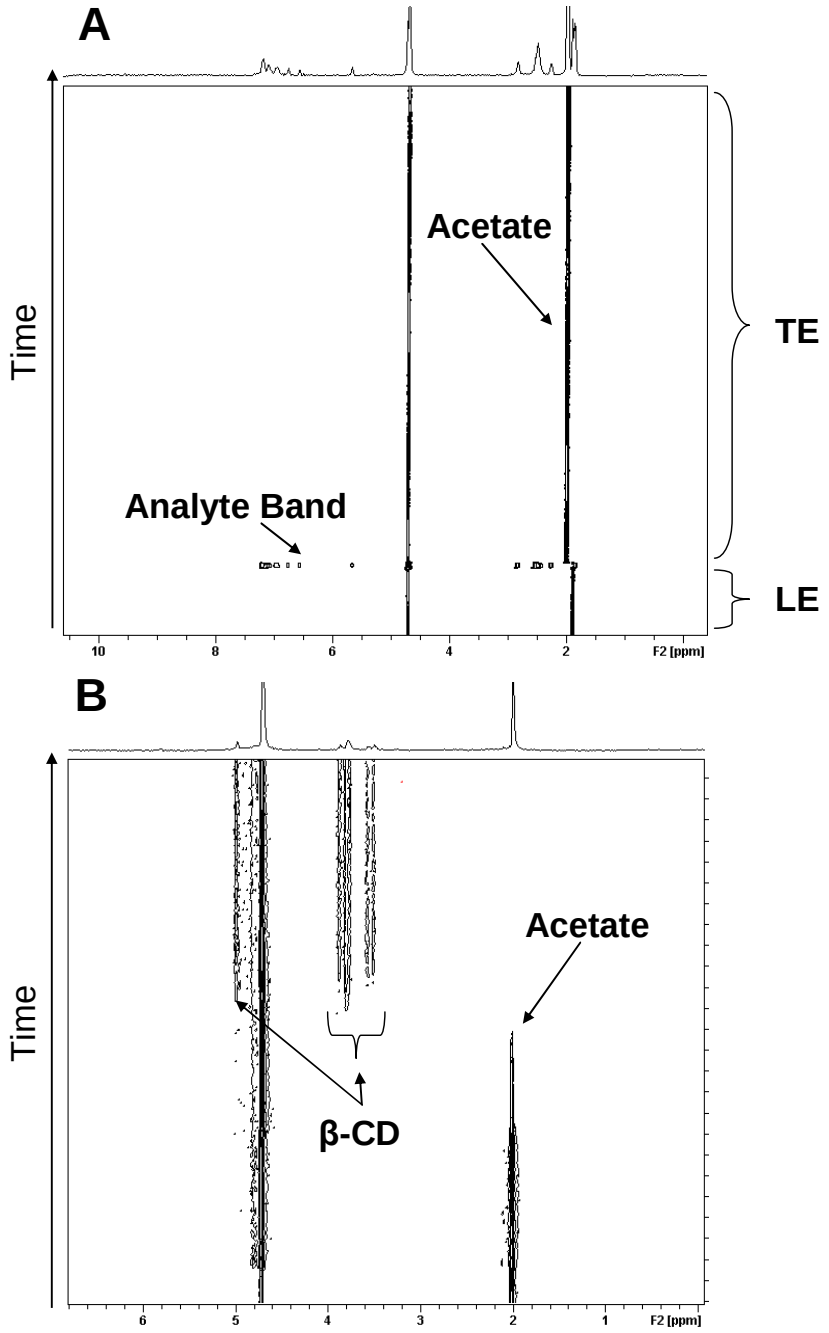

Figure 4.22. Pseudo two-dimensional plots of the online cITP NMR analysis of doxpein using a cITP buffer system of LE: 160 mM NaAcetate (pD 5.0); TE: 160 mM deuterated acetic acid, 10 mM β-CD. A) The region of the separation containing the LE, analyte band, and the beginning of the TE, and B) an expansion of the data set showing the region of the separation where the acetate from the LE stops migrating and β-CD appears.

toward the anode into the TE. To confirm this binding interaction, spectra were acquired for an acetate solution with and without β-CD. In Figure 4.23, we see a small but distinct downfield shift of the acetate resonance with the addition of 10 mM β-CD to the solution indicating a binding. Because the change in chemical shift is so small (about 3 Hz) a full NMR titration could not be performed, but the binding of acetate and β-CD might be an additional reason for the poor least squares fit of the 1:1 binding model for the NMR titration of β-CD and doxepin seen in Figure 4.3. Because acetate can also act as a counterion/ion-pair (demonstrated in Figure 4.4 by the split resonance for the methyl resonance of the E isomer) to doxepin it is possible that the acetate bound to β-CD acts to stabilize the complexation of β-CD and doxepin. This is evidenced by the binding constant we calculated for the E isomer by CE which is more than double that of the previously reported value (3.60×10^4 M^{-1} vs. 1.32×10^4 M^{-1}) that was measured in a sodium chloride solution.[20] However, the co-concentration of β-CD and doxepin in the analyte band seems to refute any idea that both acetate and doxepin bind to β-CD at the same time, as an ion-pair between doxepin and acetate would neutralize the two preventing the complex from focusing by cITP. A more likely scenario is one in which the acetate/β-CD complex migrates into the analyte band. Once in the analyte band doxepin will be attracted to both the negative charge of acetate and to the cavity of β-CD. Then the more hydrophobic doxepin forces the acetate out of the binding pocket leaving acetate free to continue migrating towards the anode and allowing the newly formed doxepin/ β-CD complex to focus in the analyte band. However, because both isomers should be equally attracted to the acetate ion it is unclear if this added interaction could

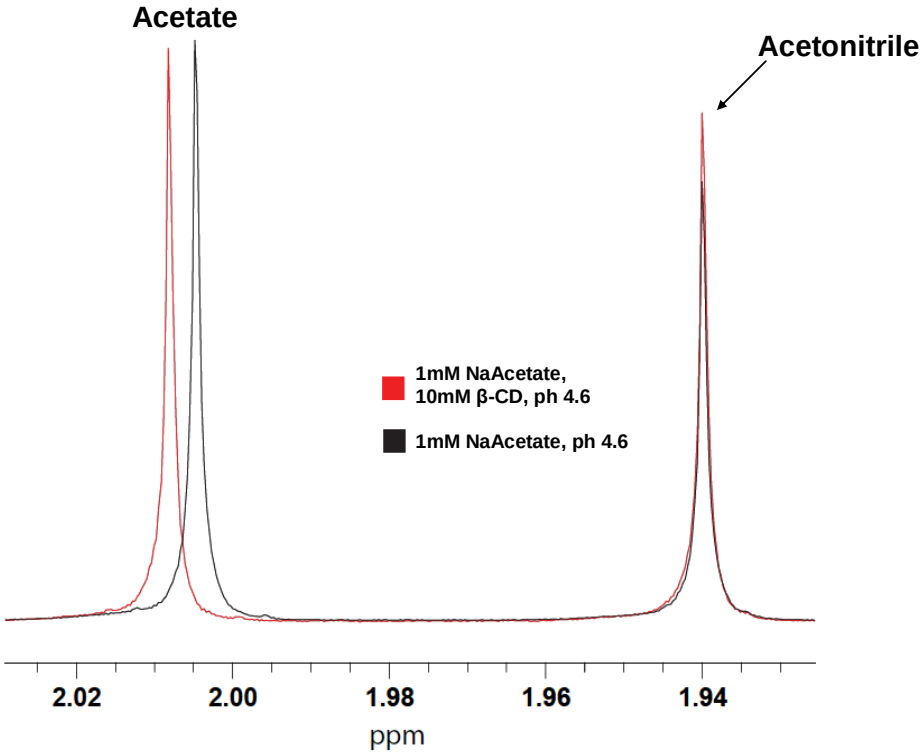

Figure 4.23. Overlay of the ^{1}H NMR survey spectra acquired in a 5mm NMR probe showing the change in chemical shift of acetate with the addition of 10 mM β-CD to the solution (red spectrum) indicating binding of acetate and β-CD.

be the reason for the poor isomer resolution in the cITP-NMR separation shown in Figure 4.10.

4.4 Conclusions

In this chapter online cationic cITP-NMR was used to concentrate and separate the components of a commercial preparation of the tricyclic antidepressant doxepin using β-CD as a buffer modifier. While the cITP separation did not yield full resolution of the less abundant Z isomer, the binding constants of both E and Z isomers to β-CD were determined using CE. To the best of our knowledge, the binding constant for the Z isomer has not been previously reported. These experiments further demonstrated the value of coupling cITP to microcoil NMR for the study of the physico-chemical processes involved in the separation such as changes in intracapillary pD and interactions between various components of the buffer and sample. In Chapter 5 the insights gained from this chapter and from previous studies are used to optimize an anionic cITP buffer system for the analysis of heparin and heparan sulfate oligosaccharides

4.5 References

1. Gökay, O.; Albert, K., From single to multiple microcoil flow probe NMR and related capillary techniques: a review. *Anal. Bioanal. Chem.* **2012,** 402, 647-669.

2. Almeida, V. K.; Larive, C. K., Insights into cyclodextrin interactions during sample stacking using capillary isotachophoresis with on-line microcoil NMR detection. *Magn. Reson. Chem.* **2005,** 43, 755-761.

3. Korir, A. K.; Almeida, V. K.; Larive, C. K., Visualizing ion electromigration during isotachophoretic separations with capillary isotachophoresis-NMR. *Anal. Chem.* **2006,** 78, 7078-7087.

4. Morris, K. F.; Froberg, A. L.; Becker, B. A.; Almeida, V. K.; Tarus, J.; Larive, C. K., Using NMR to develop insights into electrokinetic chromatography. *Anal. Chem.* **2005,** 77, 254 A-263 A.

5. Wolters, A. M.; Jayawickrama, D. A.; Larive, C. K.; Sweedler, J. V., Insights into the cITP process using on-line NMR spectroscopy. *Anal. Chem.* **2002,** 74, 4191-4197.

6. Eldridge, S. L.; Almeida, V. K.; Korir, A. K.; Larive, C. K., Separation and analysis of trace degradants in a pharmaceutical formulation using on-line capillary isotachophoresis-NMR. *Anal. Chem.* **2007,** 79, 8446-8453.

7. Jayawickrama, D.; Sweedler, J., Chiral separation of nanomole amounts of alprenolol with cITP/NMR. *Anal. Bioanal. Chem.* **2004,** 378, 1528-1535.

8. Jayawickrama, D. A.; Sweedler, J. V., Hyphenation of capillary separations with nuclear magnetic resonance spectroscopy. *J. Chromatogr., A* **2003,** 1000, 819-840.

9. Kautz, R. A.; Lacey, M. E.; Wolters, A. M.; Foret, F.; Webb, A. G.; Karger, B. L.; Sweedler, J. V., Sample concentration and separation for nanoliter-volume NMR spectroscopy using capillary isotachophoresis. *J. Am. Chem. Soc.* **2001,** 123, 3159-3160.

10. Korir, A.; Larive, C., On-line NMR detection of microgram quantities of heparin-derived oligosaccharides and their structure elucidation by microcoil NMR. *Anal. Bioanal. Chem.* **2007,** 388, 1707-1716.

11. Korir, A. K.; Almeida, V. K.; Malkin, D. S.; Larive, C. K., Separation and analysis of nanomole quantities of heparin oligosaccharides using on-line capillary isotachophoresis coupled with NMR detection. *Anal. Chem.* **2005,** 77, 5998-6003.

12. Korir, A. K.; Larive, C. K., Advances in the separation, sensitive detection, and characterization of heparin and heparan sulfate. *Anal. Bioanal. Chem.* **2009,** 393, 155-169.

13. Olson, D. L.; Peck, T. L.; Webb, A. G.; Magin, R. L.; Sweedler, J. V., High-resolution microcoil ^{1}H-NMR for mass-limited, nanoliter-volume samples. *Science* **1995,** 270, 1967-1970.

14. Bocek, P.; M. Demi; Gebauer, P.; Dolnik, V., *Analytical isotachophoresis*. VCH Publishers: New York, 1988; p 237.

15. Chankvetadze, B.; Kartozia, I.; Burjanadze, N.; Bergenthal, D.; Luftmann, H.; Blaschke, G., Enantioseperation of chiral phenothiazine derivatives in capillary electrophoresis using cyclodextrin type chiral selectors. *Chromatographia* **2001,** 53, S290-S295.

16. Gübitz, G.; Schmid, M. G., Chiral separation by capillary electromigration techniques. *J. Chromatogr., A* **2008,** 1204, 140-156.

17. Juvancz, Z.; Kendrovics, R. B.; Iványi, R.; Szente, L., The role of cyclodextrins in chiral capillary electrophoresis. *Electrophoresis* **2008,** 29, 1701-1712.

18. Scriba, G. K. E. V., Cyclodextrins in capillary electrophoresis enantioseparations – Recent developments and applications. *J. Sep. Sci.* **2008,** 31, 1991-2011.

19. Lin, S.-C.; Whang, C.-W., Capillary electrophoretic separation of tricyclic antidepressants using a polymer-coated capillary and β-cyclodextrin as an electrolyte additive. *J. Sep. Sci.* **2008,** 31, 3921-3929.

20. Valsami, G. N.; Koupparis, M. A.; Macheras, P. E., Complexation Studies of Cyclodextrins with Tricyclic Antidepressants Using Ion-Selective Electrodes. *Pharmaceut. Res.* **1992,** 9, 94-100.

21. Korir, A. K.; Larive, C. K., On-line NMR detection of microgram quantities of heparin-derived oligosaccharides and their structure eluctdation by microcoil NMR. *Anal. Bioanal. Chem.* **2007,** 388, 1707-1716.

22. Bax, A., A spatially selective composite 90° radiofrequency pulse. *J. Magn. Reson.* **1985,** 65, 142-145.

23. Terabe, S.; Otsuka, K.; Nishi, H., Separation of enantiomers by capillary electrophoretic techniques. *J. Chromatogr., A* **1994,** 666, 295-319.

24. Al Azzam, K. M.; Saad, B.; Aboul-Enein, H. Y., Determination of the binding constants of modafinil enantiomers with sulfated β-cyclodextrin chiral selector by capillary electrophoresis using three different linear plotting methods. *Electrophoresis* **2010,** 31, 2957-2963.

25. Casarotto, M. G.; Craik, D. J., Ring flexibility within tricyclic antidepressant drugs. *J. Pharm. Sci.* **2001,** 90, 713-721.

26. Casarotto, M. G.; Craik, D. J.; Munro, S. L. A., 13C NMR studies of the solution molecular dynamics of tricyclic antidepressants. *Magn. Reson. Chem.* **1990,** 28, 533-540.

27. Munro, S. L.; Andrews, P. R.; Craik, D. J.; Gale, D. J., 13C NMR studies of the molecular flexibility of antidepressants. *J. Pharm. Sci.* **1986,** 75, 133-141.

28. Wilson, J. C.; Munro, S. L. A.; Craik, D. J., ^{13}C and ^{1}H NMR studies of nitrogen inversion and molecular flexibility in the tricyclic antidepressant drug trimipramine maleate. *Magn. Reson. Chem.* **1995,** 33, 367-374.

29. Cruz, J. R.; Becker, B. A.; Morris, K. F.; Larive, C. K., NMR characterization of the host–guest inclusion complex between β-cyclodextrin and doxepin. *Magn. Reson. Chem.* **2008,** 46, 838-845.

30. Wolters, A. M.; Jayawickrama, D. A.; Larive, C. K.; Sweedler, J. V., Capillary Isotachophoresis/NMR extension to trace impurity analysis and improved instrumental coupling. *Anal. Chem.* **2002,** 74, 2306-2313.

31. Wolters, A. M.; Jayawickrama, D. A.; Webb, A. G.; Sweedler, J. V., NMR detection with multiple solenoidal microcoils for continuous-flow capillary electrophoresis. *Anal. Chem.* **2002,** 74, 5550-5555.

32. Eldridge, S. L. Development of analytical methods for trace impurity analysis and structure determination of heparin/heparan sulfate-derived oligosaccharides. University of California, Riverside, Riverside, CA, 2009.

33. Lin, M.; Jayawickrama, D. A.; Rose, R. A.; DelViscio, J. A.; Larive, C. K., Nuclear magnetic resonance spectroscopic analysis of the selective complexation of the cis and trans isomers of phenylalanylproline by β-cyclodextrin. *Anal. Chim. Acta* **1995,** 307, 449-457.

CHAPTER FIVE

Analysis of Heparin-Derived Oligosaccharides by Anionic Capillary Isotachophoresis Coupled to Microcoil NMR

The SEC hexasaccharide fractions of heparinase III digested heparan sulfate and enoxaparin were collected by Consuelo Beecher and Derek Langeslay. The SEC hexasaccharide fraction of heparinase I digested heparin was collected with the assistance of Derek Langeslay, John Limtiaco, and Szabolcs Beni.

The work presented in this chapter builds on the mechanistic details of capillary isotachophoresis (cITP) gained in Chapter 4 for the cationic cITP separation of the isomers of doxepin to create a new, optimized anionic buffer system for the focusing and separation of heparin and heparan sulfate (HS) derived oligosaccharides. While methods for cITP analysis of heparin and HS derived oligosaccharides have been published previously by our group, the spectra suffered from poor spectral resolution as a result of current induced broadening and from low S/N due to poor cITP focusing. The new buffer system described in this chapter utilizes a tricine buffer trailing electrolyte (TE) in place of the 2-(*N*-morpholino)ethanesulfonic acid (MES) TE used in our previous work. Tricine significantly reduces the electrophoretic current during cITP. The new method also uses the stop flow approach introduced in Chapter 4 to park the focused analyte bands in the active volume of the microcoil for increased signal averaging to further improve S/N.

5.1 Introduction

As was discussed in Chapter 1, NMR spectroscopy has proven to be a useful technique for the structural characterization of heparin and HS oligosaccharides.[1, 2] For highly purified, single oligosaccharides, visual examination of a simple ^{1}H NMR survey spectrum can both reveal the number of monosaccharide residues present in the oligosaccharide and give a tentative structural assignment by comparison of the resonance chemical shifts with reference data. However, NMR is often limited by poor sensitivity and for samples containing more than one compound of interest, the spectra obtained can quickly become convoluted, complicating interpretation. This is especially a concern for heparin and HS derived samples that are often highly polydisperse mixtures of microheterogeneous oligosaccharides.[3] As described in Chapters 2 and 3, to address this problem most analytical methods used for the study of heparin and HS involve some form of size- or charge-based separation prior to NMR analysis.[4]

Previously, our laboratory demonstrated the use of cITP-NMR for the measurement of ^{1}H NMR spectra for only 1-2 μg of heparin derived di- and tetrasaccharides.[5-7] However, the structural information provided by these spectra was limited by broad resonances and poor spectral resolution due to the magnetic field created by the current running through the capillary during separations. Also, because charged analytes migrate through the capillary to the microcoil for detection once they have focused and stacked into concentrated bands, ^{1}H NMR spectra have to be acquired on a transient basis which limits the ability to signal average for an extended period to

increase spectral S/N or to perform longer two-dimensional experiments. In an attempt to overcome these limitations previous experiments from our lab showed that lowering the separation voltage when the analyte band reaches the microcoil can reduce the separation current sharpening resonance line widths and slowing the movement of the peak without significant dispersion of the focused band.[6] However, the resonances in the spectra obtained were still noticeably broadened compared to static spectra, and only about 12 quick 8 scan FID's could be acquired before the analyte band moved out of the active volume of the coil. Also, the buffer system used in these experiments failed to focus the less charged heparin derived disaccharides IVA, IIH, IIIH and IVH limiting the applicability of the method.[5]

The work described in this chapter presents an optimized anionic cITP buffer system for the focusing and separation of heparin derived oligosaccharides. This buffer system utilizes a tricine TE buffer in place of the MES TE used in our previous work, significantly reducing the electrophoretic current during cITP and as a consequence, reducing spectral broadening. These experiments also use the stop flow method introduced in Chapter 4, which is similar to the approach of Kautz et al., to park the focused analyte bands in the active volume of the microcoil for increased signal averaging.[8] Finally, the new buffer system and stop-flow method will be used to focus, separate, and characterize a series of heparin derived oligosaccharides including all 12 commercially available disaccharides (including IVH, IVA, IIH, and IIIH which could not be focused using the previous buffer system and IVS which was not available commercially at the time the previous experiments were carried out), hexasaccharide

fractions of depolymerized heparin, HS, and the low molecular weight heparin (LMWH) enoxaparin obtained by size-exclusion chromatography (SEC), as well as an unfractionated enoxaparin sample.

5.2 Experimental

5.2.1. Materials and Reagents. Fused silica capillaries were purchased from Polymicro (Phoenix, AZ) and surface-modified to produce zero electroosmotic flow (EOF) by MicroSolv Technology Corporation (Eatontown, NJ). Polyurethane-coated copper wire (99.99% Cu) was purchased from the California Fine Wire Company (Grover Beach, CA). Non-magnetic trimmer capacitors were purchased from Voltronics. MES, 99%, porcine intestinal mucosa heparin sodium salt, grade 1-A, and the heparin derived disaccharides IS, IIS, IIIS, IH, IIH, IIIH, and IVH (structures shown in Table 5.1) were purchased from Sigma-Aldrich, Inc. (St. Louis, MO). Heparan sulfate was purchased from Celsus (Cincinnati, Ohio). The heparin derived disaccharides IA, IIA, IIIA, IVA, and IVS (structures shown in Table 5.1) were purchased from V-Labs (Covington, LA). Imidazole was purchased from Thermo Fisher Scientific (Waltham, Mass). Tricine was purchased from Spectrum Pharmaceuticals (Gardena, CA). Deuterium oxide (D_2O, 99.9% D low paramagnetic) and sodium deuteroxide were purchased from Cambridge Isotope Laboratories, Inc. (Andover, MA). Enoxaparin sodium was purchased from the U.S. Pharmacopeia (USP, Rockville, MD). The 0.2 μm nylon syringe filters were purchased from MicroSolv (Eatontown, NJ).

Table 5.1. Names and structures of the family of heparin disaccharides studied.

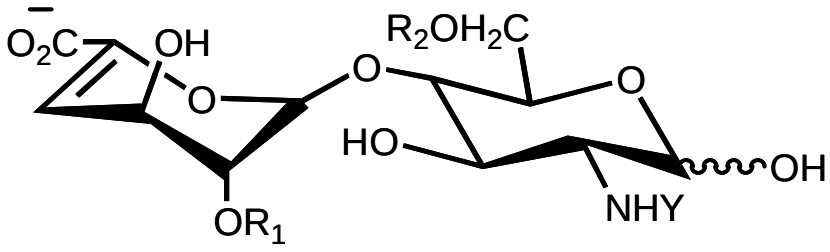

Disaccharide	R_1	R_2	Y
IS	SO_3^-	SO_3^-	SO_3^-
IIS	H	SO_3^-	SO_3^-
IIIS	SO_3^-	H	SO_3^-
IA	SO_3^-	SO_3^-	Ac
IIA	H	SO_3^-	Ac
IIIA	SO_3^-	H	Ac
IVA	H	H	Ac
IH	SO_3^-	SO_3^-	H
IIH	H	SO_3^-	H
IIIH	SO_3^-	H	H
IVH	H	H	H

5.2.2. Solenoidal Microcoil Probe Construction. The design of the solenoidal microcoil probe used in this work is described in section 4.2.2.

5.2.3. Enzymatic Depolymerization of Heparin. Digestion of 1 g of heparin was carried out in 50 mL of 100 mM pH 6.8 Tris buffer, containing 2.5 mM calcium acetate. The enzyme heparinase I (0.5 IU) (IBEX Technologies Inc., Montreal, Quebec) was added to the mixture and incubated at 28 °C in a water bath for 66 hr. The progress of the enzymatic digestion was monitored by UV absorbance at 232 nm using a Thermo Scientific NanoDrop 200 spectrophotometer (Wilmington, DE). After the digestion was complete the enzyme was quenched by placing the reaction vessel into boiling water for 5 min. The depolymerization solution was then lyophilized and reconstituted into 15 mL of the separation buffer (0.5 M NH_4HCO_3) prior to preparative scale SEC.

5.2.4. Enzymatic Depolymerization of Heparan Sulfate. Digestion of 1 g of HS was carried out in 50 mL of 0.1 M pH 7.0 sodium acetate buffer, containing 1.0 mM calcium acetate. The enzyme heparinase III (0.5 IU) (IBEX Technologies Inc., Montreal, Quebec) was added to the mixture and incubated at 32 °C in a water bath for 20 hr. The progress of the enzymatic digestion was monitored by UV absorbance at 232 nm using a Thermo Scientific NanoDrop 200 spectrophotometer (Wilmington, DE). After the digestion was complete the enzyme was quenched by placing the reaction vessel into boiling water for 5 min. The depolymerization solution was then lyophilized and reconstituted into 15 mL of the separation buffer (0.5 M NH_4HCO_3) prior to preparative scale SEC.

5.2.5. Size-exclusion Chromatography. The heparin, HS, and enoxaparin oligosaccharides were size fractionated on a 3.0 x 200 cm column packed with Bio-Rad Bio-Gel P-10 fine resin (Bio-Rad Laboratories Hercules, CA). The oligosaccharides were eluted from the column with a 0.5 M NH_4HCO_3 buffer at a flow rate of 0.08 mL/min. The eluent was collected in fractions of 4.5 mL. The progress of the separation was monitored offline by UV absorption measurements at 232 nm using the NanoDrop spectrophotometer as described above. Following SEC, fractions containing similar sized oligosaccharides were pooled and stored as a lyophilized powder at -20 °C until analysis by cITP.

5.2.6. On-line cITP-NMR Experiments. The cITP buffers were prepared in low paramagnetic D_2O. The leading electrolyte (LE) consisted of a 160 mM DCl, 80 mM imidazole solution containing 30 mM *tert*-butanol (as a chemical shift reference, 1.23 ppm) adjusted to pD 6.9 by addition of sodium deuteroxide. The TE solution consisted of 40 mM tricine adjusted to pD 8.2 with sodium deuteroxide. For cITP experiments, the capillary was filled with LE and then the sample introduced from the TE end. For experiments with the heparin disaccharides and unfractionated enoxaparin, a 1 mM sample prepared in 50/50 H_2O/TE was introduced by hydrodynamic injection at a height differential of 18 cm for 7 min. Because enoxaparin is a complex mixture of polydisperse components, the average molecular weight (4,500 g/mol) was used for calculation of the estimated molarity. Arixtra® (Fondaparinux sodium) was obtained from the University Pharmacy and Department of Pharmacy Administration of Semmelweis University, formulated as prefilled syringes. The pooled Arixtra solutions were desalted using a 1.6 x

70 cm Sephadex G10 superfine column (GE Healthcare) at a flow rate of 0.15 mL/min using HPLC grade water as the eluent. After desalting Arixtra was lyophilized and stored at -20 °C until analyzed. cITP samples were prepared by making a 1mM Arixtra solution in 50/50 H_2O/TE. For cITP experiments with the hexasaccharide SEC fractions of the heparin and HS enzymatic digests and enoxaparin, the samples were prepared by reconstituting the fractions in 1 mL of H_2O and then diluting 125 uL of that solution with 125 uL of TE. After injection of the samples at the height differential listed above, the TE was injected for a total of 7 min at the same height.

After completion of the injection protocol, the voltage across the capillary was raised to 15 kV for the duration of the cITP experiment. ^{1}H NMR spectra were acquired using a Bruker Avance spectrometer operating at 599.69 MHz. After the start of the cITP experiment, NMR acquisition was initiated to acquire an array of ^{1}H NMR spectra using 90° pulses with an acquisition time of 1.99 s and a spectral width of 11.03 ppm using the Bruker defined zg_8pulse pulse sequence which uses a composite 90° pulse to suppress background signals from the probe by only detecting resonances in the most homogeneous part of the B_1 field.[9] Each spectrum was acquired by coaddition of eight transients and zero dummy scans. Line broadening equivalent to 1.0 Hz and zero-filling to 65,536 points were applied prior to Fourier transformation. Once each sample reached the active volume of the microcoil probe a hydrodynamic back pressure was applied to the LE buffer reservoir which slowed the migration of the band through the active volume of the probe. Additionally, the separation voltage was reduced to 10 kV to further reduce the electrophoretic current to around 10 - 15μA. To improve the S/N, each

spectrum comprising the cITP array was produced by coaddition of individual 8 scan FIDs following manual alignment of the spectra to account for spectral drift during data acquisition due to the lack of a spectrometer lock. For the disaccharide cITP spectra, 20 FIDs were coadded to produce each spectrum, while 60 FIDs were coadded to produce each spectrum of the hexasaccharide samples and unfractionated enoxaparin.

5.3 Results and Discussion

5.3.1. Optimization of Anionic cITP Buffer System. Previous experiments to focus and detect heparin di- and tetrasaccharides by cITP-microcoil NMR used an anionic buffer system consisting of an LE of 160 mM DCl and 80 mM imidazole adjusted to pD 6.9 and a TE of 160 mM MES also adjusted to pD 6.9.[5-7] Although this buffer system was able to focus the most highly charged oligosaccharides, it failed to focus the lesser charged IVA, IIH, IIIH and IVH disaccharides. Additionally, the electrophoretic current produced during the experiments ranged from 35 – 70 μA. The high electrophoretic current limited the structural information that could be obtained from these spectra because of resonance broadening caused by the magnetic field created by the separation current. This broadening persisted even when the separation voltage was lowered from 15 kV to 12 kV after the focused analyte band had reached the coil.[6] The mechanism by which the separation current causes broadening of cITP-NMR resonances and alternative probe designs to minimize current-induced broadening are discussed in greater detail in Chapter 6.

To reduce the effects of resonance broadening due to the separation current and to focus a wider range of oligosaccharides, we sought an alternative buffer system that would allow effective cITP focusing of anionic analytes (including the heparin derived disaccharides IVS, IVA, IIH, IIIH, and IVH) while minimizing the electrophoretic current. Because it is predominantly the concentration of the high mobility LE ions that determines the degree to which focusing occurs, we chose to focus on modifying the TE composition.[10] In choosing a TE there are several criteria that must be met. The most important is that the TE has an effective electrophoretic mobility lower than the analyte/analytes to be focused. Because electrophoretic mobility is determined by the charge/mass ratio, to focus a heparin derived disaccharide that contained only one negative charge, such as IVA, by cITP the TE would need to have a lower net negative charge than IVA or a similar charge but a larger size.

The TE used in the previous experiments, MES (structure shown in Figure 5.1), with a pK_a of 6.15 was a zwitterion under the experimental conditions used for cITP: 160 mM MES titrated to pD 6.9 with NaOD. At pD 6.9, the morpholino group of MES would be 31% protonated reducing its net negative charge to somewhere between -1 and 0. While this is lower than the net negative charge of IVA, even with its sterically bulky morpholino group MES is still significantly smaller than the IVA disaccharide. From the effective electrophoretic mobilities, $\mu_{e,}$ calculated for MES from Equation 5.1 (where μ_a is the electrophoretic mobility of the fully deprotonated species typically measured using capillary electrophoresis) and determined by CE for IVA, MES (μ_a MES = -28×10^{-5} cm^2/sV) has a calculated effective mobility of -19.4×10^{-5} cm^2/sV and IVA has a mobility

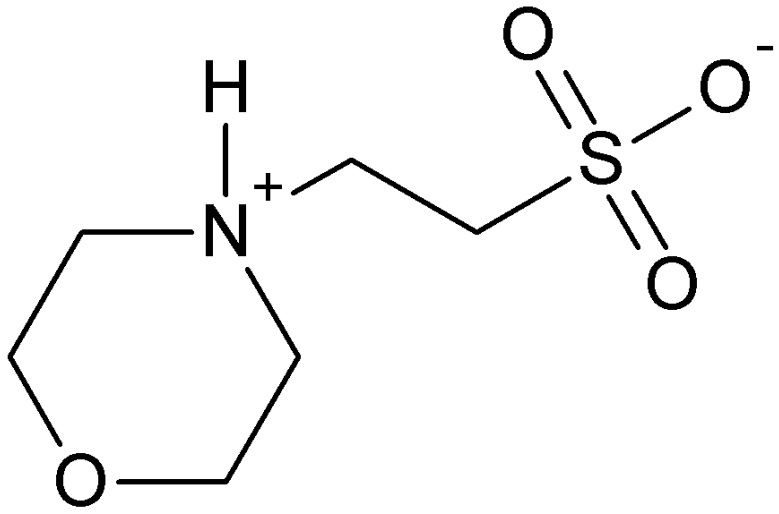

Figure 5.1. Structure of 2-(*N*-morpholino)ethanesulfonic acid (MES)

of -16.0×10^{-5} cm^2/sV, where the pK_a values of IVA and MES are 3.41 and 6.15, respectively.[5]

$$\mu_e = \frac{\mu_a}{10^{(pK_a - pH)} + 1} \tag{5.1}$$

From this simple calculation, it is clear that under these conditions IVA should not focus by cITP because its effective mobility is lower than that of the TE, MES. However, in cITP experiments solution pH can be used to modulate the effective charge of buffer components and thus change their effective mobilities. In the previous work the pD of the TE was reduced to a pD of 6.01 in an attempt to improve the cITP results. At this pD, 78% of the MES molecules should contain a charged morpholino group, decreasing the effective mobility of MES to 6.3×10^{-5} cm^2/sV, which is significantly less than the mobility of IVA (-16.0×10^{-5} cm^2/sV). However, when both IVA and MES were run by capillary electrophoresis (CE) in buffer at this pD the two had the same migration time suggesting that their effective electrophoretic mobilities were more similar than the simple calculation using equation 5.1 would suggest.[5]

In an attempt to find a TE alternative to MES, an ACES buffer which has a pK_a of 6.84 and a mobility of -24.1×10^{-5} cm^2/sV in its fully deprotonated form was tested in the previous work.[5] Unlike MES, when a CE separation of ACES and IVA was performed, ACES migrated slower than IVA with a migration time of 20.38 min compared to 11.83 min for IVA. From this result it seemed as if ACES might be a good alternative to MES, but when cITP experiments were performed using a TE of 160 mM

ACES buffer at pD 6.9, the IVA disaccharide again did not focus. Upon analysis of the intracapillary pD it was determined from this work that even with the use of a buffered LE and TE that there was a net rise in the intracapillary pD over the time period of the experiment. The most intense rise in pD (estimated to be ≥ 8.5) was at the sample/TE boundary. It was postulated that OH^- ions (produced at the cathode) were stacking at the frontal boundary of the TE due to interactions with buffer cations and Na^+ ions that migrated toward the cathode (illustrated in Figure 5.2).[5, 11] At such a high pD the ACES molecule would be completely deprotonated giving it an effective mobility of -24.1×10^{-5} cm^2/sV, higher than IVA (-16.0×10^{-5} cm^2/sV). From these results it was concluded that in future experiments, the TE should meet the minimum requirements of possessing a low μ_a ($< -24.1\times10^{-5}$ cm^2/sV) and have a pK_a in the range of 6.8-7.0 with greater buffering capacity than the ACES buffer used in the prior work.

In this study we decided to partially stray from these minimum requirements and instead search for a buffer (preferably a zwitterion) with a low μ_a ($< -24.1\times10^{-5}$ cm^2/sV) and a pK_a in the range of the pD measured at the TE frontal boundary where OH^- accumulates. In this situation the TE would be buffered at the pD that naturally arose during cITP experiments. This meant that even if OH^- stacked at the TE/sample boundary, as it had in the experiments using ACES as the TE, the new TE would have a greater buffer capacity and would remain zwitterionic during the course of the experiment thus maintaining a lower mobility than that of IVA and the other disaccharides. Another alternative would be to use a buffer with a lower pK_a but to raise

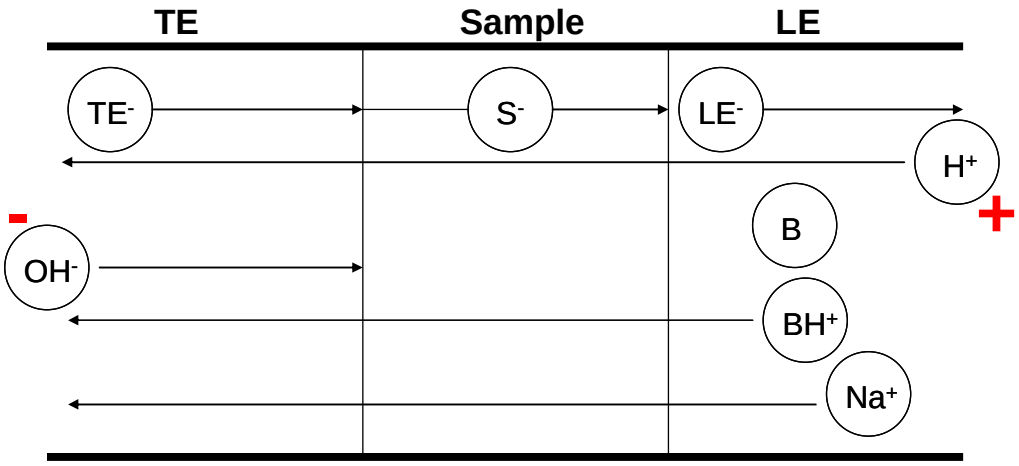

Figure 5.2. Illustration of the movement of ions through the anionic cITP system. From the illustration we see that OH^- ions produced at the cathode do not cross the boundary of the TE and the sample due to interactions/recombination with LE buffer cations (BH^+ and H^+) and Na^+ from the LE that migrate towards the cathode.

its concentration in the TE to increase its buffer capacity. This however is not really a viable option as a TE at a higher concentration would increase the electrophoretic current produced during cITP causing excessive current induced broadening which would decrease the NMR spectral resolution.

In our search we determined that a simple amino acid like glycine (shown in Figure 5.3 A) would satisfy our new TE requirements because it is a zwitterion with an amino group pKa of 9.6 which would allow it to remain zwitterionic at the pD of the TE frontal boundary. However, if glycine were to be used, the TE would need to be at a pH near the pKa of the amino group (9.6) which is outside the pH range (2 – 8) over which the zero-EOF coating of our capillaries is stable. By adding a TRIS moiety to glycine to make tricine (shown in Figure 5.3 B), the pKa of the amino group is reduced to around 8.2. This allows the TE to be buffered in a range safe for the capillary coating. Additionally, with a value of 0.00218×10^{-5} cm^2/sV at pD 8.2 its mobility should be significantly lower than that of IVA, allowing it and the other low charge disaccharides to focus.[12] Benchtop experiments were performed using tricine buffer as the TE at various concentrations. It was determined that a TE of 40 mM tricine at pH 7.8 (pD 8.2) yielded similar focusing capabilities for bromothymol blue as the previous TE of 160 mM MES, but produced a much lower electrophoretic current (~19 μA at 15 kV when the band reached the microcoil).

5.3.2. Anionic cITP of Heparin Derived Disaccharides. The newly optimized anionic cITP buffer system was tested by analyzing 12 commercially available heparin derived disaccharides by cITP-NMR. The family of heparin disaccharides shown in

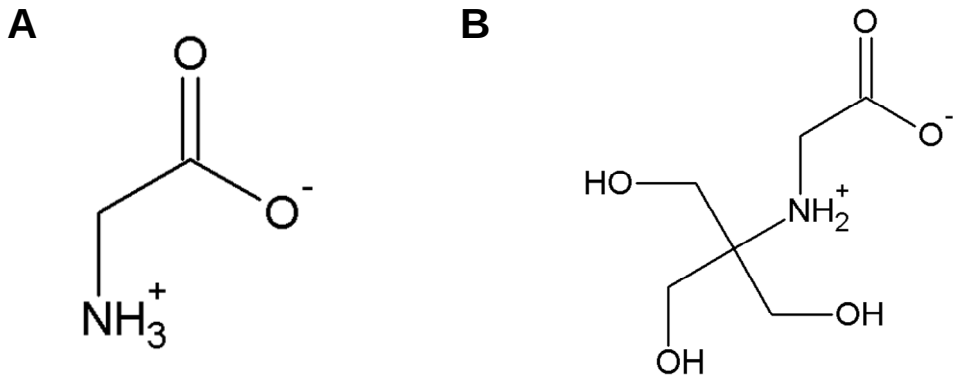

Figure 5.3. The structures of A) glycine and B) tricine.

Table 5.1 makes an interesting set of analytes for testing the new anionic cITP buffer system. As a whole they are comprised of analogs with very similar structures but charge states that range from zero net charge at neutral pH (IVH) to a charge of -4 (IS).

The first set of disaccharides tested were the disaccharides containing an unmodified glucosamine (IH, IIH, IIIH, and IVH). From the intracapillary pD study performed in previous work it is expected that the sample band pD should be somewhere between pD 7.0 and 8.5.[5] Because the pKa values of the disaccharide amino groups (listed in Table 5.2)[5] are near the sample pD, the disaccharides will be partially zwitterionic in the sample band giving net effective mobilities for IH $\geq -30.5 \times 10^{-5}$ cm^2/sV, IIH $\geq -17.1 \times 10^{-5}$ cm^2/sV, IIIH $\geq -17.3 \times 10^{-5}$ cm^2/sV, and IVH $\geq 2.09 \times 10^{-5}$ cm^2/sV, where the minimum mobilities were calculated experimentally in previous work by CE experiments at a buffer pH of 6.5 (amine groups are 99% protonated at this pH).[5] Figure 5.4 shows the online anionic cITP-NMR spectra of disaccharide IVH. The focused IVH disaccharide band migrates through the microcoil just in front of the TE with a portion of the IVH band trailing into the TE. Closer examination of the spectra in Figure 5.4 shows that only the less abundant β-anomer focused, however it is important to note that is the first successful report of the focusing of either IVH anomer by anionic cITP, validating the effectiveness of our new buffer system. Because the exact pD of the sample zone and TE are not known due to the effect of the frontal migration of OH^- ions at the sample/TE interface, we cannot precisely calculate the effective mobilities for both IVH anomers and tricine in this system.[5] Even with this limitation, an understanding of the cITP experiment can be gained by examining the relative pKas and considering the

Table 5.2. The carboxylate and amine pKa(D) values for 11 heparin disaccharide standards reported in references 5 and 13 Disaccharide IVS was not commercially available at the time this data was reported. Also reported are the pKa(D)'s for both anomers of IH-IVH.

Disaccharide	pK_a(D) of COO^-	pK_a(D) of NH_3^+ α anomer	pK_a(D) of NH_3^+ β anomer
IS	3.74 ± 0.02	-	-
IIS	3.68 ± 0.01	-	-
IIIS	3.72 ± 0.00	-	-
IA	3.58 ± 0.00	-	-
IIA	3.61 ± 0.02	-	-
IIIA	3.53 ± 0.01	-	-
IVA	3.41 ± 0.00	-	-
IH	3.26 ± 0.01	8.73 ± 0.01	8.29 ± 0.01
IIH	3.23 ± 0.02	8.65 ± 0.01	8.20 ± 0.01
IIIH	3.18 ± 0.01	8.70 ± 0.00	8.26 ± 0.00
IVH	2.96 ± 0.03	8.60 ± 0.01	8.15 ± 0.01

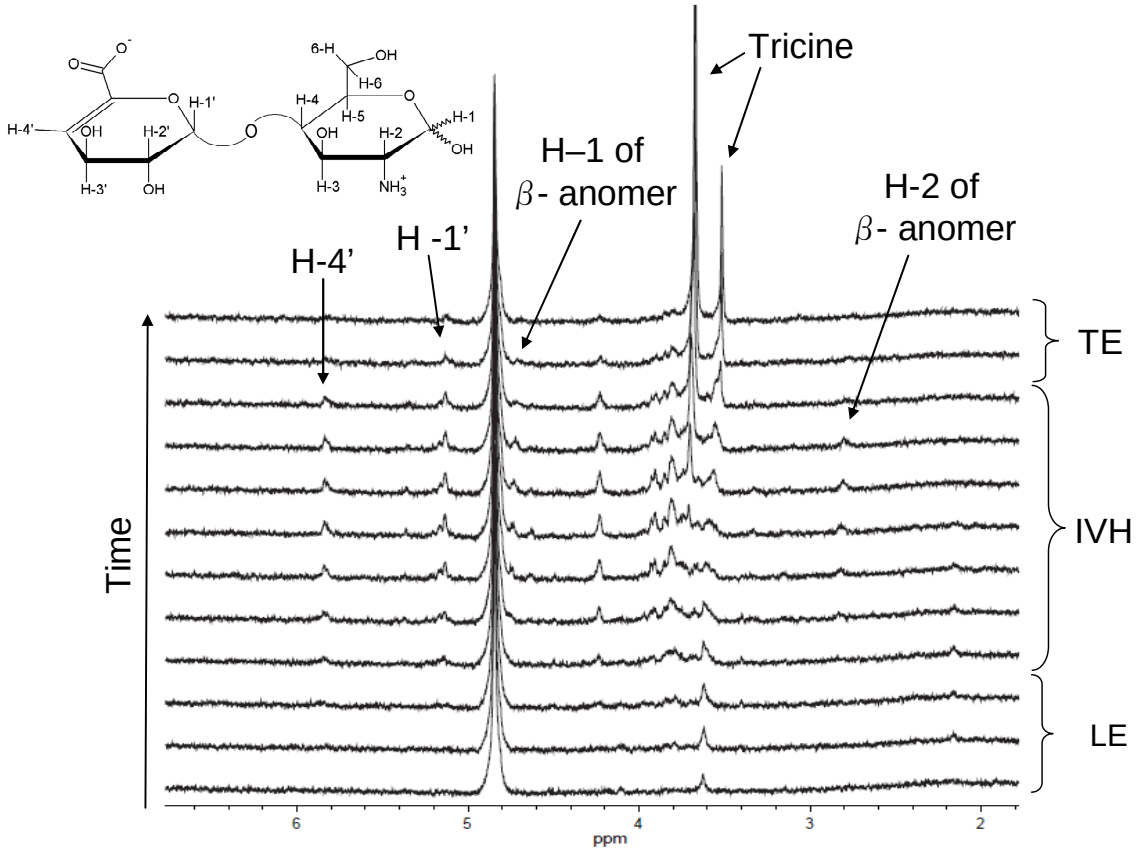

Figure 5.4. Results showing the on-line cITP-NMR spectra of 9 nmol of the heparin disaccharide IVH.

fractional protonation at the nominal pD of the TE. Furthermore, compared with prior work, the better buffer capacity of the tricine TE should minimize the increase in pH due to accumulation of OH^- and give effective pD values at the sample/TE interface that are much closer to the TE nominal pD. The pKa(D) of the IVH β-anomer amino group is 8.17,[13] significantly lower than that of tricine's amine (pKa(D) 8.75; calculated from the equation pKa(D) = pKa + 0.6),[14] where the expression pKa(D) indicates the value in D_2O solution. Because of the difference in their pKas, a smaller fraction (0.46) of the IVH β-anomer amino group will be positively charged at the nominal pD of the TE (8.2) compared to tricine (0.78), giving the IVH β-anomer a higher effective mobility than tricine and allowing it to focus under these conditions. Furthermore, the fact that the α-anomer of IVH did not focus by cITP can be attributed to its higher amino group pKa(D) (8.68)[13] which is very close to that of tricine (8.75) giving the two species very similar net charges at the TE nominal pD of 8.2.

Figure 5.5 shows the online anionic cITP-NMR spectra of disaccharide IIH; this is also the first report of the focusing of this disaccharide by cITP. Unlike the cITP-NMR spectra of IVH (Figure 5.4) where only the β-anomer focused, in Figure 5.5 there is a separation of the IIH α- and β-anomers of over the length of the analyte band. At the beginning of the band the β-anomer dominates. Moving towards the back of the band there is a gradual decrease in the intensity of the β-anomer resonances and a gradual increase in intensity of the α-anomer. Eventually, the α-anomer becomes the dominant species near the end of the analyte band just prior to the TE. However, unlike the IVH disaccharide, because of the 6-O sulfonation both anomers IIH will always have a net

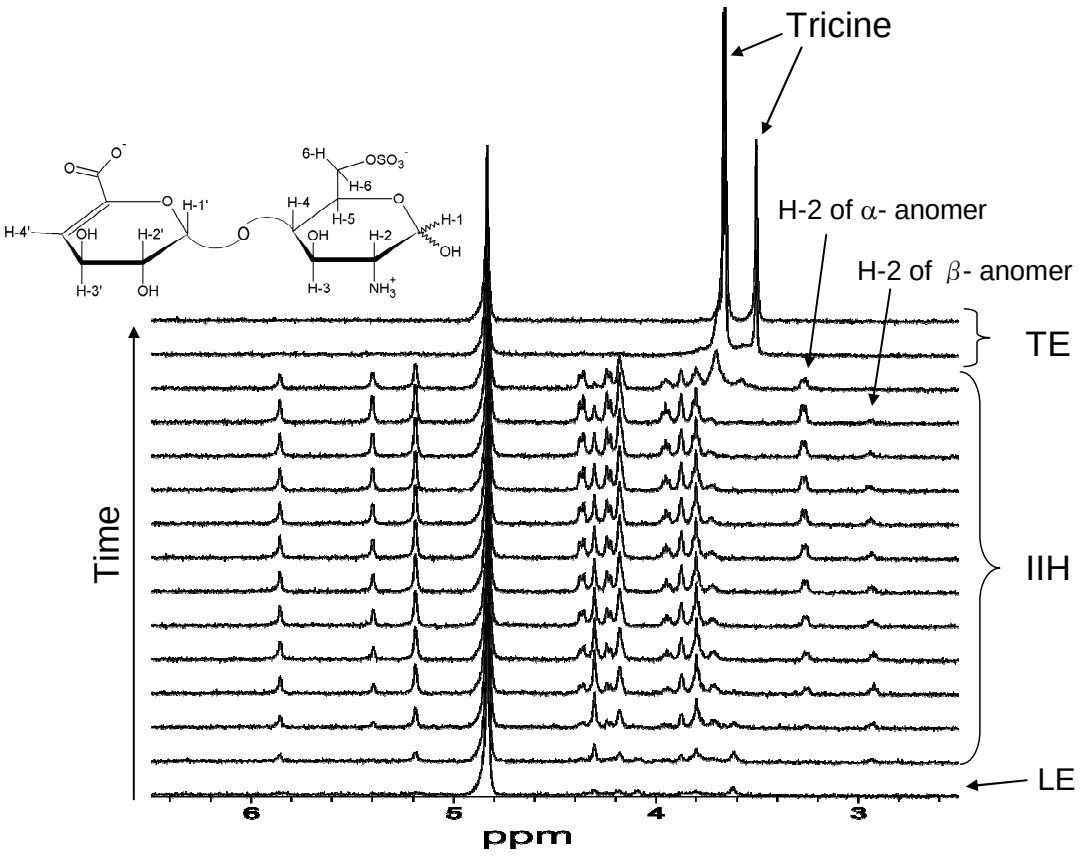

Figure 5.5. Results showing the on-line cITP-NMR spectra of 9 nmol of the heparin disaccharide IIH.

charge greater than -1 making their effective mobilities $\geq$ -17.1 $\times 10^{-5}$ cm^2/sV and allowing both anomers to focus in front of the tricine TE. The separation of the IIH anomers can be attributed to differences in the amino group pKa's (α-anomer 8.65 and β-anomer 8.20) of the amine groups of the two anomers but the difference in electrophorectic mobility between the two did not seem to be different enough to fully resolve the them.[13] In contrast, Figure 5.6 shows that the anomers of IIIH (which did not focus by anionic cITP using previous buffer systems) are almost completely resolved by cITP microcoil NMR. For much of the first half of the analyte band only the resonances of the β-anomer are observed. This is followed by a short region near the center of the analyte band where the two anomers are not fully resolved. Finally, in the latter half of the band only resonances of the α-anomer are observed. Because the two anomers of IIIH are well resolved from each other, separate spectra with high S/N can be coadded from the spectra in the online experiment for both the α-anomer (Figure 5.7 B) and β-anomer (Figure 5.7 C), or one can simply sum across the entire analyte band to yield a spectrum of the full mixture (Figure 5.7A).

Finally, Figure 5.8 shows the online anionic cITP-NMR spectra of the disaccharide IH. IH is the most sulfonated of the four disaccharides in this group and will have an effective mobility $\geq$ -30.5 $\times 10^{-5}$ cm^2/sV at the nominal pD of the experiment.[5] At first glance, it seems that the anomers of IH are not resolved by cITP-NMR. However, following the H-1 resonance for the α anomer and H-2 reonance of the β anomer we see that there is some degree of resolution of the two anomers. At the beginning of the analyte band the H-1 resonance of the α anomer is rather small and

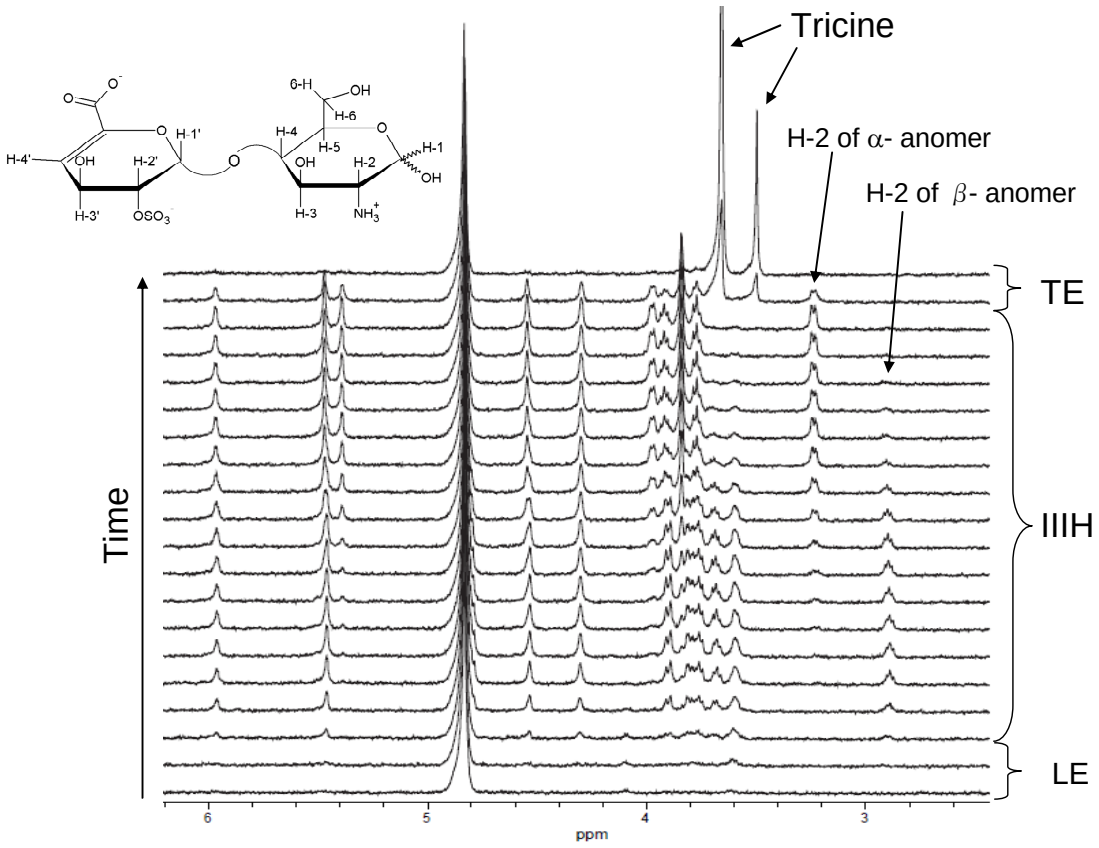

Figure 5.6. Results showing the on-line cITP-NMR spectra of 9 nmol of the heparin disaccharide IIIH.

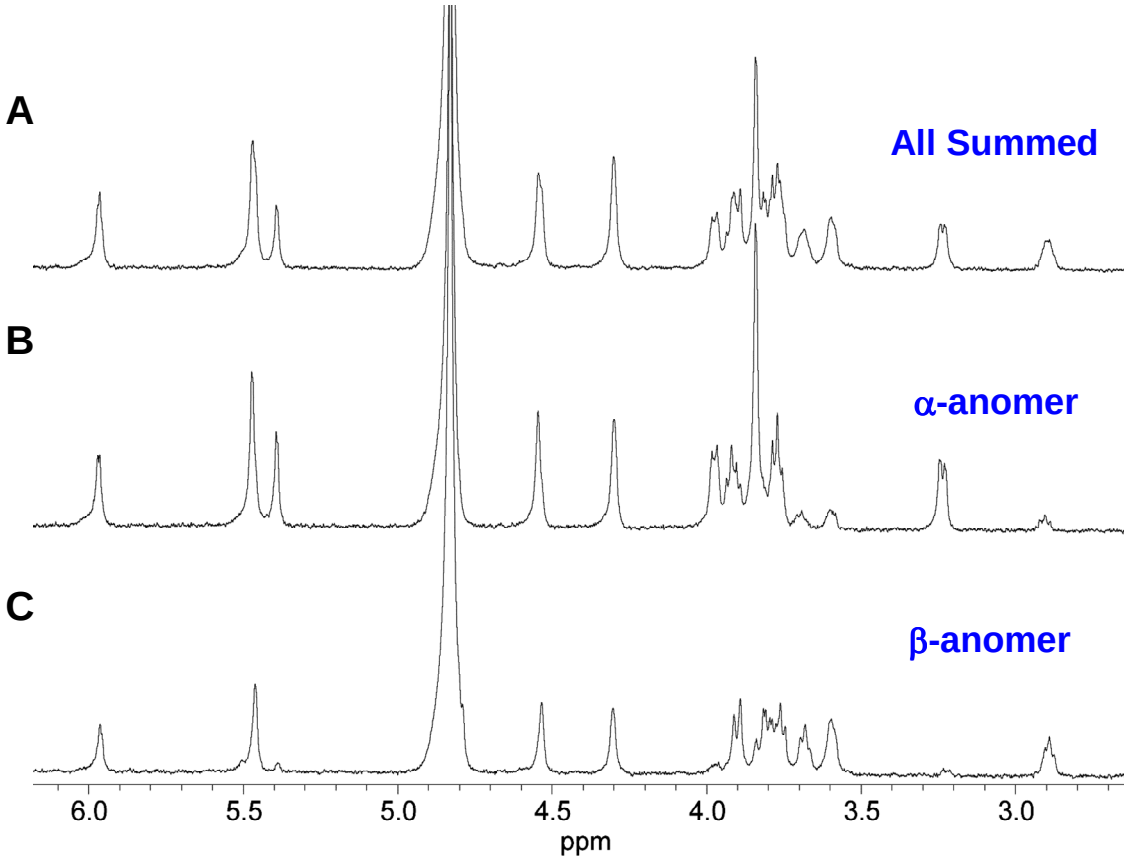

Figure 5.7. Results showing coadded cITP-NMR spectra of A) all spectra acquired for IIIH, B) the spectra containing predominantly the resonances of the α-anomer of IIIH and C) the spectra containing the resonances of the β-anomer of IIIH.

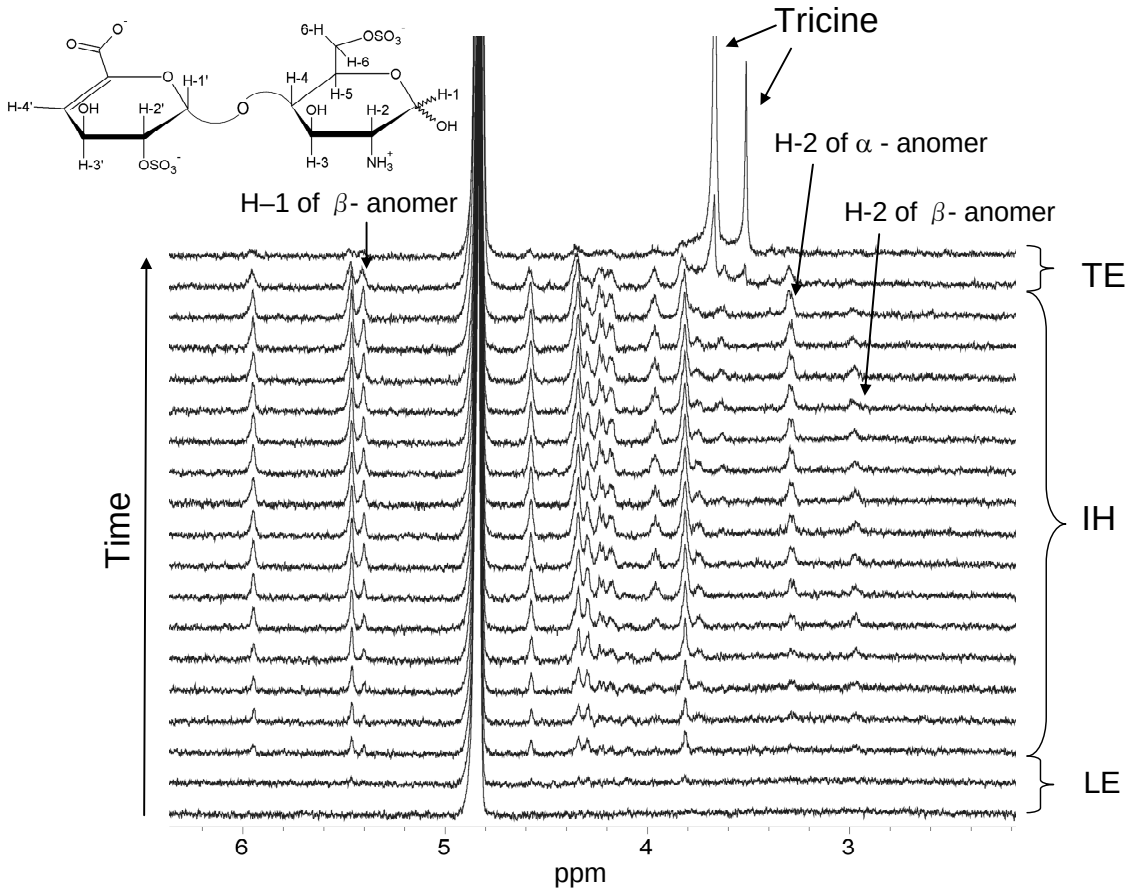

Figure 5.8. Results showing the on-line cITP-NMR spectra of 9 nmol of the heparin disaccharide IH.

grows in intensity towards the end of the band. The opposite is true for the H-2 resonance of the β anomer which decays in intensity as the back of the band is approached. It is interesting, that the addition of sulfonation at the 6-O position of the glucosamine residue in both IIH and IH causes loss of resolution of the two anomers of the disaccharides. This perhaps suggests that the resolution of the two anomers cannot be solely attributed to differences in the pKa of the amino group as first postulated, but instead is also based on conformational differences between the two anomers. Sulfonation at the 6-O position might significantly alter the hydrodynamic radius of one or both of the anomers. Because the electrophoretic mobility is determined by the ratio of molecular charge and hydrodynamic radius, 6-O sulfonation may have altered the hydrodynamic radii of one or both of the IH anomers enough to give them similar mobilities even though they have different net charges due to differences in the amino group pKa values.[15, 16]

The next set of disaccharides examined were those containing an *N*-acetylated glucosamine residue (IA, IIA, IIIA, and IVA). Unlike the previous group of disaccharides, the *N*-acetylated disaccharides cannot carry a charge on the glucosamine amino group. Therefore, the disaccharide effective charge comes from the carboxylate and the presence of sulfate groups, and deviations from the TE nominal pD should not have an affect on mobility. The effective mobilities (experimentally determined by CE at pH 6.5) of these disaccharides are IA -39.7×10^{-5} cm^2/sV, IIA -29.2×10^{-5} cm^2/sV, IIIA -39.7×10^{-5} cm^2/sV, and IVA -16.0×10^{-5} cm^2/sV, all of which should be significantly higher than that of tricine at the pD of the cITP experiment.[5] Figures 5.9, 5.10, 5.11 and

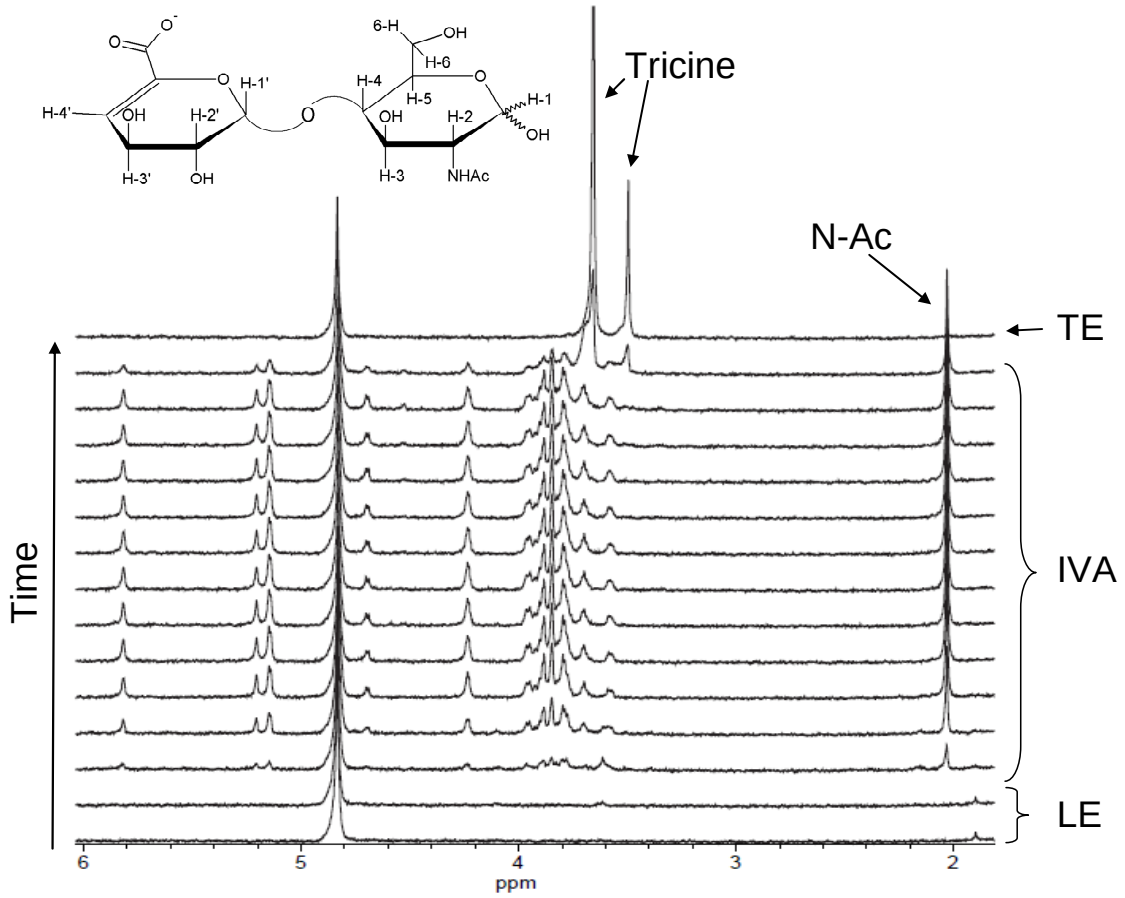

Figure 5.9. Results showing the on-line cITP-NMR spectra of 9 nmol of the heparin disaccharide IVA.

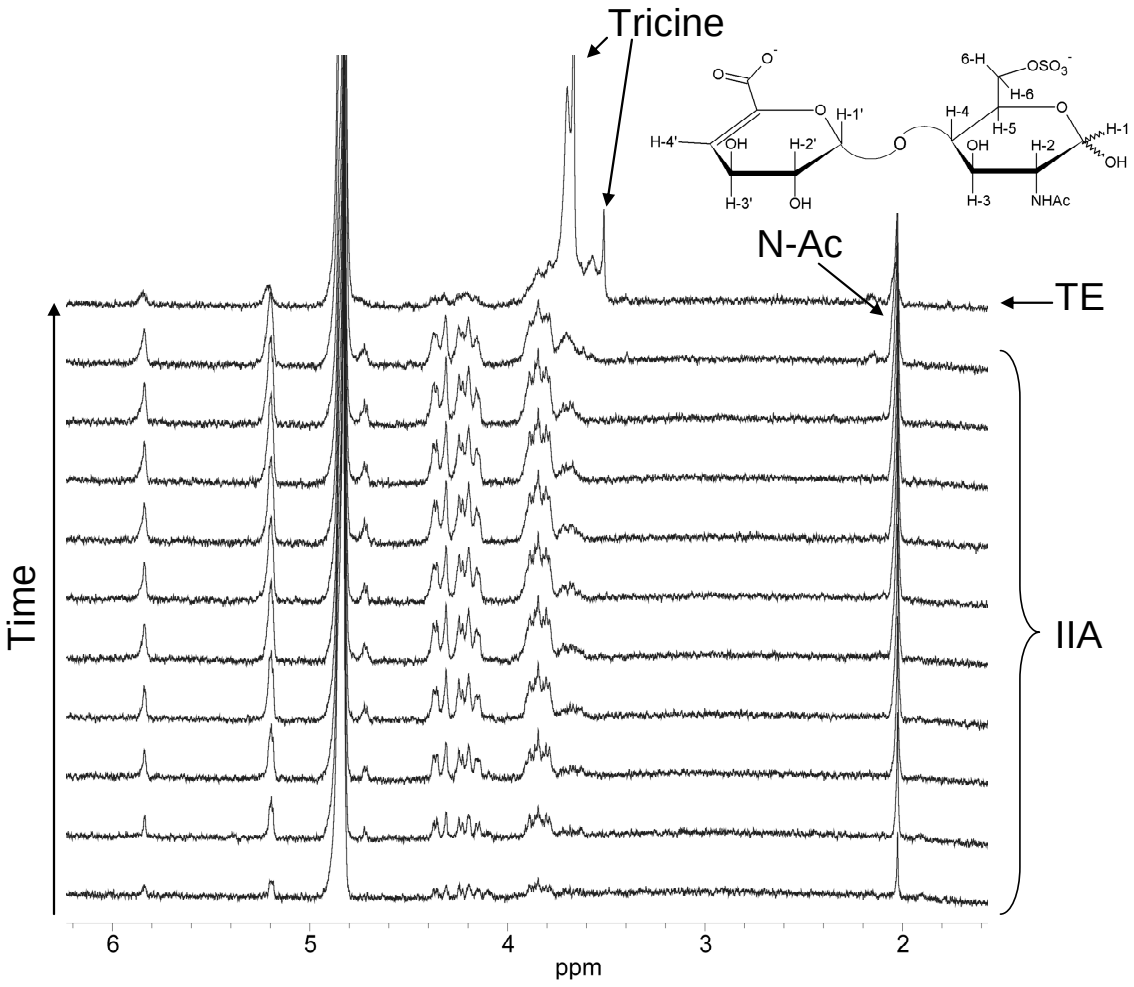

Figure 5.10. Results showing the on-line cITP-NMR spectra of 9 nmol of the heparin disaccharide IIA.

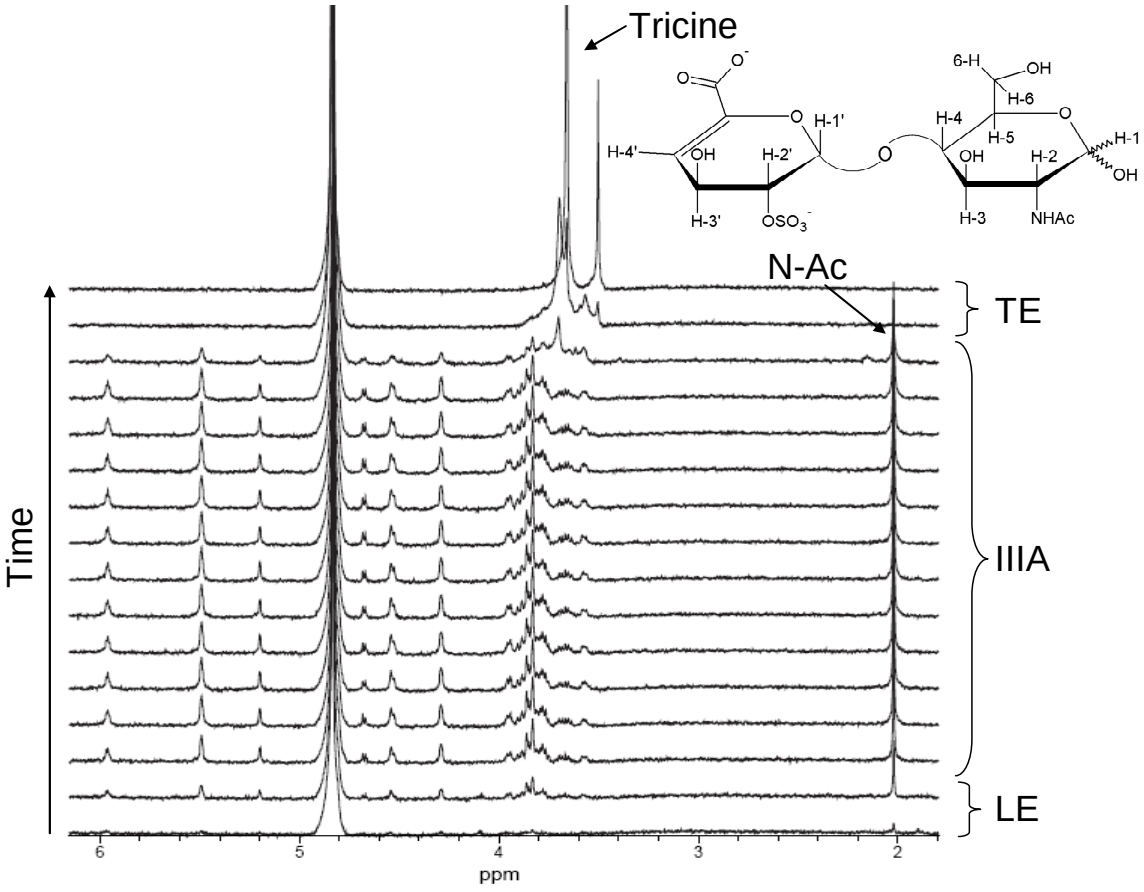

Figure 5.11. Results showing the on-line cITP-NMR spectra of 9 nmol of the heparin disaccharide IIIA.

5.12 show the online cITP-NMR spectra for IVA, IIA, IIIA, and IA, respectively. As expected, all four disaccharides easily focus using the new cITP buffer system, including IVA which previously did not focus with the MES or ACES buffers.[5] The *N*-acetyl resonance of each disaccharide is easily observable in Figures 5.9-5.12. Also noticeable in these figures is the lack of separation of the anomers of the *N*-acetylated disaccharides. This is consistent with our hypothesis that the anomers of IH, IIH, IIIH, and IVH are resolved by cITP based on differences in electrophoretic mobility that arise from pKa differences of the glucosamine amino groups and conformational differences of the two anomers. Because the *N*-acetylated disaccharides can not carry a positive charge on the amine both anomers will have identical net charges. This means that only differences in the hydrodynamic radii of the two anomers could lead to differences in electrophoretic mobility, which for the *N*-acetylated disaccharides was insufficient to resolve the anomers.

The final set of disaccharides tested were the *N*-sulfonated series of disaccharides (IS, IIS, IIIS, and IVS). These disaccharides are unique in that *N*-sulfonation of the glucosamine residue adds an extra negatively charged group giving even the least sulfonated disaccharide, IVS, a net charge of -2. The other three disaccharides IS, IIS, and IIIS have net charges of -4, -3, and -3, respectively. In fact, IS, IIS, and IIIS have been shown to be the dominant disaccharides in bovine and porcine derived heparin giving the polysaccharide its highly anionic structure.[17] Figures 5.13, 5.14, 5.15, and 5.16 show the online cITP-NMR spectra of IVS, IIS, IIIS, and IS, respectively. With such a high degree of negative charge, all four disaccharides easily focus by cITP.

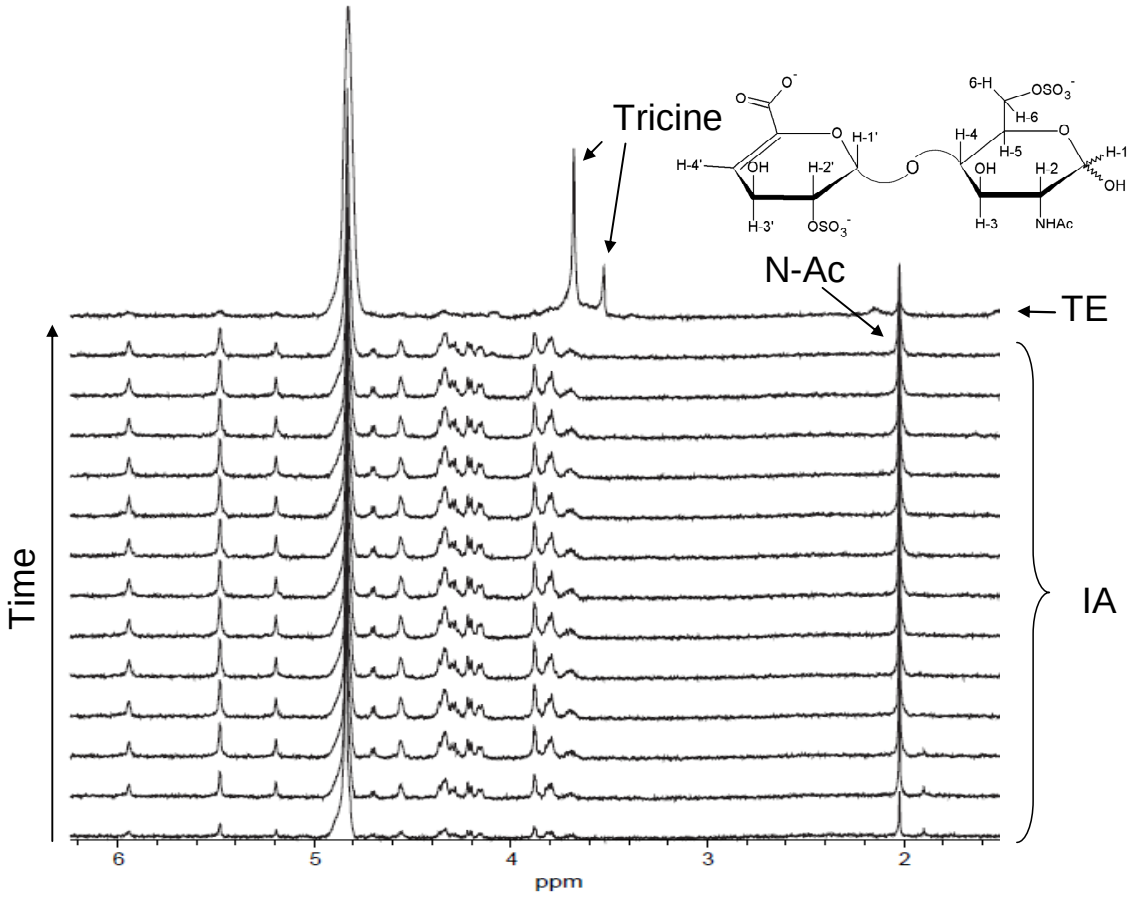

Figure 5.12. Results showing the on-line cITP-NMR spectra of 9 nmol of the heparin disaccharide IA.

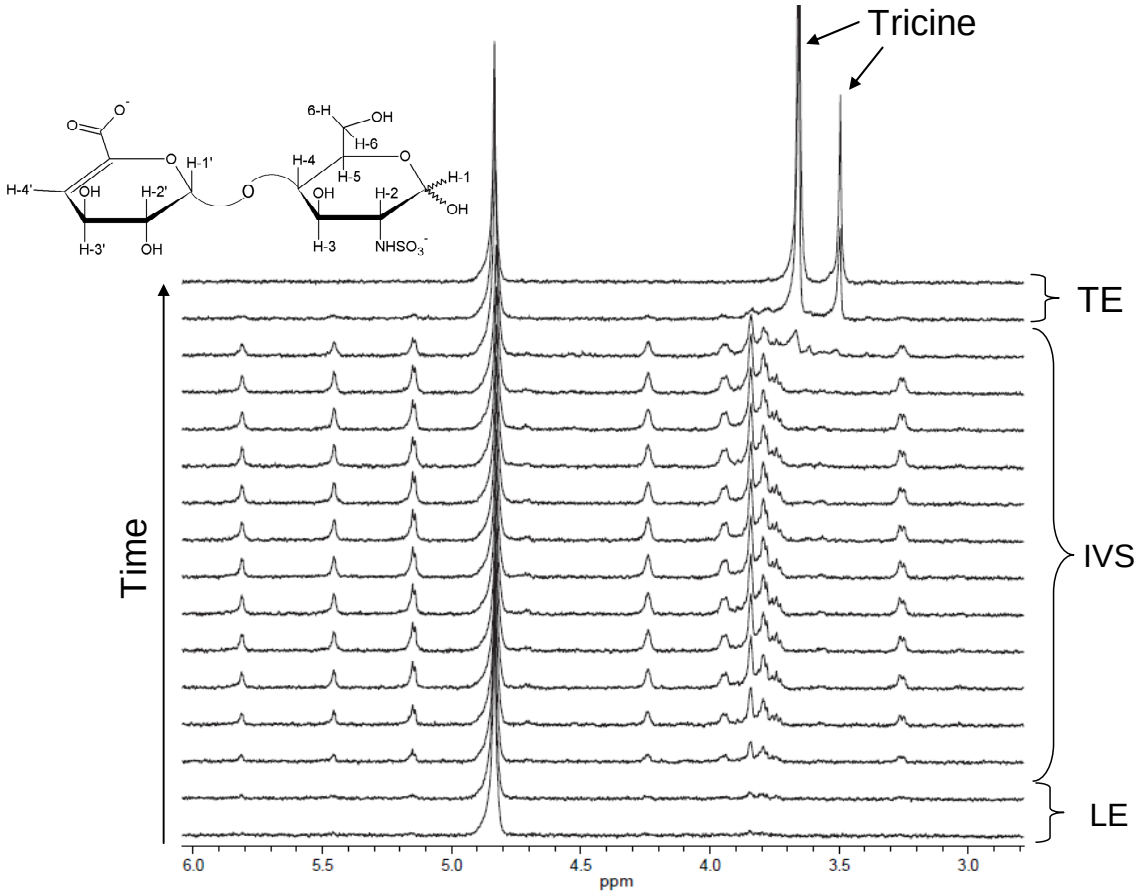

Figure 5.13. Results showing the on-line cITP-NMR spectra of 9 nmol of the heparin disaccharide IVS.

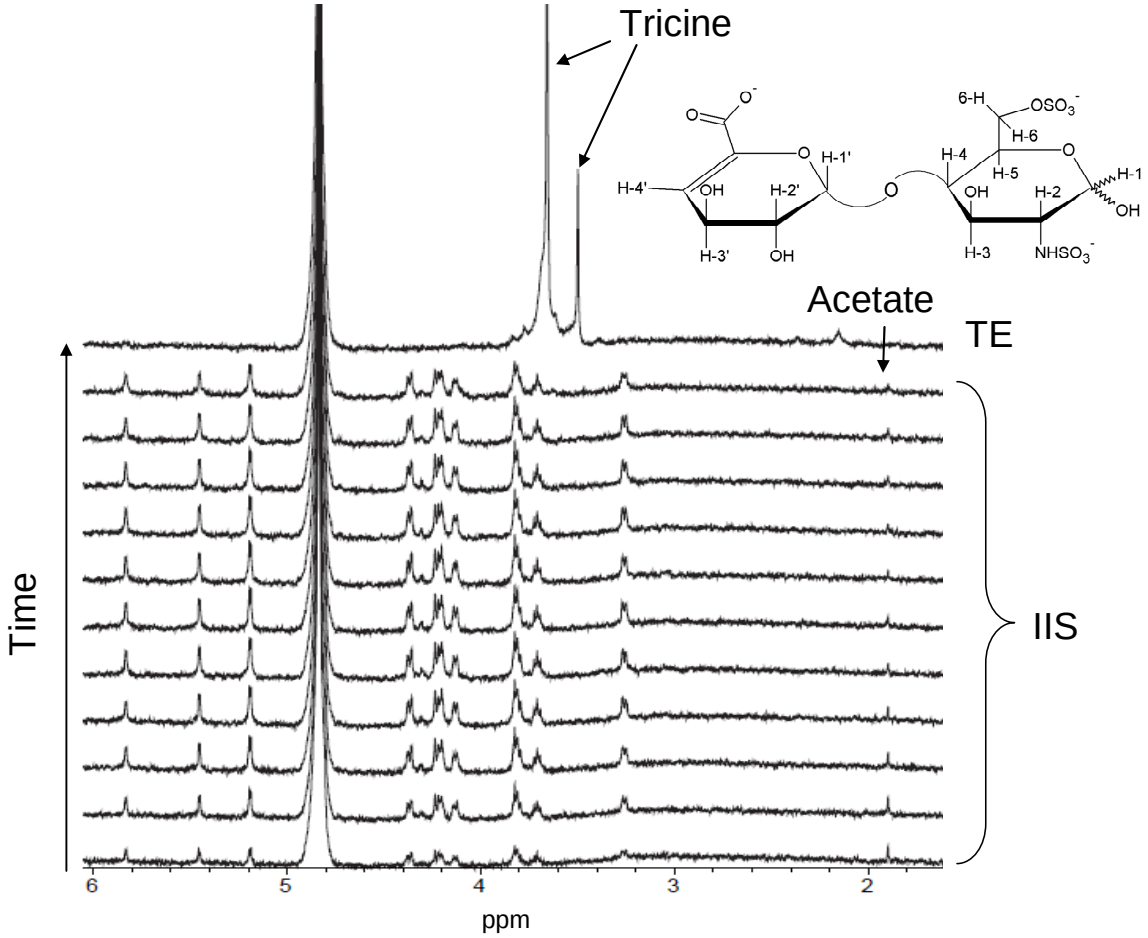

Figure 5.14. Results showing the on-line cITP-NMR spectra of 9 nmol of the heparin disaccharide IIS.

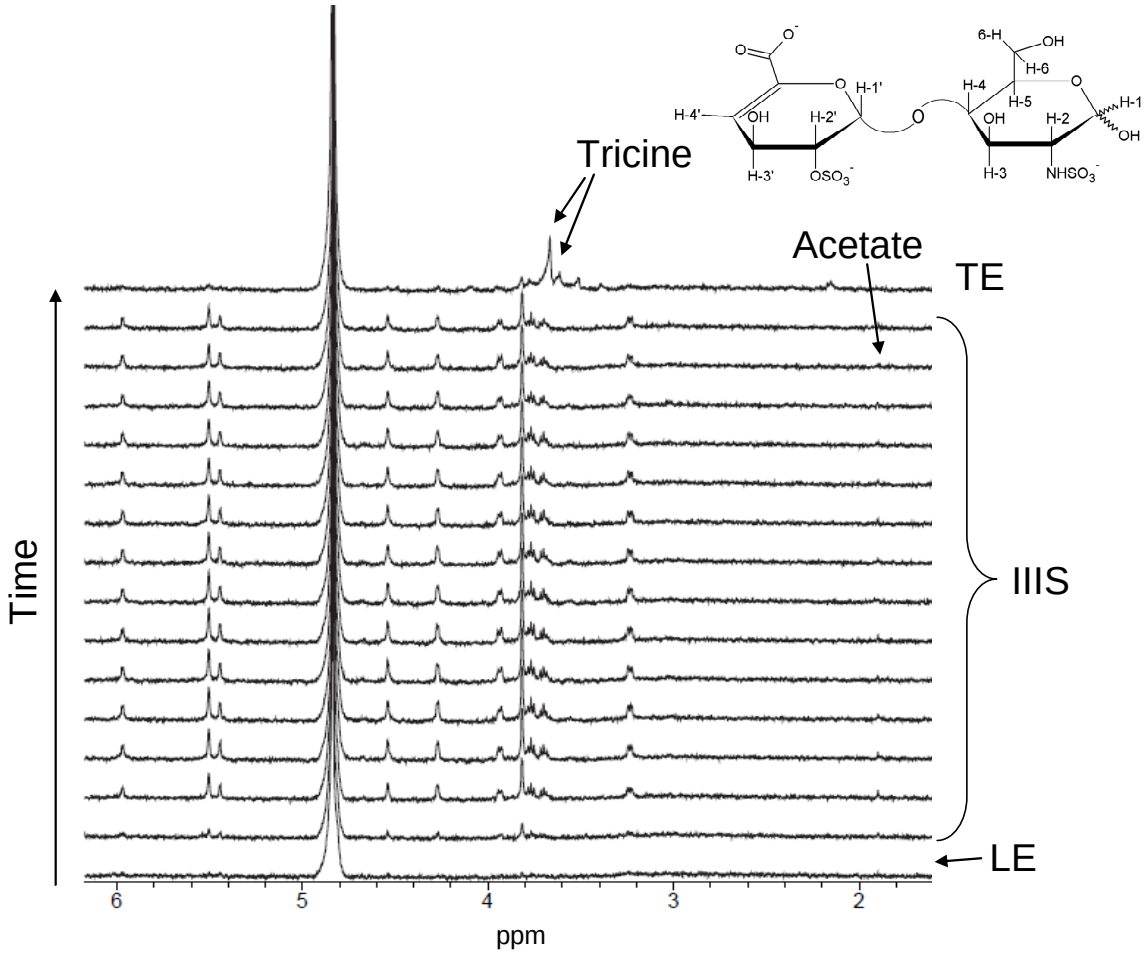

Figure 5.15. Results showing the on-line cITP-NMR spectra of 9 nmol of the heparin disaccharide IIIS.

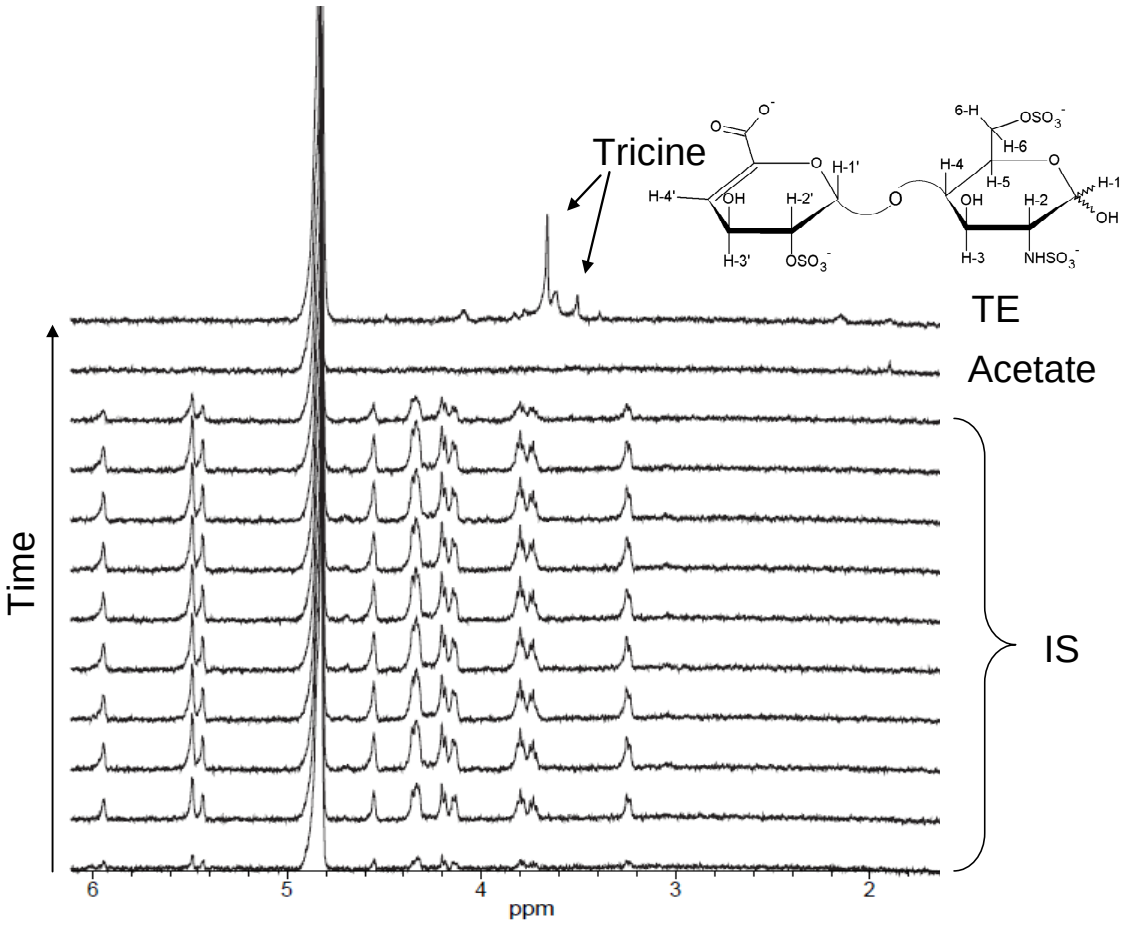

Figure 5.16. Results showing the on-line cITP-NMR spectra of 9 nmol of the heparin disaccharide IS.

Interestingly, in the spectra for IIS and IIIS we see that trace acetate (likely from the isolation of the disaccharides by the vendor) focused in the analyte band as well. In the spectra for IS, however, we see that the acetate is fully resolved from IS. This is likely due to the high negative charge of IS giving it a higher electrophoretic mobility (-50.3 $\times 10^{-5}$ cm^2/sV) than the smaller but less charged acetate (-42.5$\times 10^{-9}$ cm^2/sV).[5, 11] Disaccharide IVS, which was purchased from a different supplier (V-labs), did not appear to contain acetate as an impurity. As observed for the *N*-acetylated series of disaccharides, no separation of the anomers is observed in the cITP-NMR spectra of the *N*-sulfonated disaccharides. Because the pKa of the *N*-sulfo group is quite low (between 0.5 and 1.5)[18] compared to the pH of the buffer system, both anomers have identical net charges at the pD used for the separation. Finally, Figure 5.17 shows a summed spectrum for IIS highlighting the degree of spectral resolution achievable with the new cITP buffer system. Even the 3 Hz coupling constants of the anomeric proton resonances are clearly resolved in this spectrum. However, compared to static spectra acquired in the microcoil probe there is still a significant degree of spectral broadening resulting from the magnetic field created by the electrophoretic current.

5.3.3. Anionic cITP of Arixtra. To further test the new anionic cITP buffer system we sought to expand the capabilities of our cITP method to larger, more biologically relevant oligosaccharides. While disaccharide analysis is useful for determining the overall composition of a depolymerized heparin sample, most biologically active heparin derived oligosaccharide sequences, such as the binding sequence for antithrombin III, are generally at least pentasaccharides or larger. Figure

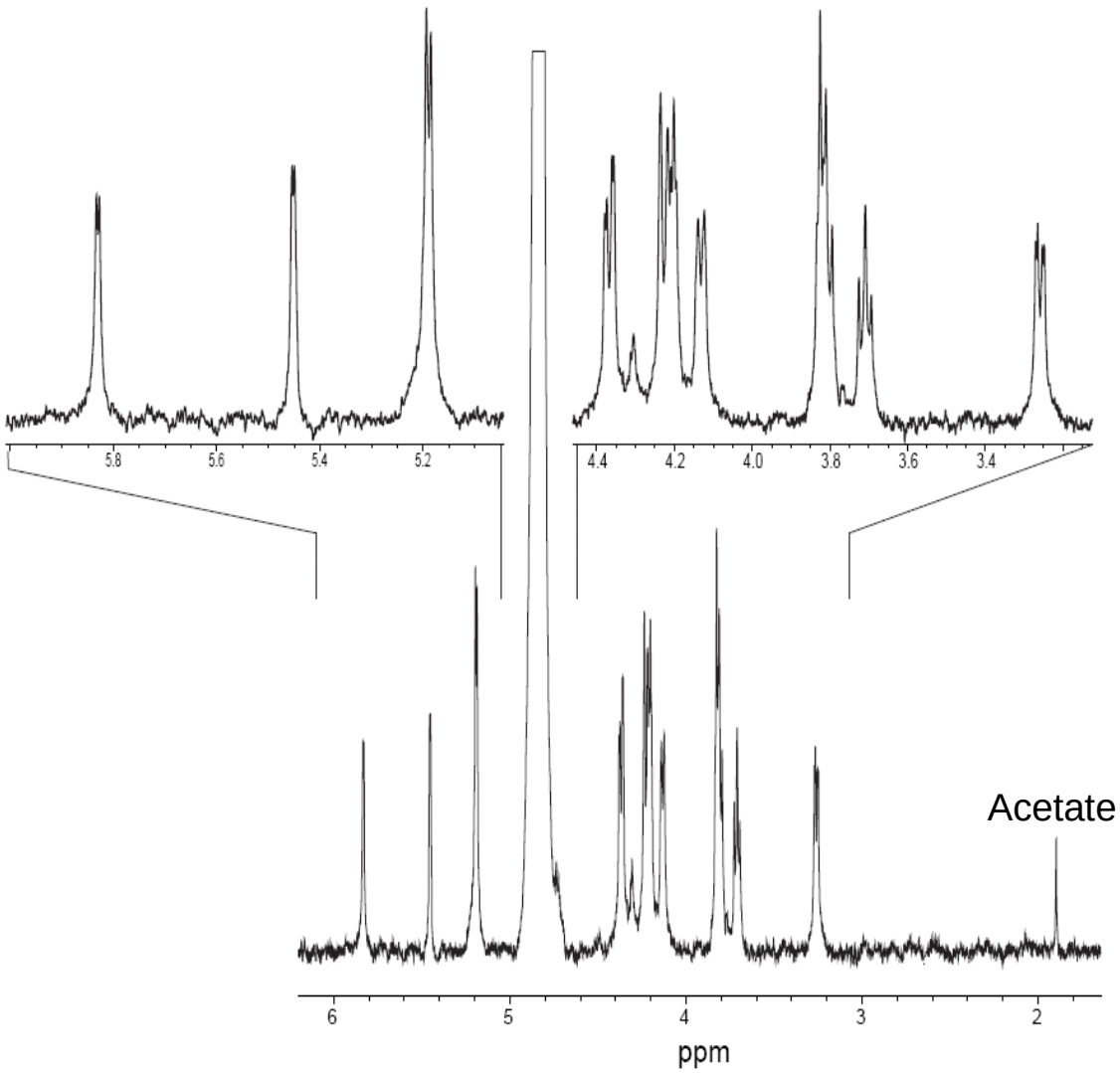

Figure 5.17. Results showing the summed cITP-NMR spectrum of 9 nmol of the heparin disaccharide IIS.

5.18 shows the online cITP-NMR spectra for the synthetic pentasaccharide Arixtra. This pentasaccharide is designed to mimic the native pentasaccharide sequence that binds to antithrombin III and is regularly prescribed as pharmaceutical anticoagulant. Quickly glancing at Figure 5.18 a few things are immediately noticeable from the spectra. First, as in the spectra for IS in Figure 5.16 we see a focused band behind the analyte and before the TE that can likely be attributed to components of the sample matrix. In this case, however, the matrix components seem to be NMR silent impurities that yield blank NMR spectra. Secondly, the spectra of Arixtra show that the pentasaccharide contains neither an N-acteyl group nor a non-reducing end double bond based on the absence of resonances around 2 (acetyl resonance) and 6 ppm (double bonded proton, ΔUA) respectively. Also by counting the number of anomeric resonances (a total of five) and by observing their chemical shifts we can easily assign the molecule as in fact being a pentasaccharide with a glucuronic acid residue (based on the anomeric residue seen at 4.6 ppm). However, given the poor spectral resolution in the sugar region of the spectra, resulting in part from current induced broadening, it is not possible to assign any more of the structure. It is also important to note that the current induced broadening in this set of spectra is particularly worse than what was observed for the disaccharide standards. This is likely due to the increased electrophoretic current (~17 μA vs the ~10 μA) produced during the heparin disaccharide analysis once the sample is parked in the active volume of the micrcoil. The source of the higher current and the NMR-silent impurity in Figure 5.18 is most likely bicarbonate which is used as the desalting buffer, which may have been incompletely removed by lyophilization after the desalting step. For this reason

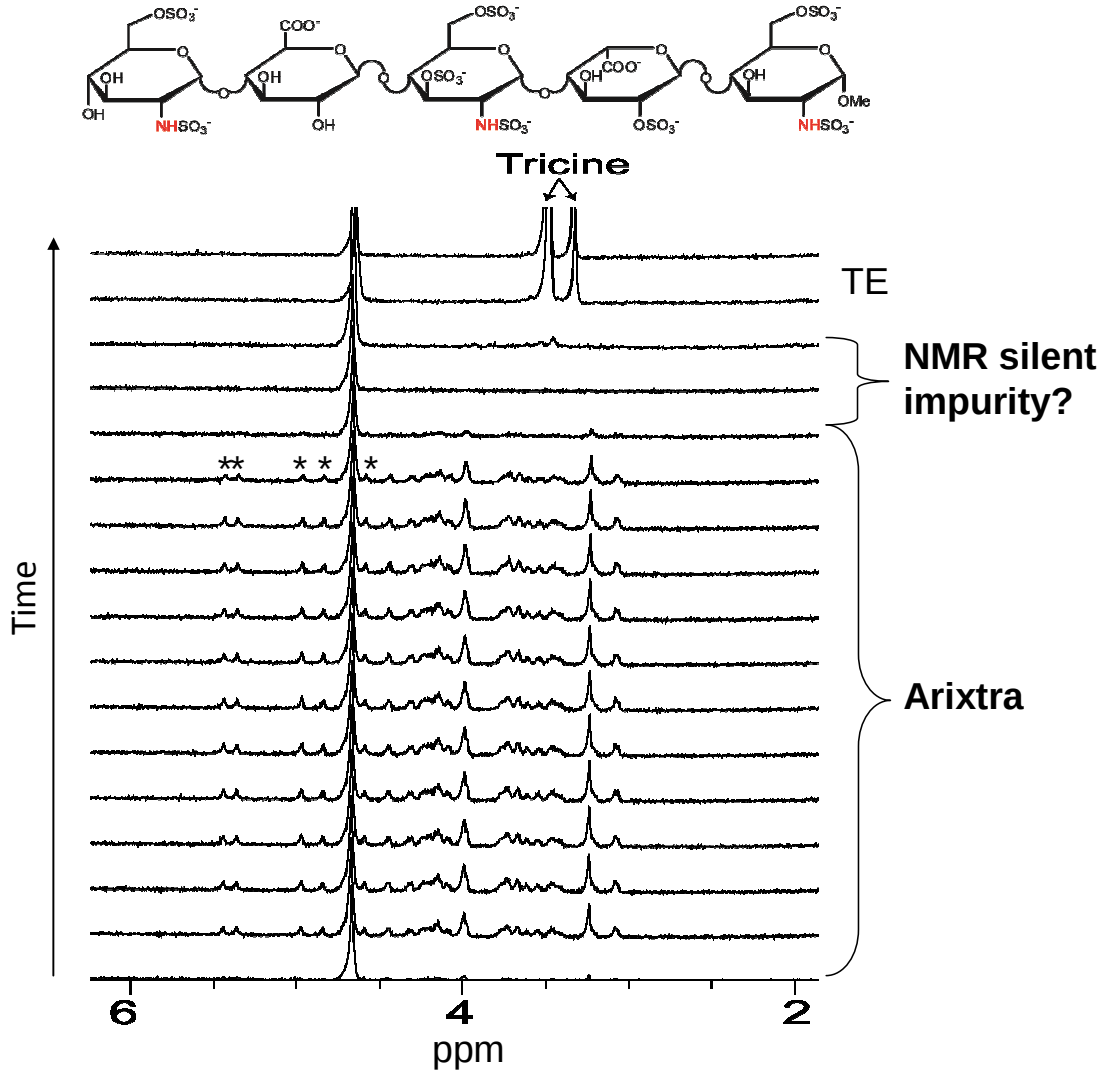

Figure 5.18. Results showing the online cITP-NMR spectra of the synthetic pentasaccharide Arixtra. Resonances marked with asterisks denote anomeric resonances.

special attention should be paid to sample ionic strength prior to analysis by cITP-NMR to avoid excess current induced broadening of spectra. Alternatively, as mentioned in Section 5.3.1, a different probe design is presented in Chapter 6 that minimizes current-induced broadening and thereby reduces the need to limit the ionic strength of samples.

5.3.4. Anionic cITP of a Hexasaccharide Mixture Derived from Heparin**.** Thus far the application of anionic cITP coupled to microcoil NMR for the study heparin and HS derived oligosaccharides has been limited to mostly single component samples. For these samples cITP acts more as a means of introducing the sample into the small active volume of the microcoil probe than as a separation technique. Figure 5.19 shows the ^{1}H-NMR spectrum of the hexasaccharide SEC fraction of a heparinase I digest of bovine intestinal mucosa heparin measured in a Bruker 5 mm NMR probe. As shown in Figure 5.19, even though this sample has already been simplified by a size-based separation, it is still a very complex mixture of components making structural analysis of the intact mixture nearly impossible. To try to address this problem, we subjected this heparin derived hexasaccharide sample to analysis by cITP-NMR (Figure 5.20) to evaluate the extent that our anionic cITP method could resolve the components of this complex mixture. Examining the series of spectra in Figure 5.20 we first see that the hexasaccharide mixture has been completely separated from the matrix components designated by an asterisk in Figure 5.19. However, from inspection of the number of resonances in the anomeric region of the spectra it is clear that each spectrum is still made up of resonances from a mixture of hexasaccharides. Additionally, an expansion of

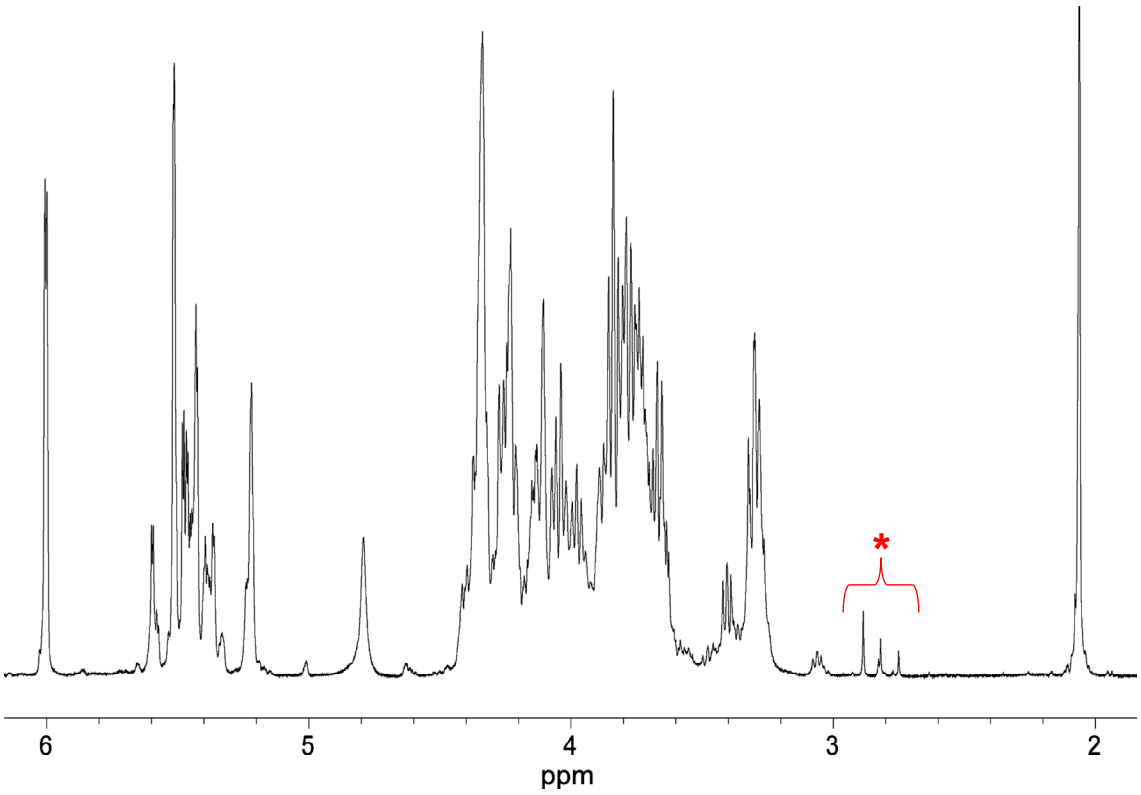

Figure 5.19. ^{1}H-NMR spectrum of a hexasaccharide SEC fraction from a heparinase I digest of bovine intestinal mucosa heparin measured in a Bruker 5 mm NMR probe. Resonances marked with an asterisk are impurities from the sample matrix.

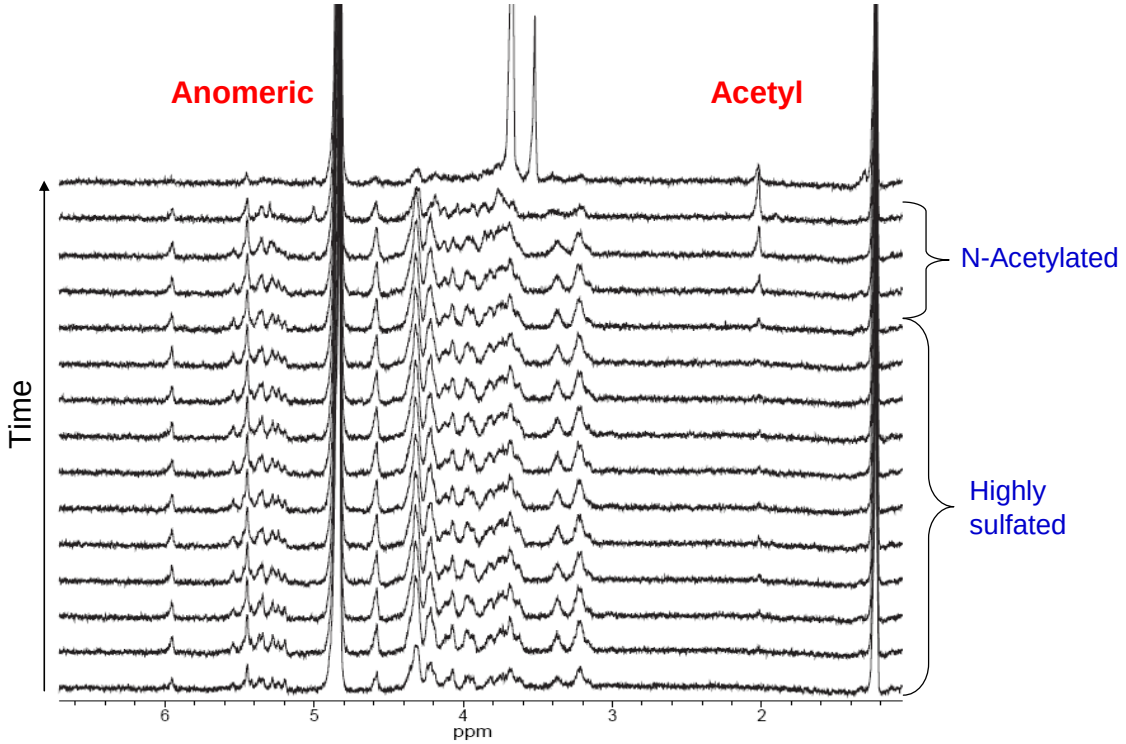

Figure 5.20. Results showing the online cITP-NMR spectra of the hexasaccharide SEC fraction from a heparinase I digest of bovine intestinal mucosa heparin.

the anomeric region of the spectra, Figure 5.21, shows that there is little change in the spectra of the sample band until the interface with the TE is approached. At this point a distinct change in the profile of the anomeric and sugar resonances is observed, with the appearance of a glucuronic acid anomeric resonance at 5.02 ppm. As shown in Figure 5.22, the appearance of the glucuronic acid signal also corresponds to the appearance of resonances of hexasaccharides containing *N*-acetylated residues suggesting the presence of oligomers containing the glucuronic acid-*N*-acetylglucosamine biosynthetic heparin precursor. Overall, while this separation did not yield resolution of individual components of the hexasaccharide mixture as we had hoped, it was able resolve the more abundant and highly sulfonated hexasaccharides of the mixture from less abundant and less charged hexasaccharides containing both *N*-acetyglucosamine and glucuronic acid residues.

5.3.5. Anionic cITP of a Hexasaccharide Mixture Derived from Heparan Sulfate.

With the promising results of the cITP-NMR separation of the hexasaccharide mixture from heparin (Figures 5.21 and 5.22) the separation of a different mixture of hexasaccharides isolated from an SEC separation of heparinase III digested HS was attempted. The HS used in these experiments was isolated as the heparinase I resistant fraction of heparin by Celsus. As discussed in Chapter 1, HS is a less sulfonated relative of heparin consisting of alternating regions of high and low sulfonation. Also unlike heparin, which is mainly isolated to the secretory granules of the mast cells, HS is primarily found on the cell surfaces and in the extracellular matrix allowing it to be involved in a whole host of biological processes.[19] For this reason being able to separate

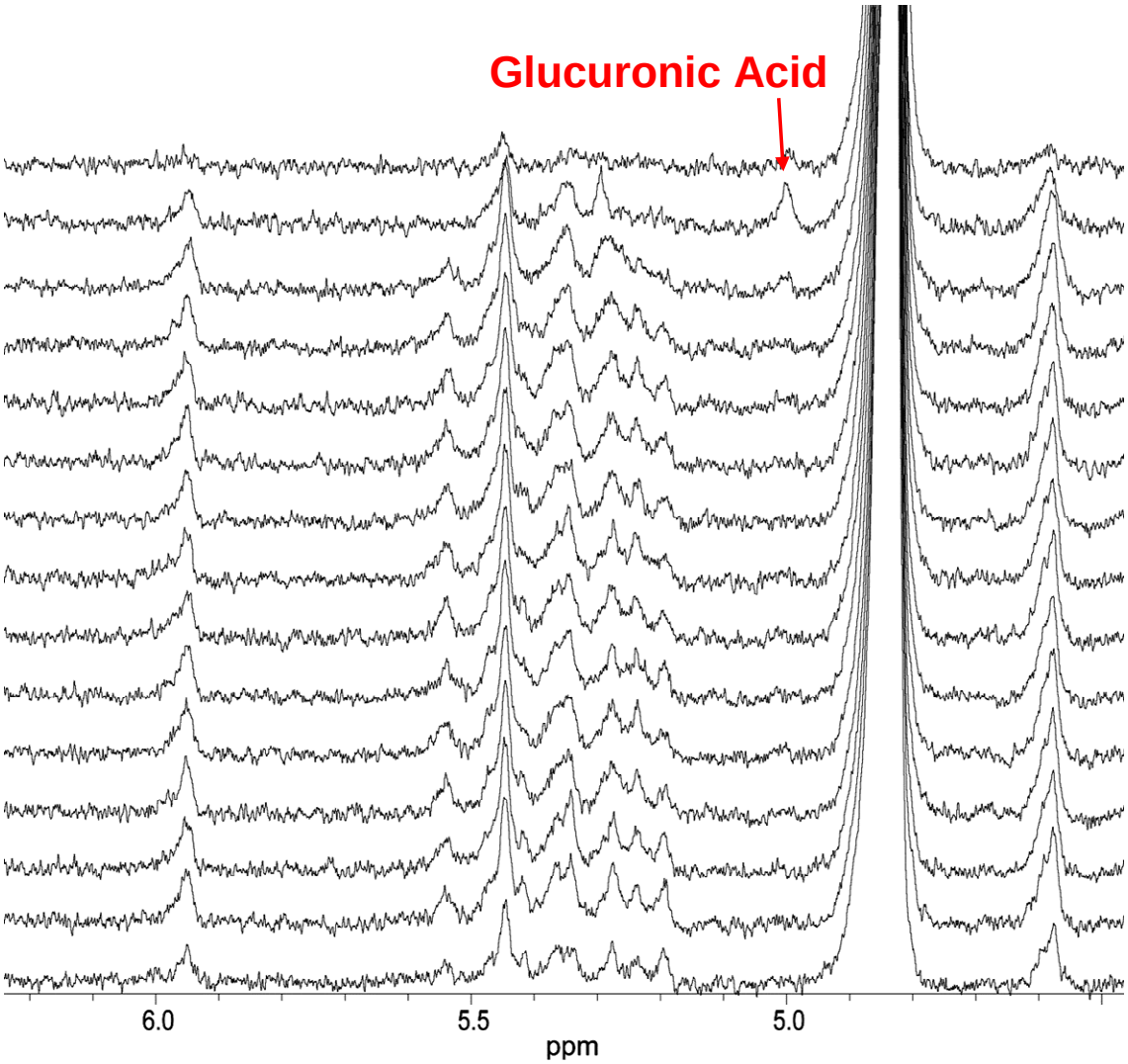

Figure 5.21. Results showing an expanded view of the anomeric region of the online cITP-NMR spectra of the hexasaccharide SEC fraction from a heparinase I digest of bovine intestinal mucosa heparin.

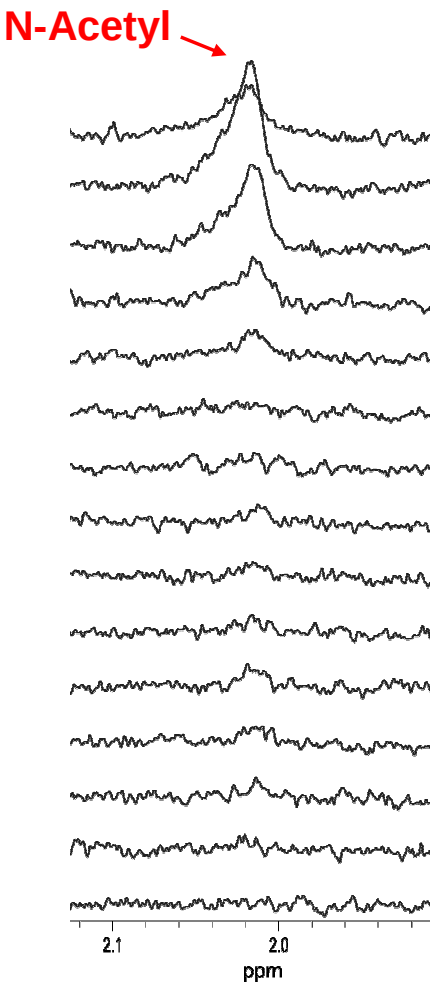

Figure 5.22. Results showing an expanded view of the acetyl region of the online cITP-NMR spectra of the hexasaccharide SEC fraction of a heparinase I digest of bovine intestinal mucosa heparin.

and characterize the specific structural motifs responsible for HS activity is key to better understanding its structure-function relationships.

From the survey spectrum of the HS hexasaccharide mixture, Figure 5.23, one immediately notices a very different spectral profile than was obtained for the corresponding spectrum of the heparin hexasaccharide mixture (Figure 5.19). Examining the acetyl region of the spectra (shown in the inset), we see that the *N*-acetyl resonance is clearly divided into two distinct chemical shifts. The less abundant downfield resonance likely represents a unique substitution pattern near the *N*-acetyl group such as 2-*O* sulfonation.

Figure 5.24 shows the online cITP-NMR spectra of the HS hexasaccharide mixture. The beginning of the analyte band is comprised of what seems to be (based on the poor S/N of the spectra) a poorly focused set of hexasaccharides. Because of their higher electrophoretic mobility, these are likely the hexasaccharides derived from the more sulfonated portions of the HS polysaccharide, but it is difficult to say much more about their structure because of the poor S/N of the spectra. Moving towards the latter half of the analyte band we see a gradual increase in the S/N of all resonances indicating stronger focusing near the back of the band. The expansion of the acetyl, sugar, and anomeric regions of the spectra (Figure 5.25) show that there is a distinct change in the resonances of the sugar region (resonances marked with asterisk) near the back of the band. Interestingly, this change in the sugar region also corresponds with the appearance of the downfield acetyl resonance seen in the inset of Figure 5.23. Examining the resonances near 6 ppm, which correspond to the double bond created at the non-reducing

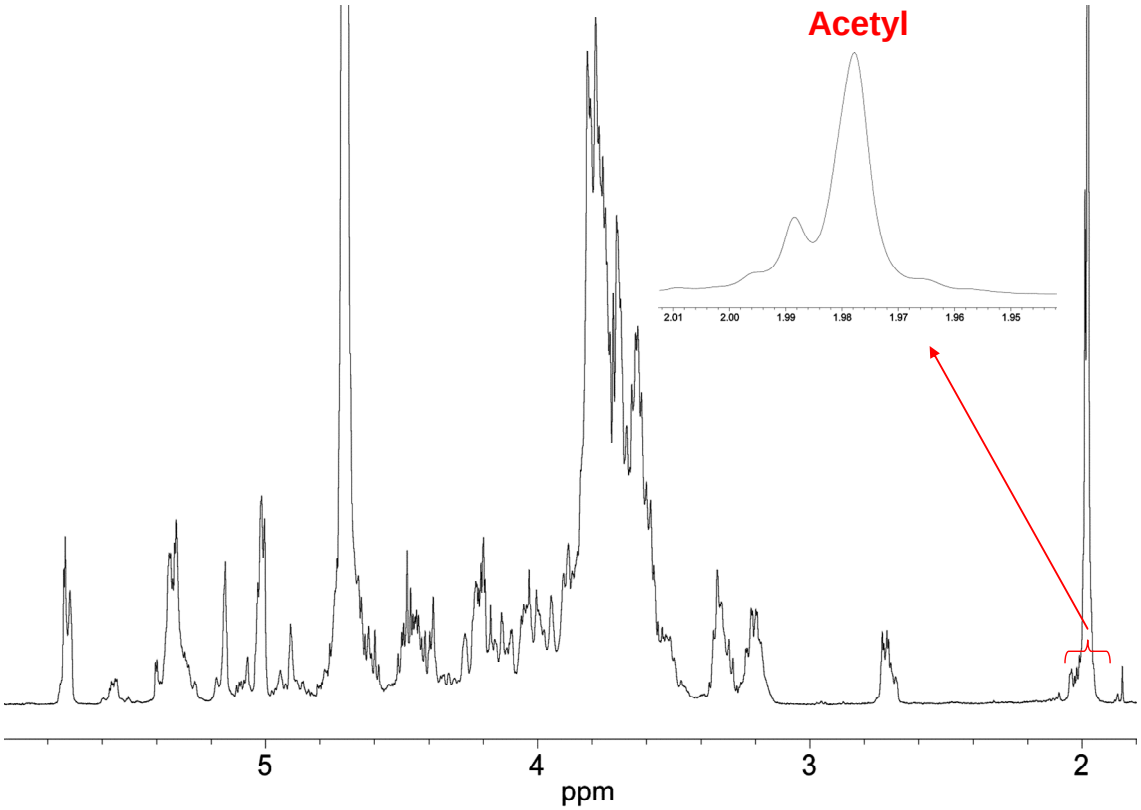

Figure 5.23. ^{1}H NMR spectrum of the hexasaccharide SEC fraction from a heparinase III digest of heparan sulfate measured in a Bruker 5 mm NMR probe. The inset shows an expansion of the acetyl region of the spectrum.

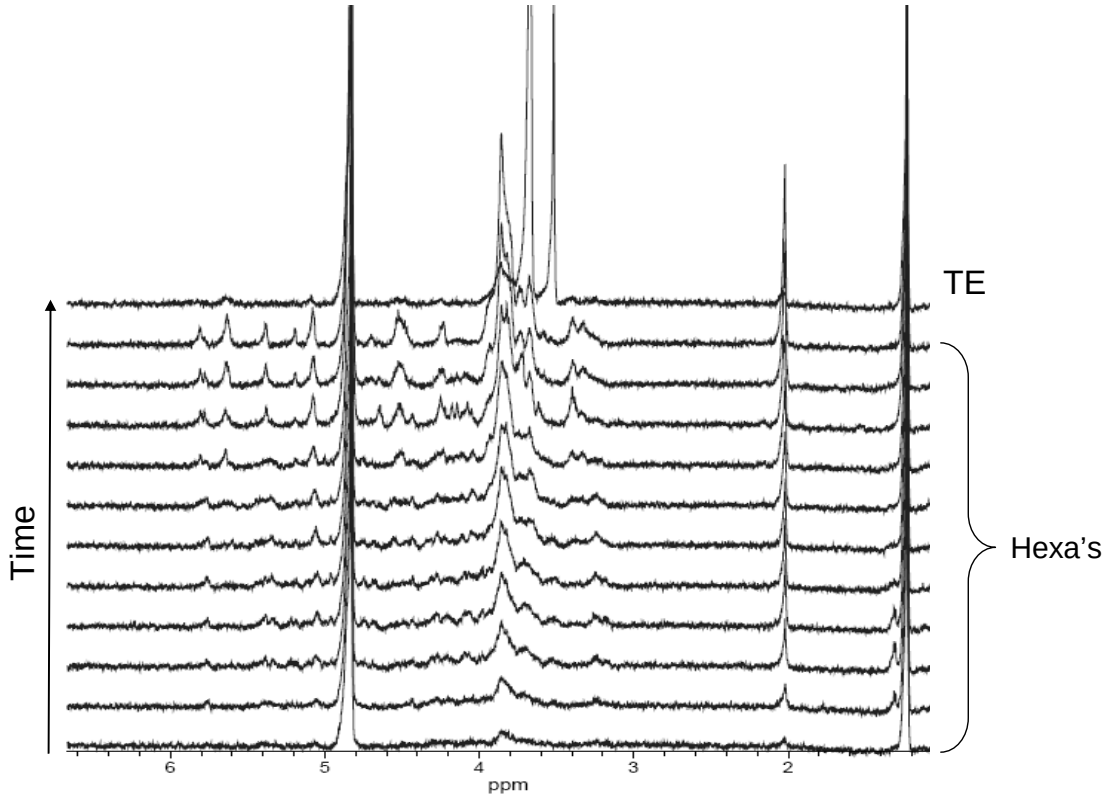

Figure 5.24. Results showing the online cITP-NMR spectra of the hexasaccharide SEC fraction from a heparinase III digest of heparan sulfate.

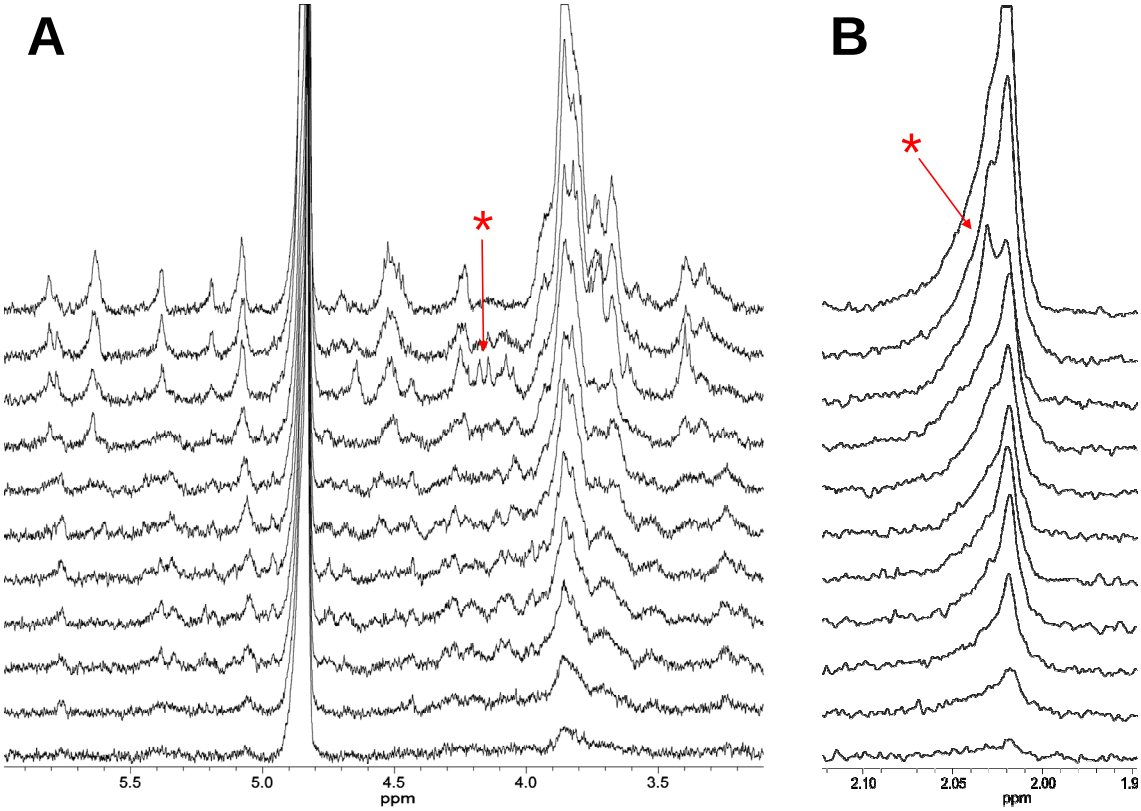

Figure 5.25. Results showing an expanded view of A) the anomeric region and B) the acetyl region of the online cITP-NMR spectra of a hexasaccharide SEC fraction from a heparinase III digest of heparan sulfate. Resonances marked with asterisks mark significant changes in chemical shift.

end of the hexasaccharides during enzymatic digestion, we see that the presence of this unique *N*-acetyl resonance also corresponds to a downfield shift of the proton resonance of the double bond suggesting sulfonation at the 2-*O* position of the double bond containing uronic acid residue.[2] Furthermore, moving through the spectra towards the end of the analyte band it can be observed that the chemical shift of the double bond proton is maintained in the rest of the spectra even after the downfield shifted *N*-acetyl resonance disappears. In all, the online cITP-NMR separation of the HS hexasaccharide mixture showed that even the relatively low abundance series of hexasaccharides that could only be identified in the survey spectrum in Figure 5.23 by the downfield shift of their N-acetyl resonances could be concentrated and separated reasonably well from the larger mixture of hexasaccharides, providing unique spectral information about their structure.

5.3.6. Anionic cITP of a Hexassaccharide Mixture from Enoxaparin. Next we subjected the hexasaccharides obtained by the SEC fractionation of the commercial LMWH drug enoxaparin to our cITP-NMR separation method. Enoxaparin is amongst the most prescribed LMWH anticoagulants. It is produced by chemically digesting the intact heparin polymer by a β-elimination reaction that mimics enzymatic cleavage through a chemical reaction that introduces a double bond at the non-reducing end of each cleaved oligosaccharide. However, unlike the enzymatic digestions, side reactions at the reducing end of the molecule (such as production of a 1,6 anhydro ring) may also occur further increasing the complexity of the oligosaccharides created.[20] From the survey spectrum in Figure 5.26 we see that the hexasaccharide mixture features only a

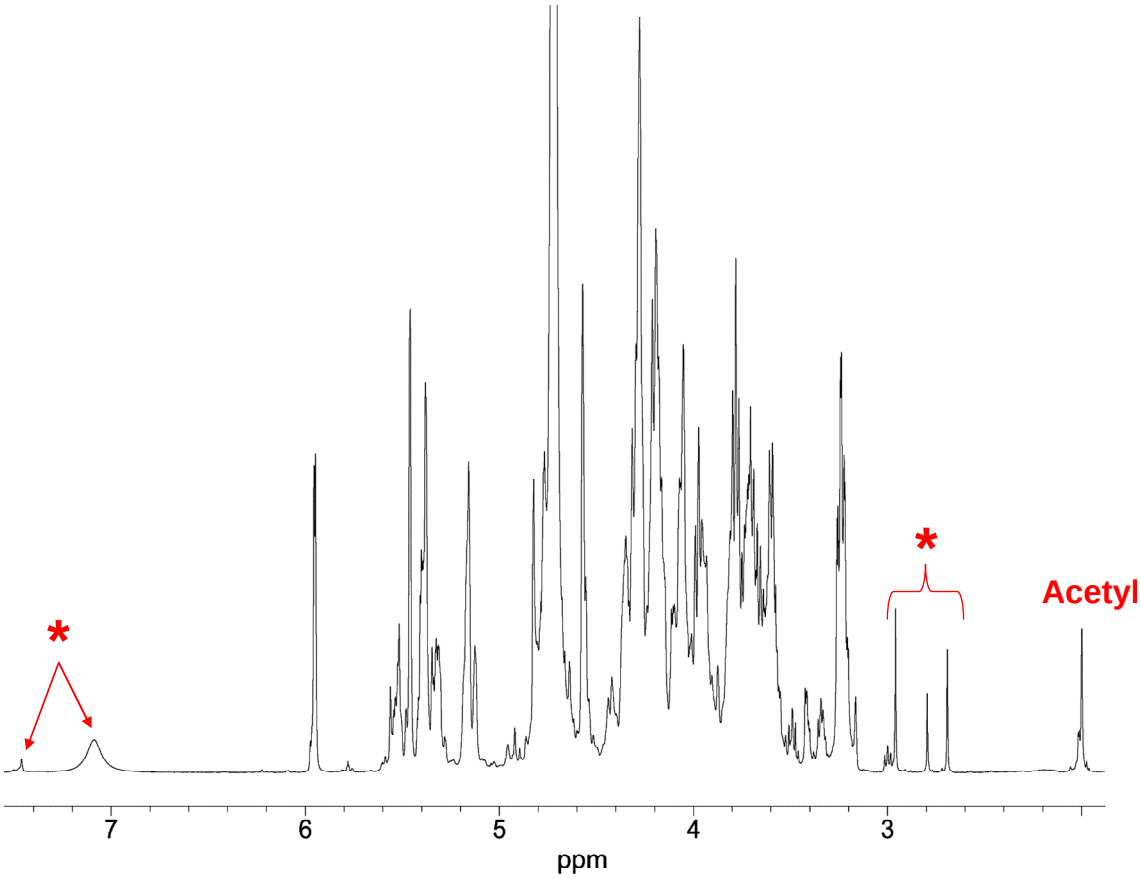

Figure 5.26. ^{1}H-NMR spectrum of the hexasaccharide SEC fraction from the LMWH enoxaparin measured in a Bruker5 mm NMR probe. Peaks marked with asterisks are impurities from the sample matrix.

small degree of N-acetylation compared to the components of the previous two separations. Several resonances (marked by asterisks) can also be observed that correspond to components of the sample matrix. As we saw previously for the heparin hexasaccharide mixture (Figure 5.20), in the online cITP-NMR separation of the mixture of enoxaparin hexasaccharides (Figure 5.27) these matrix components are not focused along with the hexasaccharides. Closer observation of the spectra shows very little change in the chemical shift of resonances in the spectra across almost the entire band. In fact the only observable change is at the very end of the analyte band where the N-acetylated components focused. This suggests that there is little difference in the electrophoretic mobilities between the individual hexasaccharides that make up the sample. This would likely result from a similar degree of sulfonation and charge of the enoxaparin hexasaccharides in the mixture. Even so, Figure 5.27 showed that the method easily separated and focused the less abundant *N*-acetylated compounds from the rest of the mixture and purified the oligosaccharides from the sample contaminants.

5.3.7. Anionic cITP-NMR of Unfractionated Enoxaparin. The previous section showed that cITP could separate a complex mixture of size uniform oligosaccharides and yield useful structural information about groups of similarly charged species in the mixture. However, these samples were isolated from polydisperse digestion mixtures through a time consuming semi-preparative SEC separation. Direct injection of the enzymatic digestion mixture or unfractionated enoxaparin sample into a cITP capillary without any prior separation would require that cITP separation adequately resolve of the mixture components. Because charge and chain length can be related in these

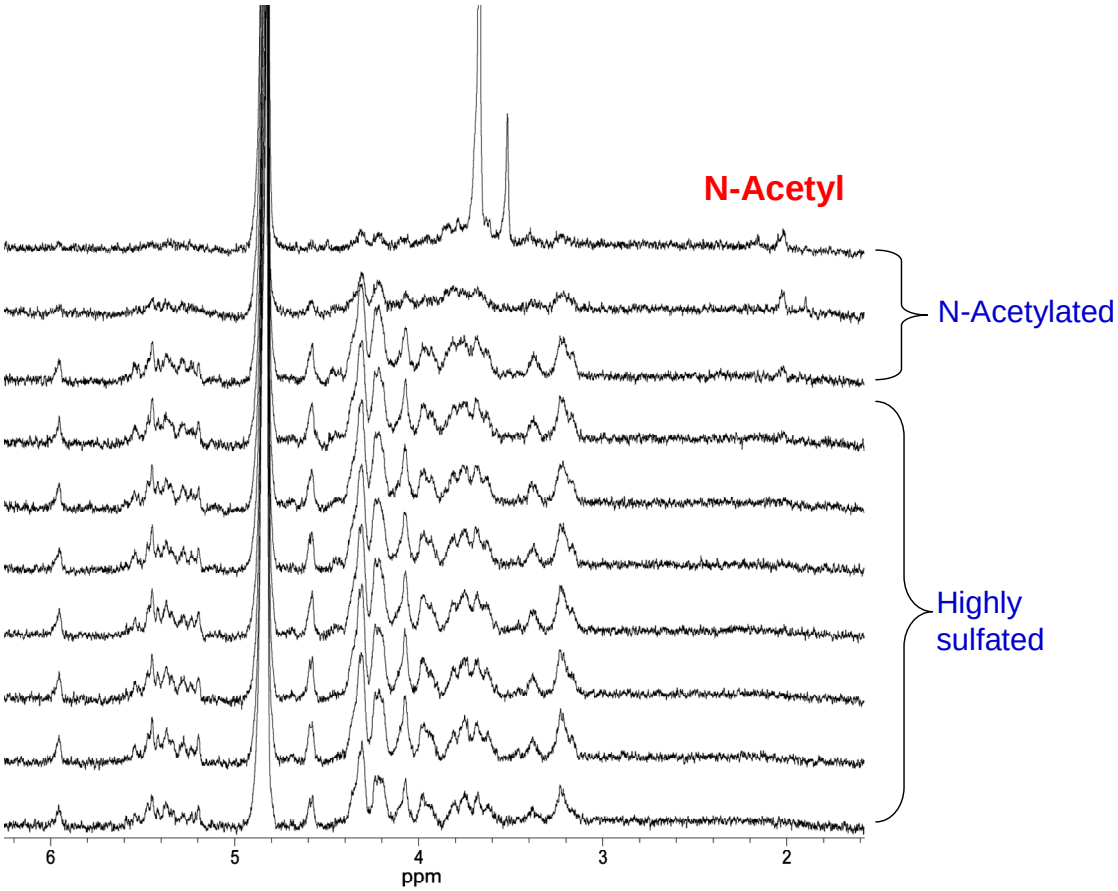

Figure 5.27. Results showing the online cITP-NMR spectra of the hexasaccharide SEC fraction of the LMWH enoxaparin.

oligosaccharides, it could be difficult to resolve components in such a complex mixture. For example, in the analysis of DNA ladders by CE, the use of a sieving gel is required to effect a high-resolution separation because the differently sized oligomers cannot be resolved by their electrophoretic mobilities alone.[21, 22]

To test the potential of cITP-NMR to reveal elements of structure for an unfractionated oligosaccharide mixture, the intact enoxaparin sample with an average molecular weight of 4500 daltons was analyzed using our optimized online anionic cITP-NMR method (Figure 5.28). In examining Figure 5.28 there are several noticeable trends in the spectra. First, looking in the acetyl region of the spectra a gradual increase in the intensity of the *N*-acetyl resonances is observed moving from the front to the back of the analyte band. Also, in the expansion of the anomeric region of the spectra (Figure 5.29) it can be observed that the oligosaccharides that focused at the beginning of the analyte band contained an intense ΔUA resonance indicating the presence of a double bond created during the β-elimination chemical reaction. Because each oligosaccharide should contain only one ΔUA resonance, the compounds that migrated at the front of the band were likely smaller oligosaccharides for which the ΔUA resonance represents a more significant fraction of the overall spectral intensity compared to larger oligosaccharides. This hypothesis is supported by the observation that the spectra containing a more intense ΔUA resonance also feature sharper resonances than the later eluting oligosaccharides. Interestingly, these higher mobility oligosaccharides appear to also be the species with the lowest degree of *N*-acetylation. This is consistent with the formation of selective heparin esters at the carboxylate moieties of sulfated iduronic acid linkages during the β-

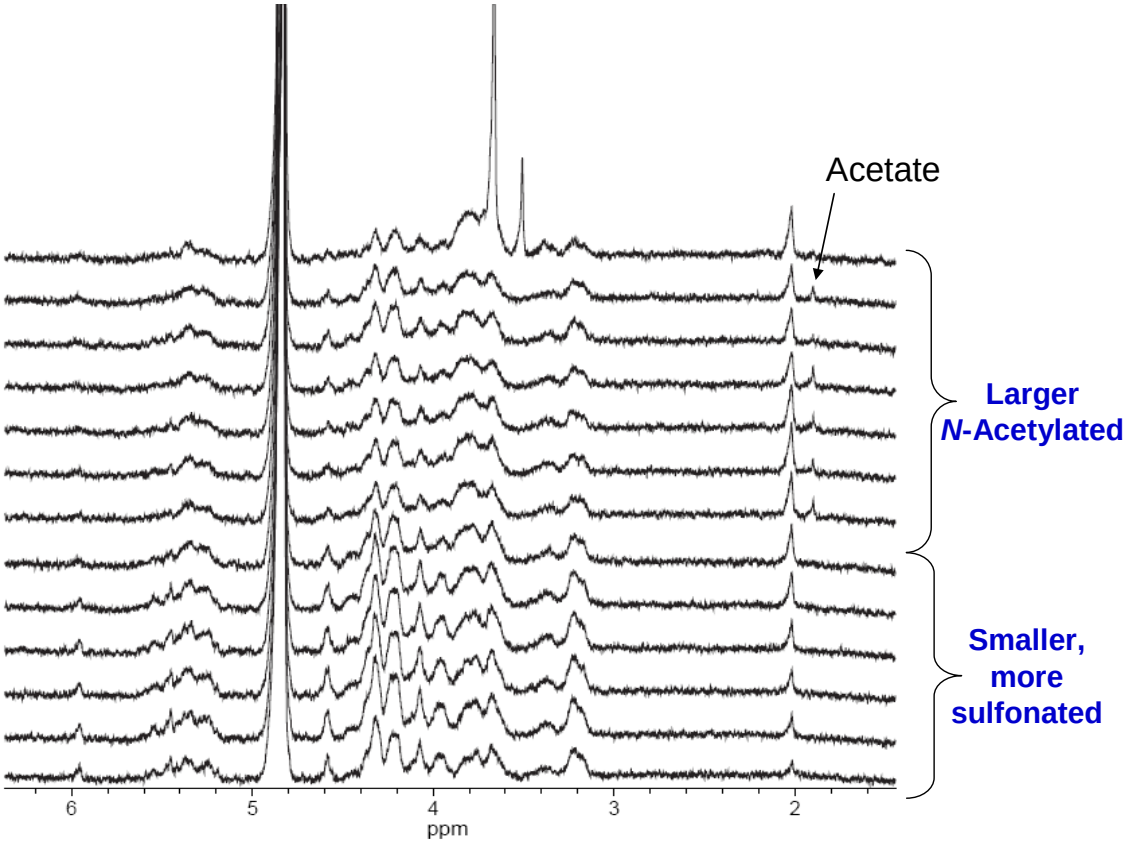

Figure 5.28. Results showing the online cITP-NMR spectra of an unfractionated enoxaparin sample.

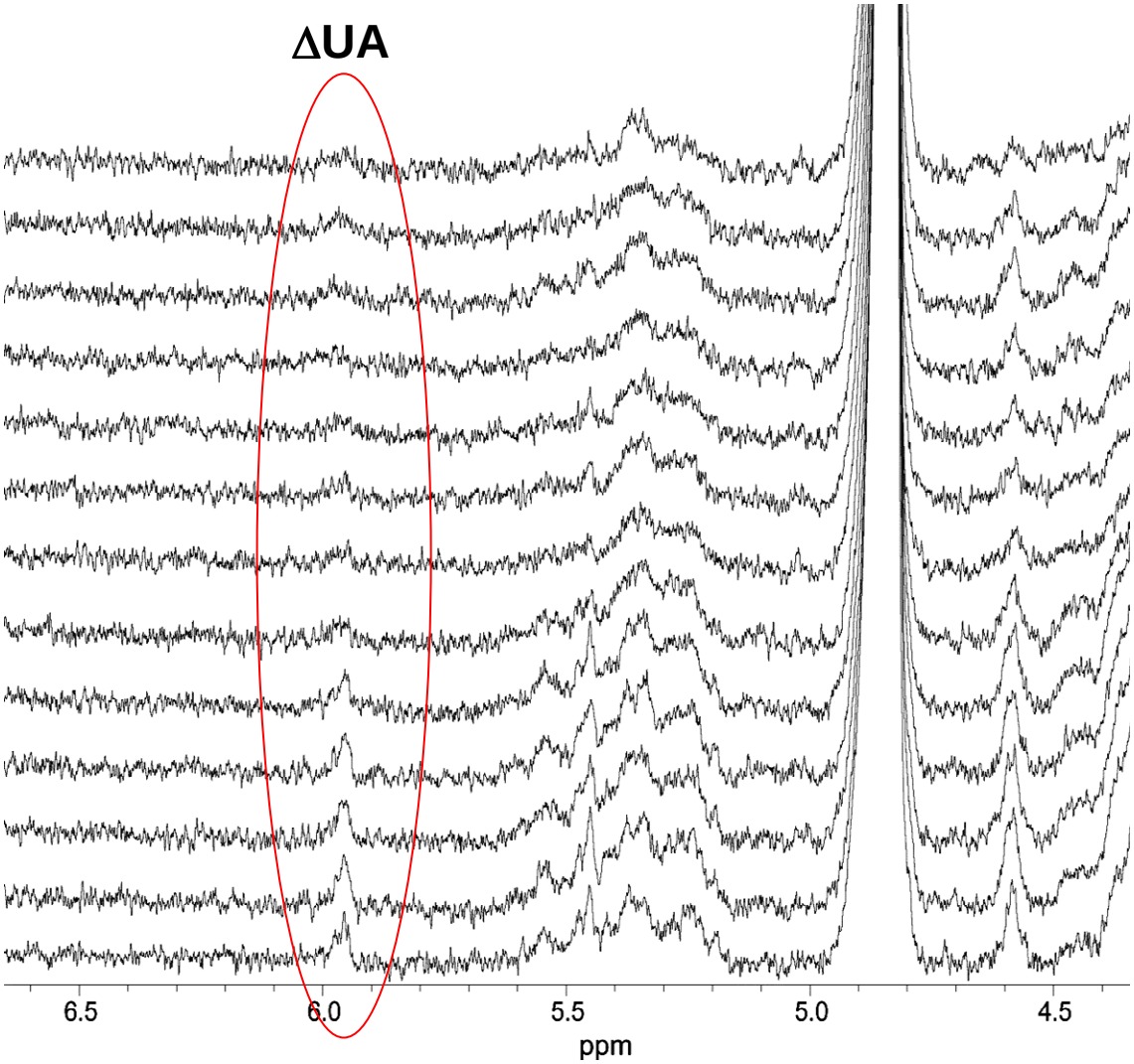

Figure 5.29. Results showing an expansion of the anomeric region of the online cITP-NMR spectra of an unfractionated enoxaparin sample.

elimination process, producing smaller oligosaccharides that are more highly sulfated.[23] The absence of the ΔUA resonance in the larger, more *N*-acetylated oligosaccharides suggests that they are larger because of their lower degree of sulfonation and were not further depolymerized during the β-elimination reaction. Ultimately, while the separation did not provide a high degree of resolution of the components in the complex unfractionated enoxaparin sample, it did provide useful insights into the activity of the β-elimination reaction used to prepare enoxaparin by separating components of the mixture based on size and overall charge. The ability to directly visualize structural modifications, such as the degree of *N*-acetylation and the presence of a double bond and to relate that information to relative size and charge in complex samples containing a diverse array of oligosaccharides could be of significant value for future studies of chemical and enzymatic digestion products and in the quality assurance of commercial preparations.

5.4. Conclusions

This chapter demonstrated the use of a new anionic cITP buffer system for online cITP-NMR experiments for heparin and HS derived oligosaccharides. The new buffer system featured a tricine TE buffer which significantly lowered the electrophoretic current produced during the experiment compared with the previously used MES buffer, reducing the effects of current induced broadening on the NMR spectra acquired. This tricine buffer was able to focus all 12 commercially available heparin derived disaccharides with far superior signal-to-noise ratio and spectral resolution than those spectra published previously by our group. The buffer system also successfully

resolved components in the complex mixtures of hexasaccharides from heparin, HS, and enoxaparin to provide useful structural information about groups of similarly charged species, even those in low abundance. Finally, the cITP buffer system was used to focus and partially resolve components of an unfractionated enoxaparin sample. The results demonstrate the potential of anionic cITP-NMR as a useful tool for evaluating sample purity, composition, and reaction processes for mass-limited heparin and HS samples. It is also likely that this anionic buffer system could be useful for the cITP NMR analysis of wide range of other anionic analytes. In the next chapter, a new type of NMR probe will be presented that has the potential to improve the spectral resolution in cITP-NMR experiments like those shown in this chapter and in Chapter 4 by eliminating the effects of current induced broadening.

5.5. References

1. Chuang, W. L.; Christ, M. D.; Peng, J.; Rabenstein, D. L., An NMR and molecular modeling study of the site-specific binding of histamine by heparin, chemically modified heparin, and heparin-derived oligosaccharides. *Biochemistry* **2000,** 39, 3542-3555.

2. Chuang, W. L.; Christ, M. D.; Rabenstein, D. L., Determination of the primary structures of heparin- and heparan sulfate-derived oligosaccharides using band-selective homonuclear-decoupled two dimensional H-1 NMR experiments. *Anal. Chem.* **2001,** 73, 2310-2316.

3. Korir, A. K.; Larive, C. K., Advances in the separation, sensitive detection, and characterization of heparin and heparan sulfate. *Anal. Bioanal. Chem.* **2009,** 393, 155-169.

4. Jones, C. J.; Beni, S.; Limtiaco, J. F. K.; Langeslay, D. J.; Larive, C. K., Heparin characterization: challenges and solutions. *Annu. Rev. Anal. Chem.* **2011,** 4, 439-465.

5. Eldridge, S. L. Development of analytical methods for trace impurity analysis and structure determination of heparin/heparan sulfate-derived oligosaccharides. University of California, Riverside, Riverside, CA, 2009.

6. Korir, A.; Larive, C., On-line NMR detection of microgram quantities of heparin-derived oligosaccharides and their structure elucidation by microcoil NMR. *Anal. Bioanal. Chem.* **2007,** 388, 1707-1716.

7. Korir, A. K.; Almeida, V. K.; Malkin, D. S.; Larive, C. K., Separation and analysis of nanomole quantities of heparin oligosaccharides using on-line capillary isotachophoresis coupled with NMR detection. *Anal. Chem.* **2005,** 77, 5998-6003.

8. Kautz, R. A.; Lacey, M. E.; Wolters, A. M.; Foret, F.; Webb, A. G.; Karger, B. L.; Sweedler, J. V., Sample concentration and separation for nanoliter-volume NMR spectroscopy using capillary isotachophoresis. *J. Am. Chem. Soc.* **2001,** 123, 3159-3160.

9. Bax, A., A spatially selective composite 90° radiofrequency pulse. *J. Magn. Reson.* **1985,** 65, 142-145.

10. Bocek, P.; M. Demi; Gebauer, P.; Dolnik, V., *Analytical isotachophoresis*. VCH Publishers: New York, 1988; p 237.

11. Korir, A. K.; Almeida, V. K.; Larive, C. K., Visualizing ion electromigration during isotachophoretic separations with capillary isotachophoresis-NMR. *Anal. Chem.* **2006,** 78, 7078-7087.

12. Poon, G. M. K.; Abu-Ghazalah, R. M.; Macgregor, R. B., Ionic mobilities of duplex and frayed wire DNA in discontinuous buffer electrophoresis: Evidence of interactions with amino acids *Biochemistry* **2004,** 43, 16337-16347.

13. Eldridge, S. L.; Higgins, L. A.; Dickey, B. J.; Larive, C. K., Insights into the capillary electrophoresis separation of heparin disaccharides from nuclear magnetic resonance, pKa, and electrophoretic mobility measurements. *Anal. Chem.* **2009,** 81, 7406-7415.

14. Good, N. E.; Winget, G. D.; Winter, W.; Connolly, T. N.; Izawa, S.; Singh, R. M. M., Hydrogen ion buffers for biological research. *Biochemistry* **1966,** 5, 467-477.

15. El Rassi, Z.; Mechref, Y., Recent advances in capillary electrophoresis of carbohydrates. *Electrophoresis* **1996,** 17, 275-301.

16. Mittermayr, S.; Guttman, A., Influence of molecular configuration and conformation on the electromigration of oligosaccharides in narrow bore capillaries. *Electrophoresis* **2012,** 33, 1000-1007.
17. Korir, A. K.; Limitiaco, J. F. K.; Gutierrez, S. M.; Larive, C. K., Ultraperformance ion-pair liquid chromatography coupled to electrospray time-of-flight mass spectrometry for compositional profiling and quantification of heparin and heparan sulfate. *Anal. Chem.* **2008,** 80, 1297-1306.

18. Casu, B.; Gennaro, U., A conductimetric method for the determination of sulphate and carboxyl groups in heparin and other mucopolysaccharides. *Carbohydr. Res.* **1975,** 39, 168-176.

19. Rabenstein, D. L., Heparin and heparan sulfate: structure and function. *Nat. Prod. Rep.* **2002,** 19, 312-331.

20. Bianchini, P.; Mascellani, G., Few bicyclic acetals at reducing end of low-molecular-weight heparins: might they restrict specification of pharmacopoeia? *Pharmaceur. Sci. Notes* **2005,** 1, 1-3.

21. Albargheuthi, M. N.; Barron, A. E., Polymeric matrices for DNA sequencing by capillary electrophoresis. *Electrophoresis* **2000,** 21, 4096-4111.

22. Lerman, L. S.; Frisch, H. L., Why does the electrophoretic mobility of DNA in gels vary with the length of the molecule? *Biopolymers* **1982,** 21, 995-997.

23. Mardiguian, J. Heparin esters and processes for their preparation. U.S. Patent No. 4440926, 1984.

CHAPTER SIX

Hyphenation of Capillary Isotachophoresis to a Microslot NMR Probe

The work in this chapter is based on a paper submitted to Analytical Chemistry, 2012. Some text and figures in the introduction are also based on a paper published in Analytical and Bioanalytical Chemistry: *Anal. Bioanal. Chem.*, 2012, 402, 61-68.

In this chapter we demonstrate the coupling of cITP with a microslot NMR probe design.. While the work in chapters 4 and 5 coupled cITP with solenoidal microcoil NMR probes, the structural information provided by these spectra were limited by broad resonances and poor spectral resolution due to the magnetic field created by the current running through the capillary during separations. Coupling cITP to a microslot NMR probe design allows the separation capillary to be oriented parallel to the static magnetic field of the NMR eliminating the deleterious affects of the magnetic field produced in the capillary.

6.1 Introduction

While the work in chapters 4 and 5 coupled cITP with solenoidal microcoil NMR probes, the structural information provided by these spectra were limited by broad resonances and poor spectral resolution due to the magnetic field created by the current running through the capillary during separations. A promising alternative to solenoidal microcoils are microstrip (or stripline) and microslot probe designs.[1-3] Both types of

probes use a thin metal strip positioned parallel to the static magnetic field of the magnet, B_0, to produce the B_1 magnetic field and to act as a receiver of the NMR signal. Similar to a wire that produces a magnetic field that encircles it when current is applied, the B_1 magnetic field lines produced by these probes encircle the strips and run parallel to the surface. In the stripline design B_1-field homogeneity is realized by sandwiching the metal strip between two ground planes creating a nonradiative closed system.[1] In the microslot design a small hole is cut into a microstrip waveguide to create a pure series inductance.[2, 3] Both designs have shown great promise in terms of the sensitivity and resolution of the spectra acquired.

Because of their planar designs, the capillaries used for CE or cITP separations can be oriented parallel to B_0 in microstrip or microslot probes. Figure 6.1 shows the magnetic fields created by the NMR magnet, B_0, the probe, B_1, and the electrophoretic current running through the separation capillary during a separation, B_2 for both a solenoidal microcoil (Figure 6.1A) and a microslot (Figure 6.1B). Because the direction of B_2 is perpendicular to B_0 for the microslot, the separation current should not contribute to B_0 inhomogeneity and, compared to solenoidal coils, better quality spectra should be obtained.

Another promising feature of microstrip and microslot probe designs is their ease of manufacture. Although automated fabrication techniques do exist for solenoidal microcoils, they are often hand wound by skilled probe designers. In contrast, microstrip and microslot probes are created using well established lithographic methods which could

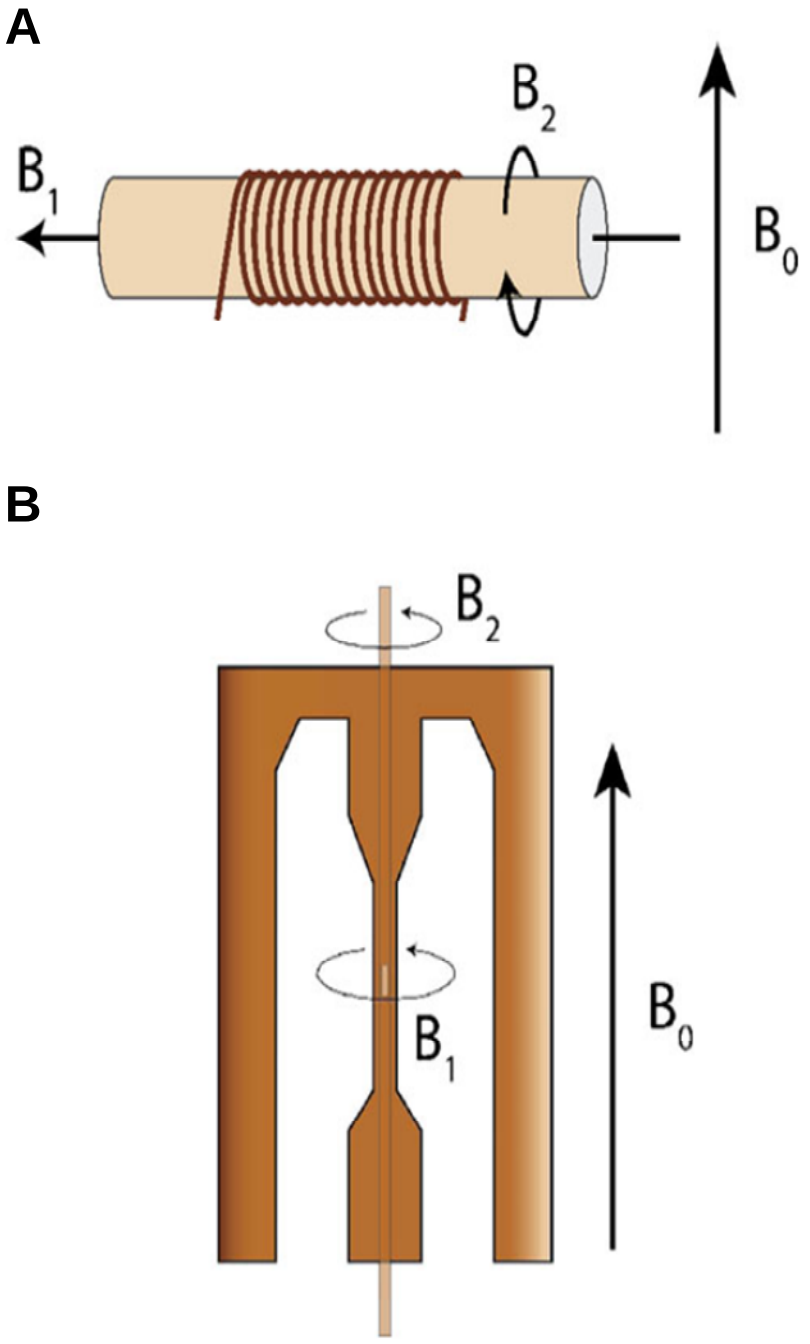

Figure 6.1. Illustrations of a solenoidal microcoil (A) and a microslot (B), showing the direction of the magnetic fields created by the coil or slot (B_1), the current running through the separation capillary during a separation (B_2), and the magnet (B_0)

easily be translated to a commercial design process. The microstrip probe is constructed using only a single layer lithographic process, which offers a full range of scalability, while in the case of the microslot, scalability is limited by the laser wavelength used to create the slot in the microstrip.

The work described in this chapter demonstrates the coupling of cITP with a microslot NMR probe design that was constructed by me at the ISAS institute for analytical sciences in Dortmund, Germany during collaboration with the Hergenroder group in the summer of 2010. In this probe design the separation capillary is oriented parallel to the static B_0 magnetic field of the NMR, eliminating the deleterious effects of the magnetic field produced in the capillary. The benefits of this approach will be demonstrated by the cITP focusing and online NMR analysis of the commercially available β-blocker, atenolol.

6.2 Experimental

6.2.1 Materials and Reagents. Fused silica capillaries were purchased from Polymicro (Phoenix, AZ) and surface-modified to produce zero electroosmotic flow by MicroSolv Technology Corporation (Eatontown, NJ). Polyurethane-coated copper wire (99.99% Cu) was purchased from California Fine Wire Company (Grover Beach, CA). Non-magnetic trimmer capacitors were purchased from Voltronics Corporation (Denville, NJ). The Rogers RT/duroid 5880 high-frequency laminate used for microslot fabrication was purchased from the Rogers Corporation (Chandler, AZ). The dielectric of this laminate is glass microfiber reinforced PTFE (thickness 3.175 mm) with electrodeposited copper on both sides (thickness 35 μm). The photoresist used for chemical etching was

AR-U 4040 Alresist (Alresist). The development of the exposed substrate was accomplished with sodium hydroxide solution (7 g/L). The etching bath (Hema) consisted of sodium persulfate. Sodium acetate was purchased from Sigma-Aldrich, Inc. (St. Louis, MO). Deuterium oxide (D_2O, 99.9% D low paramagnetic) and deuterated acetic acid were purchased from Cambridge Isotope Laboratories, Inc. (Andover, MA). The 0.2 μm nylon syringe filters were purchased from MicroSolv (Eatontown, NJ).

6.2.2. Solenoidal Microcoil Probe Construction. The design of the solenoidal microcoil probe used in this work is described in section 4.2.2.

6.2.3. Microslot Probe Construction. The construction of the micrslot probe used in this chapter was done at the ISAS institute for analytical sciences in Dortmund, Germany. The method used to construct the microslot has also been reported previously.[4] To begin construction of the structure and microstrip, one side of the of the Rogers substrate was cleaned with ethanol and polished to micron root-mean-square roughness. The substrate was then coated with a thin layer of photoresist and the mask (seen in Figure 6.2) for the structure and microstrip was pressed on the surface. The surface and mask were then exposed to UV light for 25s in a vacuum chamber. Next, the mask was removed and the substrate was developed by immersing the substrate in a sodium hydroxide bath for several seconds. The exposed copper was then etched away from the substrate by immersing the it in an etching bath of sodium persulfate for 20min. This left only the copper structure and microstrip on the substrate. A 400 x 500μm microslot (shown in Figure 6.3) was then machined into the center of the microstrip by

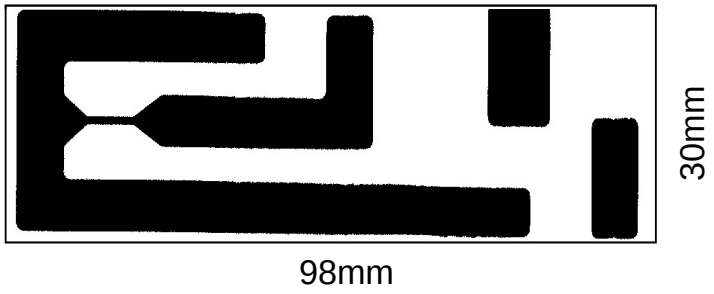

Figure 6.2 Illustration of the mask used for the photolithographic production of the microstrip structure for the microslot probe

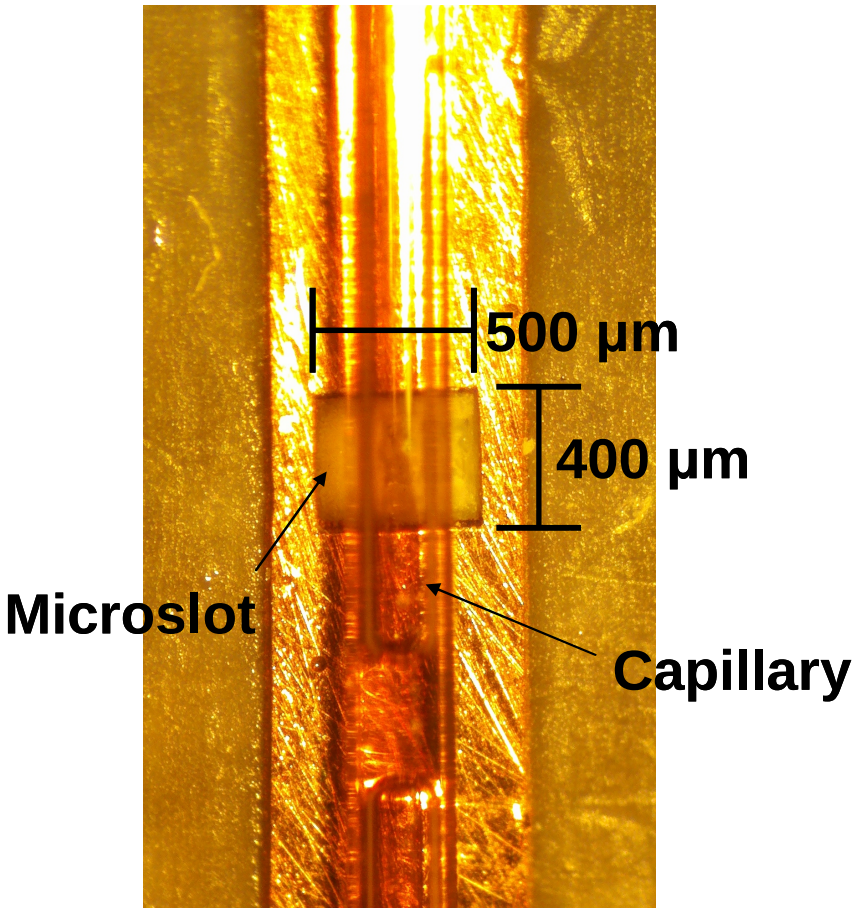

Figure 6.3 Digital image taken through the lens of a microscope of a sample capillary positioned on top of the slot in the microstrip of a microslot NMR probe.

femtosecond laser ablation. The finished microslot chip was then fastened (with a custom built mount) to the top of a 500 MHz bruker broadband probe with the coil removed. Electrical connections to the tuning and matching capacitors of the probe were made according to the circuit diagram shown in Figure 6.4. An additional trimmer capacitor (C2) was added to the circuit in order to tune the resonant frequency of the probe into the range of 600MHz. The separation capillary was then taped with kapton tape across the microslot in an orientation parallel to B_0.

6.2.4. Experiments to Test the Effect of Electrophoretic Current on ^{1}H NMR Lineshape in Microcoil and Microslot Probes. A 50 mM sodium acetate buffer was prepared in H_2O and titrated to pH 4.6 with deuterated acetic acid. The capillary of each probe was filled with buffer and each end placed into a buffer reservoir. The appropriate voltage was applied across the capillary using platinum electrodes and an NMR spectrum was subsequently measured. All ^{1}H NMR spectra were acquired using a Bruker Avance spectrometer operating at 599.69 MHz. The spectra were acquired by averaging 16 transients with 0 dummy scans. A relaxation delay of 1.00 s was used, and FIDs were acquired into 33,066 data points following the application of the 90° pulse. FIDs were apodized by multiplication by an exponential function equivalent to 1.0 Hz line broadening prior to Fourier transform and zero-filled to 65,536 points.

6.2.5. Experiment to Test the Effect of Electrophoretic Current on Radio Frequency Homogeneity in the Microslot Probe. A 50 mM sodium acetate buffer was prepared in H_2O and titrated to pH 4.6 with deuterated acetic acid. The capillary of the microslot probe was filled with the buffer and each end placed into a buffer reservoir.

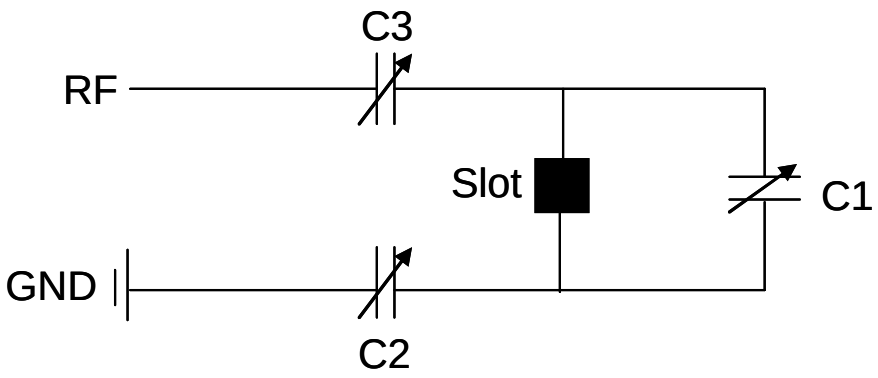

Figure 6.4 Circuit diagram for microslot probe

For the nutation plot, ^{1}H NMR spectra were measured with either 0 or -20 kV applied across the separation capillary by averaging 8 transients with 0 dummy scans for each pulse width, incremented from 2 μs to 60 μs in 2μs increments. A relaxation delay of 30 s was used, and FIDs were acquired into 33,066 data points following the application of the appropriate pulse. FIDs were apodized by multiplication by an exponential function equivalent to 1.0 Hz line broadening prior to Fourier transform and zero-filled to 65,536 points. In the high voltage nutation experiment, the -20 kV voltage applied resulted in a current of -85 μA. For both experiments, integrals of the water resonance were plotted vs. the pulse length in Excel (Microsoft, Redmond, WA) to produce the plots in Figure 6.10.

6.2.6. On-line Microslot cITP-NMR of Atenolol. The cITP buffers were prepared in D2O. The leading electrolyte (LE) consisted of a 260 mM sodium acetate solution adjusted to pD 5.0 by addition of deuterated acetic acid. A solution containing 160 mM deuterated acetic acid served as the trailing electrolyte (TE). For the cITP experiment, the capillary was filled with LE and the 2 mM atenolol sample (prepared in 50/50 H2O/TE) was introduced by hydrodynamic injection at a height differential of 18 cm for 7 min resulting in injection of 18 nmol. Next the TE was injected for a total of 7 min. After completion of the injection protocol, the voltage across the capillary was raised to -15 kV for the duration of the cITP experiment. After the start of the cITP experiment, NMR acquisition was initiated to acquire an array of ^{1}H NMR spectra using 90° pulses with an acquisition time of 1.99 s and a spectral width of 11.03 ppm. Each spectrum was acquired by coaddition of eight transients and zero dummy scans. Line broadening equivalent to 1.0 Hz and zero-filling to 65,536 points were applied prior to Fourier

transformation. Once atenolol reached the active volume of the microslot probe a hydrodynamic back pressure was applied to the LE buffer reservoir which slowed the migration of the atenolol band through the probe active volume. The spectrum was produced by coaddition of thirty FIDs containing the resonances for atenolol after first manually aligning the spectra to account for spectral drift during data acquisition due to the lack of a spectrometer lock.

6.2.7 Improving Background Suppression in the Microslot Probe. A 100 mM sucrose solution was prepared in low paramagnetic D_2O and filtered through a 0.2 μm filter. The capillary of the microslot probe was filled with the sucrose solution and the ends were closed off to prevent loss of sample during NMR acquisition. NMR acquisition was initiated to acquire an array of ^1H NMR spectra using 90° pulses with an acquisition time of 1.99 s and a spectral width of 11.03 ppm. Each spectrum was acquired by coaddition of sixteen transients and zero dummy scans and a relaxation delay of 2.00 s. Line broadening equivalent to 1.0 Hz and zero-filling to 65,536 points were applied prior to Fourier transformation. The spectra shown in Figures 6.8-6.11 were prepared by co-adding sixty four FID's after first manually aligning the spectra to account for spectral drift during the acquisition of the spectra. In each Figure the spectrum was only phased, but no baseline correction was applied.

6.3. Results and Discussion

Previous work has demonstrated the effects that the electrophoretic current has on the line width of NMR resonances when CE is coupled to solenoidal microcoil NMR.[5, 6] Coupling electrophoretic driven separations with a microslot NMR probe

should reduce the impact of current-induced broadening because the separation capillary can be oriented parallel to the static B_0 field of the NMR magnet. In this geometry, the magnetic field induced by the electrophoretic current is oriented perpendicular to B_0 and therefore does not contribute to resonance broadening (Figure 6.1).

6.3.1 Experiments to Test the Effect of Electrophoretic Current on ^{1}H NMR Lineshape in Microcoil and Microslot Probes. Figure 6.5 compares of the effects of electrophoretic current on the line width of the ^{1}H NMR resonance of water in spectra measured using a solenoidal microcoil probe (Figure 6.5A) and a microslot probe (Figure 6.5B). The 180 μm ID/360 μm OD capillary contains a 50 mM sodium acetate buffer in H_2O at pH 4.6. For both sets of spectra in Figure 6.5, the electrophoretic current increased proportionally from 0 to around -115.0 μA as the voltage across the capillary increased from 0 to -20.0 kV. For the ^{1}H NMR spectra acquired using the solenoidal microcoil probe (Figure 6.5A), as the electrophoretic current increases the water resonance is significantly broadened, resulting in a significant loss in S/N. Additionally, as the current is increased we see that the lineshape of the water resonance also degrades becoming an asymmetrical lump at -115.0 μA. Identical spectra measured with the microslot probe (Figure 6.5B) show little current-induced broadening because of the orientation of the separation capillary parallel to B_0. The slight broadening of the water resonance at the highest values of the applied voltage is likely due to an increase in bulk solvent flow due to a small residual EOF in the zero-EOF capillary used for this experiment.[7]

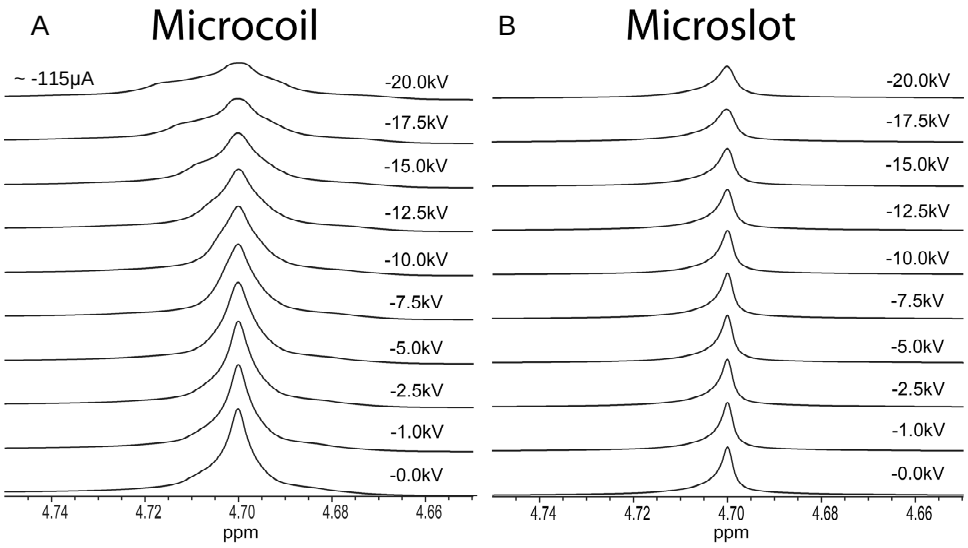

Figure 6.5 Comparison of the effects of electrophoretic current on the line width of the ^{1}H resonance of water for A) a solenoidal microcoil probe and B) a microslot probe. In both experiments the capillary contains 50 mM sodium acetate buffer in H_2O at pH 4.6.

6.3.2 Experiment to Test the Effect of Electrophoretic Current on Radio Frequency Homogeneity in the Microslot Probe. To evaluate the effect of electrophoretic current on the RF homogeneity of the microslot probe, nutation experiments were conducted in which the width of a single pulse was varied as a function of time at a constant pulse power and electrophoretic currents of 0 and -85 μA (Figure 6.6). One might expect that the magnetic field induced by the electrophoretic current would have some deleterious effect on RF homogeneity because of its orientation parallel to B_1. However, Figure 6.6 shows that the 90°, 180°, 270°, and 360° nutation angles match well at both high and low electrophoretic currents. Only near a nutation angle of 450° are the pulse lengths slightly different (0 μA: 54 μs and -85 μA: 52μs). Additionally, the ratio of the peak intensities obtained for tip angles of 90° and 270°, 0.91 with a separation current of -85 μA and 0.93 with no separation current, demonstrates the preservation of RF (B_1) field homogeneity even at high electrophoretic currents.

6.3.3 On-line Microslot cITP-NMR of Atenolol. The final experimental objective was to demonstrate the coupling of cITP to microslot NMR by focusing and detecting the commercially available β-blocker, atenolol. Atenolol was chosen because it is positively charged at the acidic pH of our cationic cITP buffer system and because its ^{1}H NMR spectrum spans 6 ppm including both methyl and aromatic resonances. Figure 6.7 shows the on-flow cITP-NMR spectrum of 18 nmol of atenolol obtained by coaddition of 30, 8 scan FID's. The inset containing the expansion of the aromatic region of the atenolol spectrum shows that the 8.3 Hz J-coupling of the aromatic protons is well resolved even

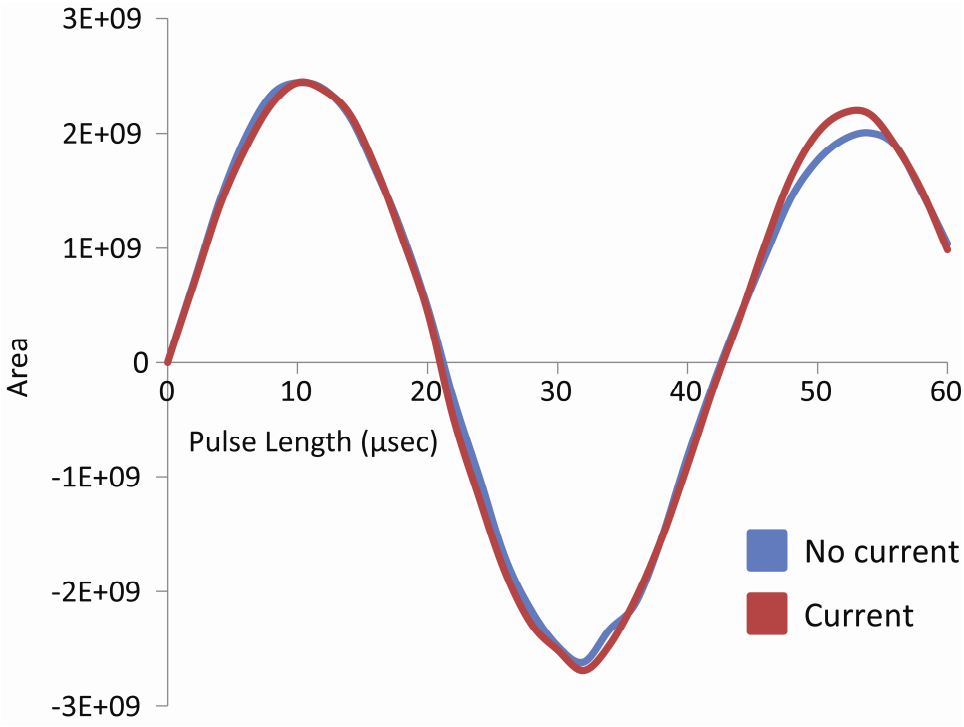

Figure 6.6. Nutation plots showing the effect of current on RF homogeneity for the microslot probe.

with the application of 1-Hz line-broadening to the FID. The inset showing the expansion of the spectral region between 3.0 and 4.2 ppm shows the resolution of even smaller proton couplings (some as low as 1.8 Hz). The presence of the resonances around 4.52, 4.17, 3.36, and 1.77 ppm, which do not arise from atenolol, suggests that either a contaminant in the sample or an atenolol degradation product was focused during the experiment.

Even after the application of baseline correction, the baseline distortion in Figure 6.7 would make it difficult to extract accurate integrals from this spectrum. These distortions are likely a result of background resonances produced by the probe. The bruker defined zg_8pulse pulse sequence used to acquire the spectrum in Figure 6.7 uses a composite 90° pulse in the place of a single 90° pulse that should have suppressed some of the background signals by only detecting resonances in the most homogeneous part of the B_1 field.[8] To achieve better background suppression other pulse sequences can be explored. Section 6.3.4 discusses several alternate pulse sequences that could be used to improve background suppression in spectra acquired with microslot NMR probes and presents results obtained for each sequence using a 100 mM sucrose solution (Figures 6.8-6.11).

6.3.4 Improving Background Suppression in the Microslot Probe. Figure 6.8 shows the microslot NMR spectra of sucrose acquired with a basic single pulse Bruker zg pulse sequence which features a simple 90° pulse followed by acquisition. It would be difficult to learn much from the spectrum in Figure 6.8 due to the degree of baseline distortion present. These distortions are likely a result of background from stray

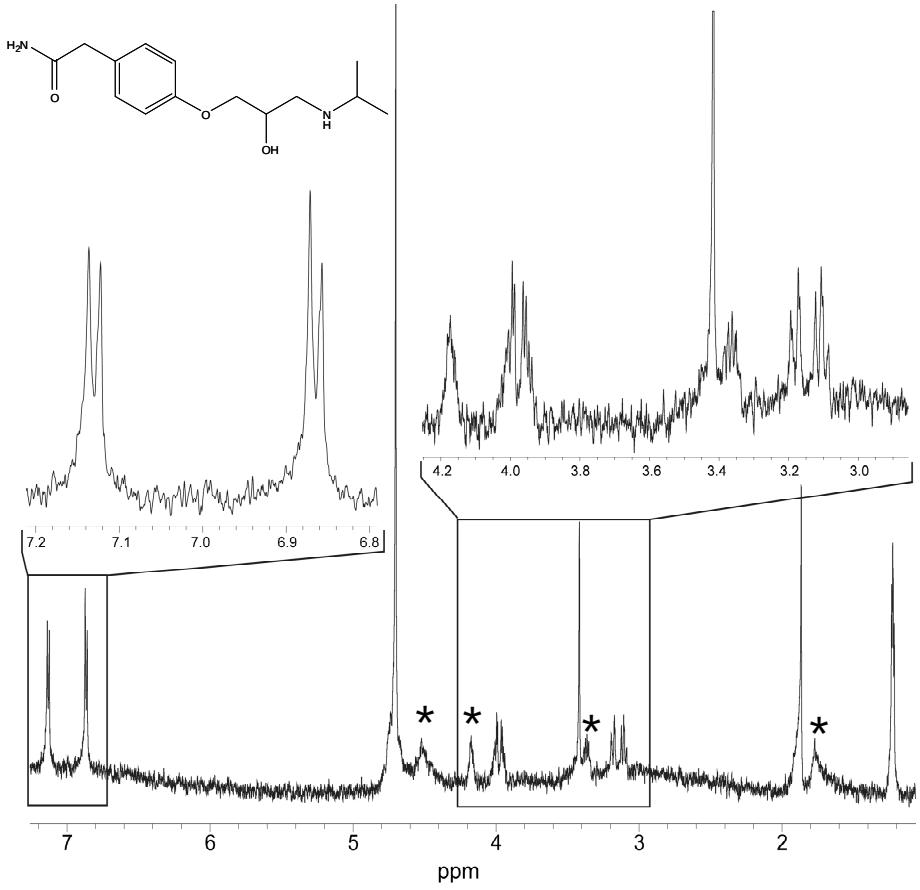

Figure 6.7 An on-flow cITP-microslot NMR spectrum resulting from injection of 18 nmol of atenolol produced by summing 30 FIDs each comprised of 8 transients. Resonances marked with an asterisk are likely from a contaminant or an atenolol degradation product.

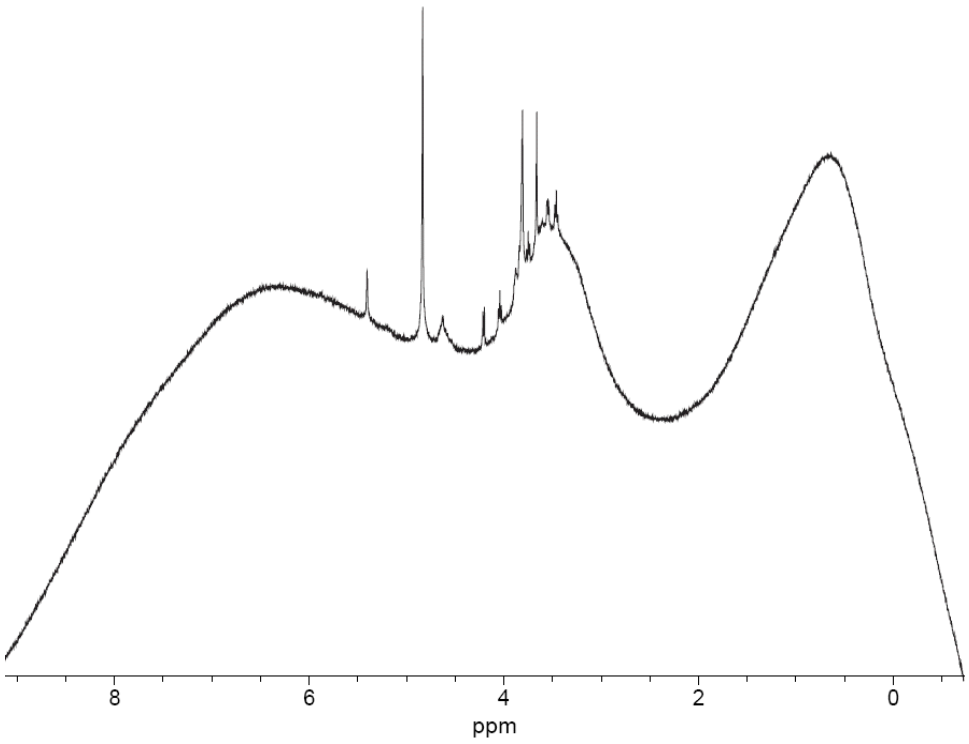

Figure 6.8. Static microslot NMR spectrum of a 100mM sucrose solution acquired with the Bruker defined ZG pulse sequence.

magnetic fields created along the length of the microstrip resulting from imperfections in the strip. In previous work, Olson et al. showed that a composite 90° pulse could suppress the signals originating from protons in the Fluorinert in which their solenoidal microcoil was immersed.[9] This composite pulse and associated phase cycling of this pulse sequence (Bruker zg_8pulse) allows detection of only the resonances in the most homogeneous part of the B_1 field.[8] In a solenoidal microcoil this corresponds to the sample inside the microcoil. In a microslot probe this pulse sequence should limit sample detection to the region directly around the slot in the microstrip minimizing the effects of the probe background. Figure 6.9 shows the microslot NMR spectrum measured for the 100 mM sucrose sample using the zg_8pulse pulse program. This spectrum is much improved from that in Figure 6.8 as all of the sucrose resonances fall along a fairly linear portion of the baseline which extends from the acetyl region out past the aromatic region. Because of the linearity of the baseline in this region, the sharp baseline slope in Figure 6.9 should be correctable using a simple algorithm. However, for samples containing resonances covering a larger spectral region, especially below 2 ppm, this approach would be less useful.

An alternative approach to suppressing background signals from the probe was presented by Cory and Ritchey in 1988.[10] Their method uses a 90° pulse followed by two 180° refocusing pulses with the appropriate phase cycling (zgbs in the Bruker pulse sequence catalog). Figure 6.10 A shows the static microslot NMR spectrum for sucrose acquired using the zgbs pulse sequence. In this spectrum we again see that the baseline is

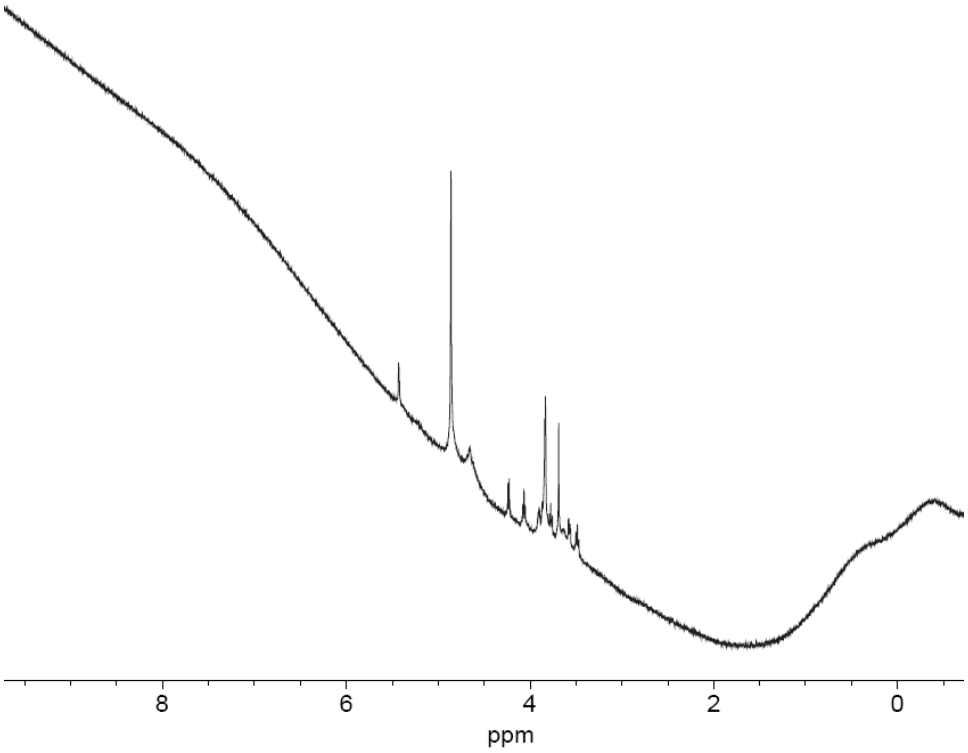

Figure 6.9 Static microslot NMR spectrum of a 100mM sucrose solution acquired with the Bruker defined zg_8pulse sequence.

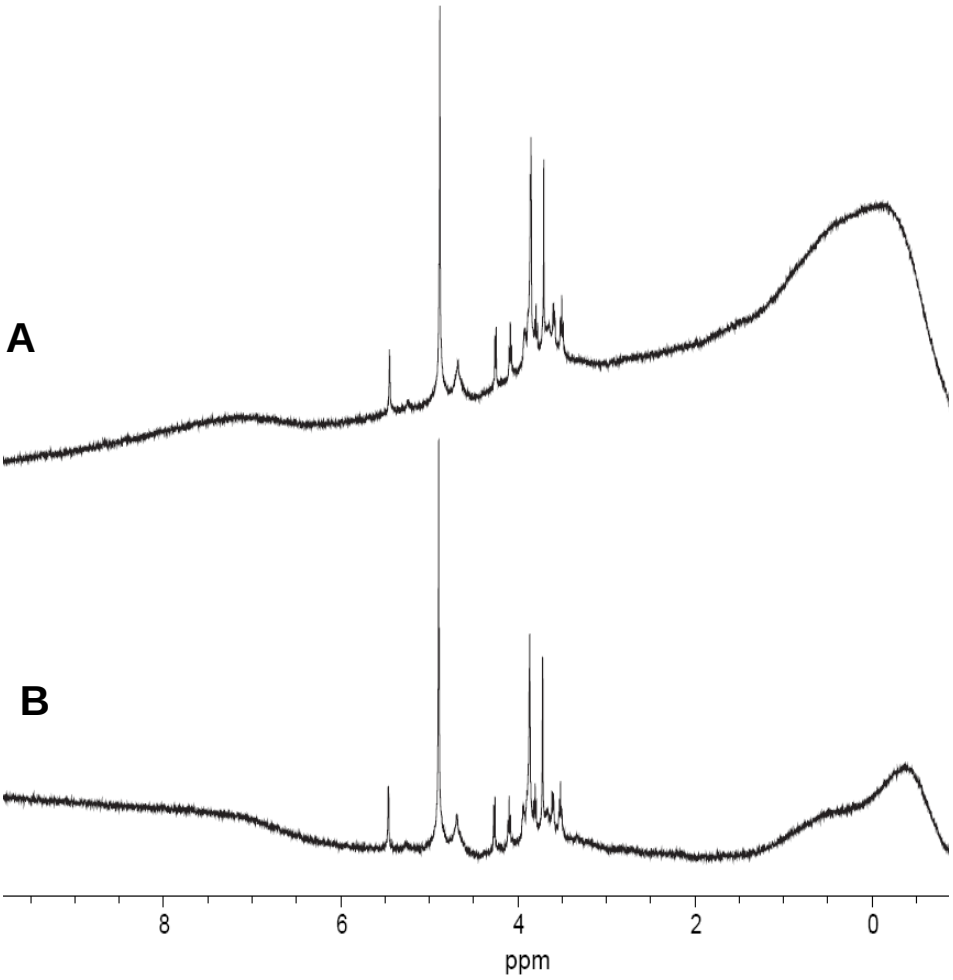

Figure 6.10A Static microslot NMR spectra of a 100mM sucrose solution acquired with A)the Bruker defined zgbs pulse sequence and B) a hybrid pulse sequence combing both the zgbs and zg_8pulse pulse sequences.

fairly flat from the acetyl region out to the aromatic region, but again there is a large baseline distortion below ~1.5 ppm.

In an attempt to obtain better baselines with our microslot NMR probe, a hybrid pulse sequence was designed that utilizes a composite 90° pulse for excitation followed by two 180° refocusing pulses. The full pulse sequence code for a Bruker spectrometer can be found at the end of this document. In this sequence the 8-pulse composite pulse from the zg_8pulse sequence is used to replace the 90° pulse in the zgbs sequence. Figure 6.10B shows the results obtained for a static sucrose sample with this hybrid pulse sequence. Comparing this spectrum to that in Figure 6.10A for the zgbs sequence, a significant reduction in baseline distortion below 1.5 ppm is observed. Figure 6.11 shows an expansion of the sucrose resonances in Figure 6.10B. Both Figures 6.10B and 6.11 demonstrate the superior performance of the hybrid pulse sequence in terms of background suppression of NMR signals from the probe. Figure 6.11 also demonstrates the quality, in terms of spectral resolution, of NMR spectra that can be acquired using the microslot probe with a static sample of high concentration. However, due to the complexity of phase cycling during both the zgbs and hybrid pulse sequences it is difficult to use these sequences with our current implementation of online cITP microslotNMR experiments because visual detection of the analyte is used to determine the presence of the focused band and apply a counterflow to park it in the probe active volume. In these pulse sequences only 1 in every 8 scans will result in a completely in-phase NMR spectrum making it difficult to visualize the presence of the analyte. For this

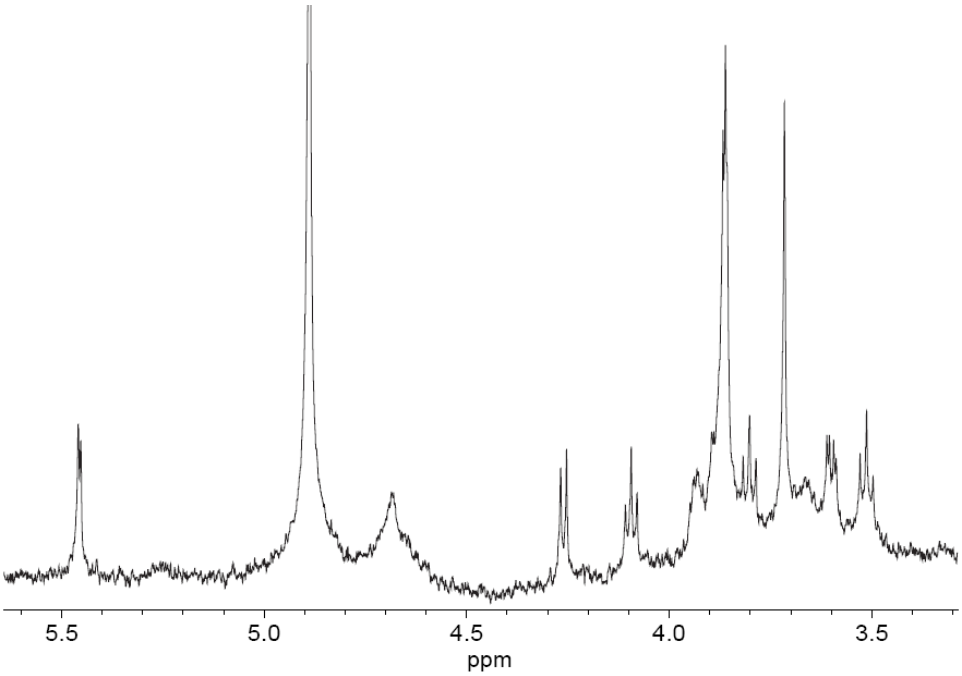

Figure 6.11 Static microslot NMR spectra zoomed in on the resonances of a 100mM sucrose solution acquired with a hybrid pulse sequence combining both the zgbs and zg_8pulse pulse sequences.

reason the atenolol cITP-microslot NMR spectrum shown in Figure 6.7 was acquired using a simple composite 90° pulse using the zg_8pulse sequence.

6.3.5 Hybrid Pulse Sequence for Improved Background Correction.

```
;zgbs_8pulse
;avance-version (02/05/31)
;1D sequence for suppression of background signals
;using composite pulse
;
;Chris Jones 08/12/11
;
;$CLASS=HighRes
;$DIM=1D
;$TYPE=
;$SUBTYPE=
;$COMMENT=
#include <Avance.incl>
"p2=p1*2"

1 ze
2 30m
  d1
  p1 ph1
  p1 ph2
  p1 ph3
  p1 ph4
  p1 ph3
  p1 ph4
  p1 ph1
  p1 ph2
  2u
  (p2 ph5):f1
  2u
 (p2 ph6):f1

  go=2 ph31
  30m mc #0 to 2 F0(zd)
exit

ph1=0 0 0 0 1 1 1 1 2 2 2 2 3 3 3 3
ph2=1 1 1 1 2 2 2 2 3 3 3 3 0 0 0 0
ph3=2 2 2 2 3 3 3 3 0 0 0 0 1 1 1 1
```

```
ph4=3 3 3 3 0 0 0 0 1 1 1 1 2 2 2 2
ph5=0 1 2 3
ph6=0 0 0 0 2 2 2 2 3 3 3 3 1 1 1 1
ph31=0 2 0 2 1 3 1 3

;pl1 : f1 channel - power level for pulse (default)
;p1 : f1 channel -  90 degree high power pulse
;p2 : f1 channel - 180 degree high power pulse
;d1 : relaxation delay; 1-5 * T1
;NS:  16 * n, total number of scans: NS * TD0
```

6.4 Conclusions

This work demonstrates that the planar geometry of the microslot NMR probe permits the separation capillary to be oriented parallel to the static magnetic field in cITP-NMR experiments, minimizing the B_0 inhomogeneity induced by the electrophoretic current of the separation. The results of nutation experiments show that B_1 homogeneity is minimally affected by the electrophoretic current. With the current boom in the commercial development of lab-on-a-chip devices, including those capable of electrophoretic separations, the added wealth of chemical and structural information that can be gained by incorporating NMR detection could be invaluable. However, further improvements in sensitivity and background suppression are still required for the coupling of cITP with microslot NMR probes.

6.5 References

1. Kentgens, A. P. M.; Bart, J.; van Bentum, P. J. M.; Brinkmann, A.; van Eck, E. R. H.; Gardeniers, J. G. E.; Janssen, J. W. G.; Knijn, P.; Vasa, S.; Verkuijlen, M. H. W., High-resolution liquid- and solid-state nuclear magnetic resonance of nanoliter sample volumes using microcoil detectors. *J. Chem. Phys.* **2008,** 128.

2. Krojanski, H. G.; Lambert, J.; Gerikalan, Y.; Suter, D.; Hergenroeder, R., Microslot NMR Probe for Metabolomics Studies. *Anal. Chem.* **2008,** 80, 8668-8672.

3. Maguire, Y.; Chuang, I. L.; Zhang, S.; Gershenfeld, N., Ultra-small-sample molecular structure detection using microslot waveguide nuclear spin resonance. *Proc. Natl. Acad. Sci. U.S.A* **2007,** 104, 9198-9203.

4. Krojanski, H. G.; Lambert, J.; Gerikalan, Y.; Suter, D.; Hergenröder, R., Microslot NMR probe for metabolomics studies. *Anal. Chem.* **2008,** 80, 8668-8672.

5. Olson, D.; Lacey, M.; Webb, A.; Sweedler, J., Nanoliter-volume ^{1}H NMR detection using periodic stopped-flow capillary electrophoresis. *Anal. Chem.* **1999,** 71, 3070-3076.

6. Wolters, A. M.; Jayawickrama, D. A.; Webb, A. G.; Sweedler, J. V., NMR detection with multiple solenoidal microcoils for continuous-flow capillary electrophoresis. *Anal. Chem.* **2002,** 74, 5550-5555.

7. Webb, A., Radiofrequency microcoils in magnetic resonance. *Prog. Nucl. Magn. Reson. Spectrosc.* **1997,** 31, 1-42.

8. Bax, A., A spatially selective composite 90° radiofrequency pulse. *J. Magn. Reson.* **1985,** 65, 142-145.

9. Olson, D. L.; Lacey, M. E.; Sweedler, J. V., High-resolution microcoil NMR for analysis of mass-limited, nanoliter samples. *Anal. Chem.* **1998,** 70, 645-650.

10. Cory, D. G.; Ritchey, W. M., Suppression of signals from the probe in bloch decay spectra. *J. Magn. Reson.* **1988,** 80, 128-132.

CHAPTER SEVEN

Conclusions and Future Directions

7.1 Conclusions

The high degree of structural diversity of heparin and HS is primarily responsible for their wide range of biological functions. However, it is this same structural diversity and it's highly ionic nature that complicates the molecular-level characterization of these important GAGs. To address this challenge, new and more sensitive separation and characterization techniques have to be developed. In chapter 2, we explored the mechanism of RPIP chromatography through the use of the RPIP-UPLC. The ability of this method to resolve heparin disaccharides based on differences in charge and subtle variations in compound structure makes it a useful probe of the mechanism of RPIP separations. The investigation also addressed the specific interactions between the IPR tributylamine (TrBA) and heparin as well as the potential role that competition between TrBA and other IPRs can play in the resolution of isomeric disaccharides. Finally, in chapter 2 we used the mechanistic insights gained to design and optimize a new reverse-phase ion-pair UPLC separation for heparin- and heparan sulfate-derived disaccharides. Compared to the results of previous studies, this method yielded higher resolution and improved ionization efficiency when coupled to ESI-MS.

In chapter 3, the RPIP-HPLC separation mechanism was examined further by probing the effects of ion-pairing reagent (IPR) concentration, counterion and mobile phase pH on the quality of the RPIP-UPLC separation with emphasis on how these

factors impact the separation of disaccharide anomers. The results highlighted the role of the IPR counterion and demonstrated that the resolution of the disaccharide anomers can be minimized by conducting the separation at low pH, simplifying chromatographic analysis and improving resolution. The results presented in both chapters 2 and 3 provided insights into strategies that could be used for developing more sensitive and efficient reverse-phase separations for other charged analytes including larger GAG oligosaccharides.

Chapter 4 describes experiments designed to investigate the effects of binding in capillary isotachophoresis, (cITP) separations. The work examined the cITP separation of the isomers of the tricyclic antidepressant doxepin to gain insights into intermolecular interactions that occur during cITP. These results showed that acetate binds weakly to beta-cyclodextrin (β-CD). The work also compared the use of CE and NMR to determine the association equilibrium constants for the binding of both doxepin isomers and β-CD.

In Chapter 5, the insights gained from the results reported in Chapter 4 were used to develop an improved anionic cITP separation method for heparin-derived oligosaccharides. The optimized buffer system using an LE of 160 mM DCL/80 mM immidazole (pD 6.9) and a TE of 40 mM tricine (pD 8.2) was shown to effectively focus all 12 commercially available disaccharides (including IVH, IVA, IIH, and IIIH which could not be focused using previous buffer systems and IVS which was not previsouly available commercially), hexasaccharide fractions of depolymerized heparin, heparan sulfate, and the low molecular weight heparin (LMWH) enoxaparin obtained by size-exclusion chromatography (SEC), as well as an unfractionated enoxaparin sample. The

results demonstrate the potential of anionic cITP microcoil NMR as a useful tool for evaluating sample purity, composition, and reaction processes for mass-limited heparin and HS samples.

In Chapter 6, we demonstrated the coupling of cITP with a microslot NMR probe design that allowed us to orient the separation capillary parallel to the static B_0 magnetic field of the NMR magnet, eliminating current-induced broadening produced in the cITP separations. The benefits of this approach were demonstrated by the cITP focusing and online NMR analysis of 18 nmol of the commercially available β-blocker, atenolol. The resulting spectrum showed that by elimination of current induced broadening that J-couplings as low as 1.8 Hz could be resolved. With the current boom in the commercial development of lab-on-a-chip devices, including those capable of electrophoretic separations, the added wealth of chemical and structural information that can be gained by incorporating NMR detection could be invaluable.

7.2 Future Directions

7.2.1 Redesign of Microslot Probe. The microslot design presented in chapter 6 is effective in reducing the broadening of NMR resonances that results from the current induced magnetic field created in the cITP capillary during focusing. However, there is still a need to improve the overall sensitivity of the probe. The microslot probe described in chapter 6 is about 4 times less sensitive than the solenoidal microcoil probe used in chapters 4 and 5. This made it difficult to distinguish most analyte resonances from baseline noise during online cITP-NMR microslot experiments. Additionally, without being able to visualize where the analyte is relative to the active volume of the coil, it is

difficult to perform stop flow experiments that would enable additional signal averaging to enhance spectra signal-to-noise.

To address this sensitivity limitation, a major redesign of the microslot probe is needed. As Figure 7.1 shows that the current slot is not only too wide for the dimensions of our capillaries (ID 180μm and OD 360μm), at a length of 500 μm it is only half the length of the 16-turn microcoils used in the solenoidal microcoil probe. At best, this limits the active volume of the microslot probe to half that of the solenoidal microcoil probe, and the added noise from the reduced filling factor are likely major contributors to the poorer sensitivity. A better design would increase the length of the slot to 1,000 μm and would reduce the width of the slot to a value closer to the O.D. of the capillaries used (~360 μm) as illustrated in Figure 7.2. This would greatly improve the filling factor of the probe while also roughly doubling its active volume.

7.2.2 Lab-on-a-chip Coupled to Microslot NMR. The planar design of the microslot probe makes it ideally suited for coupling to lab-on-a-chip applications. Recent work by Quist et al. showed that isotachophoretic separations could be triggered at the border of a nanochannel-induced ion-depleted zone.[1] The technique coined depletion zone isotachophoresis (dzITP) uses a nanochannel that connects two microchannels as a perm-selective barrier between the channels leading to concentration polarization with respect to the nanochannel when an electric field is applied across the microchannels. This concentration polarization leads to a zone of depleted ions (or a depletion zone) in the separation microchannel and ion enrichment in the other microchannel. A tangential EOF created by the interaction of buffer cations with the negative charge of the walls of

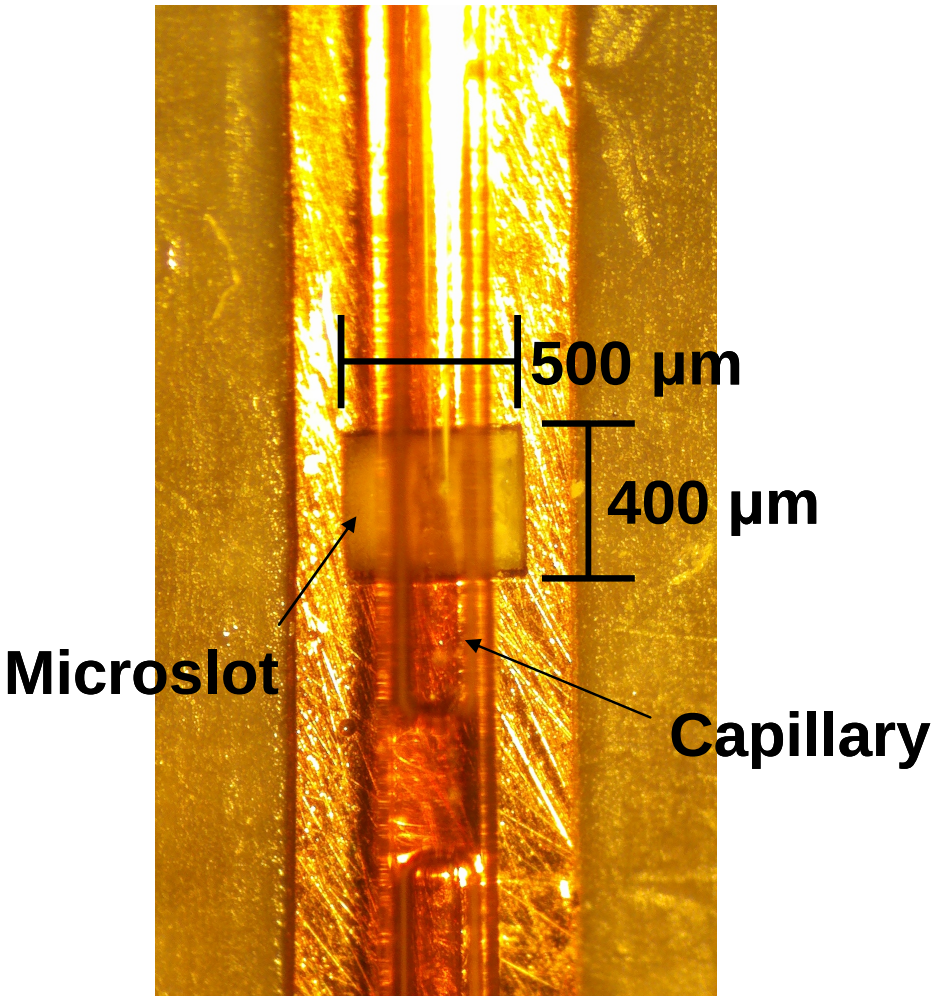

Figure 7.1. Digital image taken through the lens of a microscope of a sample capillary positioned on top of the slot in the microstrip of a microslot NMR probe used in chapter 6.

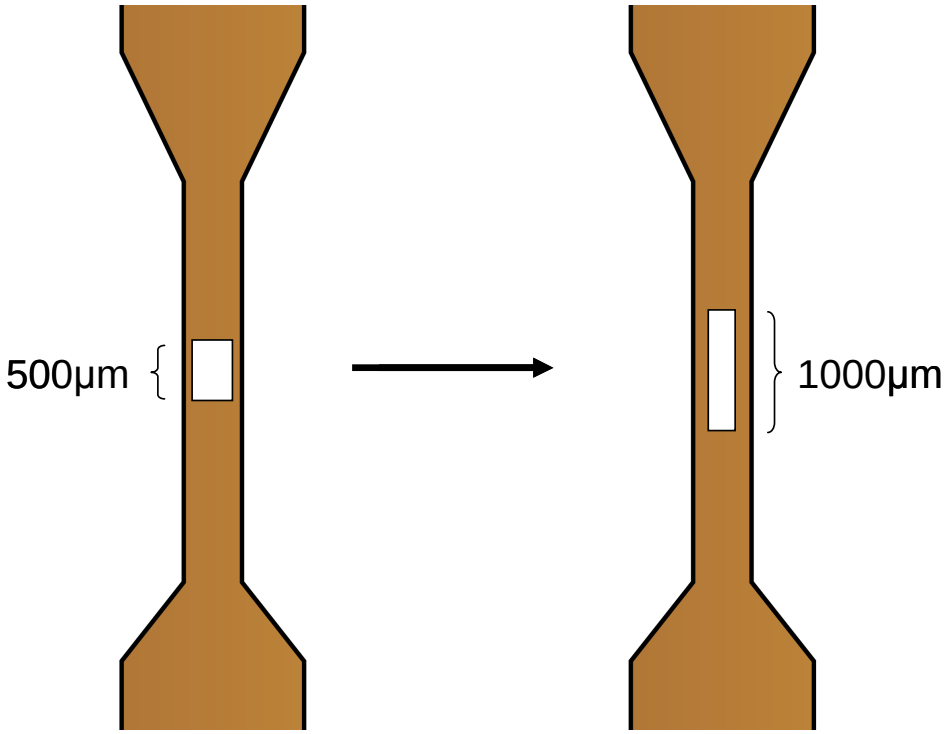

Figure 7.2. Illustration depicting the proposed changes to the current microslot probe design to increase the overall sensitivity of the probe.

the microchannel (in this case the walls were pyrex) transports analytes toward the border of the depletion zone where they are trapped. In dzITP, the depletion zone also acts as a trailing electrolyte and the background electrolyte would act as a leading electrolyte inducing an isotachophoretic separation. Since the walls of the chip are negatively charged it is ideally suited for the dzITP of anionic molecules such as heparin and heparan sulfate oligosaccharides. Additionally, using the same three point voltage actuation utilized by Quist et al., the position of the analyte zones can be fully controlled (by function of controlling the position of the depletion zone) without the need to apply a backpressure as in normal cITP, which often results in partial dispersion of the analyte band. For coupling to microslot NMR, a dzITP chip similar to that illustrated in Figure 7.3 could be fabricated which could be mated to the microslot NMR chip as shown in Figure 7.4. To maximize the filling factor, the width of the separation channel can be fabricated to the width of the microslot. The proposed dzITP chip would also need to be positioned such that the nanochannel is beyond the microslot allowing the analyte bands to be focused between the nanochannel and buffer reservoir "A". This would allow the ITP analyte bands to be focused directly above the microslot by adjusting the voltages applied at buffer reservoirs "A" and "B", allowing unlimited signal averaging capabilities for microslot NMR spectra.

7.2.3 Multinuclear Microcoil/Microslot Probes. As discussed in chapter 1, one dimensional ^{13}C and two-dimensional heteronuclear ^{1}H-^{13}C NMR experiments can provide invaluable information about the type, number, and position of C-H bonds within analytes and offers improved spectral resolution by taking advantage of the greater

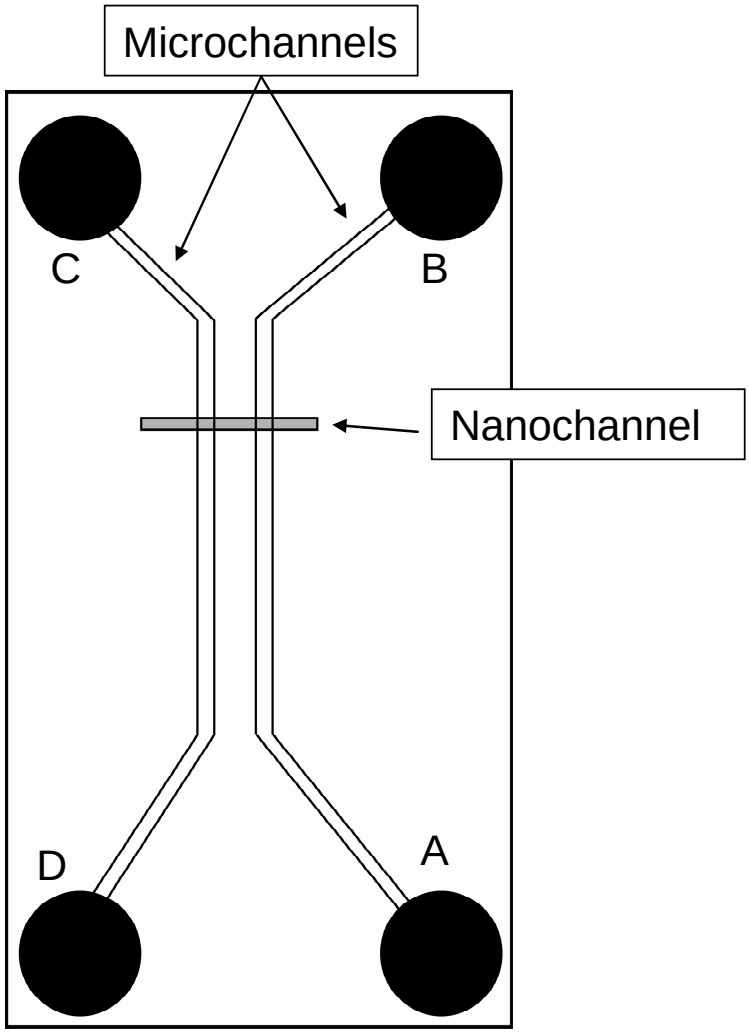

Figure 7.3. Chip layout for dzITP consisting of two microchannels and one nanochannel. In this setup A is the downstream voltage and B the upstream voltage while C and D are connected to ground. By varying the A and B voltages relative to each other the position of the depletion zone and thus the position of the focused ITP bands can be controlled.

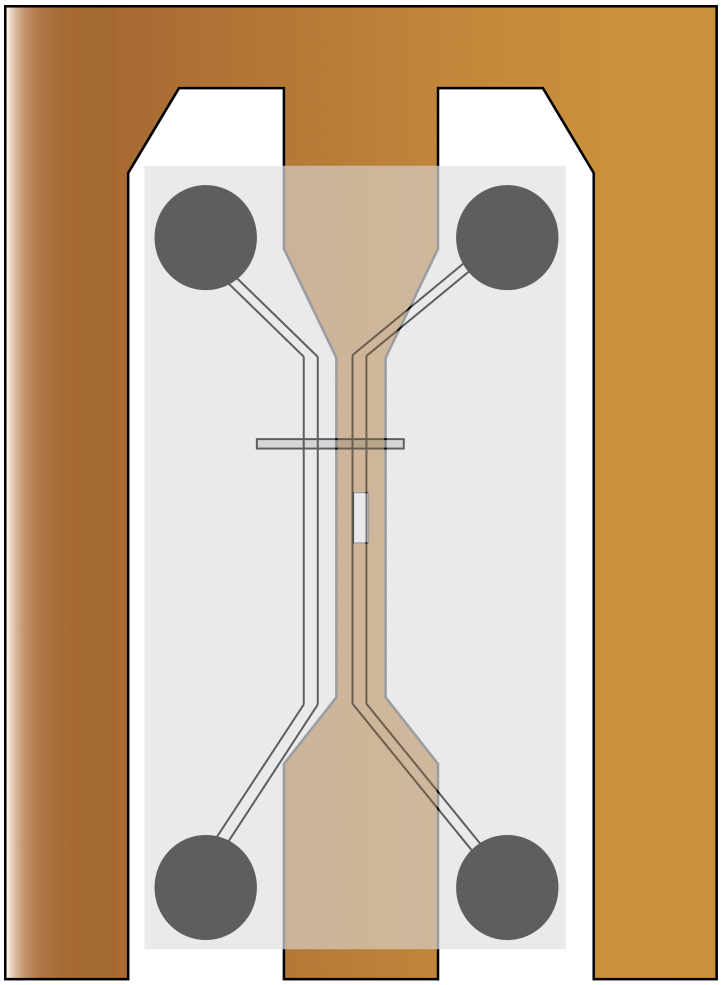

Figure 7.4. Illustration of the dzITP chip mated on top of the microslot probe.

dispersion of the ^{13}C chemical shift dimension.[2] Langeslay et al. demonstrated experimental conditions that allowed the detection of the sulfamate ($NHSO_3^-$) ^1H NMR resonances of heparin and HS derived mono- and oligosaccharides in 90% H_2O.[3] These authors further showed that by using a $^1H,^{15}N$ HSQC experiment, the sulfamate protons could be efficiently used to detect the glucosamine ^{15}N chemical shifts greatly simplifying the analysis of complex mixtures of heparin- and HS-derived oligosaccharides. However, the poor sensitivity of NMR makes detecting the less abundant ^{13}C and ^{15}N nuclei in mass-limited samples difficult. A potential solution is to add multinuclear capabilities to the solenoidal microcoil and microslot probes coupled to cITP. While some sensitivity will be lost by adding additional channels to the probes, the increased mass sensitivity of these probes along with the concentration and separation capabilities of cITP could allow the detection of ^{13}C and ^{15}N nuclei from molecules isolated in trace quantities.

7.2.4. Top-down Analysis of Heparin and HS by MS. Recent work by Ly et al. described efforts to structurally characterize and sequence the simplest proteoglycan, bikunin.[4] Bikunin is a serine protease inhibitor and is unique in that its core protein has a single site for glycan attachment. Additionally, it is readily available in high purity due to its use in the treatment of acute pancreatitis in Japan. Prior to analysis, the bikunin proteoglycans were enzymatically cleaved into peptidoglycans and then the glycan portion was further enzymatically cleaved into smaller and more easily analyzed oligosaccharides. The smaller peptidoglycans were then fractionated into size and charge uniform pools using continuous elution polyacrylamide gel electrophoresis (PAGE).

These fractions were characterized by MS and CID-MS/MS experiments with both FT-ICR and FTMS instruments. All of the isolated peptidoglycans contained a linkage region consisting of a single hexasaccharide sequence *O*-glycosidically linked to serine. Surprisingly, even beyond this linkage region the MS results revealed that the peptidoglycan chains contained a predictable pattern of 4-*O*-sulfogalactosamine residues showing a defined sequence for bikunin.

This breakthrough will likely change the glycosaminoglycan community's thinking about the structure of proteoglycans and their biosynthesis. Unlike the genome and proteome for which we understand how template-driven biosynthetic processes impart specific sequences, no such understanding exists for the glycome. In fact, there is still much debate as to whether glycans possess any true sequence or even how that would be possible given their complex biosynthetic assembly from an unmodified proteoglycan into their final form within the Golgi complex.[5] Furthermore, given the known similarity in biosynthetic pathways of all proteoglycans these results suggest that other more complex proteoglycans, such as heparan sulfate, may also have regions of defined sequence.

This work also aptly illustrates the role that the advances in the technologies available for glycan separation and analysis play in this rapidly evolving field. In particular, the application of FT-ICR and FTMS/MS^n and their success in efficiently providing sequence information, even for oligosaccharides with labile constituents. This is a significant advance in glycomics technology that will certainly see more extensive application to more complex oligosaccharides such as those in the GAG family.

However, further improvements in proteoglycan isolation techniques and the development of a detailed understanding of the regulation of glycan biosynthetic pathways will likely be required to address any role that defined sequence elements play in more complex proteoglycans.

7.3 References

1. Quist, J.; Janssen, K. G. H.; Vulto, P.; Hankemeier, T.; van der Linden, H. J., Single-electrolyte isotachophoresis using a nanochannel-induced depletion zone. *Anal. Chem.* **2011,** 83, 7910-7915.

2. Guerrini, M.; Naggi, A.; Guglieri, S.; Santarsiero, R.; Torri, G., Complex glycosaminoglycans: profiling substitution patterns by two-dimensional nuclear magnetic resonance spectroscopy. *Anal. Biochem.* **2005,** 337, 35-47.

3. Langeslay, D. J.; Beni, S.; Larive, C. K., Detection of the ^{1}H and ^{15}N NMR resonances of sulfamate groups in aqueous solution: A new tool for heparin and heparan sulfate characterization. *Anal. Chem.* **2011,** 83, 8006-8010.

4. Ly, M.; Leach, F. E.; Laremore, T. N.; Toida, T.; Amster, I. J.; Linhardt, R. J., The proteoglycan bikunin has a defined sequence. *Nat Chem Biol* **2011,** 7, 827-833.

5. Ly, M.; Laremore, T. N.; Linhardt, R. J., Proteoglycomics: Recent Progress and Future Challenges. *Omics* **2010,** 14, 389-399.

Appendix 1

MicroMath Scientist Statistics Report

Goodness-of-fit statistics for data set:c:\scientis\try.mmd

Data Column Name: D

	Weighted	Unweighted	
Sum of squared observations :	302.595715	302.595715	
Sum of squared deviations :	0.00448339022	0.00448339022	
Standard deviation of data :	0.0201886337	0.0201886337	
R-squared :	0.999985184	0.999985184	
Coefficient of determination :	0.398681355		0.398681355
Correlation :	0.964937665	0.964937665	

Data Set Name: c:\scientis\try.mmd

	Weighted	Unweighted	
Sum of squared observations :	302.595715	302.595715	
Sum of squared deviations :	0.00448339022	0.00448339022	
Standard deviation of data :	0.0201886337	0.0201886337	
R-squared :	0.999985184	0.999985184	
Coefficient of determination :	0.398681355		0.398681355
Correlation :	0.964937665	0.964937665	
Model Selection Criterion :	0.341963627	0.341963627	

Confidence Intervals:

Parameter Name :	K		
Estimate Value =	37731.9134		
Standard Deviation =		2988.91538	
95% Range (Univar) =		31153.3551	44310.4718
95% Range (S-Plane) =		31153.3551	44310.4718

Variance-Covariance Matrix:
8933615.1199

Correlation Matrix:
1.00000000

Residual Analysis:

The following are normalized parameters with an expected value of 0.0. Values are in units of standard deviations from the expected value.

The serial correlation is 2.40 which indicates a systematic non-random trend in the residuals.

Skewness is -4.52 indicating the likelihood of a few large negative residuals having an unduly large effect on the fit.

Kurtosis is 0.30 which is probably not significant.

The weighting factor was 0.00 leading to a heteroscedacticity of -201.49 which suggests an optimal weight factor for this fit of about -201.49

```
// MicroMath Scientist Model File
IndVars: PTOT
DepVars: D
Params: K

DS=5.06668
DSP=4.99593
STOT=0.001
SP=STOT-S

A=K
B=(K*PTOT)+(K*STOT)+1
C=-STOT

DD=sqrt((B*B)-(4*A*C))
S=(-B+DD)/(

XSP=SP/STOT
XS=S/STOT
D=(DS*XS)+(DSP*XSP)
0<SP<0.001

Key:
D = Doxepin concentration
S = β-CD
```